

(200)  
R290  
no.80-1171



3 1818 00074568 5

# IMPROVED STRESS DETERMINATION

## PROCEDURES BY HYDRAULIC FRACTURING

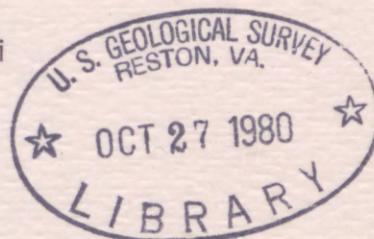
--Rock Fracture Extension in Hydraulic Fracturing for Conditions where the Principal Stresses are Inclined to the Axis at the Pressurized Borehole.

by

Yoshiaki Mizuta

&

Hideo Kobayashi



FINAL REPORT

to the

U.S. Geological Survey  
on research carried out under Grant No. USDI-14-08-0001-17775

John Santich

&

Charles Fairhurst

Co-Principal Investigators

April 1980

MINERAL RESOURCES RESEARCH CENTER

DEPARTMENT OF CIVIL AND MINERAL ENGINEERING  
INSTITUTE OF TECHNOLOGY

UNIVERSITY OF MINNESOTA









✓  
U.S. Geological Survey,

[Reports-Open file series]

TM.  
cm ✓

IMPROVED STRESS DETERMINATION

Laboratory PROCEDURES BY HYDRAULIC FRACTURING

--Rock Fracture Extension in Hydraulic Fracturing for Conditions where the Principal Stresses are Inclined to the Axis at the Pressurized Borehole.

of varying borehole inclination with respect to the in-situ stress field and of varying pressurization flow rates.

Experiments were carried out on relatively large specimens of compact brittle and impermeable rock containing vertical or inclined boreholes.

by

Yoshiaki Mizuta

&

Hideo Kobayashi

Fracture orientation was determined by overcoring the borehole in the specimen. The pressure-time records obtained were of two types, dependent on fracture orientation to the borehole axis. In fracturing corresponding to a first type of pressure-time record, the direction of fracture initiation at the borehole is determined primarily by the borehole axis; the fracture

FINAL REPORT

to the

U. S. Geological Survey

on research carried out under Grant No. USDI-14-08-0001-17775 on

breakdown pressure. Inclined type fractures can be initiated away from the borehole, propagating away from and back to the borehole and its direction is perpendicular to minimum principal stress. Numerical analyses were also

John Santich

&

Charles Fairhurst

Co-Principal Investigators

of pressure-time records produced experimentally.

April 1980

Analysis and experimental studies indicate that: 1) the minimum principal stress is perpendicular to the normal stress component perpendicular to a fracture directed away from the borehole; 2) the minimum principal stress is the minimum stress component in the plane perpendicular to the borehole axis; 3) the minimum principal stress is the minimum stress component in the plane perpendicular to the borehole axis.

312575

Mineral Resources Research Center  
Department of Civil and Mineral Engineering  
Institute of Technology  
University of Minnesota







## Abstract

Laboratory hydraulic fracturing tests using a straddle packer with inflatable rubber sealing elements were conducted to investigate the effects of varying borehole inclination with respect to the in-situ stress field and of varying pressurization flow rates.

Experiments were carried out on relatively large specimens of competent, brittle and impermeable rock containing vertical or inclined boreholes. These specimens were fractured hydraulically under biaxial loading, the fractures then being reopened by cycling the pressure at different flow rates.

Fracture orientation was determined by overcoring the borehole in the specimen. The pressure-time records obtained were of two types, dependent on fracture orientation to the borehole axis. In fracturing corresponding to a first type of pressure-time record, the direction of fracture initiation at the borehole is determined primarily by the borehole axis, the fracture orienting itself to the far field stress with propagation depending on breakdown pressure. Second type fractures can be initiated away from the borehole, propagating away from and back to the borehole and its direction is perpendicular to minimum principal stress. Numerical analyses were also carried out on experimental configurations to assist in the interpretation of pressure-time records produced experimentally.

Analytical and experimental studies indicate that: 1) it is possible to determine the normal stress component perpendicular to a fracture direction, from a first type of pressure-time record along with observation of the fracture on the borehole surface. If the fracture was produced by hydrostatic pressure, that normal stress component is the minimum stress component in the plane perpendicular to the borehole axis; 2) the minimum principal



stress and its direction can be estimated from a second type of pressure-time record along with observation of the fracture at the borehole wall.

Laboratory hydraulic fracturing tests using a straddle packer with inflatable rubber sealing elements were conducted to investigate the effects of varying borehole inclination with respect to the in-situ stress field and of varying pressurization flow rates. Experiments were carried out on relatively large specimens of compact brittle and impermeable rock containing vertical or inclined boreholes. These specimens were fractured hydraulically under biaxial loading, the first then being reopened by cycling the pressure at different flow rates. Fracture orientation was determined by overcoring the borehole in the specimen. The pressure-time records obtained were of two types, dependent on fracture orientation to the borehole axis. In fracturing corresponding to a first type of pressure-time record, the direction of fracture initiation at the borehole is determined primarily by the borehole axis, the fracture orienting itself to the far field stress with propagation depending on breakdown pressure. Second type fractures can be initiated away from the borehole, propagating away from and back to the borehole and its direction is perpendicular to minimum principal stress. Numerical analyses were also carried out on experimental configurations to assist in the interpretation of pressure-time records produced experimentally. Analytical and experimental studies indicate that: (1) it is possible to determine the normal stress component perpendicular to a fracture direct from a first type of pressure-time record along with observation of the fracture on the borehole surface. If the fracture was produced by hydrostatic pressure, that normal stress component is the minimum stress component in the plane perpendicular to the borehole axis; (2) the minimum principal



## Disclaimer

## TABLE OF CONTENTS

This report is based upon research supported by U. S. Geological Survey under Grant No. USDI-14-08-0001-17775. Any opinions, findings and conclusions or recommendations expressed in this report are those of the author and should not be interpreted as necessarily representing the official policies, either expressed or implied, of the U. S. Government.

1.0	INTRODUCTION	5
2.0	STATE OF THE ART	6
3.0	EXPERIMENTAL AND ANALYTICAL CONDITIONS	10
4.0	EXPERIMENTS	15
4.1	Sample Preparation	16
4.2	Equipment	15
4.3	Procedure for Fracturing Test	24
4.4	Procedure for Reopening Test	28
4.5	Results	30
4.6	Fracture Orientation	57
5.0	NUMERICAL ANALYSIS	102
5.1	Techniques and Assumptions	102
5.2	Results	107
6.0	DISCUSSION	116
6.1	Fracturing Tool	116
6.2	Breakdown Pressure	116
6.3	Steady Flow Pressure	117
6.4	Fracture Extension Pressure and Shut-In Pressure	126
6.5	Pre-Existing Fracture	126
7.0	CONCLUSIONS	131
8.0	REFERENCES	133
	APPENDIX A Program Listing	
	APPENDIX B Coupled Stress Flow Model of Rock Fracture	



# TABLE OF CONTENTS

	Page
LIST OF FIGURES	8
LIST OF TABLES	14
SUMMARY	
	Page
1.0 INTRODUCTION	1
2.0 BASIC CONCEPTS	5
3.0 EXPERIMENTAL AND ANALYTICAL CONDITIONS	10
4.0 EXPERIMENTS	15
4.1 Sample Preparation	15
4.2 Equipment	15
4.3 Procedure for Fracturing Test	24
4.4 Procedure for Reopening Test	28
4.5 Results	30
4.6 Fracture Orientation	67
5.0 NUMERICAL ANALYSIS	102
5.1 Techniques and Assumptions	102
5.2 Results	107
6.0 DISCUSSION	116
6.1 Fracturing Tool	116
6.2 Breakdown Pressure	116
6.3 Steady Flow Pressure	117
6.4 Fracture Extension Pressure and Shut-In Pressure	126
6.5 Pre-Existing Fracture	126
7.0 CONCLUSIONS	131
8.0 REFERENCES	133
APPENDIX A Program Listing	76
APPENDIX B Coupled Stress Flow Model of Rock Fracture	7
Figure 4.6.3 An Example of Half Shell New Cut and Dried	7
Figure 4.6.4 An Example Pair of 6-Inch Cores and a Transparent Cylindrical Coordinate	7
Figure 4.6.5 The 6-Inch Cores Cut in Two Longitudinally	7

# LIST OF FIGURES

	Page
Figure 2.1	8
Figure 3.1	14
Figure 4.1	16
Figure 4.2.1	18
Figure 4.2.2	19
Figure 4.2.3	20
Figure 4.2.4	20
Figure 4.2.5	22
Figure 4.2.6	23
Figure 4.3.1	25
Figure 4.3.2	25
Figure 4.4.1	31
Figure 4.4.2	31
Figure 4.5.1	36-65
Figure 4.5.2	69
Figure 4.6.1	70
Figure 4.6.2	71
Figure 4.6.3	72
Figure 4.6.4	73
Figure 4.6.5	75-76



# LIST OF FIGURES (continued)

	Page
Figure 4.6.6 The Fracture Trace of Specimens	77-101
Figure 5.1.1 Finite Element Meshes used in Stress Analysis and Flow Analysis	103-104
Figure 5.1.2 Flow Chart of Coupled Stress-Flow Analysis	106
Figure 5.2.1 Computed Results	108
Figure 5.2.2 Computed Results	109
Figure 5.2.3 Computed Results	110
Figure 5.2.4 Computed Results	111
Figure 5.2.5 Computed Results	112
Figure 5.2.6 Computed Results	113
Figure 5.2.7 Computed Results	114
Figure 5.2.8 Stress Distribution, Boundary Condition, Vertical Borehole	115
Figure 6.2 Analyzed Breakdown Pressure-Borehole Inclination Curves and Experimental Results	118
Figure 6.3.1 Analyzed Fluid Pressure - Flow Rate Curves and Experimental Results	119
Figure 6.3.2 Analyzed Fluid Pressure - Flow Rate Curves and Experimental Results	120
Figure 6.3.3 Analyzed Fluid Pressure - Flow Rate Curves and Experimental Results	121
Figure 6.5.1 Comparison of Experimental Results with Analytical Results with Respect to $P_t$ - $P_y$ Relationship	128
Figure 6.5.2 Mechanical Fracture creating Perpendicular to the Hydraulic Fracture	130

## LIST OF TABLES

Table 3.1	Experimental and Analytical Conditions	11
Table 3.2	Experimental Conditions of the Series C	13
Table 4.3.1	Equipment Parameter Settings	27
Table 4.5.1	Experimental Conditions and Results of Each Test	32-35
Table 6.3.1	Classification of Fracture Pattern	124



## SUMMARY

The hydraulic fracturing technique as a method for determination of in-situ stresses has the advantage over other stress measuring methods in that it can be used at considerably greater depths from a point of access. However, hydraulic fracturing will not give correct results below a depth where the bedrock experiences an horizontal shear stress in the vertical plane exceeding the shear strength of the rock, as long as breakdown pressure is used to estimate the state of stress. Even at lesser depths, breakdown pressure cannot be relied upon for accurate determination of in-situ stress because it relies on the concept of "tensile strength" of rock and thus is a structure sensitive property as well as being controlled by rock composition. One must depend, therefore, only on reopening pressure and shut-in pressure to determine the state of stress, since they are structure insensitive properties. However, reopening pressure and breakdown pressure will be influenced by the flow rate of pumping fluid.

In general, the borehole axis is not parallel to a principal stress direction. The interpretation of hydraulic fracturing data in such cases with respect to both stress magnitudes and directions has been unclear. This research was conducted to probe the possibilities of determination of rock stress by using reopening pressure and to investigate the effects of borehole inclination with respect to the in-situ stress field and of flow rate. Experiments were carried out on relatively large specimens of brittle, competent and impermeable rock containing either vertical or inclined boreholes. These specimens were fractured hydraulically under biaxial loading and the fractures reopened by cycling the pressure at different flow rates. Numerical analyses were also carried out on the experimental configurations

to assist in the interpretation of experimental data.

A summary of the significant findings to date is as follows.

- (1) Pressure-time records from hydraulic fracturing fall into two categories. The first type occurs when a fracture is initiated vertically at the borehole wall and extends past the sealing elements forming a fluid flow path back into the free part of the borehole. The second type occurs with either horizontal or sub-vertical initiation followed by fracture extension away from the borehole without breaching the packers or forming a re-entrant fluid path. The distinction between these types of fracture as reflected in the pressure time record on reopening yields important information on the in-situ stress field.
- (2) In the case that a fracture is initiated by fluid pressure for the first time, a fracture parallel to the borehole axis will be created, provided that borehole inclination to the in-situ stress field is slight or that differences between principal stresses are small. The least normal stress component perpendicular to the borehole axis can then be estimated from a reopening test pressure-time record, in which a relatively low flow rate has been employed. Use is made of analytical solutions of the hydraulic conductivity equations, enabling prediction of the pressure-flow relationship, to provide a linear multiplier relating fluid pressure and the normal stress magnitude. The fracture direction is obtained from observation of the trace on the borehole wall.
- (3) If it is possible to create a fracture in a specified direction perpendicular to the borehole axis prior to hydraulic fracturing (for

example, through the use of a mechanical tool), stress components perpendicular to this fracture can be determined. In the case that the direction is chosen to be perpendicular to a formerly induced hydraulic fracture, with the mechanical fracture being created in another section of the same borehole, the maximum normal stress in the plane perpendicular to the borehole axis will be determined.

Where a fracture has already been induced by the drilling of the borehole, as in the case of very high in-situ stresses, it is possible to estimate the normal stress component perpendicular to the fracture from the pressure-time record obtained from a reopening test employing low flow rates. In general a pre-existing fracture in the hydraulic fracturing chamber will enable an estimate of the normal stress perpendicular to the fracture to be made, although the fracture must parallel the borehole axis to some extent.

- (4) The minimum principal stress can be determined from a second type of pressure-time record which indicates the presence of a fracture with no fluid outlet back into the free borehole, whether or not this fracture was induced by hydraulic pressure. This second type of pressure-time trace is obtained by using a relatively high flow rate of pressurizing fluid.

Where the initial fracture is initiated by hydraulic fluid pressure, the fracture path will be perpendicular to the minimum principal stress in cases where the borehole is considerably inclined to the in-situ stress field and where differences in principal stress magnitudes are large. The direction of minimum principal stress may then be determined by observation of the fracture trace on the borehole wall.



The complete stress state can be determined by following the above procedures. From tests on three fractures the minimum principal stress as well as the maximum and minimum normal stresses on the plane perpendicular to the borehole axis, can be determined in magnitude and direction. In the case where there is a pre-existing fracture the number of known quantities is decreased. A pair of tests, using boreholes with differing inclinations, will then be required to determine the complete state of stress.

## 1.0 INTRODUCTION

Over-coring stress relief techniques have been widely used for the determination of in-situ stresses. The method relies on the deformation of a rock annulus as it is relieved in the extraction process of overcoring. So long as one is concerned with low stress values and with competent rock, there is little difficulty in registering the absolute value of stress in the bedrock, but it is under those conditions that it is normally less important to ascertain the precise state of stress. Difficulties arise in the case of very high stress values, under which conditions it becomes extremely important to know accurately the state of stress.

Hydraulic fracturing of rock is a technique developed approximately 30 years ago as a method of stimulating oil production from wells. More recently, the technique has been examined as a potential method for determination of in-situ stress at depth, through studies both in the laboratory and in the field (Haimson 1963, Von Schoenfeldt 1970, Rogiers 1975, and Cornet 1977).

The hydraulic fracturing technique as a method for determination of in-situ stresses has the advantage over other stress measuring methods in that it can be used at considerably greater depths from a point of access. This is of great significance in earthquake regions where stresses at hundreds or thousands of meters are of interest.

Despite the increasing use of hydraulic fracturing, however, there are uncertainties associated with the interpretation of the resulting data. In particular, confidence in the calculated maximum principal stress is less than in the minimum principal stress, although the former is often of great moment. Furthermore, where the borehole axis is not parallel to a principal stress direction, the interpretation of hydraulic fracturing data with respect to stress magnitudes and directions is unclear.

Previous laboratory experiments on hydraulic fracturing have primarily been concerned with the relationships existing between applied stresses and breakdown pressures (Haimson 1968). However, if one depends on breakdown pressure, the hydraulic fracturing method will not give correct values below the depth where the bedrock is subjected to a shearing stress exceeding the shear strength of the rock. This usually occurs at depths greater than about 1200 m (Hast 1979).

Even if the depth is less than 1200 m or so, breakdown pressure can not be relied on for accurate determination of the rock stress since it is concerned with tensile strength. The tensile strength of rock is a structure sensitive property (Yokobori 1955) as well as being controlled by rock composition.

It is necessary, therefore, to depend on reopening pressure and shut in pressure to determine the state of stress since these parameters are structure insensitive. However, both reopening pressure and breakdown pressure will be influenced by the flow rate of pumping fluid.

Another interesting possibility is indicated by the laboratory experiments of Cornet 1977. Cornet showed that the fracture path can extend perpendicular to a maximum principal stress indicating that once initiated the fracture may extend away from the hole in its own plane without turning to grow perpendicularly to the minimum principal stress.

This study seeks to probe the possibilities of the determination of rock stress by using reopening pressure and controlled flow rates to contribute to an improved stress determination procedure by hydraulic fracturing.

In this research, hydraulic fracture due to internal pressurization of the chamber between two inflatable packers is discussed. A series of experiments have been undertaken to clarify the effect of borehole orientation with respect

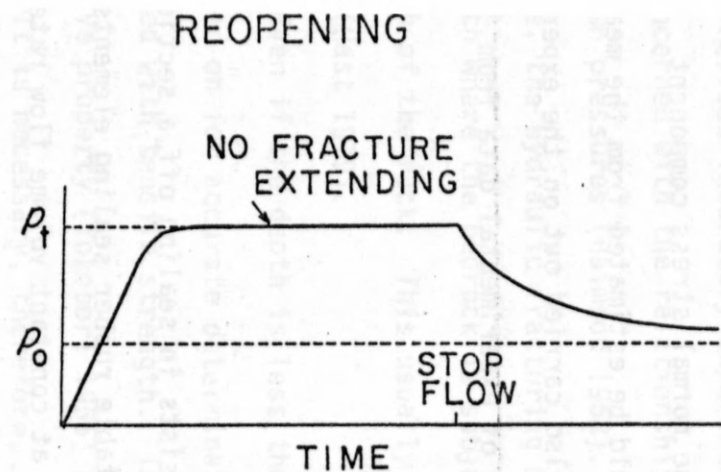
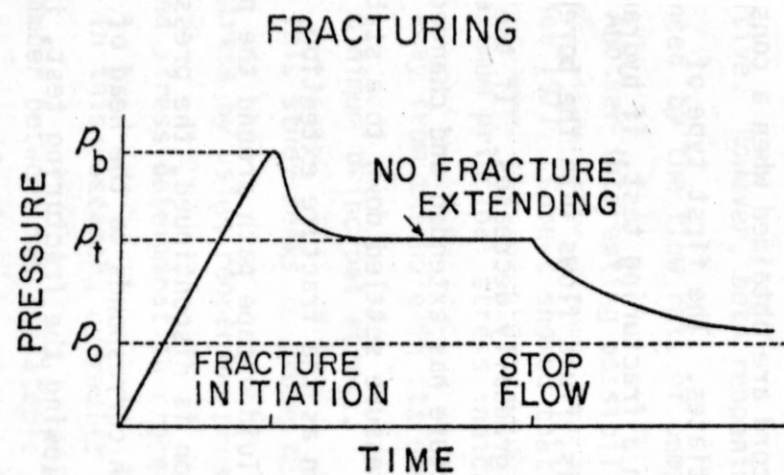


to the in-situ stress field, as well as the influence of pressurization rate on the resulting hydraulic fracturing data. Another series of experiment have also been undertaken to investigate whether the normal stress component perpendicular to a pre-existing fracture could be estimated from the measured reopening pressure. Numerical analysis were also carried out on the experimental configurations to assist in the interpretation of experimental data from reopening tests.

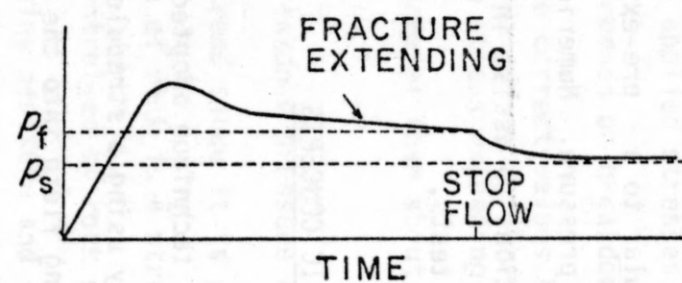
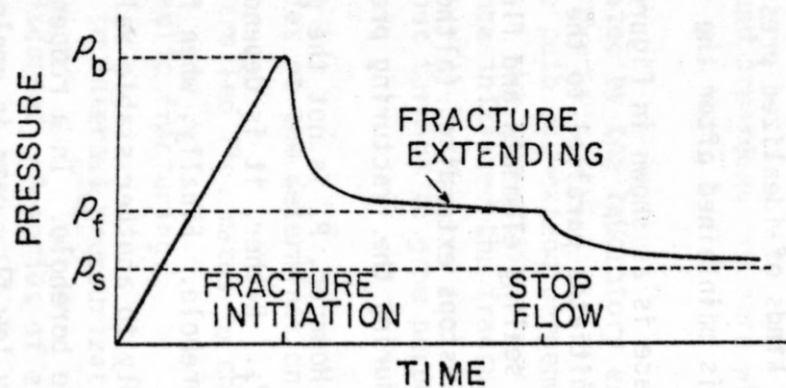
## 2.0 BASIC CONCEPTS

The technique adopted in this study consists in sealing off a section of borehole by using a straddle packer with inflatable rubber sealing elements, then pumping fluid into the sealed-off section at constant volume flow rate until fracture occurs at the so called breakdown pressure  $P_b$ .

Two kinds of idealized pressure-time record are obtained when a constant flow rate is maintained after the fracture initiates. The first type of typical trace is as shown in Figure 2.1(a). In a fracturing test, if hydraulic fracture initiates parallel to the borehole axis, fluid flows into the borehole beyond the sealing elements and fluid pressure gradually decreases. If the fracture stops extending, (although the fracture has extended and changed its direction during the fracturing process) the pressure settled down to a stable value  $P_t$ . However,  $P_t$  is not the pressure known as the fracture extension pressure,  $P_f$ . Rather, it is dependent on the fluid escape path around the packer(s) into the borehole. Finally, when fluid injection is discontinued, the pressure drops rapidly to another stable value,  $P_0$ , which corresponds to the head of fluid in the borehole. In a reopening test following the fracturing test, in which a relatively low flow rate is employed, the peak pressure overshoot on reopening disappears and fluid pressure stabilized at a value  $P_t$ , which is



(a)



(b)

Figure 2.1 Typical pressure-time record

little greater than the value  $P_t$  at fracturing. This is because the fluid pressure  $P_t$  may be affected by the existence of a peak pressure overshoot which is presumed to depend on the value of initial packer pressure. Usually, the initial packer pressure at fracturing will be required to be greater than that at reopening.

The second typical or idealized pressure-time record is as shown in Figure 2.1(b). If a fracture initiates across the sealed-off section, perpendicular or inclined to the borehole axis, the fluid is injected into the fracture causing it to extend. When fluid injection is discontinued, the pressure falls to a stable value known as the instantaneous shut-in pressure,  $P_s$ . In this report, the pressure just before termination of flow was used as the fracture extension pressure,  $P_f$ . In a reopening test following fracturing a relatively high flow rate may be used. In such a case, the fluid pressure reaches a peak at reopening and then gradually decreases. If such reopening tests are repeated, the fluid pressure at reopening will achieve a lower and lower peak, until the pressure asymptotes to the minimum principal stress.

The steady flow pressure  $P_t$  is related to the least normal stress component in the plane perpendicular to the borehole axis. The fracture extension pressure is related to the minimum principal stress. Hence, usually, the value of  $P_t$  will be greater than the value of  $P_f$ .

In the reopening test involving the first type of fracture, secondary fracture of the second type may be produced if a relatively high flow rate compared with that used on fracturing is employed. In such a case, the second type of pressure-time record may be obtained. Conversely, if relatively low flow rates are used in a reopening test involving the second type of fracture, the shape of the pressure-time record obtained may be like that of the first type, even though the registered pressure is much smaller than that of the first type.



It has been proposed that the shut-in pressure is a reliable estimate of the least compressive stress (Haimson, 1968). This is so, providing that the hydraulic fracture is of the second type, not bypassing the sealing elements. In the present study, shut-in pressure was found to be asymptotic to zero for all of the fractures of the second type, agreeing with the minimum applied stress of zero.

In general, the first type of fracture bypassing the sealing elements is apt to occur when differences among principal stresses are small, borehole inclinations are slight, flow rate are low and packer pressures are not much higher than chamber pressure at fracture initiation. When these conditions are reversed, the second type of fracture is likely to be observed.

### 3.0 EXPERIMENTAL AND ANALYTICAL CONDITIONS

The experiments were divided into three series. The first two series of tests were performed to simulate and examine the effect of varying borehole orientation on the fracture and reopening process. The third series of tests were undertaken to probe the possibilities for determination of the normal stress component in the plane perpendicular to a pre-existing fracture.

The tests of the three series are summarized in Table 3.1. In the first two series of experiments, borehole inclinations ranging from zero to  $36^\circ$  to the vertical were employed, and two different stress states were applied. Stress states A ( $P_1 = 2,000$  psi,  $P_2 = 1,000$  psi,  $P_3 = 0$ ) represents the case where the differences among principal stresses are relatively large. Stress state B ( $P_1 = 1,200$  psi,  $P_2 = 1,000$  psi,  $P_3 = 0$ ) represents the case where the difference between maximum and intermediate principal stresses is relatively small. In the third series of experiments, stress state C1 ( $P_1 = 1,000$  psi,  $P_2 = 500$  psi,

Table 3.1

## Experimental and Analytical Conditions

borehole inclination	stress state	Experiment						Analysis			
		$P_x$ (psi)	$P_y$ (psi)	$P_z$ (psi)	$P_{zx}$ (psi)	$P_{yz}$ (psi)	flow rate	$P_x$ (psi)	$P_y$ (psi)	$P_z$ (psi)	$P_t$ (psi)
0°	A	2000	1000	0	0	0	S,H,M,L	2000	1000	0	1200, 1400, 1600, 1750
$\phi = 9$	AI	1951	1000	49	309	0	H,M				
18	AI	1809	1000	191	588	0	H,M,L,S				
27	AI	1588	1000	412	809	0	H,M,L				
36	AI	1309	1000	691	951	0	S,H,M,L	1309	1000	691	1600
$\beta = 9$	AII	2000	976	24	0	155	H,M,L				
18	AII	2000	905	95	0	294	H,M				
27	AII	2000	794	206	0	405	H,M,L				
36	AII	2000	655	345	0	476	H,M,L	2000	655	345	1000,1080
0	B	1200	1000	0	0	0	M,L,H				
$\phi = 9$	BI	1171	1000	29	185	0	M,L				
18	BI	1085	1000	115	353	0	M,L				
27	BI	953	1000	247	485	0	M,L				
36	BI	785	1000	415	571	0	M,L				
$\beta = 9$	BII	1200	976	24	0	155	M,L				
18	BII	1200	905	95	0	294	M,L				
27	BII	1200	794	206	0	405	M,L				
36	BII	1200	655	345	0	476	M,L				
0	C1	1000	500	0	0	0	H,M				
$\phi=18$	C1-I	905	500	95	294	0	H,M				
$\beta=18$	C1-II	1000	452	48	0	147	H,M				

$P_3 = 0$ ) was applied for three fracturing tests. In this case, differences among principal stresses are relatively small. Thirteen different stress states were then applied for reopening tests. These states are summarized in Table 3.2. In case of stress state C2, for example, normal stress perpendicular to the fracture is the maximum stress component in the plane perpendicular to borehole axis.

In the stress state I, the borehole axis was inclined to the major principal stress direction while remaining in the  $P_1$ - $P_3$  plane, as shown in Figure 3.1(I). The borehole axis is thus perpendicular to the intermediate principal stress,  $P_2$ , whatever the angle of inclination of the particular test. In the stress state II, the borehole axis remains in the  $P_2$ - $P_3$  plane, as shown in Figure 3.2(II). Thus, the borehole axis is perpendicular to the major principal stress for all tests. Effectively, the tests of stress state I investigates the influence of shear stress  $P_{zx}$  while the tests of stress state II investigates the influence of shear stress  $P_{yz}$ .

Since a large triaxial loading frame was not available, stress states in which values of principal stresses were large, with differences among them relatively small, could not be applied. And will be mentioned later, very high stresses could not be applied to the specimens because both the stiffness and capacity of the biaxial loading frame were too small to realize such stress states.

Each test was carried out at one or more of the following flow rates representing a thirty-two fold range in flow rates.

$$L = 4.01 \times 10^{-4} \text{ in}^3/\text{sec}$$

$$M = 1.60 \times 10^{-3}$$

$$H = 6.41 \times 10^{-3}$$

$$S1 = 1.28 \times 10^{-2} \text{ in}^3/\text{sec}$$

$$S2 = 3.62 \times 10^{-3}$$

$$S3 = 9.05 \times 10^{-4}$$

Finite element analyses were carried out on the experimental configuration to establish model results with which the experimental results could be

Table 3.2  
Experimental Conditions of the Series C

$P_x$ (psi)	$P_y/\cos^2 \beta$ (psi)				
	250	375	500	750	1000
250	C9		C5		
500	C8		C4	C3	C2
750		C7	C6	C10	
1000			C1		C11
1500				C12	C13



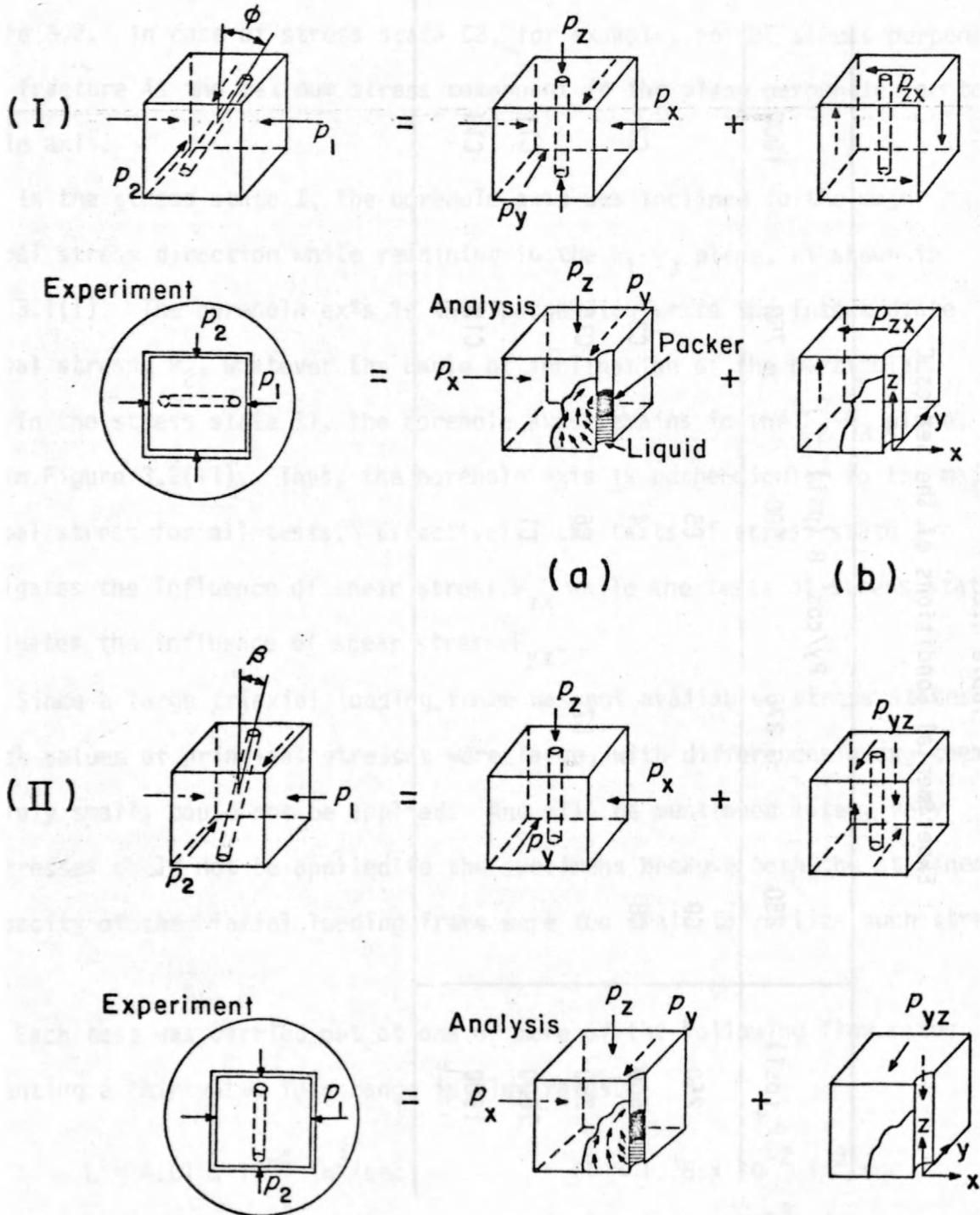


Figure 3.1 Description of analytical(a) and Experimental(a+b) stress state.

compared. In particular, the effect of shear stress components on the reopening pressure at stable flow rate could be assessed by comparing the numerical results for the triaxially compressed vertical borehole model, Figure 2(a), with experimental results of tests on biaxially compressed specimens containing inclined borehole Figure 2(a & b).

Table 3.1 shows the parameters of three series of experiments and the parameters of the corresponding analyses. As shown in the Table, seven analyses were performed.

#### 4.0 EXPERIMENTS

##### 4.1 Sample Preparation

Previous laboratory experiments on hydraulic fracturing were performed on relatively small samples. The present tests were performed in specimens of Charcoal Gray granite of  $14.5 \pm 0.25$  inches on a side and  $15.0 \pm 0.25$  inches on the height. Those specimens were produced in Cold Spring, Minnesota, the geologic name of the rock being St. Cloud Gray Granodiorites. The first specimen tested, however, was a 12 inch cube (Specimen Number 1).

A vertical or inclined borehole of one inch diameter was drilled in each specimen. The specimens were then cast in hydrostone to insure planeness and parallelism between opposite faces, by using a steel box mold of exactly 15 inch cube. A ratio of water to gypsum of 33/100 was adopted for hydrostone, giving a uniaxial compressive strength of about 10,000 psi. A completed specimen and the mold are shown in Figure 4.1.1.

##### 4.2 Equipment

Tests were performed under biaxial loading conditions in a specially

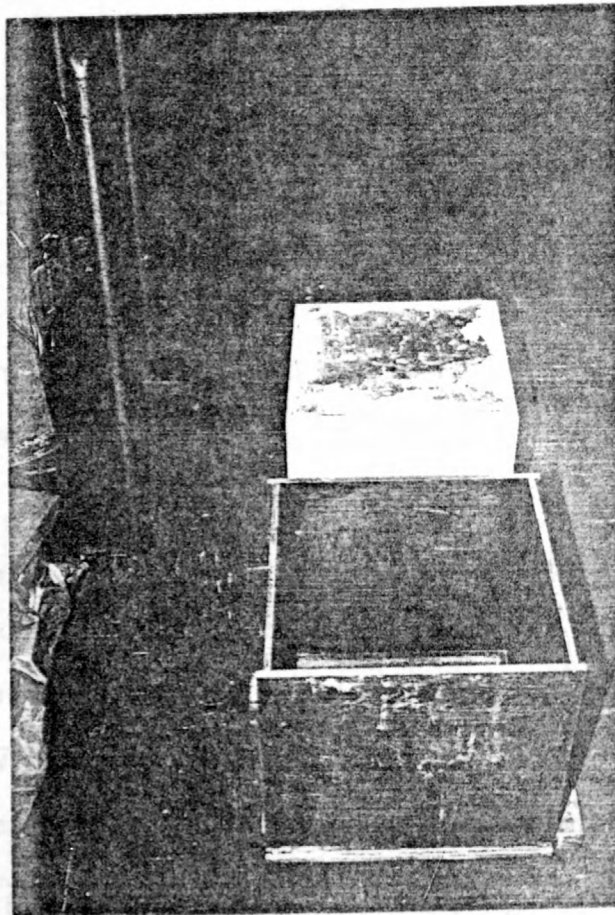


Figure 4.1.1 A specimen cast in hydrostone and the mold used for casting.

constructed loading frame capable of applying stresses of 2,500 psi to the specimens (Gronseth, 1979).

The equipment used in these experiments consisted of a miniature straddle packer (Figure 4.2.1, fully described by Roegiers, 1975), two types of pressurization system, a biaxial loading system and pressure monitoring and recording systems as shown in Figure 4.2.2. The borehole was pressurized for fracturing through the use of a 1.22 inch<sup>3</sup> displacement, 15,000 psi pressure generator. This pressure generator could be manually operated and was so used to covering out the initial hydraulic fracturing, with a metronome employed for timing. The manual pressurization system, the biaxial loading system and the pressure monitoring system are shown in Figure 4.2.3.

For reopening, however, a servo-controlled system capable of 0.769 inch<sup>3</sup> displacement and 3,000 psi were used. The hydraulic actuator and the linear variable differential transducer (LVDT) used for feedback are shown in Figure 4.2.4.

Light hydraulic oil (American industrial oil No. 32, formerly No. 15) was used as the fracturing fluid.

With the biaxial loading frame stainless steel flat jacks were employed to stress the rock specimens. Samples of up to 15 inches on a side could be accommodated. However, the stiffness of the loading frame was such that pressures greater than about 1,000 psi gave rise to displacements that were detrimental to the flat jacks. Loading values were, therefore, limited to 1,000 psi to preserve the flat jacks. The flat jack applying maximum principal stress tended to expand too much to survive the loading states in which the difference between the principal stresses was more than 1,000 psi. On the other hand, the flat jack applying minimum principal stress tended to close and was not able to maintain the given stress state because of contact of the insides of the flat jack. It is considered that stress state A was close to a critical



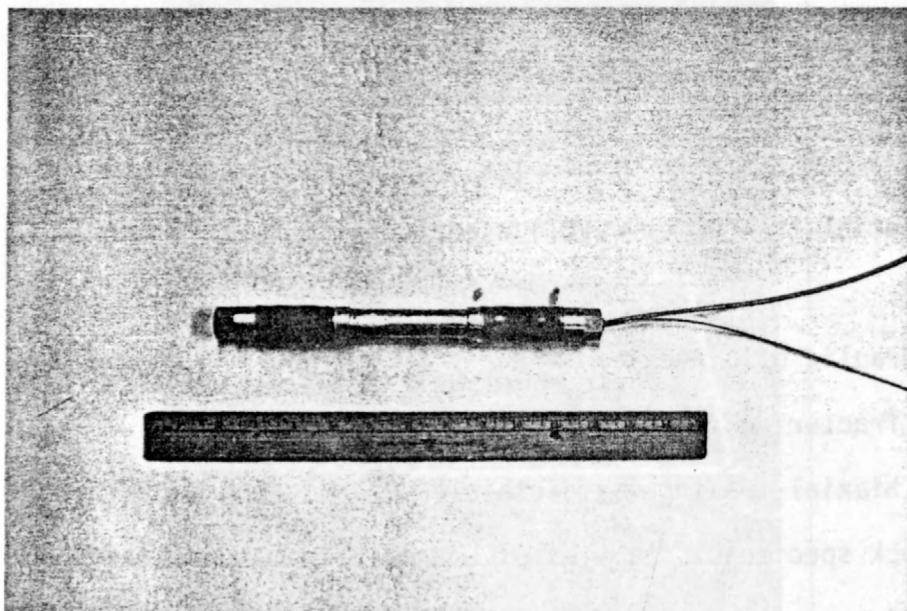


Figure 4.2.1 Miniature straddle packer.

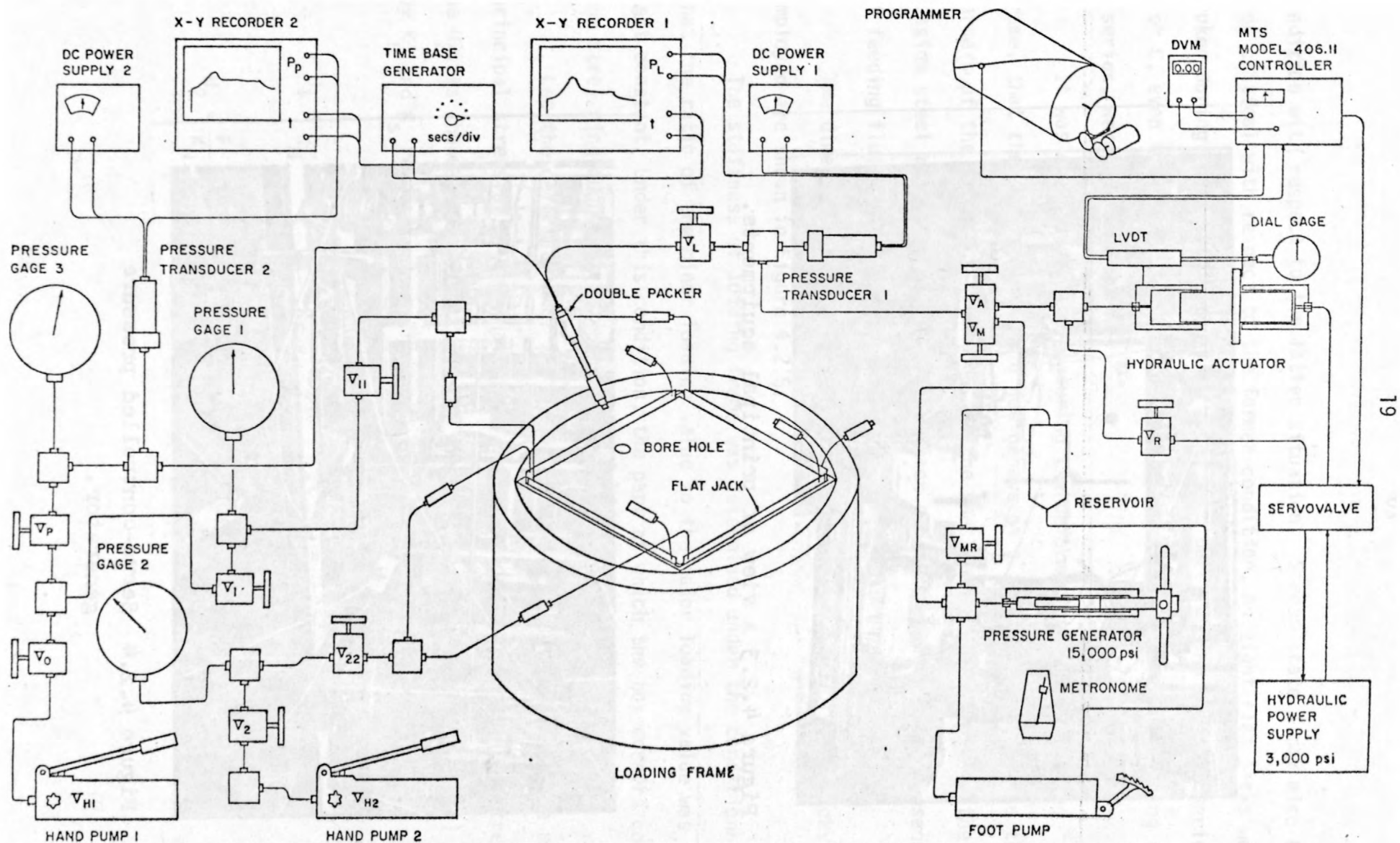


Figure 4.2.2 The outline of experimental equipment.

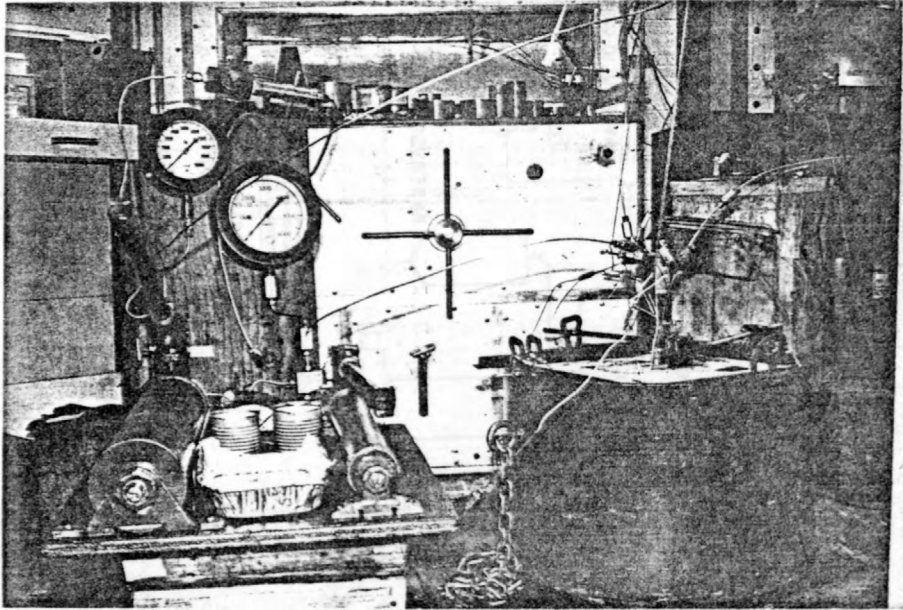


Figure 4.2.3 A view of principal equipments.

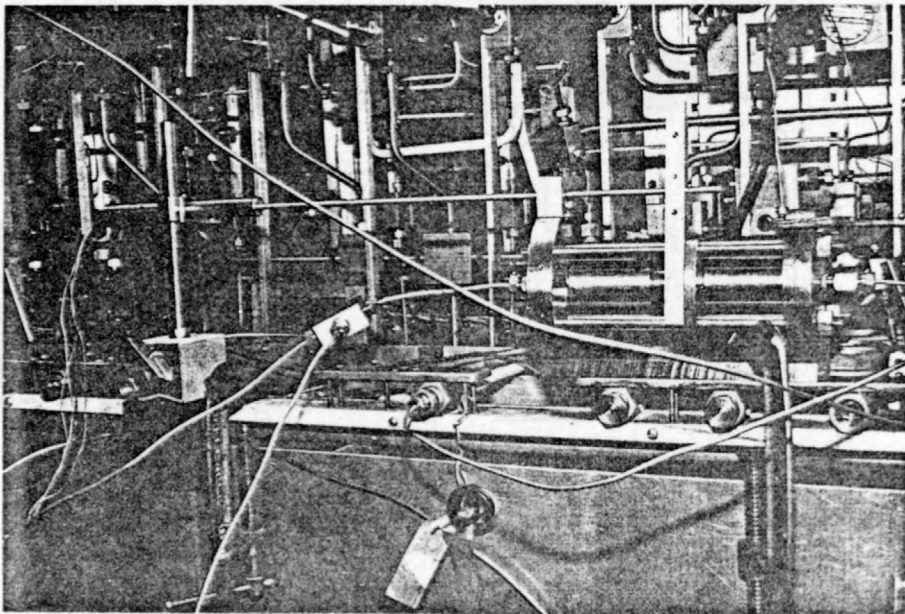


Figure 4.2.4 Servo-controlled pressure generator.

condition with respect to the latter situation. Stress state A may also have been critical with respect to the former condition, as eight flat jacks were broken during these tests. No flat jacks were burst during tests of series B or C, even though the 0.025 inch thick spacers, which were used during the A series, were not employed.

It was also proven, by measuring the deformations of the loading frame, that the loading frame did not behave as a single unit. Because the corners of the steel box accommodating the specimen are very close to the outside steel ring, the degree of flat jack expansion depended on the sequence of feeding fluid into the flat jacks.

The dimensions of the loading frame and the two kind of flat jacks employed are shown in Figure 4.2.5.

The stiffness of loading frame was determined under the condition that the ratio of the minor loading value to the major loading value was kept constant. Under this condition, the part at which the box corners contact the steel ring ought not to translate under increased loading.

Let the deformation of the loading frame in the direction of the major principal stress be  $U_1$  and that of in the direction of the principal stress be  $U_2$ , as shown in Figure 4.2.6. Let the stiffnesses in the case of (a) and (b) by  $K_n$  and  $K_s$  respectively. Then, the following equations are given:

$$U_1 = \frac{F}{K_n} \frac{\sigma_1 + \sigma_2}{2} + \frac{F}{K_s} \frac{\sigma_1 - \sigma_2}{2}, \quad K_n = \frac{F}{v} \frac{\sigma_1 + \sigma_2}{2}$$

$$U_2 = \frac{F}{K_n} \frac{\sigma_1 + \sigma_2}{2} + \frac{F}{K_s} \frac{\sigma_1 - \sigma_2}{2}, \quad K_s = \frac{F}{u} \frac{\sigma_1 - \sigma_2}{2}$$



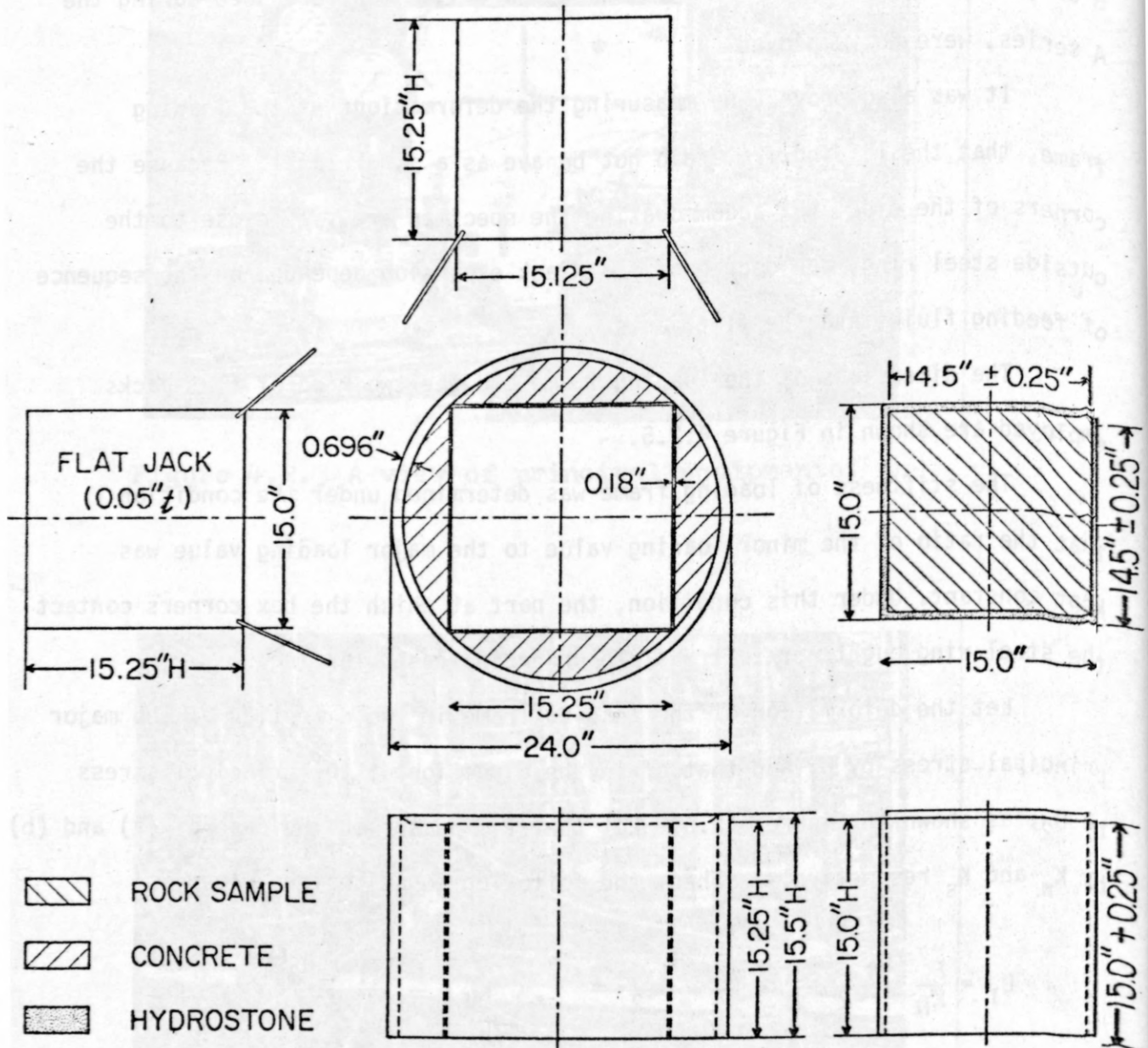


Figure 4.2.5 The dimensions of the loading frame and two kind of flat jacks.

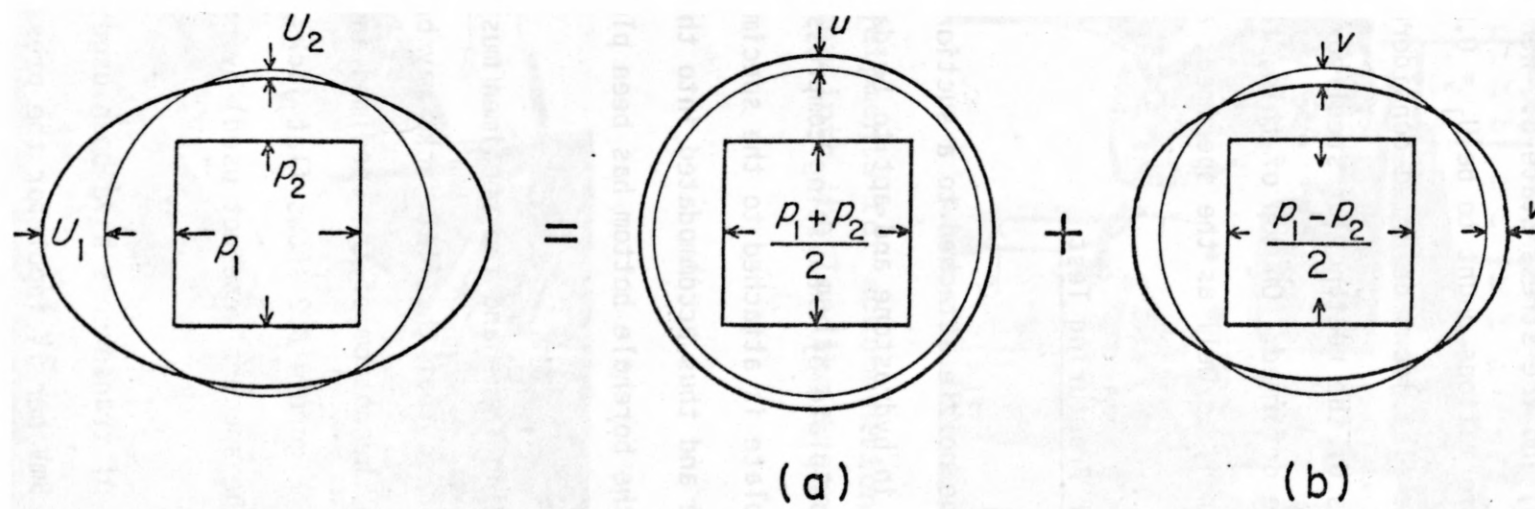


Figure 4.2.6 Deformations of loading frame.

The stiffnesses were found to be  $K_n = 2.4 \times 10^7$  psi and  $K_s = 2.0 \times 10^6$  psi from the difference of the deformations between the stress state ( $\sigma_1 = 600$ ,  $\sigma_2 = 500$ ) and the stress state B. Hence, if stress state A was applied, the deformations ought to be  $U_1 = 0.070$  inch and  $U_2 = 0.042$  inch. Actually, the flat jacks deformed considerably more because the points at which the corners of the rectangular steel box contact the outer ring moved as the loading frame deformed. On top of this, the concrete between the loading frame and the specimen, as well as the specimen, are deformed.

#### 4.3 Procedure for Fracturing Test

A venturi-type nozzle attached to a suction plate was employed to lift rock specimens cast in hydrostone and apt to be damaged. The nozzle produces vacuum at the suction plate by exhausting compressed air fed through a rubber hose. The suction plate is attached to the specimen which can be suspended from a removal crane and thus accommodated into the loading frame, as Figure 4.3.1 shows. Of course, the borehole bottom has been plugged by a rubber stopper to obtain the vacuum.

Both the loading frame and the specimen must be set up a quarter inch higher than the floor so that the flat jacks may be pushed down one eighth inch lower than both the bottom of the specimen and the loading frame (see Figure 4.2.5). Figure 4.3.2 shows flat jacks being pushed down for a test of stress state B (the spacers were not used) by pounding them with a rubber hammer.

The same type of transducers have been used for both pressure transducers 1 and 2. Output was 3mV per 1V input for the pressure of 100 percent of the capacity (10,000 psi). Hence, the pen sensitivity of the Y ranges of X-Y recorders are 4cm per 1,000 psi, because input voltages and range sensitivities

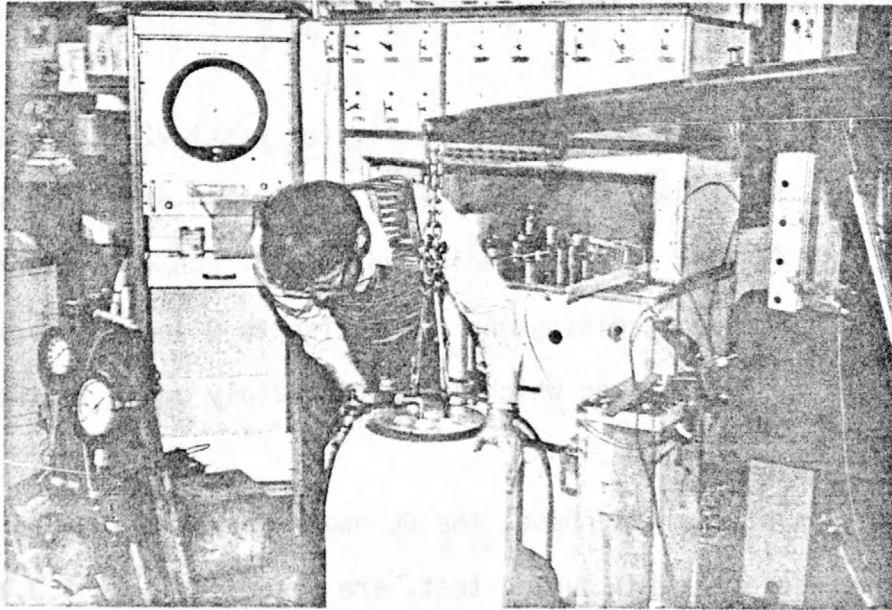


Figure 4.3.1 The equipments for accomodation of a specimen into the loading frame.

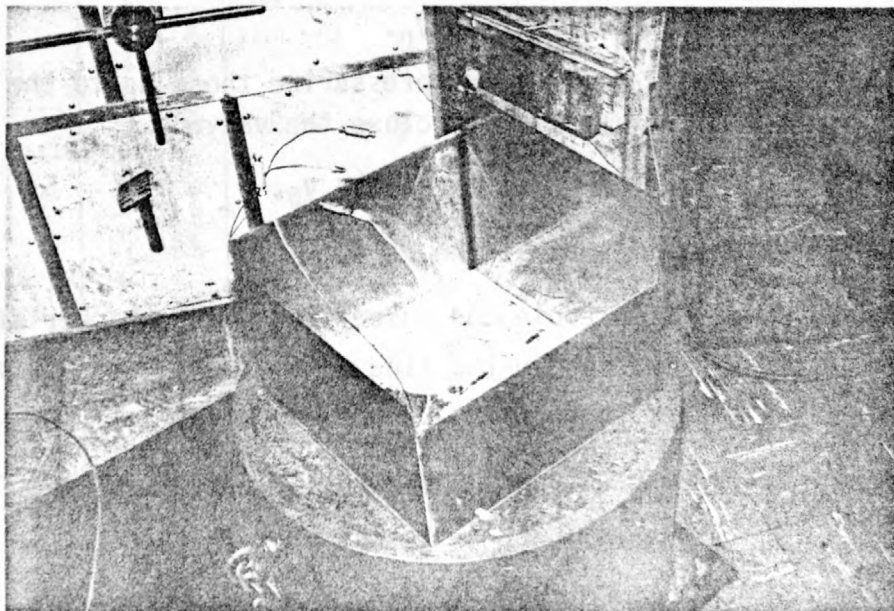


Figure 4.3.2 Appearance of the flat jacks being pushed down.



have been chosen to be 6.64 V and 0.5 mV/cm respectively. However, recording of packer pressure was not done except for several records during fracturing tests. Usually, the values of initial packer pressure and peak packer pressure were read from pressure gage 3.

The volume capacity of the pressure generator was  $1.22 \text{ inch}^3$  (20cc) and the total stroke length was 6 inches. Each revolution of the handle moves the piston  $1/13$ th of an inch so that feeding volume for one revolution is  $0.0145 \text{ inch}^3/\text{sec}$ . Hence, controlling one revolution to 9 seconds corresponds to a feed of  $1.61 \times 10^{-3} \text{ inch}^3/\text{sec}$  which is approximately equal to the flow rate M.

The parameters of the time base, the DC power supplies and the X-Y recorder, to be set before a fracturing test, are shown in Table 4.3.1.

The following procedures were followed during fracturing tests:

1. Completion of line connection to the flat jacks and the double packer.
  - a) Eliminate air bubbles in the lines.
  - b) Connect and complete the lines to the flat jacks and the double packer
  - c) Open the valves  $V_0$ ,  $V_1$ ,  $V_2$ ,  $V_{11}$ ,  $V_{22}$ , and  $V_L$ .
  - d) Close the valves  $V_{H1}$ ,  $V_{H2}$ , and  $V_p$ .
  - e) Feed fluid into flat jacks and pressurize those up to the directed principal stress values. Then close the valve  $V_2$ .
  - f) Close the valve  $V_1$  and open the valve  $V_p$ .
  - g) Open the valve  $V_M$  and close the valve  $V_{MR}$ .
  - h) Pour oil into the borehole and insert the double packer after eliminating air bubbles in the line going through the chamber between two packers by pumping up the foot pump.
  - i) Pressurize the line going through the inside of the packers up to certain value and close the valve  $V_p$ .

Table 4.3.1  
Equipment Parameter Settings

Flow Rate	Time Base (sec/mV)	DC Power Supply (V)	X - Y Recorder				Manual Control		Servo-Control		Controller	
			Time Range (mV/cm)	Pen (10 <sup>-2</sup> cm/sec)	Pressure Range (mV/cm)	Pen (10 <sup>-3</sup> cm/psi)	Pressure Generator (cnt./rev.)	Metronome (cnt./min.)	Programmer (Number of Teeth)		SPAN	CAL.FACTOR
L	50	6.64	2.5	0.8	0.5	4	36	60	16	64	520	610
M	10	6.64	2.5	4	0.5	4	9	60	48	48	520	610
H	2	6.64	2.5	20	0.5	4	4	108	64	16	520	610
S1	1	6.64	2.5	40	0.5	4	2	108	64	16	1000	778
S2	5	6.64	2.5	8	0.5	4	4	60				
S3	20	6.64	2.5	2	0.5	4	16	60				

## 2. Fracturing test

- a) Confirm the input voltages (6.64V) of the pressure transducers by using digital volt meter (DVM).
- b) Open the valve  $V_{MR}$  and wait until fluid pressure settle down to zero.
- c) Draw a zero pressure line on the chart of the X-Y recorder.
- d) Confirm the values of each range of the X-Y recorder and the time base.
- e) Feed fluid into the borehole by foot pump up to certain value (400 p
- f) Feed fluid into the borehole with constant increase of fluid volume by constantly revolving of the handle of the pressure generat
- g) Stop revolving of the handle (shut in) after ascertaining that the record is sufficient.

## 4.4 Procedure for Reopening Test

The controller (MTS, Model 406.11), the curve-following programmer (Research Incorporated, Model FGE5110) and a small actuator of our own making (Cornet, 1977) were employed for servo-control.

The fluid pressure in the chamber between two packers is induced by the servo-controlled actuator feeding fluid into the chamber at a constant volume flow rate. This volume is measured through the displacements of a rigid piston. The displacements are transmitted as feedback to the controller through a linear variable differential transducer (LVDT). The programmer transmits the voltages to the controller to set the position of the piston.

Maximum piston travel for reopening test has been set at 0.868 inch, with the cylinder diameter 1.062 inch, the volume capacity of the actuator is  $0.769 \text{ inch}^3$  (12.64 cc). The LVDT output was to be zero at the start point and 5.26V at the end point to correspond with the programmer. Values of

SPAN and CALIBRATION FACTOR on the MTS 406 controller to achieve this were 520 and 610 respectively. However, for a test using the flow rate S1, these values were set to 1,000 and 778 respectively. In this latter condition, when the pen of programmer reached the midpoint, the piston of the actuator was at the end point. Hence, running of the programmer had to be stopped when the LVDT output showed the value of 5.26V for the case of the flow rate S1.

The following procedures were followed during reopening test.

1. Before reopening test

- a) Connect the DVM to the controller to ascertain the position of the actuator.
- b) Remove fluid from packers as the pressure settle down to certain value by opening the valve  $V_P$  a little. Then close the valve.
- c) Open the valve  $V_R$  and close the valves  $A_A$  and  $V_M$ .
- d) Turn on the hydraulic power supply and adjust the SET POINT (646) for the DVM reading of 0.00V, then power off.
- e) Remove fluid from the chamber between the packers as the pressure settle down to certain value by opening the valves  $V_M$  and  $V_{MR}$ . Then close the valves.

2. Reopening test.

- a) Close the valve  $V_R$  and open the valve  $V_A$ .
- b) Circulate the cooling water.
- c) Confirm the sensitivity and change it if necessary.
- d) Turn on the hydraulic power supply. Run the programmer and the time base.
- e) When the pen of programmer close to the ending point, close the valve  $V_A$  (shut in), open the valve  $V_R$  and turn off the hydraulic power supply quickly in sequence while the programmer goes on.
- f) Stop the pen of programmer when it returns to starting point.



3. In the midst of recording, after shut in.
  - a) Turn the SET POINT and adjust the reading of the controller to zero, which shows the difference of voltage between command and feedback.
  - b) Turn on the hydraulic power supply. Turn back the SET POINT (646) gradually for the DVM reading of 0.00V.
  - c) If necessary in the midst of recording following shut in, turn back the pen of X-Y recorder (up the pen, return the time base, down the pen and run the time base). Figure 4.4.1 shows that this operation was done and the recording has reached final stage.
4. After reopening test
  - a) Open the valves  $V_P$  and  $V_{M1}$  as pressure goes down to zero.
  - b) Open the valves  $V_1$ ,  $V_2$  and  $V_{M2}$  as flat jack pressured go down to zero.
  - c) Disconnect the lines of flat jack.
  - d) Take out the specimen from the loading frame by using a hydraulic jack. Figure 4.4.2 shows this operation being done part way.
  - e) Move away the specimen and settle again the loading frame.

#### 4.5 Results

All of the experimental configurations for fracturing and reopening tests are shown in detail in Table 4.5.1. The breakdown pressure and steady flow pressures obtained from reopening tests are also shown in the table. Twenty five fracturing tests and 137 reopening tests were carried out. The fracturing tests in which stress state A was applied were mostly fractured by using flow rate H, as well as employing relatively high initial packer pressures.

All of the pressure-time records from these tests are shown in Figure 4.5.1. The coded titles in the figures indicate the following:

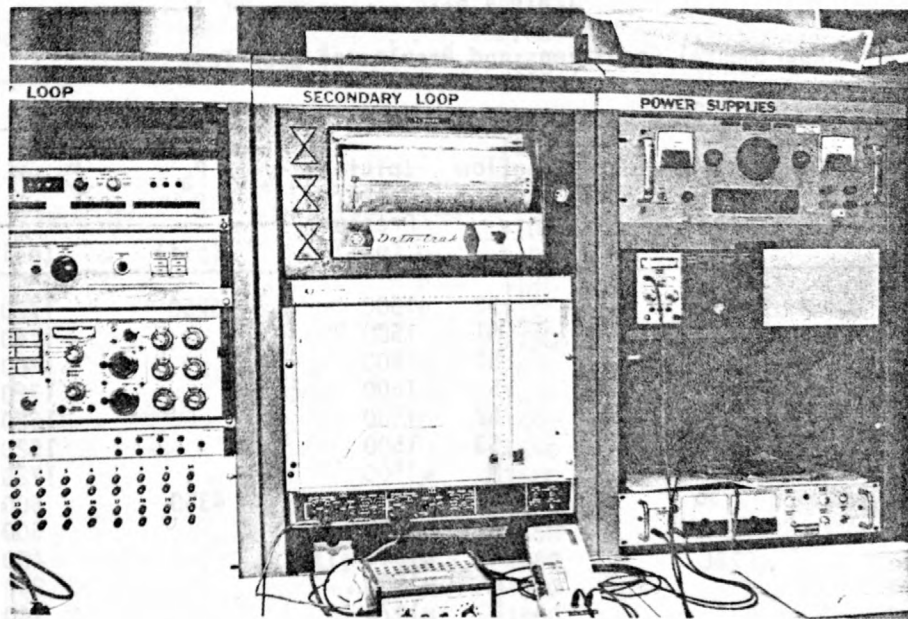


Figure 4.4.1 Servo-control system and recording system.

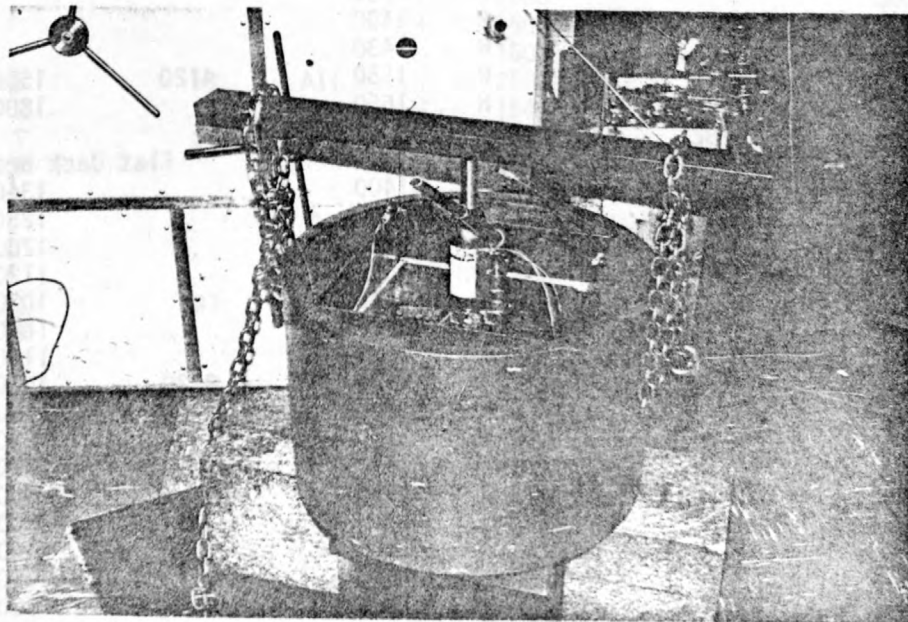


Figure 4.4.2 The equipments taking out the specimen from loading frame.

Table 4.5.1

Experimental Conditions and Results of Each Test

Block No.	Run No.	Fracturing or Reopening	Angle (°)	Stress State	Flow Rate	Initial Packer Pressure (psi)	P <sub>b</sub> (psi)	P <sub>t</sub> or P <sub>f</sub> (psi)	Note
1	1	F	0	A	S2	1500	3750	1720	12" cube
	2	R		A	S1	1500		1740	
	3			A	S2	1500		1700	
	4			B	S1	1500		1720	
	5			B	S2	1500		1620	
	6			A	S3	1500		1520	
	7			A	M	1500		1720	
2	1	F	36	AI	S1	1500	4350	600	
	2	R			S1	1460		500	
	3				H	1520		400	
	4				M	1500		240	
	5				L	1470		140	
	6				S1	820		350	
	7				H	500		300	
	8				M	510		170	
	9				L	500		40	
3	1	F	0	A	L	1750	3920		no fracture pkr. broken
	2	F			L	1750			
	3	F			M	2350		1620,900	
	4	R			M	1500			
	5				M	1700			
	6				M	1400			
	7				H	1430			
4	1	F	9	AI	H	1550	4120	1580	pkr. broken (unloaded)
	2	R			H	1650		1800	
	3								
	4								
	5				H	1400		1340	
	6				H	1500		1260	
	7				H	1540		1200	
	8				M	1500		1120	
	9				M	1550		1020	
	10				M	1420		1080	
	11				H	1520		1100	
5	1	F	18	AI	H	2500	3320	1000	
	2	R			H	1580		1000	
	3				H	1500		880	
	4				H	1550		780	
	5				M	1500		500	
	6				M	1430		500	
	7				M	1510		500	
	8				L	1470		460	
	9				H	1420		520	

Table 4.5.1 continued, page 2

Block No.	Run No.	Fracturing or Reopening	Angle (°)	Stress State	Flow Rate	Initial Packer Pressure (psi)	P <sub>b</sub> (psi)	P <sub>t</sub> or P <sub>f</sub> (psi)	Note
6	10			S1		1520		500	
	11			S1		1500		440	
	1	F	27	AII	H	2550	3370	760	
	2	R			M	1100		600	
	3				L	1100		280	
	4				H	1180		700	
7	5				M	1140		520	
	6				L	1150		280	
	1	F	0	A	H	2670	3750		
	2	R			M	1600		640	
	3				L	1600		500	
	4				H	1560		650	
8	5				M	1580		480	
	6				L	1560		340	
	7				M	1560		460	
	1	F	27	AII	H	2650	3490	740	
	2	R			M	1560		540	
	3				M	1600		520	
9	4				L	1550		360	
	5				H	1500		640	
	6				M	1500		440	
	7				L	1500		240	
	8				H	1450		620	
	1	F	9	AII	H	2600	3640		
10	2	R			M	1550		1000	
	3				L	1500		940	
	4				H	1500		500	
	5				M	1500		180	
	6				L	1500		80	
	1	F	18	AII	H	2500	3400		
11	2	R			M	1540		940	
	1	F	0	A	H	2560	3850		
	2	R			M	1550			
	3				M	1570		1520	
	4				L	1550			
	5				L	1520		1320	
12	6				L	1450			Put in die
	1	F	27	AI	H	2480	3920		
	2	R		B	M	1560		620	
	3			B	L	1400		380	
	1	F	36	AII	H	1630	3700		
	2	R			M	640		750	
13	3				M	720		750	
	4				L	730		600	
	1	F	0	B	M	1500	3080	1620	
	2	R			M	750		1700	
	3				M	570		1700	
	4				L	750		1450	
14	5				H	830		1700	
	6				M	750		1570	



Table 4.5.1 continued, page 3

Block No.	Run No.	Fracturing or Reopening	Angle (°)	Stress State	Flow Rate	Initial Packer Pressure (psi)	P <sub>b</sub> (psi)	P <sub>t</sub> or P <sub>f</sub> (psi)	Note
15	7				L	750		1420	
	1	F	18	BI	M	1500	3720	1500	
	2	R			M	640		1720	
	3				L	800		1650	
16	4				L	670		1650	
	1	F	36	BI	M	1550	3360	620	
	2	R			M	500		600	
	3				L	530		480	
17	1	F	9	BI	M	1600	2950	1750	
	2	R			M	650		1750	
	3				L	630		1550	
	4			BII	M	640			
18	1	F	27	BI	M	1640	3120	390	
	2	R			M	680		370	
	3				L	750		240	
	4	F	9	BII	M	1520	3670		o-ring pused out
19	2	R			M	600			" "
	3				M	800			" "
	4				M	800			" "
	5				M	780		1680	" "
20	6				M	1470		680	reloading
	7				M	740		470	
	1	F	18	BII	M	1520	3180	750	
	2	R			M	900		1000	
21	3				L	650		810	
	1	F	36	BII	M	1550	2910	530	
	2	R			M	700		400	
	3				L	780		370	
22	1	F	27	BII	M	1550	2730	590	
	2	R			M	760		630	
	3				L	670		480	
	4	F	0	C1	H	1300	2170		
23	2	R			M	400		1040	
	3				M	400		1000	
	4			C2	M	400		1500	
	5			C3	M	400		1250	
	6			C4	M	400		880	
	7				M	400		900	
	8			C5	M	400		910	
	9			C6	M	400		920	
	10			C7	M	400		790	
	11			C8	M	400		660	
	12			C9	M	400		690	
	13			C10	M	400		1160	
	14			C11	M	400		1420	
	15			C12	M	400		1190	
	16			C13	M	400		1400	

Table 4.5.1 continued, page 4

Block No.	Run No.	Fracturing or Reopening	Angle (°)	Stress State	Flow Rate	Initial Packer Pressure (psi)	P <sub>b</sub> (psi)	P <sub>t</sub> or P <sub>f</sub> (psi)	Note
24	1	F R	18	C	H	1700	2400	1120	
	2				M	670		920	
	3				M	700		990	
	4				C6	690		980	
	5				C7	620		860	
	6				C4	620		940	
	7				C8	600		710	
	8				C9	600		690	
	9				C5	680		960	
	10				C3	680		1220	
	11				C10	600		1230	
	12				C2	580		1470	
	13				C11	560		1500	
	14				C12	680		1250	
	15				C13	620		1430	
25	1	F R	18	C	H	1690	2820	1030	
	2				M	680		830	
	3				C6	700		810	
	4				C4	710		820	
	5				C5	520		940	
	6				C5	500		920	
	7				C9	430		680	
	8				C8	500		650	
	9				C7	400		710	
	10				C3	440		1010	
	11				C10	570		1000	
	12				C2	500		1250	
	13				C11	440		1250	

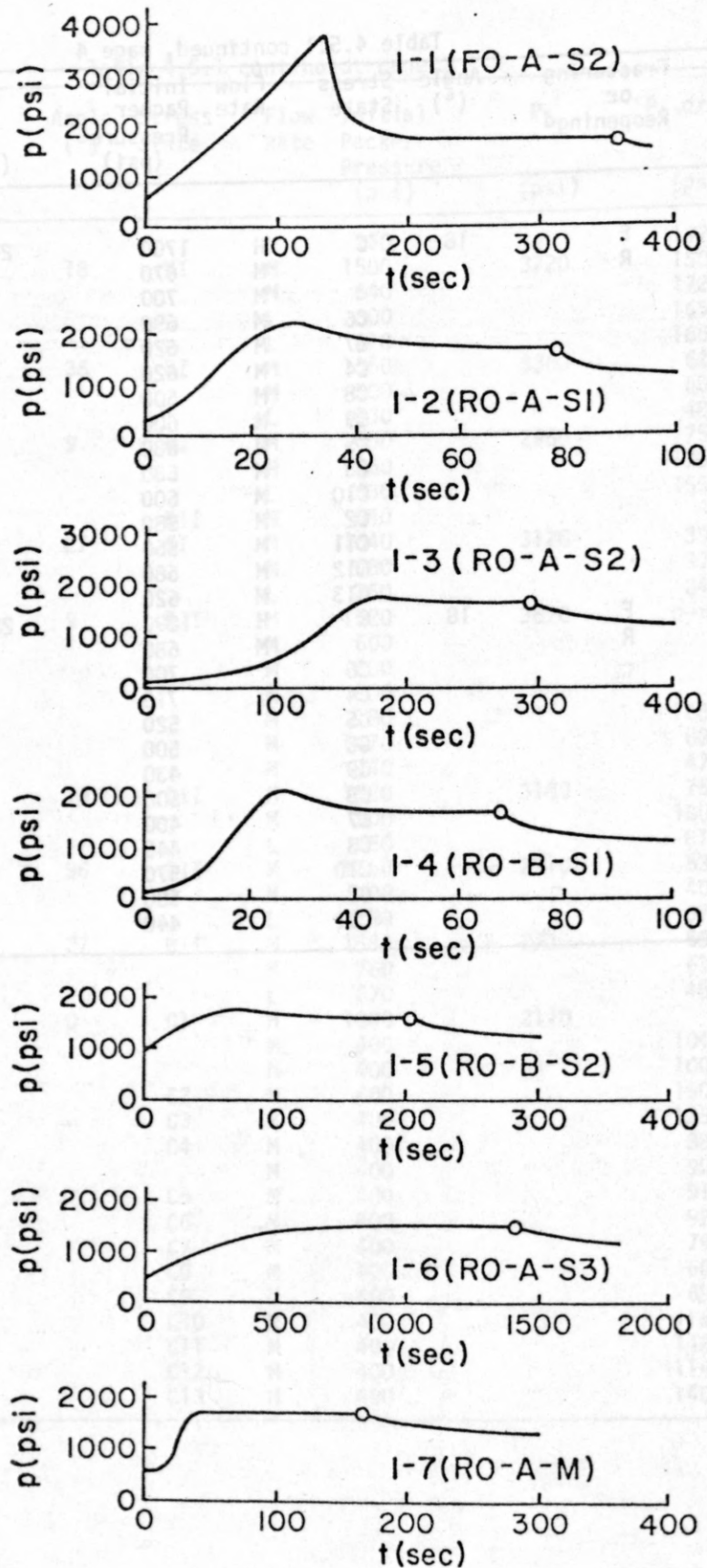


Figure 4.5.1 (1) The pressure-time record of specimen No.1

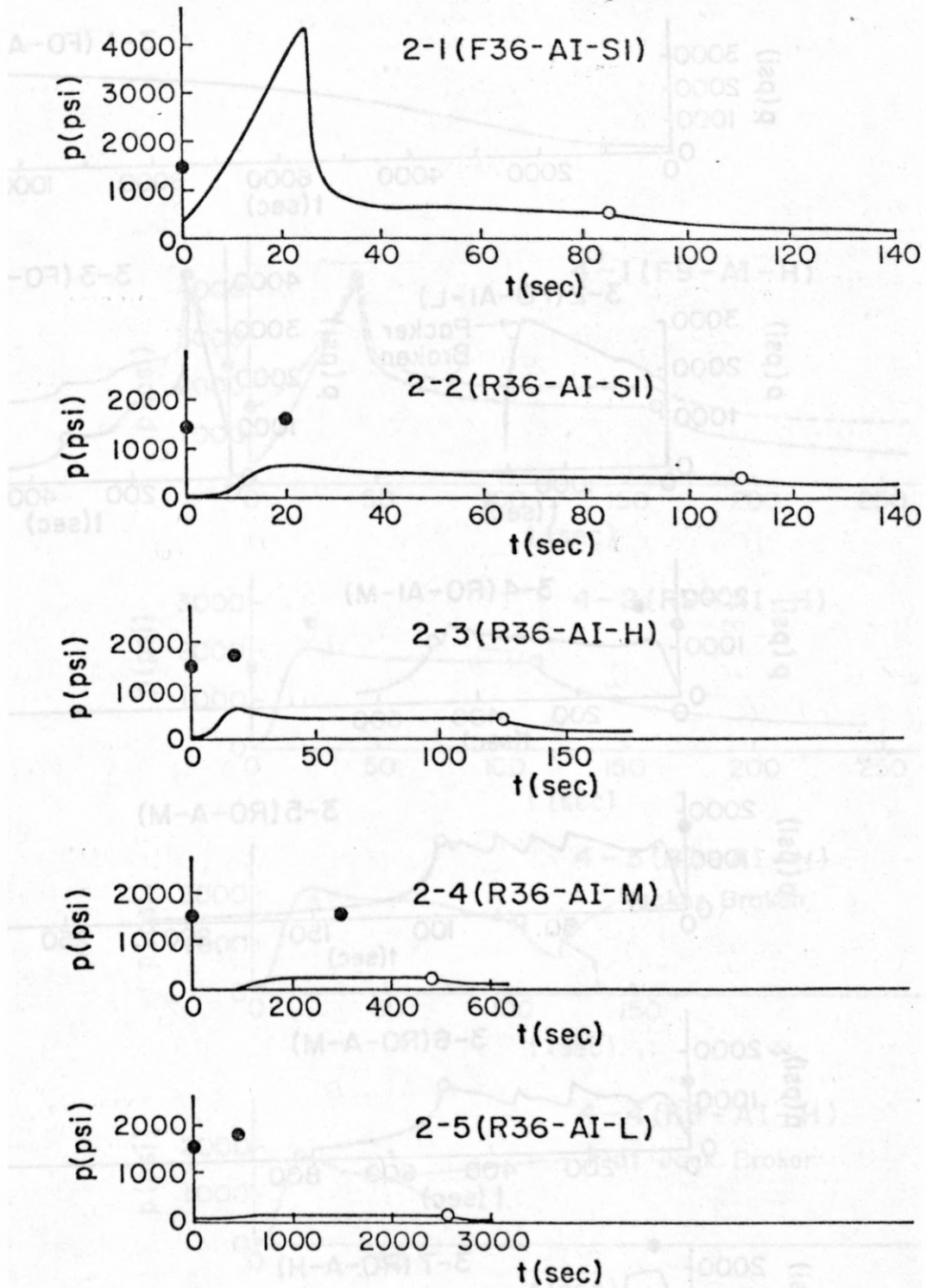


Figure 4.5.1 (2) The pressure-time record of specimen No.2



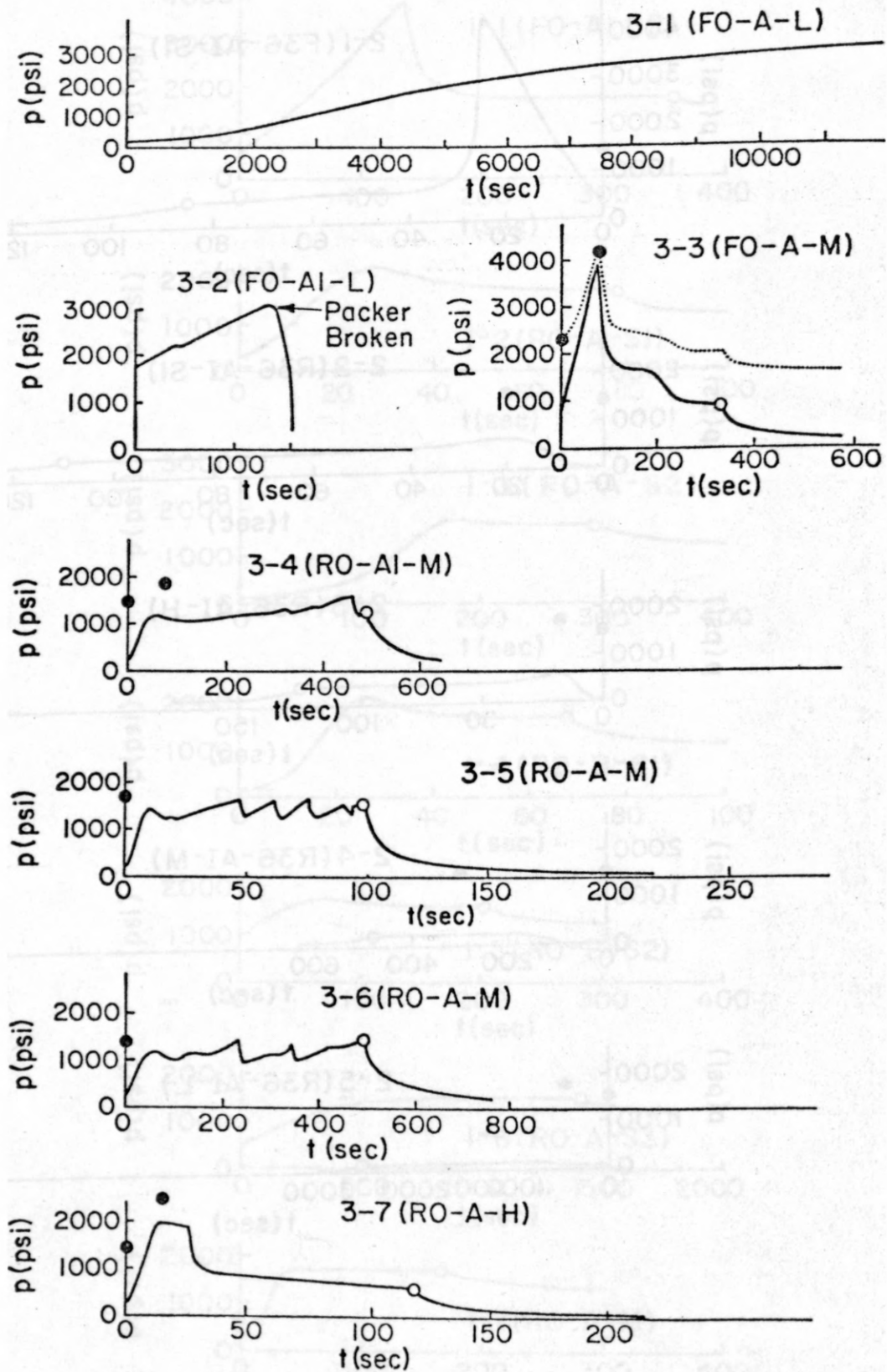


Figure 4.5.1 (3) The pressure-time record of specimen No.3

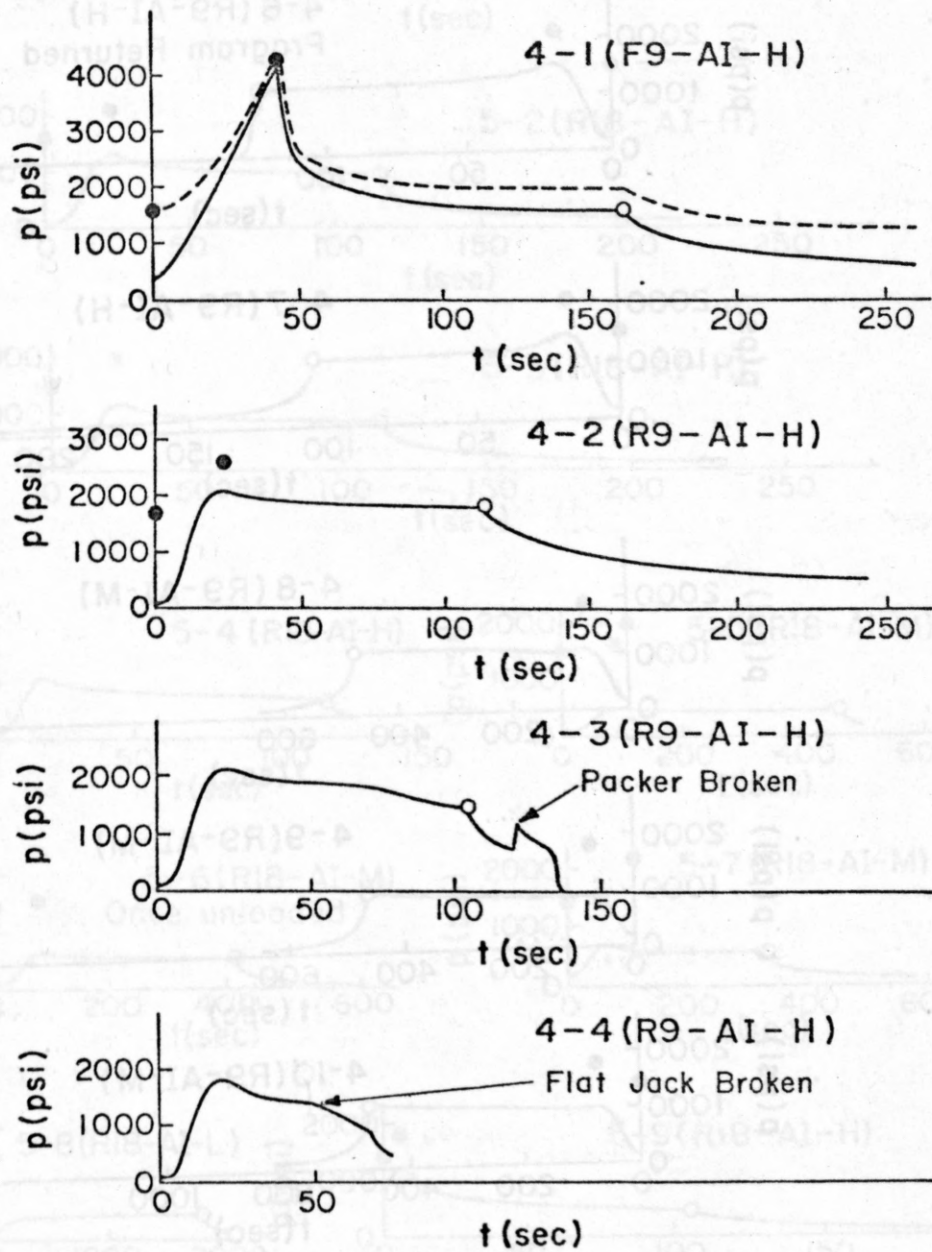


Figure 4.5.1 (4) The pressure-time record of specimen No.4 (continued)

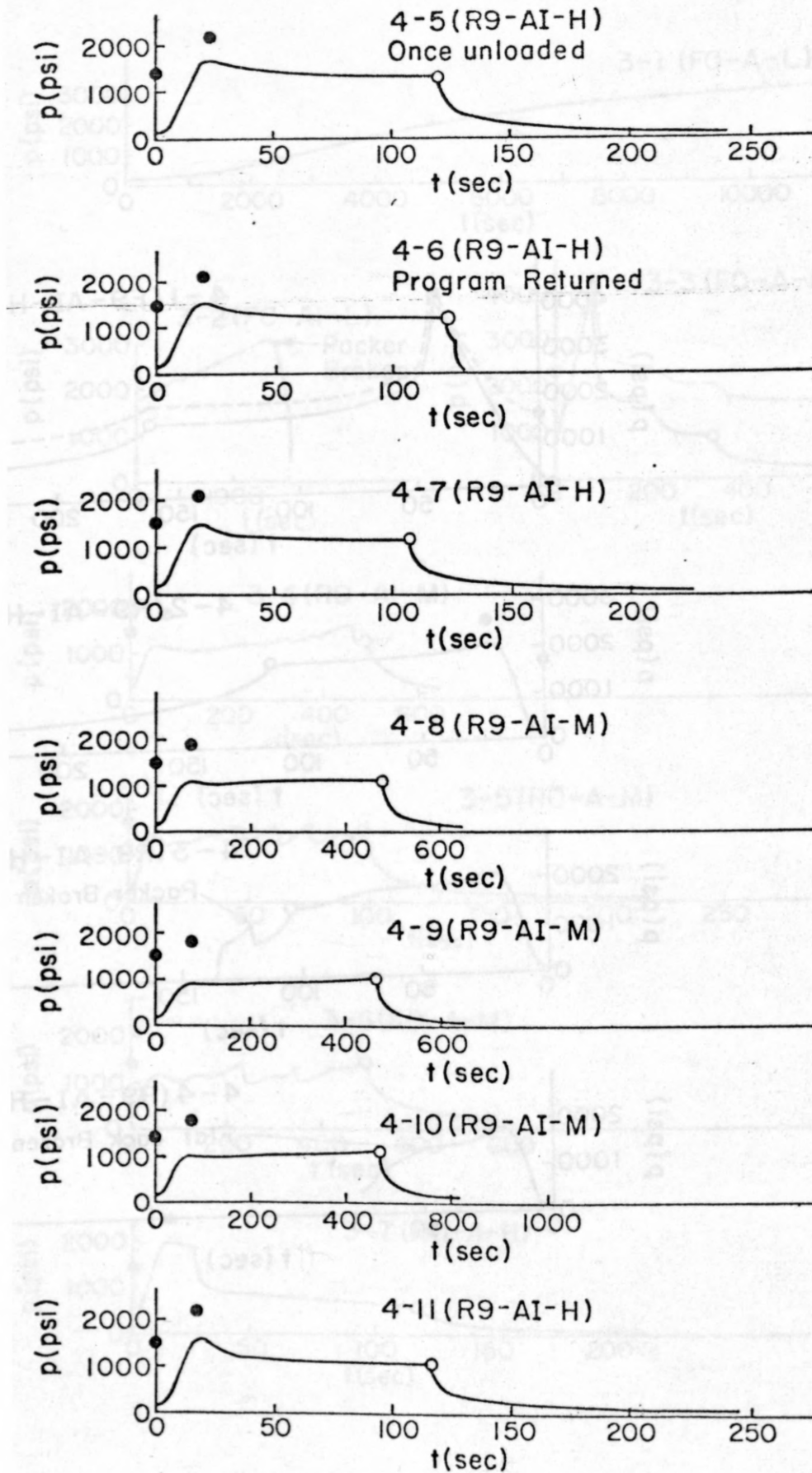


Figure 4.5.1 (4) (continued)

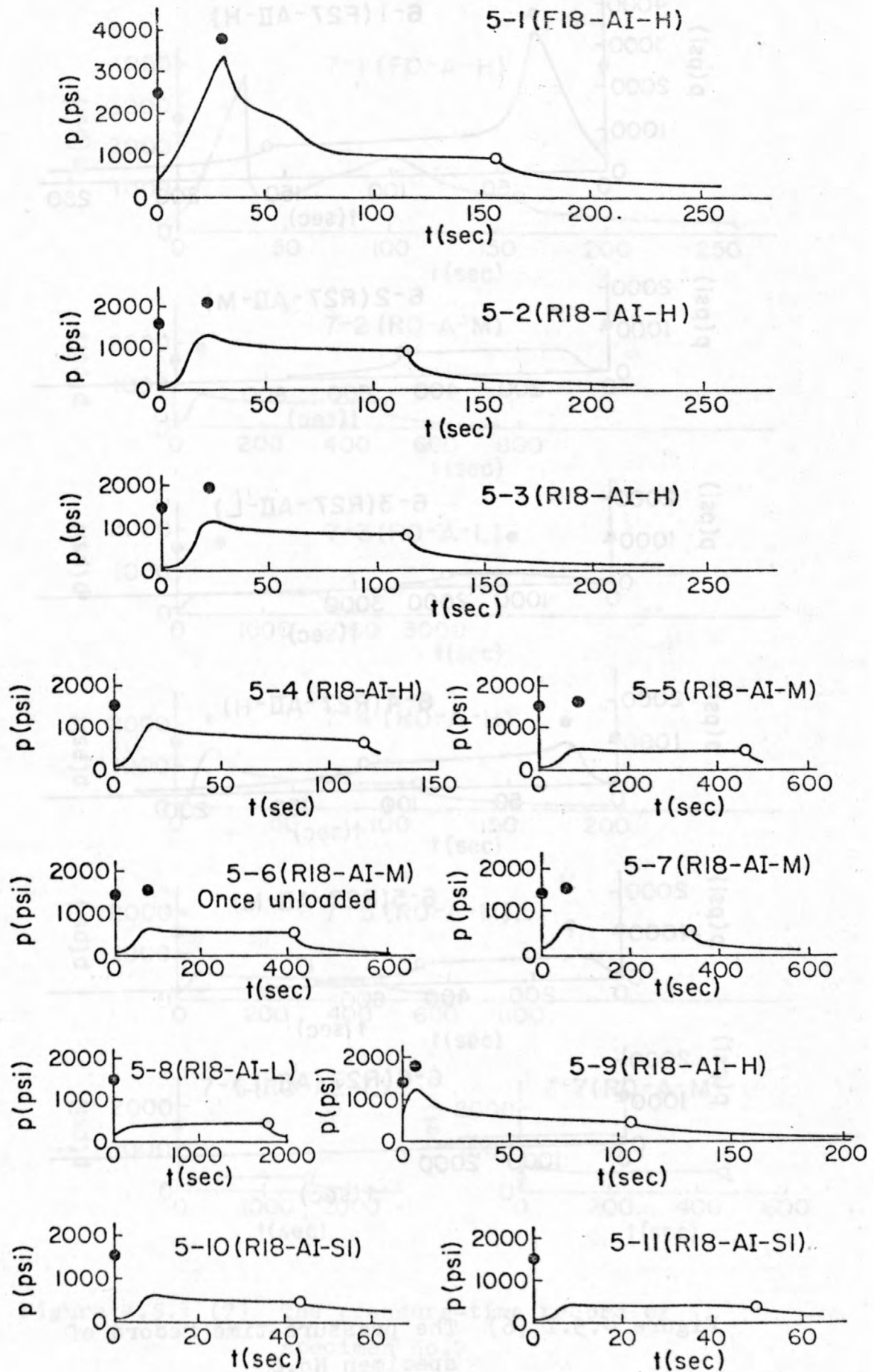


Figure 4.5.1 (5) The pressure-time record of specimen No.5



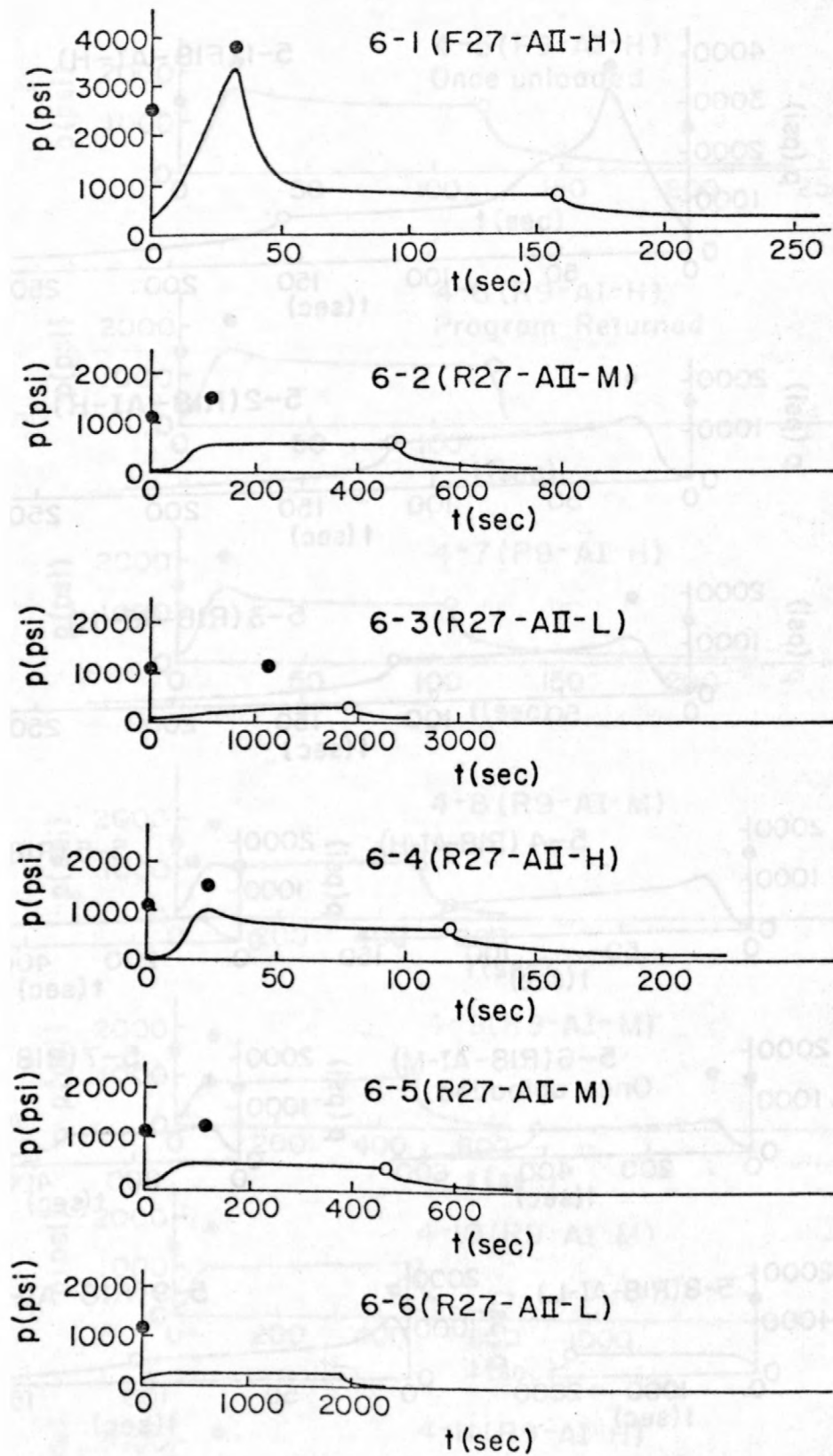


Figure 4.5.1 (6) The pressure-time record of specimen No.6

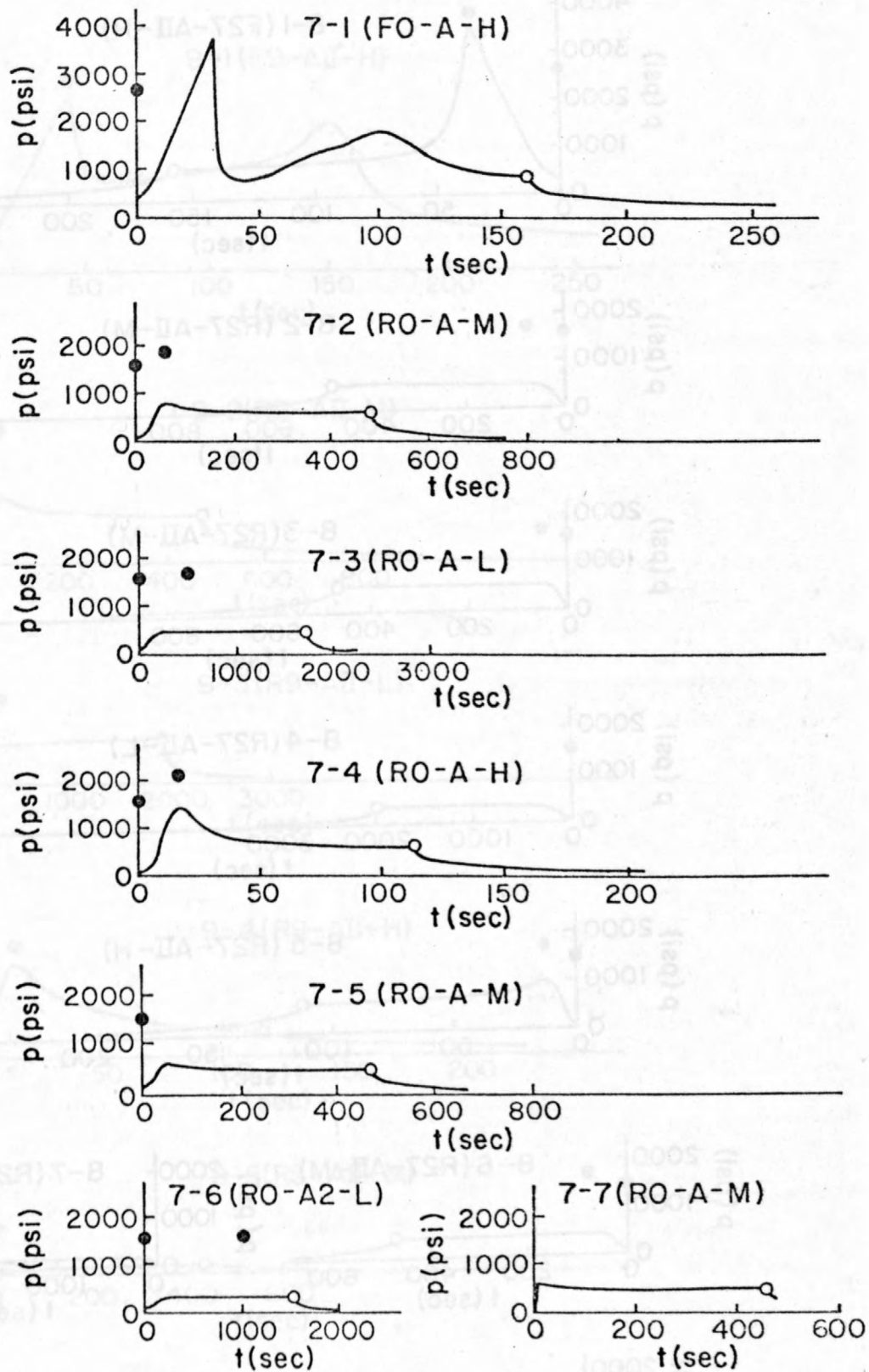


Figure 4.5.1 (7) The pressure-time record of specimen No.7

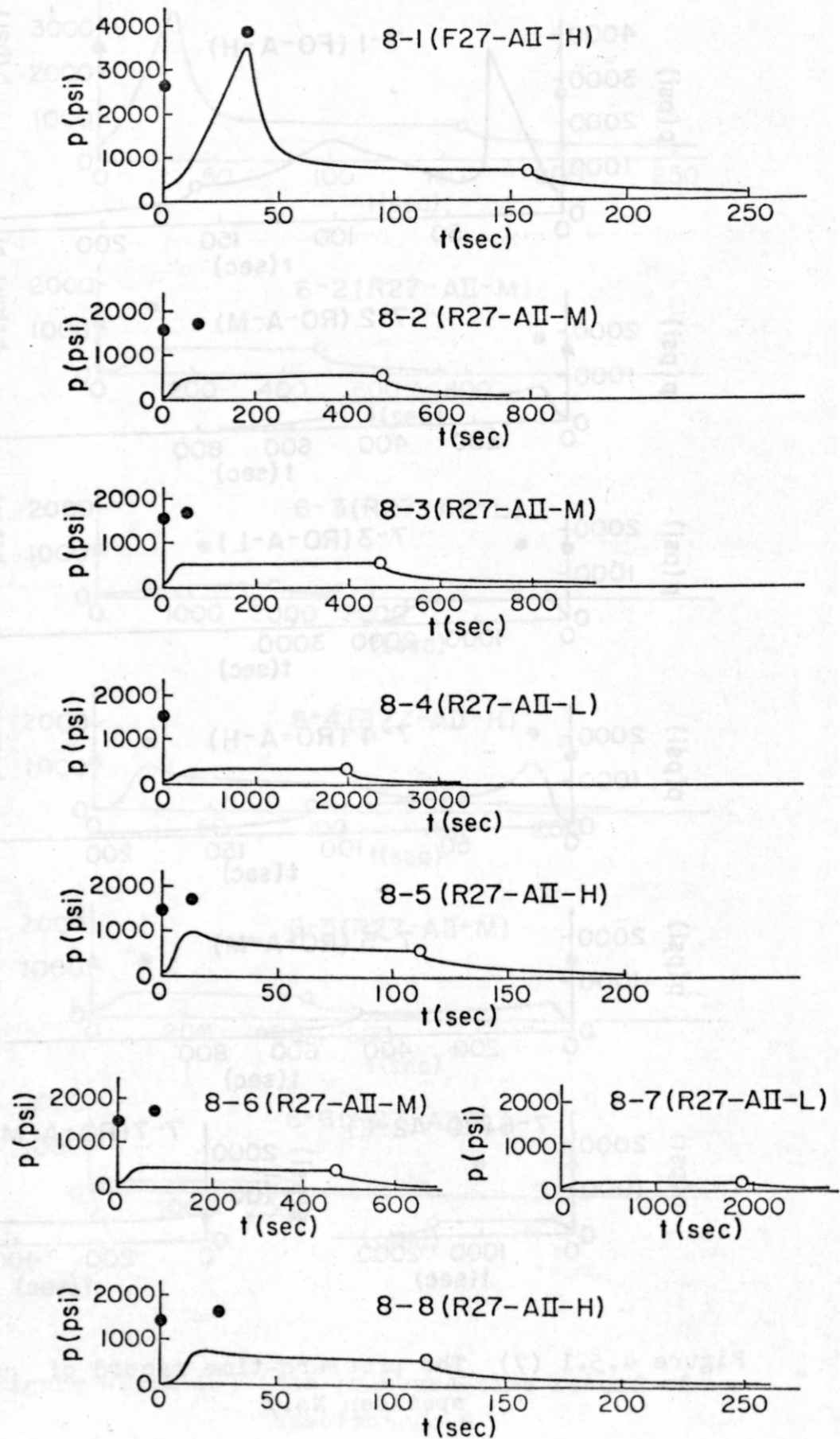


Figure 4.5.1 (8) The pressure-time record of specimen No.8

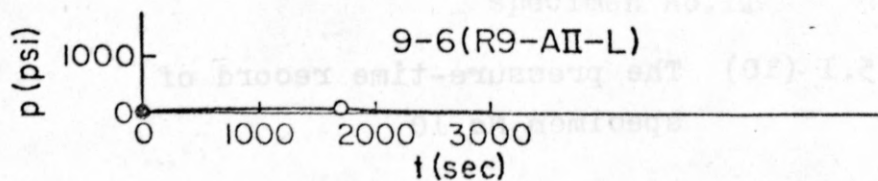
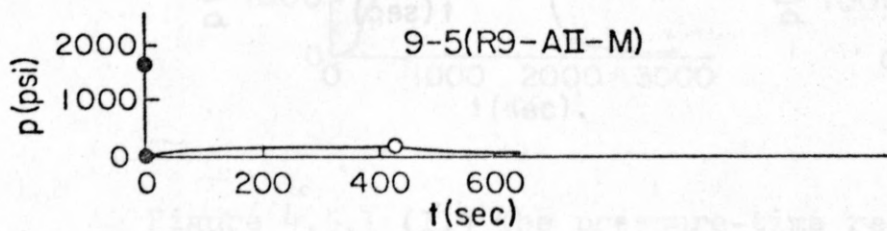
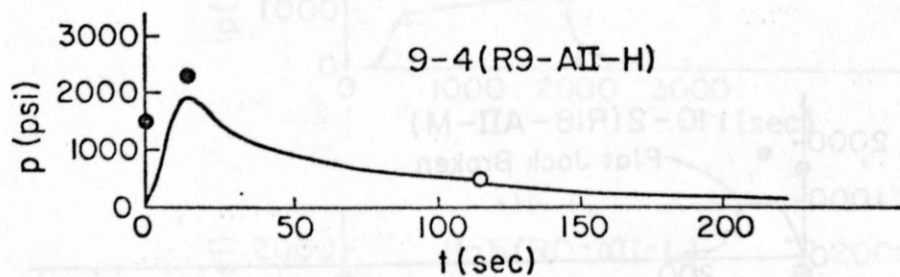
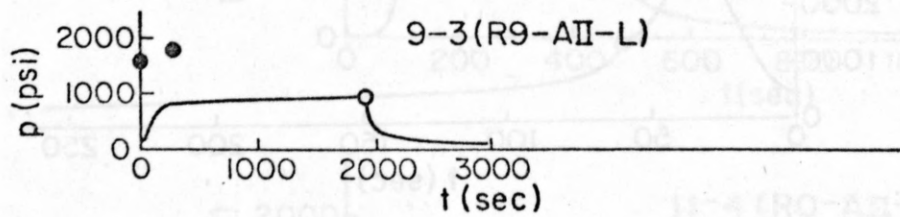
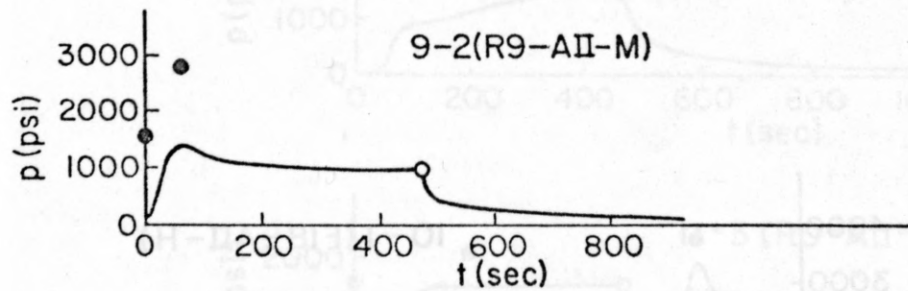
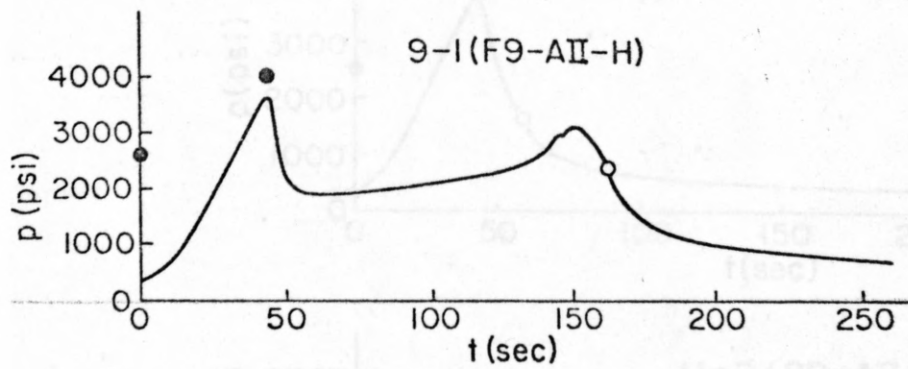


Figure 4.5.1 (9) The pressure-time record of specimen No.9



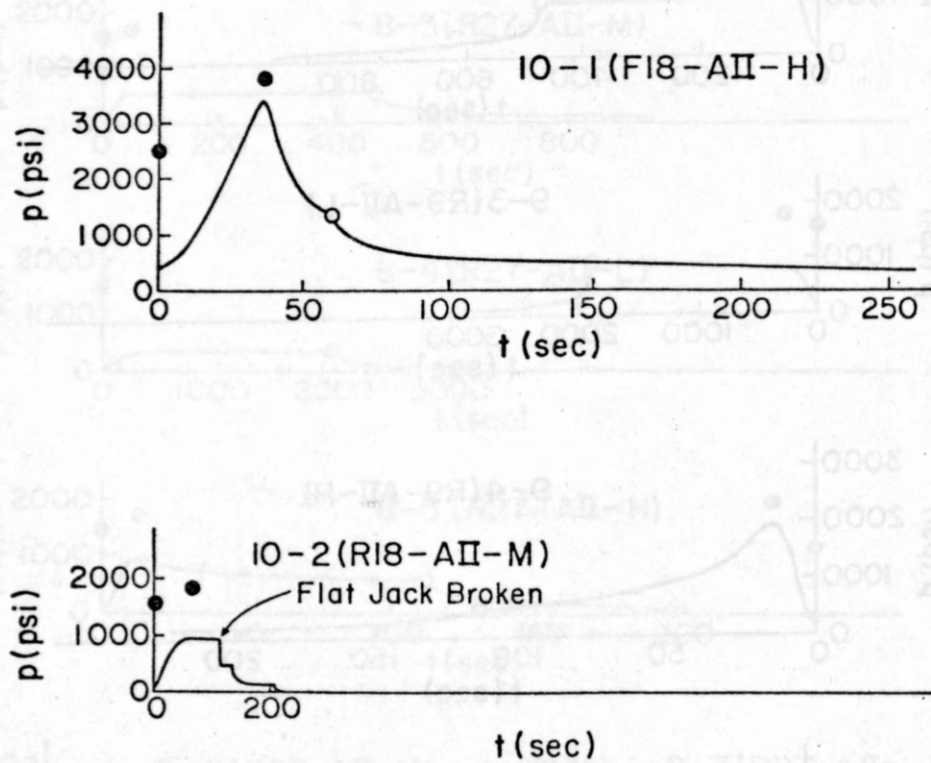


Figure 4.5.1 (10) The pressure-time record of specimen No.10

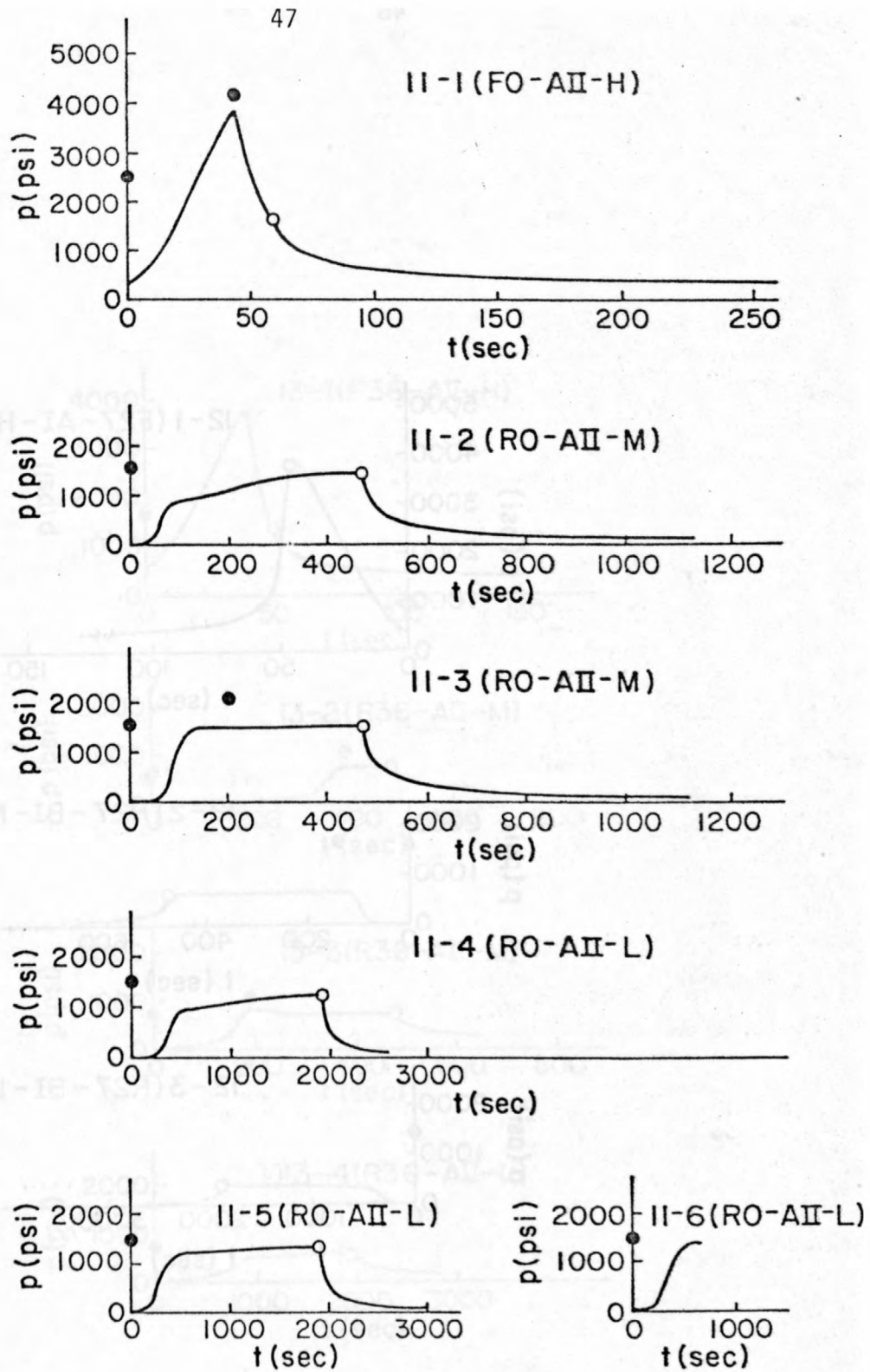


Figure 4.5.1 (11) The pressure-time record of specimen No.11

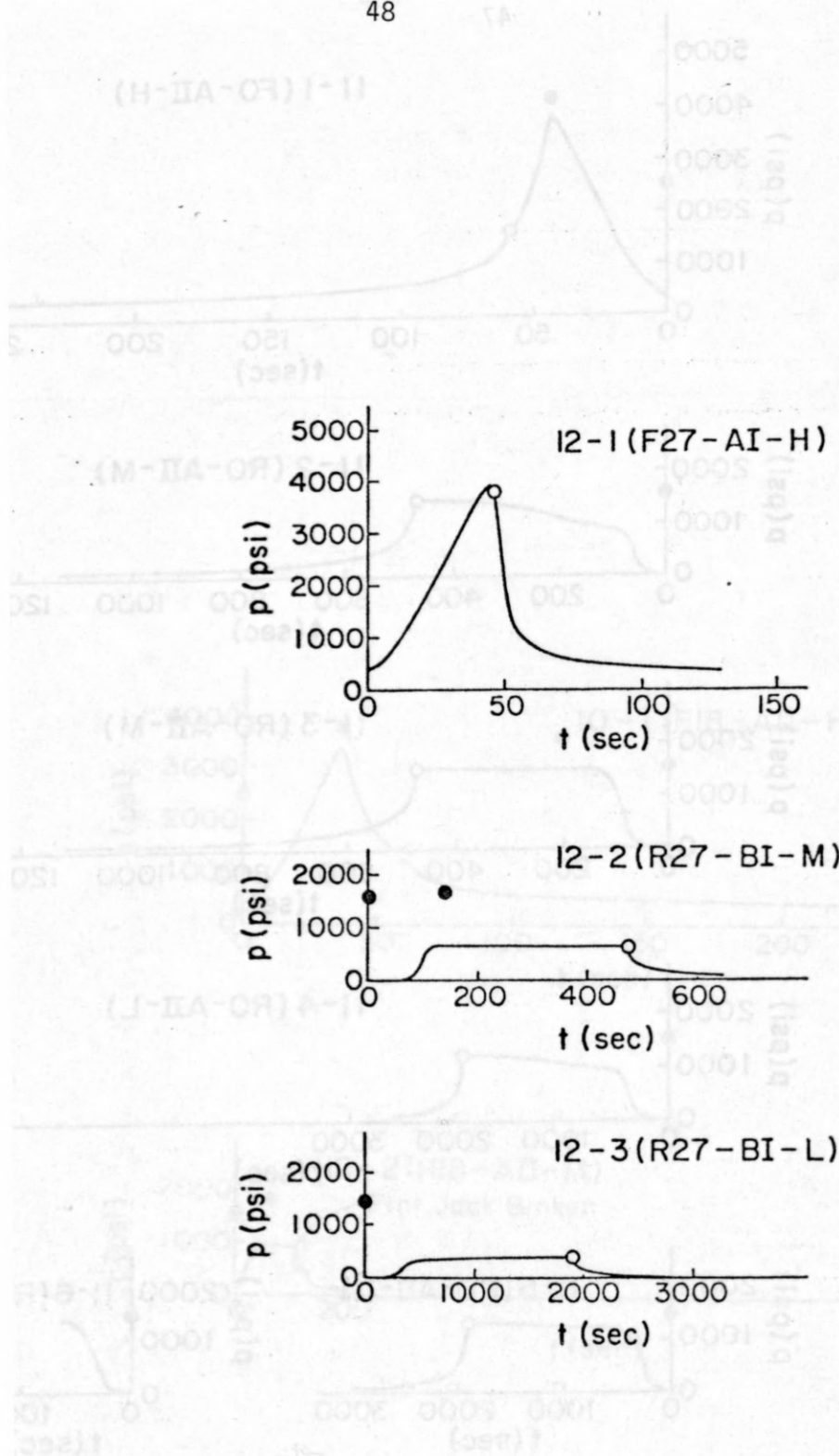


Figure 4.5.1 (12) The pressure-time record of specimen No.12

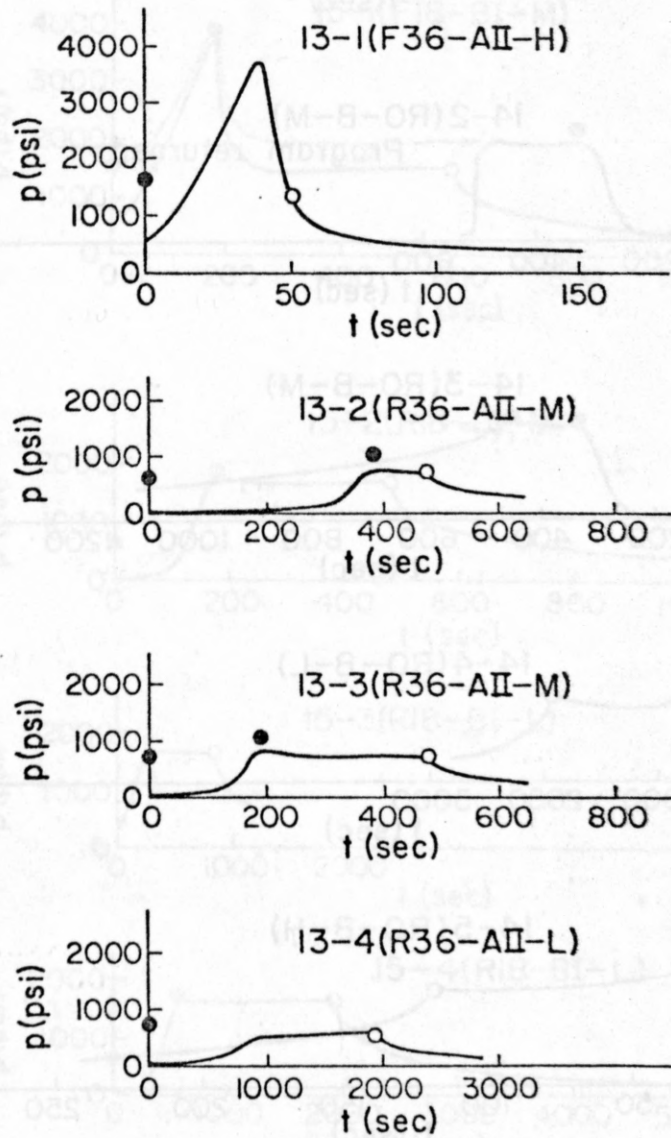


Figure 4.5.1 (13) The pressure-time record of specimen No.13



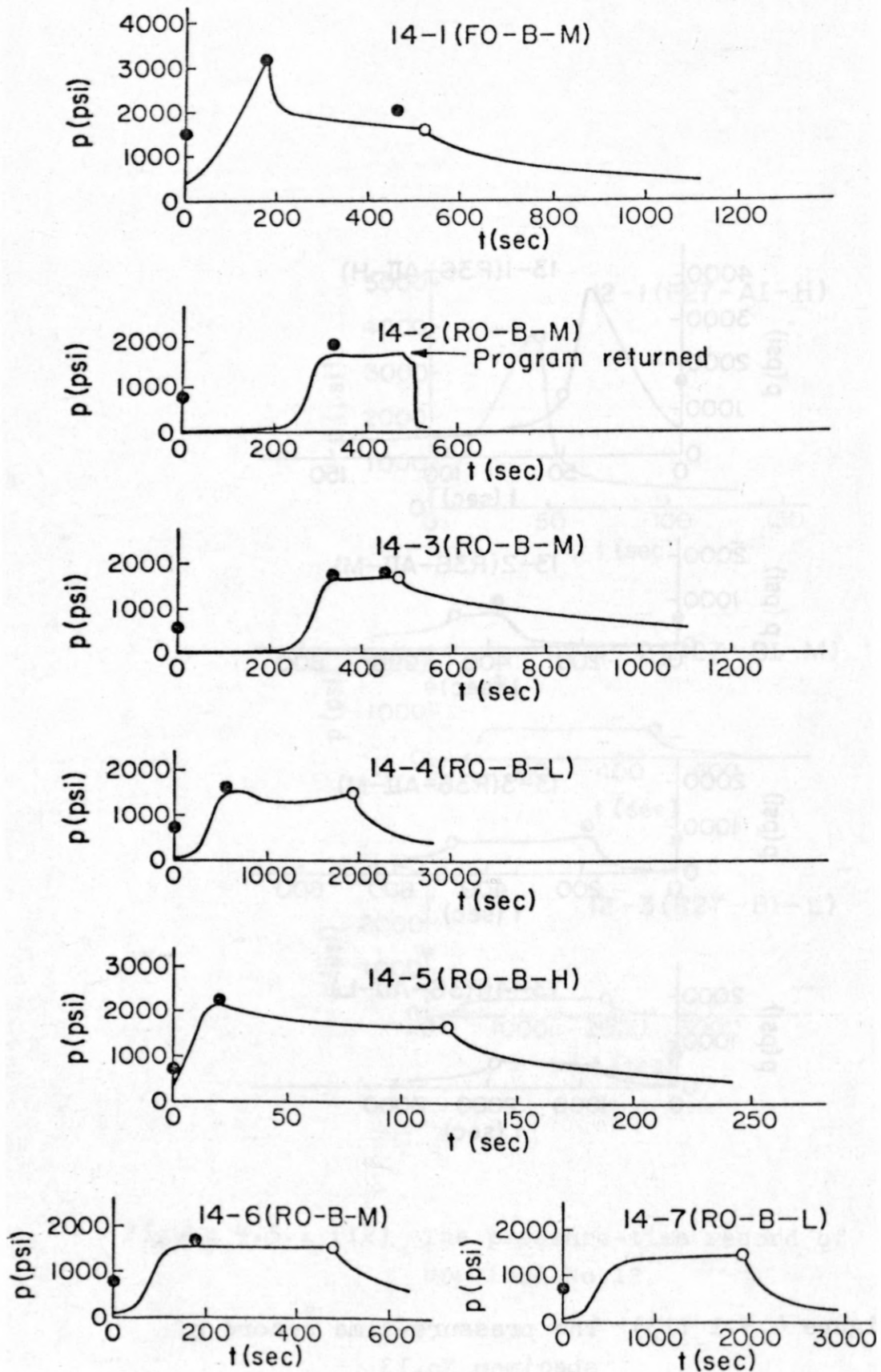


Figure 4.5.1 (14) The pressure-time record of specimen No.14

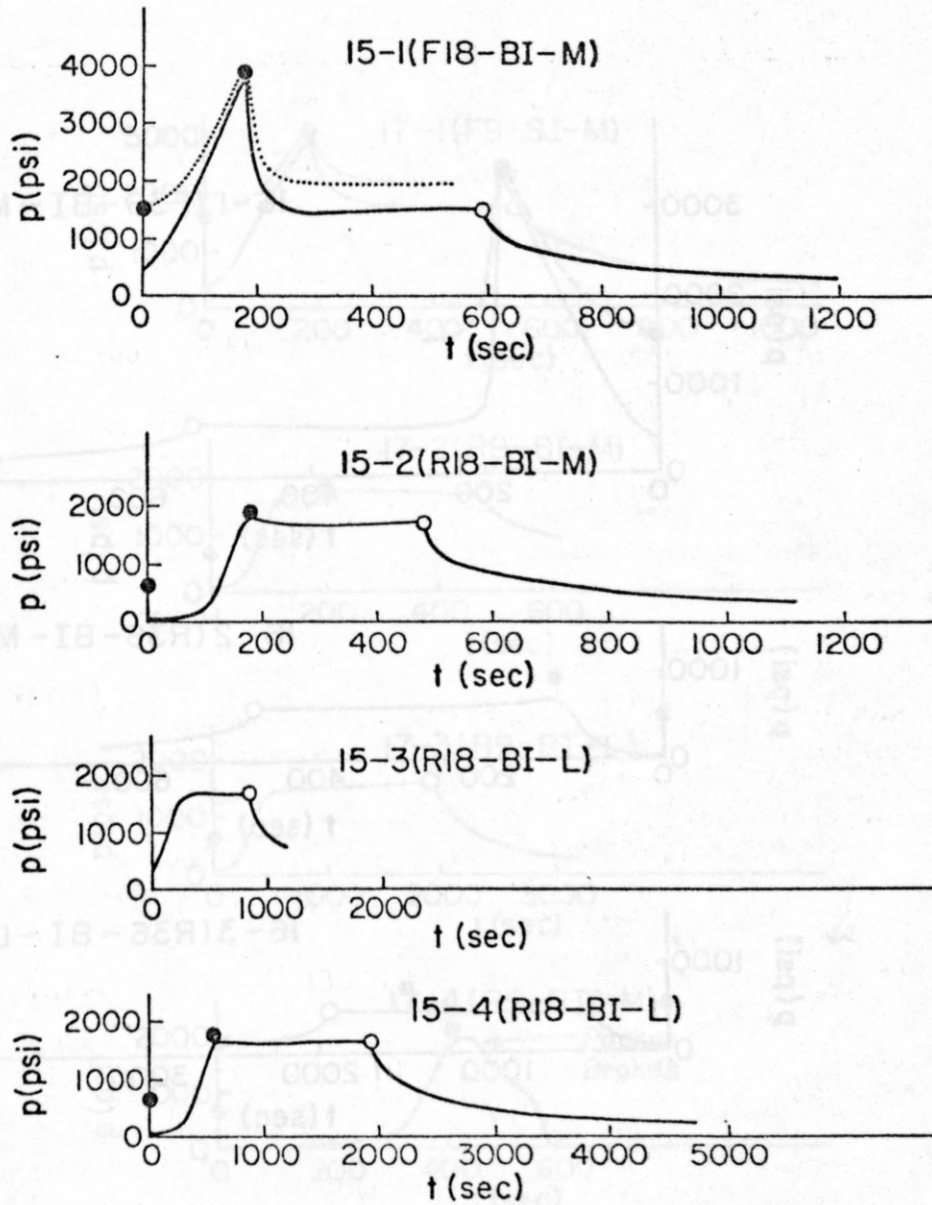


Figure 4.5.1 (15) The pressure-time record of specimen No.15

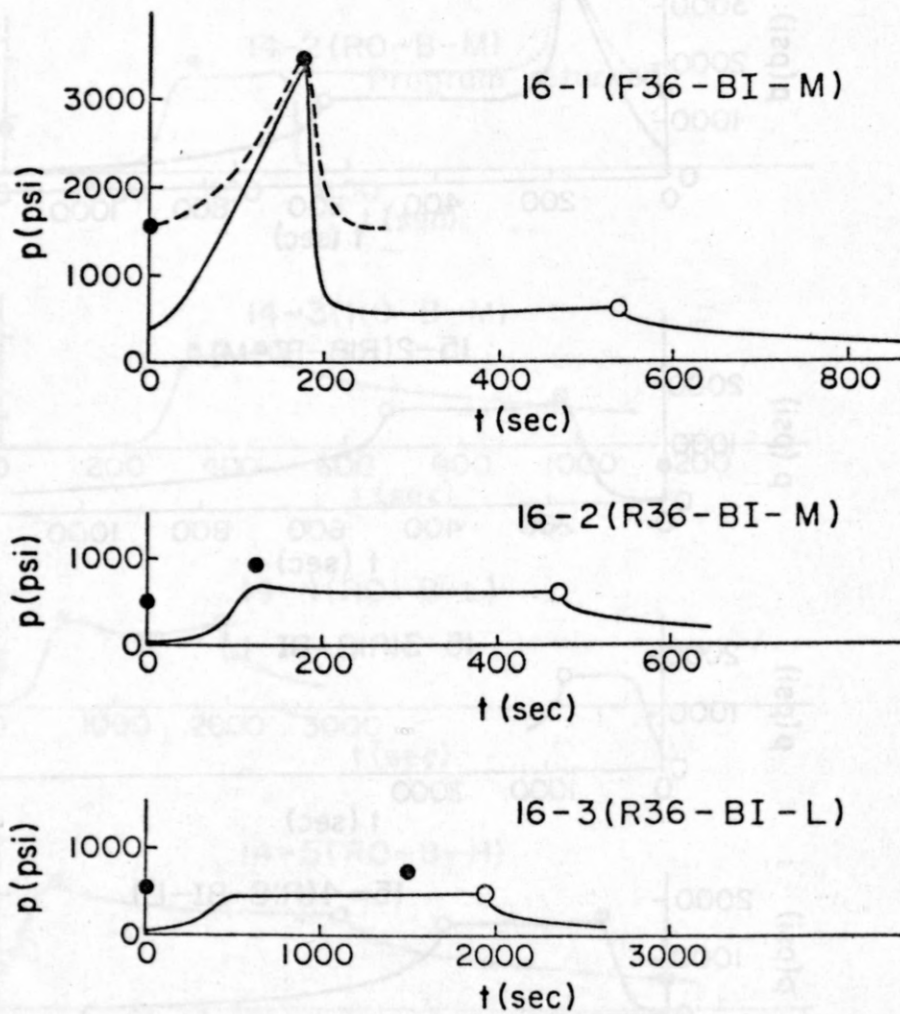


Figure 4.5.1 (16) The pressure-time record of specimen No. 16

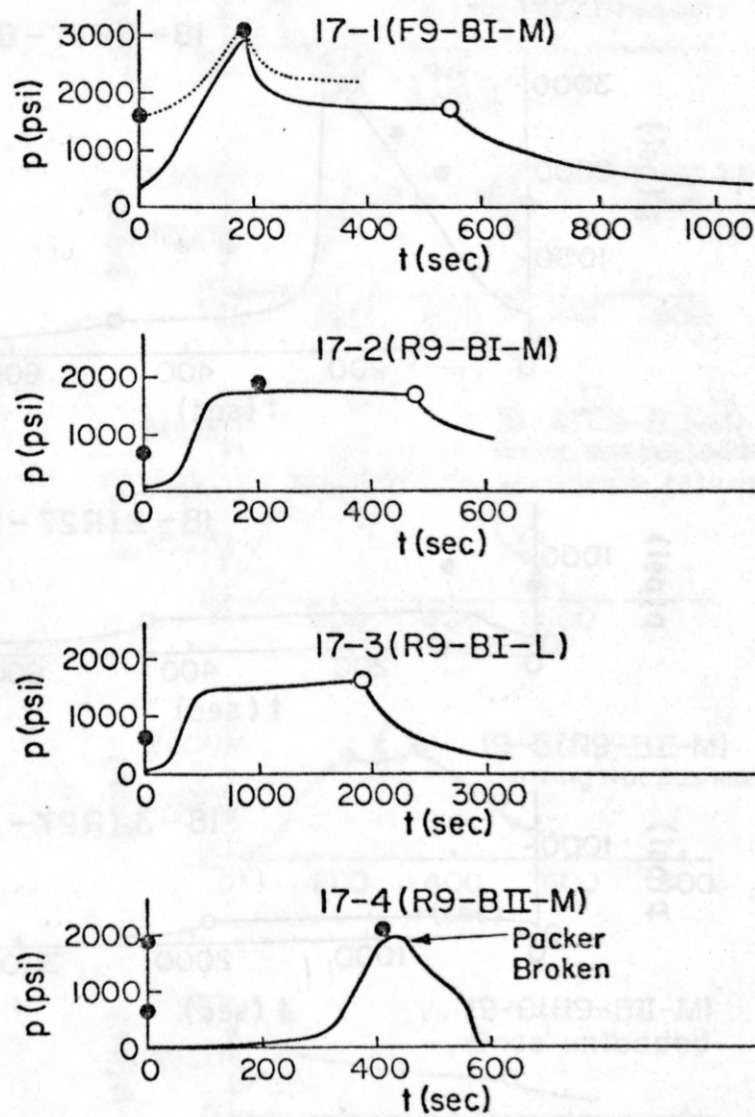


Figure 4.5.1 (17) The pressure-time record of specimen No.17



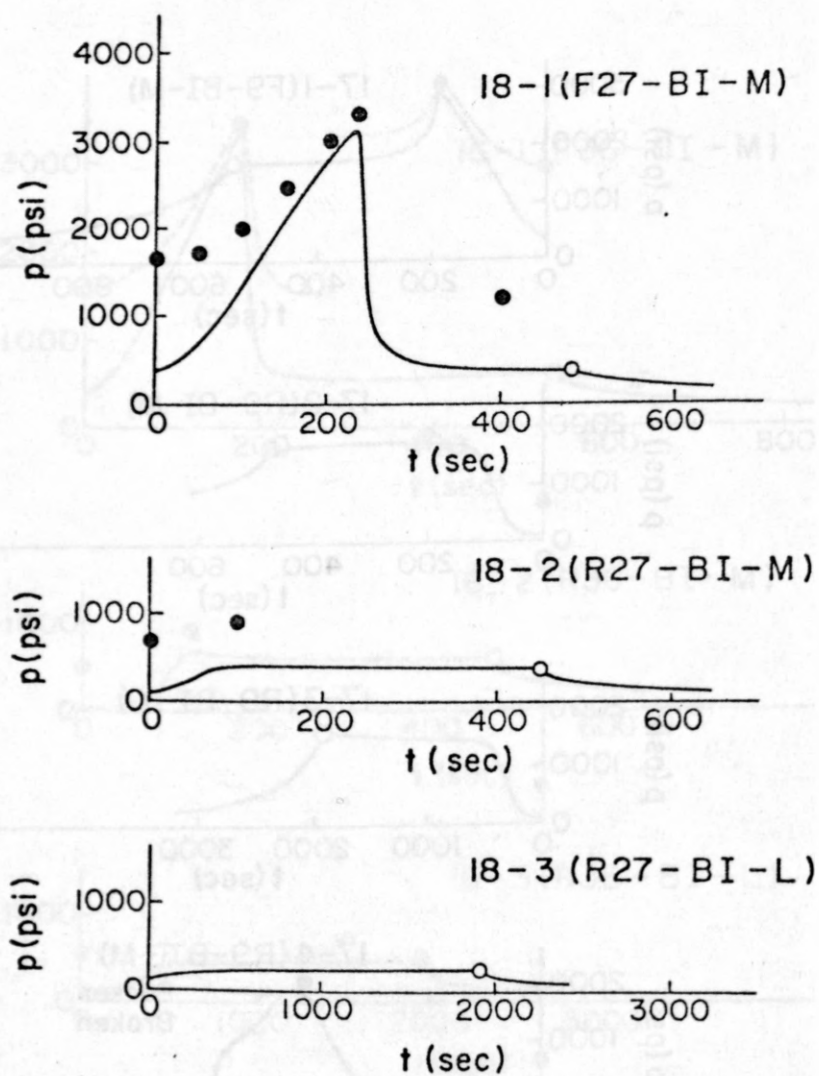


Figure 4.5.1 (18) The pressure-time record of specimen No.18

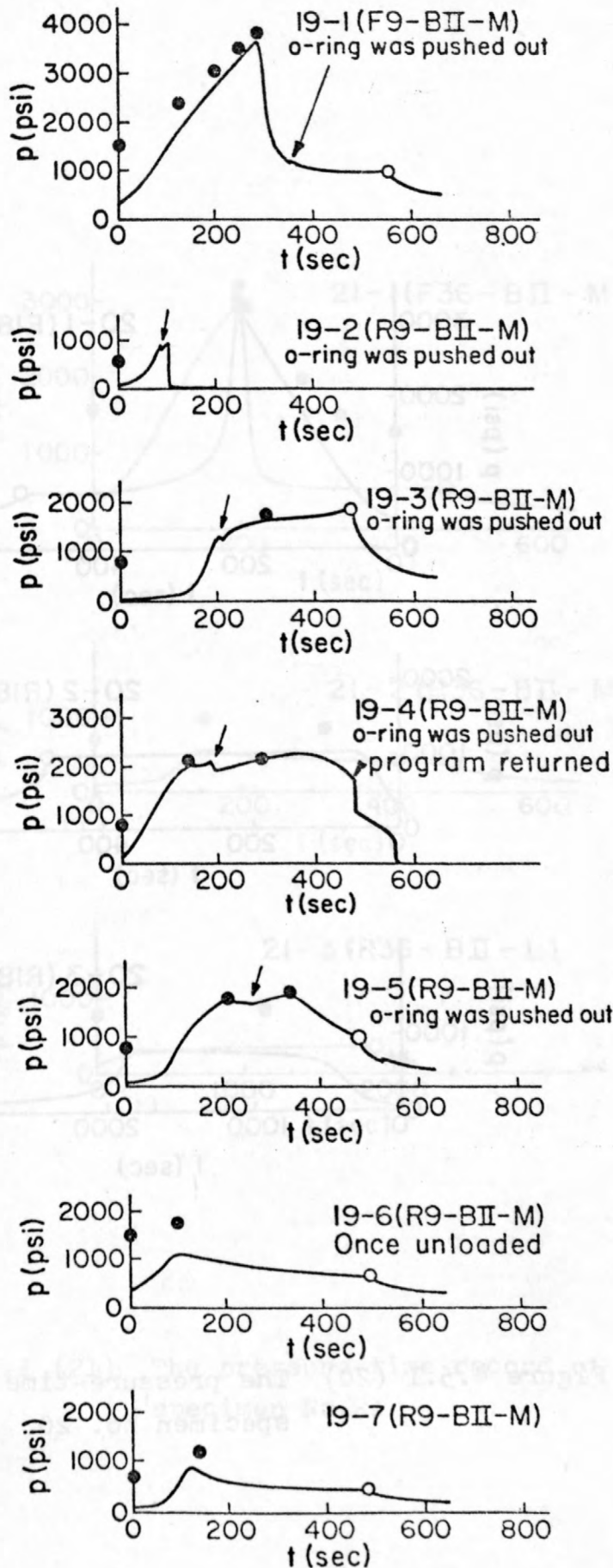


Figure 4.5.1 (19) The pressure-time record of specimen No. 19

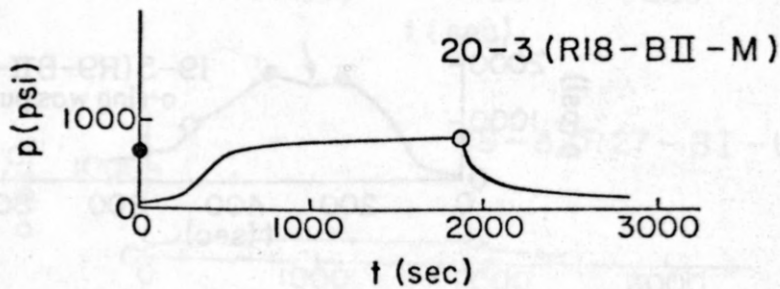
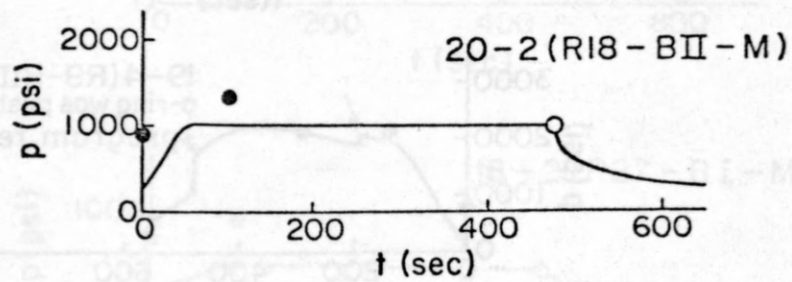
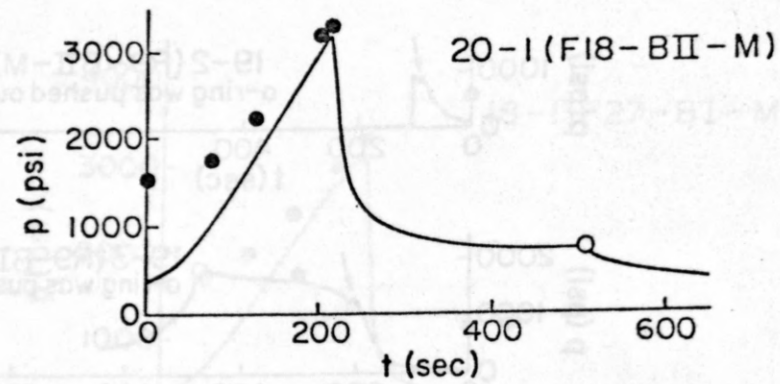


Figure 4.5.1 (20) The pressure-time record of specimen No. 20

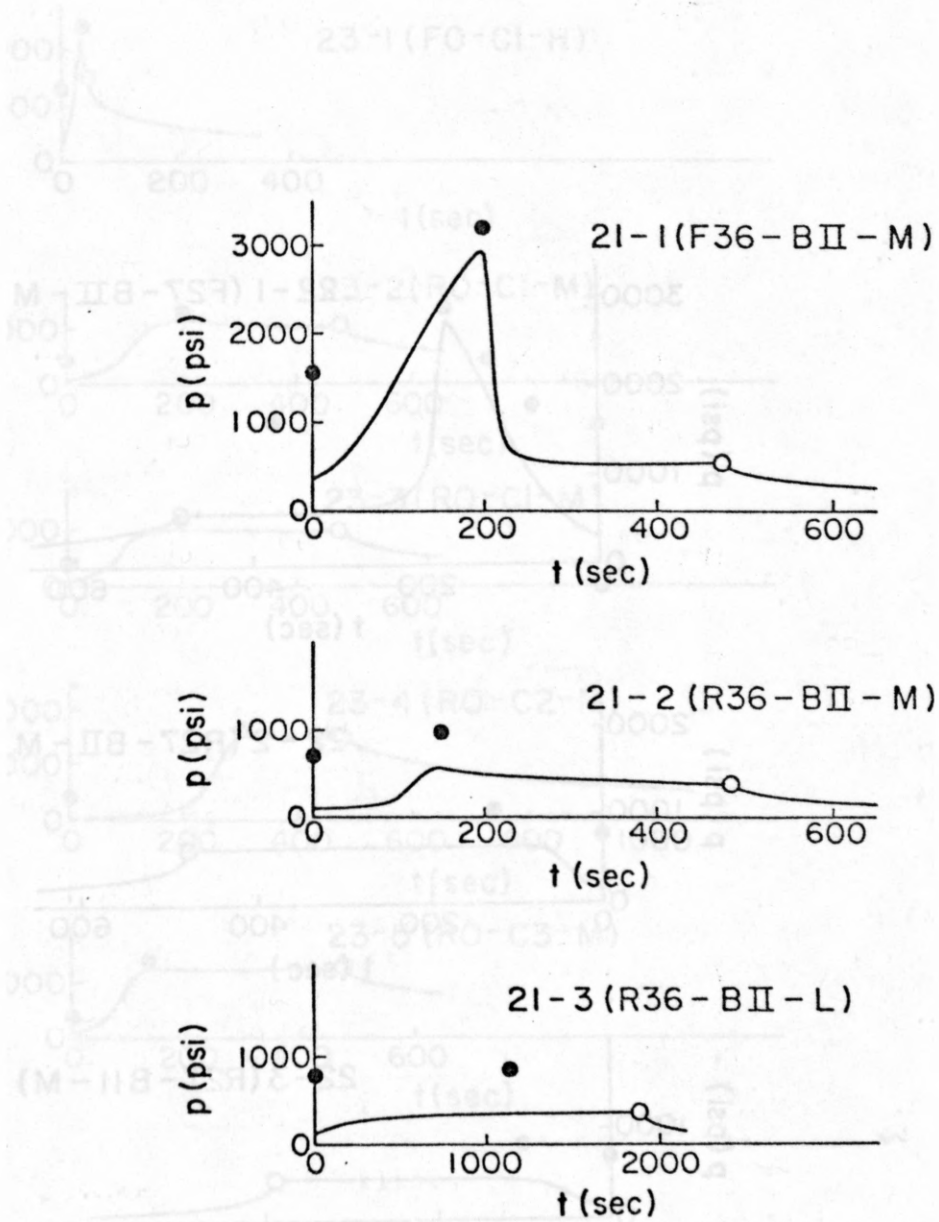


Figure 4.5.1 (21) The pressure-time record of specimen No. 21 (continued)

Figure 4.5.1 (21) The pressure-time record of specimen No. 21

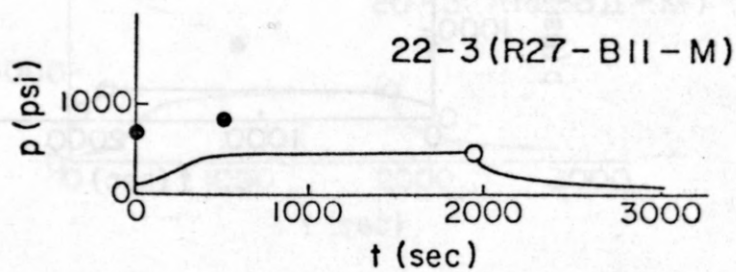
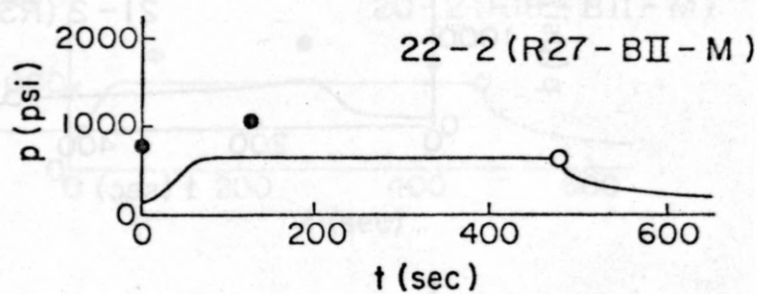
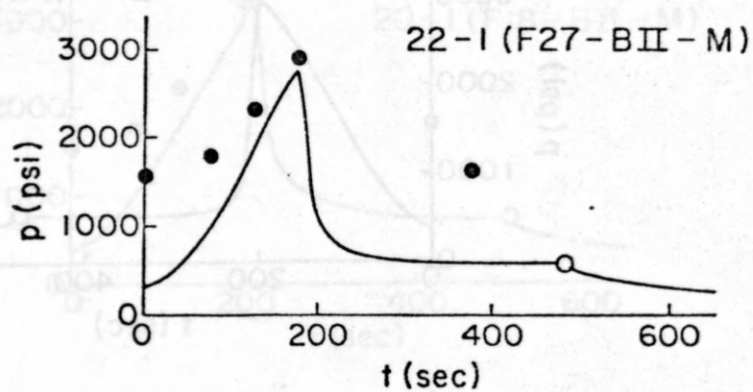


Figure 4.5.1 (22) The pressure-time record of specimen No.22



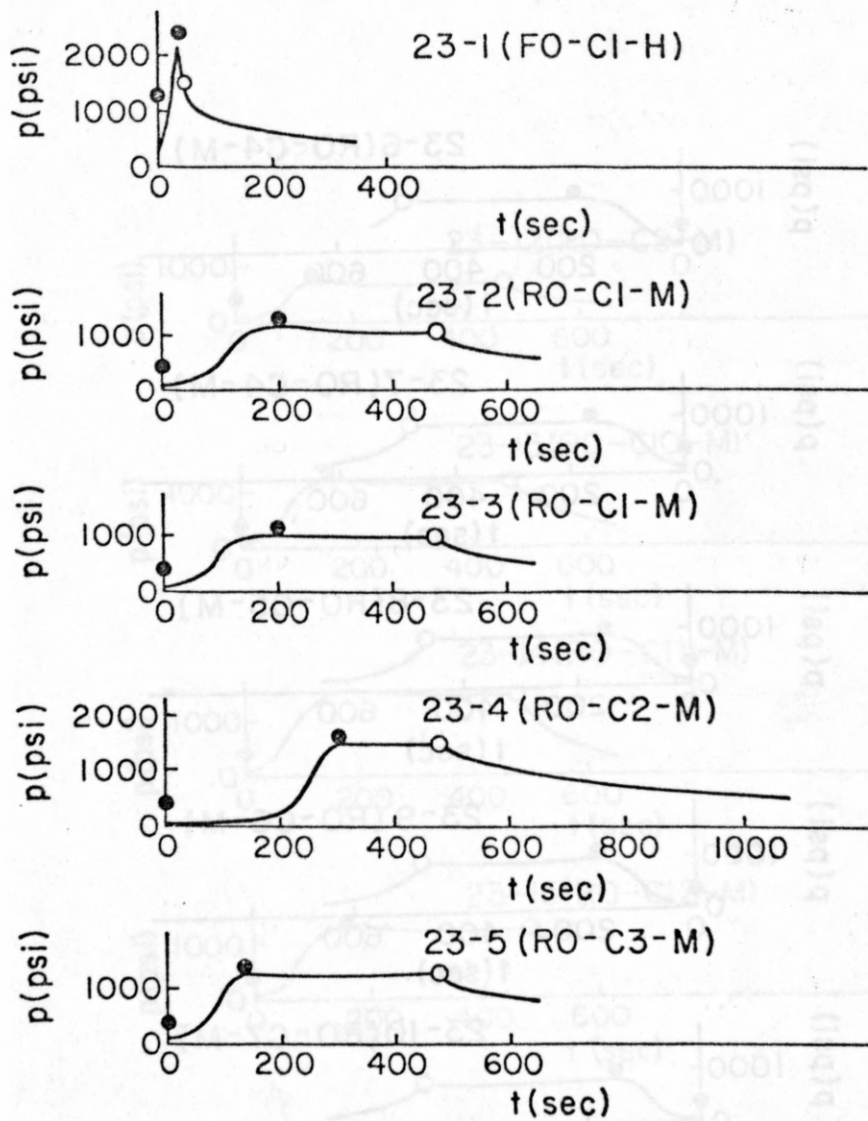


Figure 4.5.1 (23) The pressure-time record of specimen No.23 (continued)

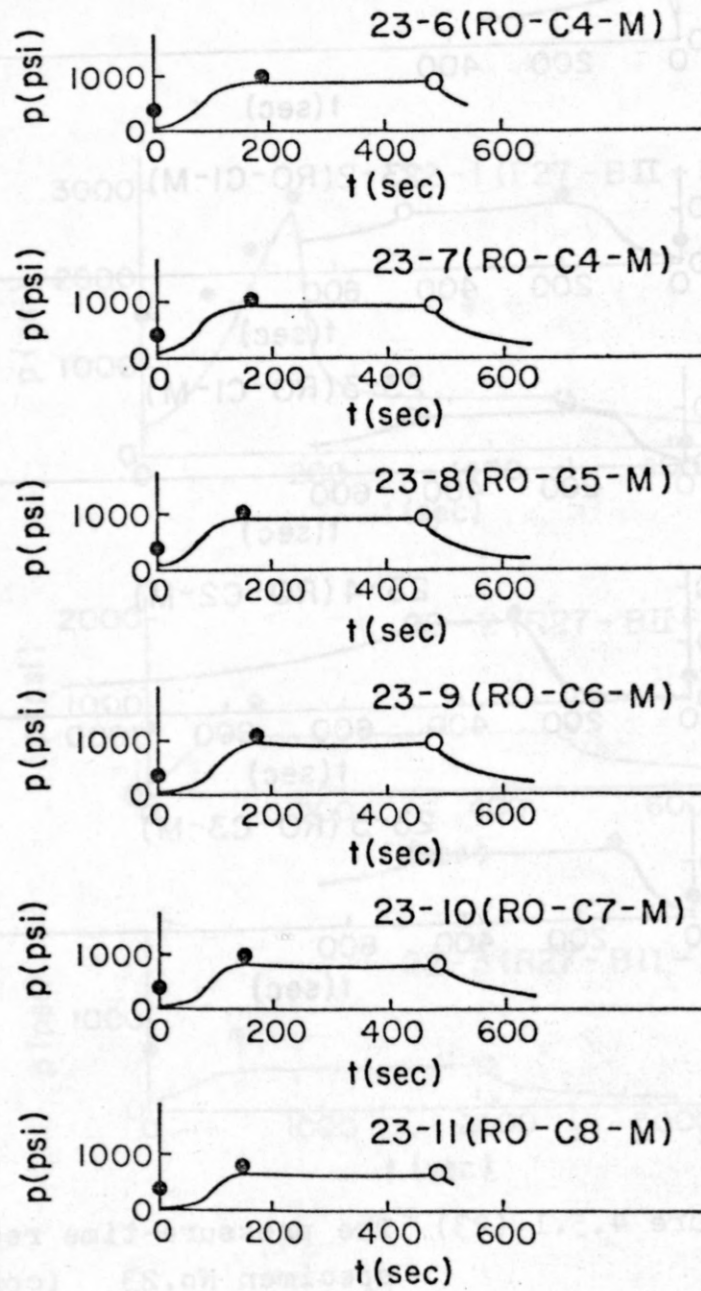


Figure 4.5.1 (23) (continued)

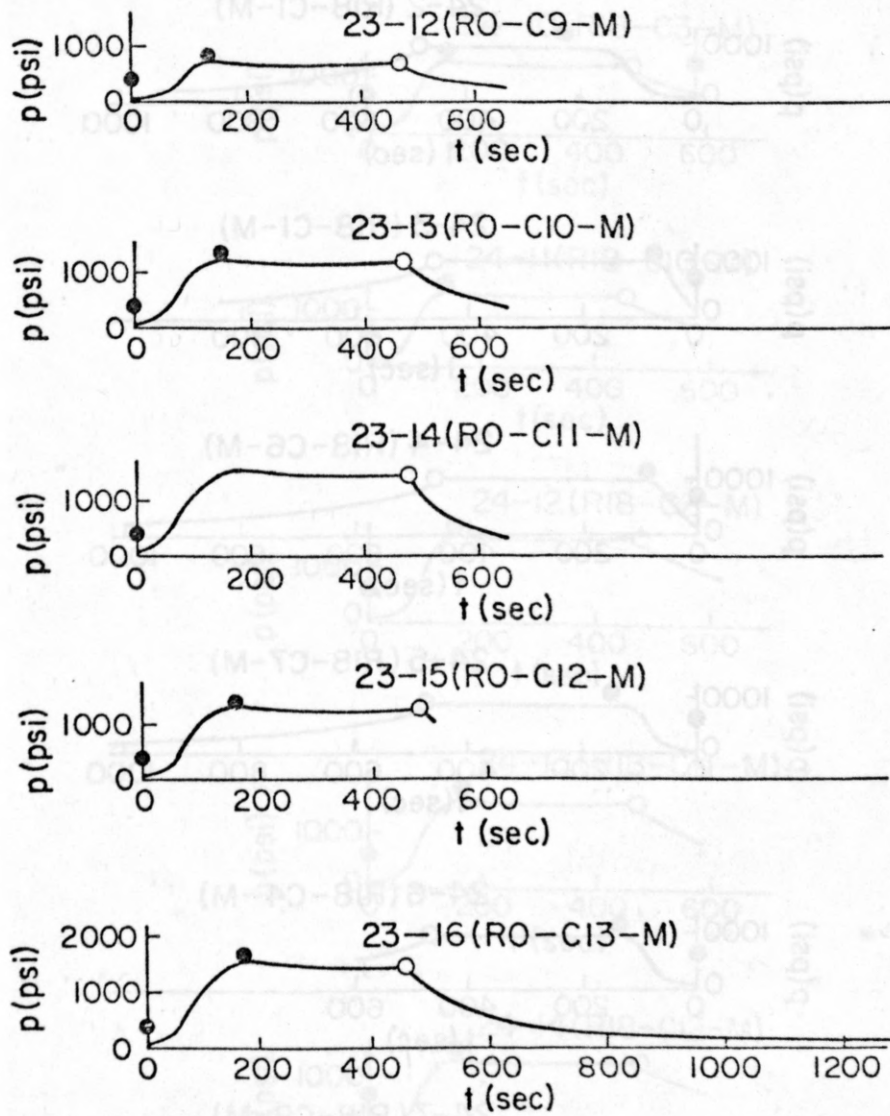


Figure 4.5.1 (23) (continued)

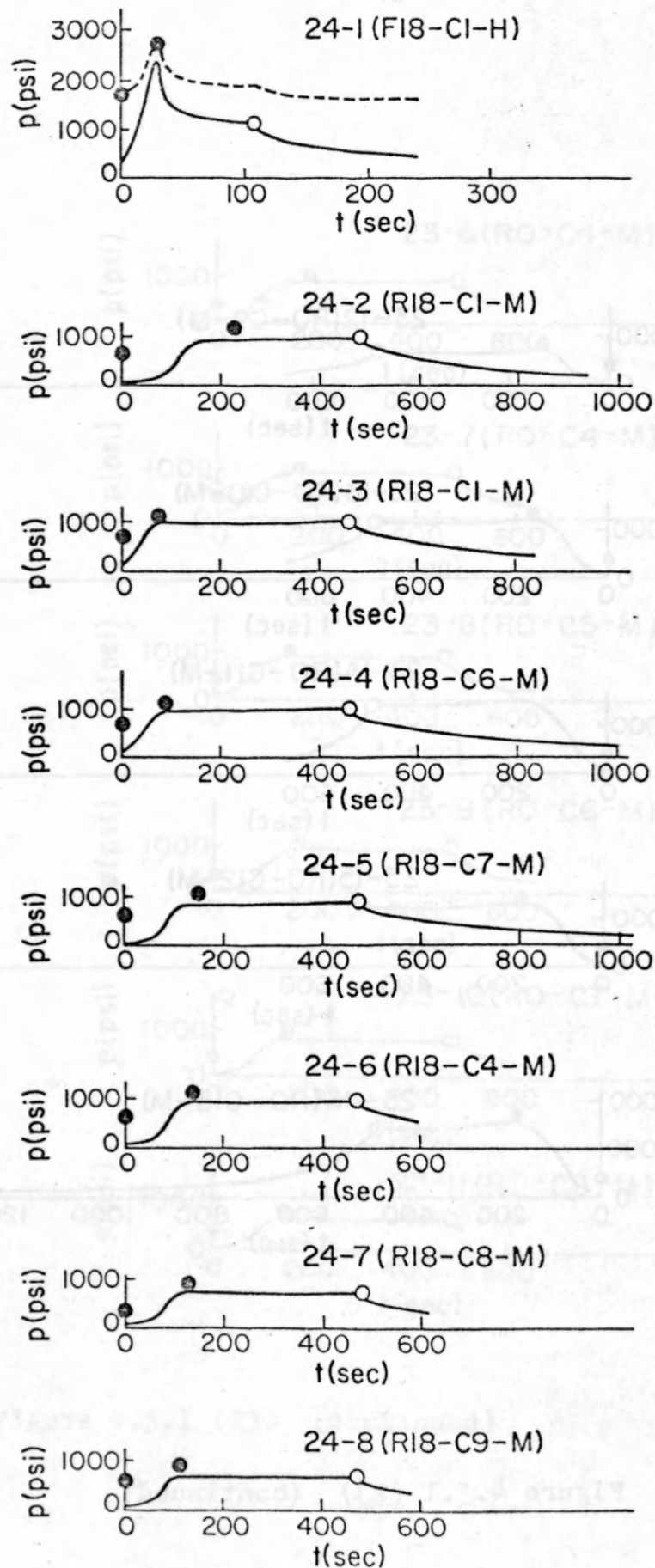


Figure 4.5.1 (24) The pressure-time record of specimen No. 24 (continued)

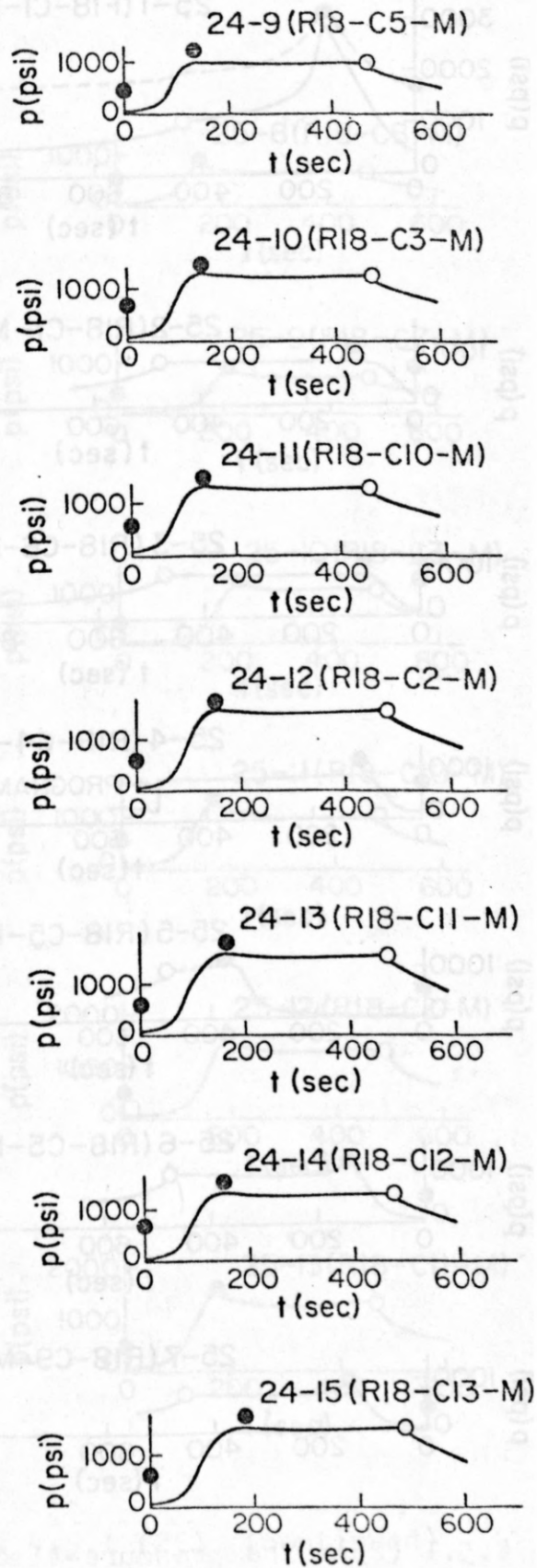


Figure 4.5.1 (24) (continued)



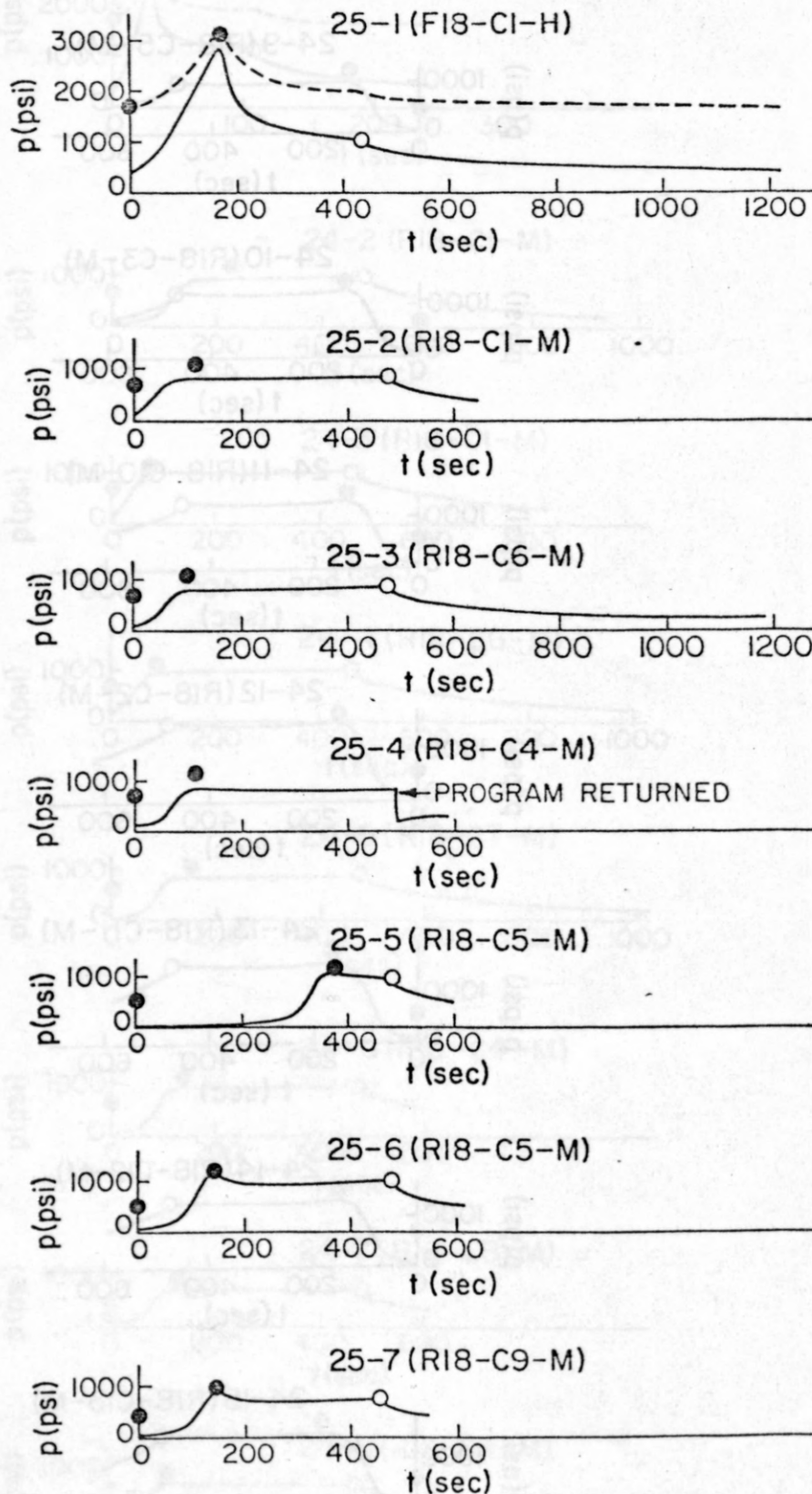


Figure 4.5.1 (25) The pressure-time record of specimen No. 25 (continued)

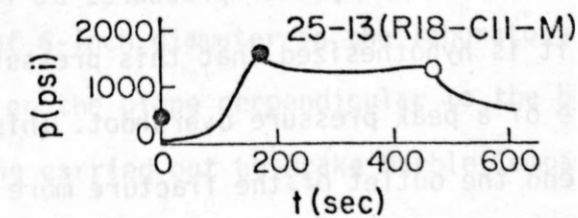
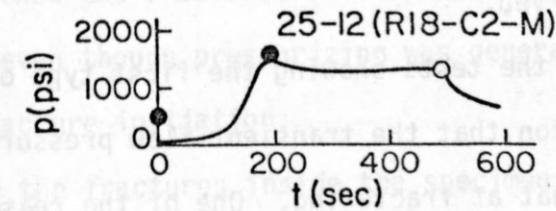
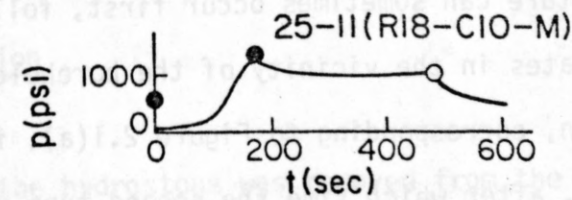
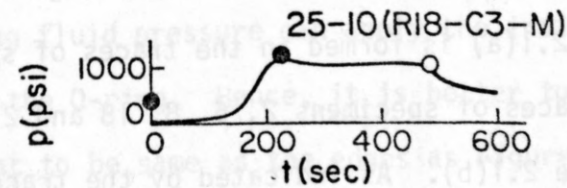
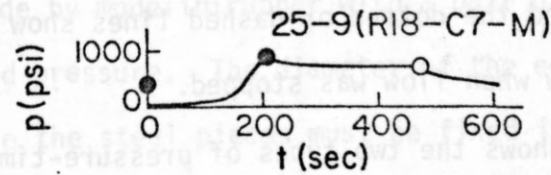
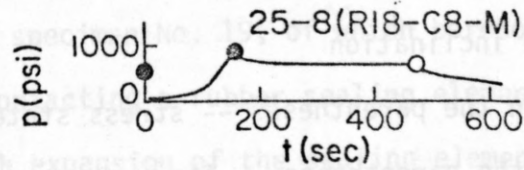


Figure 4.5.1 (25) (continued)

First number -- specimen number

Second number -- run number for each specimen

First cipher in the parentheses -- letter; means fracturing or reopening, number; shows borehole inclination

Second cipher in the parentheses -- stress state

Last letter in the parentheses -- flow rate

The closed circles and the dotted or dashed lines show the packer pressures.

The open circles show when flow was stopped.

Figure 4.5.1 shows the two types of pressure-time trace from various specimens, corresponding to the typical cases of Figure 2.1. The pattern indicated in Figure 2.1(a) is formed in the traces of specimens 1, 4, 15, 17 and 23, while the traces of specimens 2, 6, 8, 18 and 21 reproduce the general shape shown in Figure 2.1(b). As indicated by the traces for specimens 3 and 5, vertical fracture can sometimes occur first, followed by secondary fracture which indicates in the vicinity of the borehole. The initial pressure-time pattern, corresponding to Figure 2.1(a), is not maintained. The fluid pressure falls, after which time the second type of typical trace, Figure 2.1(b) is observed.

In a number of the tests showing the first type of pressure-time record, there is some indication that the transient flow pressure at reopening is a little greater than that at fracturing. One of the reasons is presumed to be the difference between the initial packer pressures at fracturing and at reopening. However, it is hypothesized that this pressure increase also reflects the existence of a peak pressure overshoot. This is because a momentary peak pressure may extend the outlet of the fracture more than that of steady flow. Farther, the aperture, once extended, is not closed, even after fluid pressure settles down to a stable value. Hence, even at reopening it is desirable to use a flow rate at which peak the pressure overshoot on reopening

virtually disappears.

The tests of specimens No. 6 and No. 8 were performed under the same condition, so that the results are similar as shown in Figure 4.5.1.

During the test of specimen No. 19, of which borehole diameter is 1.15 inch, one of the O-ring contacting a rubber sealing element was pushed out five times over. Too much expansion of the sealing element was a cause of this. The sealing element is made by modeling rubber with a pair of steel end pieces under high temperature and pressure. The diameter of the edges of it must be a little larger because the steel pieces must be fixed in the mold. The detail of the straddle packer used is shown in Figure 4.5.2(a). As Figure 4.5.2(a) shows, fracturing fluid pressure can apply the inside edges and assist in pushing out of the O-ring. Hence, it is better to enlarge the parts holding the rubber element to be same as the edges as Figure 4.5.2(b) shows.

#### 4.6 Fracture Orientation

After each test, the hydrostone was removed from the rock. Without exception, it was found that the fractures arrived at the divider between the rock and the hydrostone even though pressurizing was generally terminated immediately after the fracture initiation.

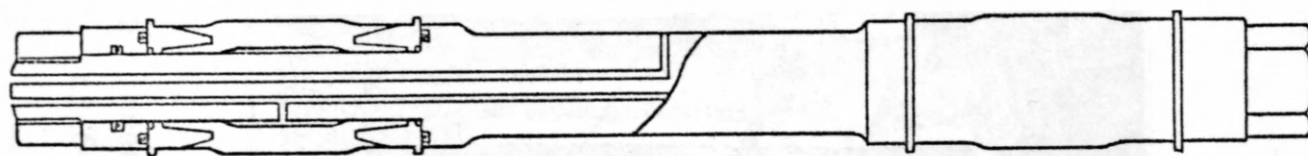
In order to trace the fractures inside the specimen, overcorings of both 2-inch and 6-inch diameter were performed. It is difficult, however, to drill an inclined hole of 6-inch diameter in the laboratory. Hence, each specimen was cut in two on the plane perpendicular to the borehole axis at the midpoint, this work being carried out by Drake Marble Company of St. Paul. Figure 4.6.1 shows some of the resulting halves thus produced. Both 2-inch and 6-inch coring was performed on each half. A view of the 6-inch drilling process

as well as of 2-inch and 1-inch drill bits, is shown in Figure 4.6.2. For each specimen, core of one of the pair of block halves was cut into four or more lengths to detect the location of the fracture on the surface of the 1-inch borehole.

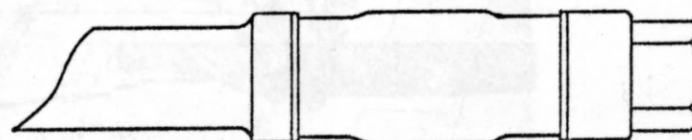
This procedure allows the precise determination of the fracture produced in each specimen on three cylindrical surfaces (inside of 1-inch borehole, outside of 2-inch core and outside of 6-inch core) as well as on the plane where the specimen was cut in two, and on the six outer surfaces of the specimen (Figure 4.6.3). The fractures appearing on the surfaces of 2-inch and 6-inch core were traced by using a transparent thin cylinder with a marked coordinate system. Figure 4.6.4 shows a sample pair of 6-inch core with a transparent cylindrical grid. Another transparent grid was used to trace the fracture appearing on the planes.

The fractures appear once on each surface was easily observed due to the exuding of oil from the fissure. Sometimes detergent was used to wash off excess oil that had been exuded and spread over the surface, after which a fresh trace could be seen in the expression of fresh oil. Colored dye was tried (pressure-time record 11-6) with the intent of making the trace easier to see, but this procedure was no advance on the earlier method. One 12-inch cube (specimen No. 1) was overcored in the laboratory without being first cut in two. The last two specimens have not been overcored. An earlier batch of four blocks (specimen No. 2-5) were overcored at Cold Spring Granite Company before being cut in two. The fractures on the borehole surfaces of those blocks have not been recorded because the 2-inch core was broken into pieces and lost during the coring. For these four blocks, the inside surfaces of 6-inch cores gave the same information as would have been obtained from the outer surface of the 2-inch core, on cutting of the 6-inch cores longitudinally.





(a)



(b)

Figure 4.5.2 The detail of the straddle packer.



Figure 4.6.1 Some of pieces cut in two.

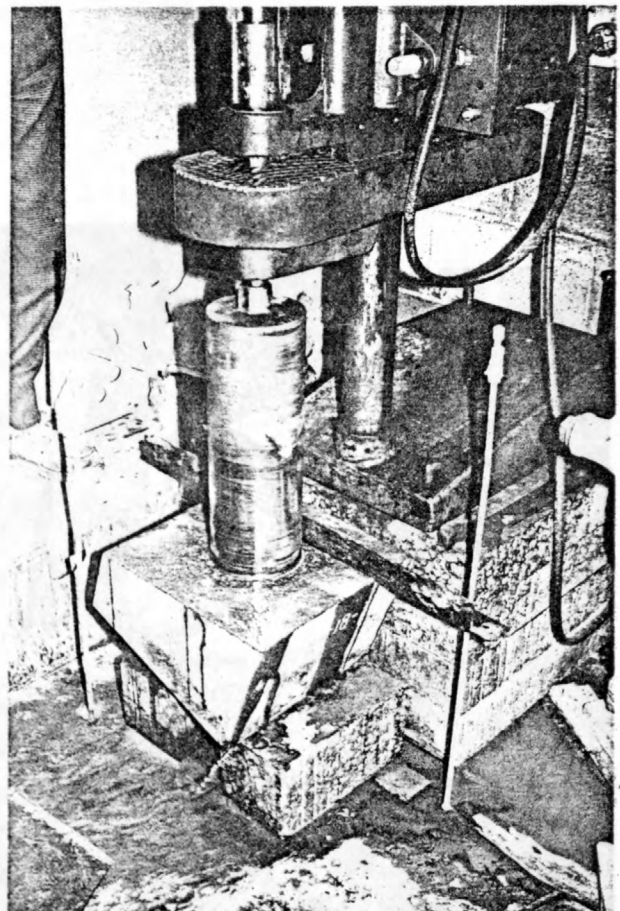
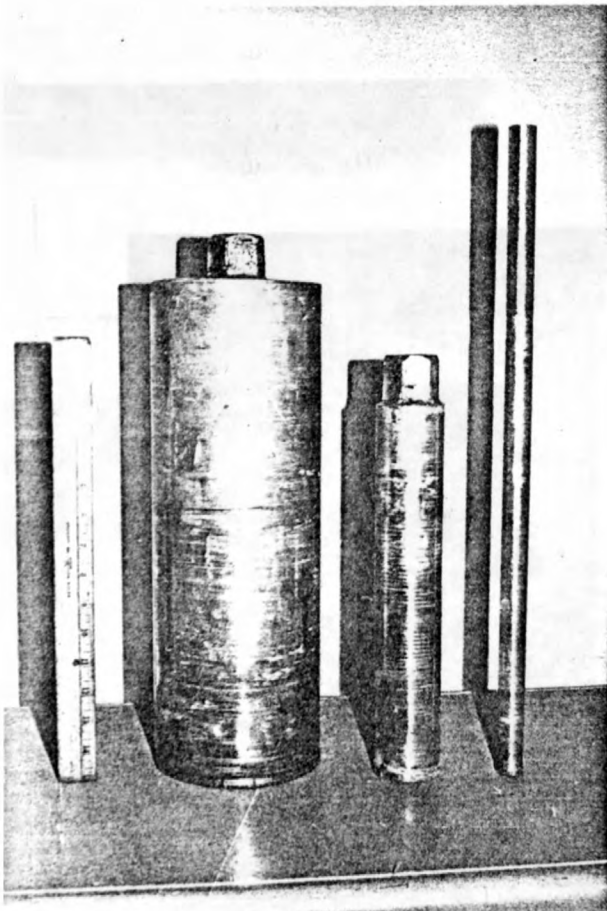


Figure 4.6.2 Three kind of drill bits and a view of 6-inch drilling.

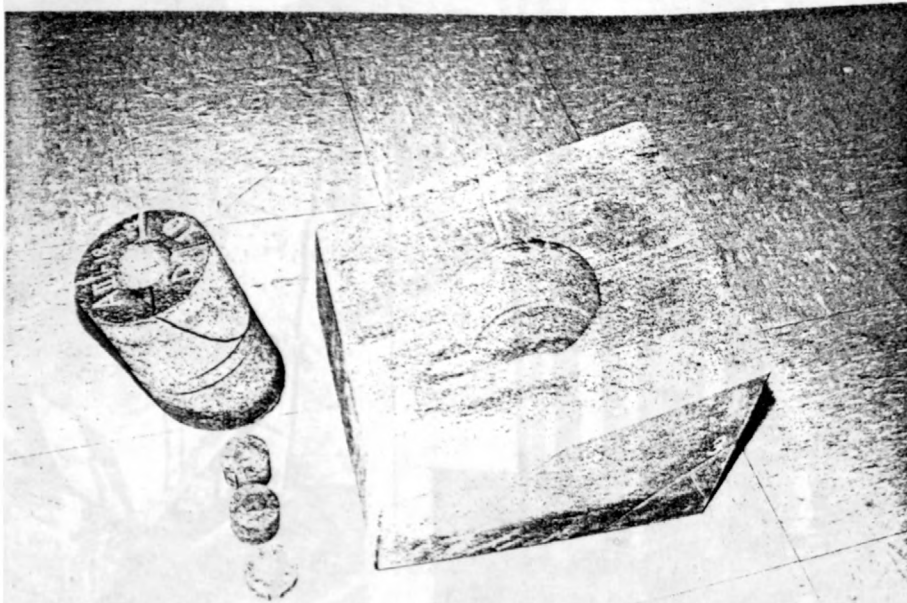


Figure 4.6.3 An example of half specimen cut and cored.

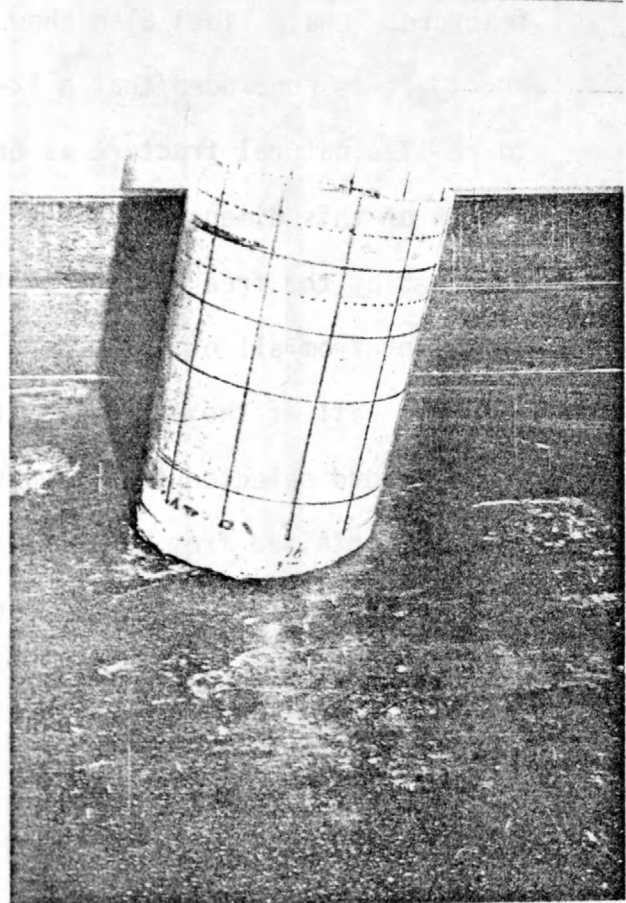


Figure 4.6.4 An example pair of 6-inch cores and a transparent cylindrical coordinate.



Figure 4.6.5 shows the core, disclosing the inside.

Some additional 2-inch coring was carried out on several blocks in which fracture was complete. In this way, a record of the fracture path of all specimens was built up.

All data were transferred to graph paper representing three dimensional coordinates which were prepared in advance. The resulting traces are shown in Figure 4.6.6. In this Figure, the thick lines show the fracture actually observed, the thin lines show the presumed fracture based on the observed fracture. Chain lines also show the plane where the blocks were cut in two.

It is concluded that a 12-inch cubical specimen is not large enough to realize natural fracture as created in the field, so long as a straddle packer of this dimension is used. The fracture of specimen No. 1 must be affected by the free surface of the top, this fracture pattern being very different from all of the others having the same stress state applied.

In all of these Figures, the pressure-time record of the fracturing test and a record selected from the reopening tests are placed above each traced fracture obtained from some specimen. It can thus be seen that the Figures clearly support the explanation given in Chapter 2, where it is hypothesized that the fracture, F, occurred first and the fracture, S, occurred next; this can be seen to be supported.

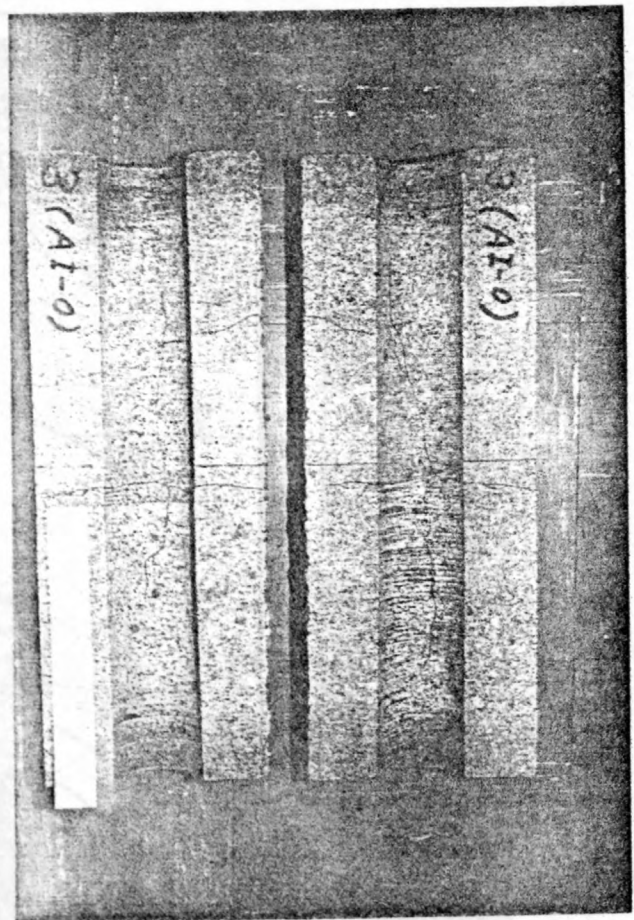
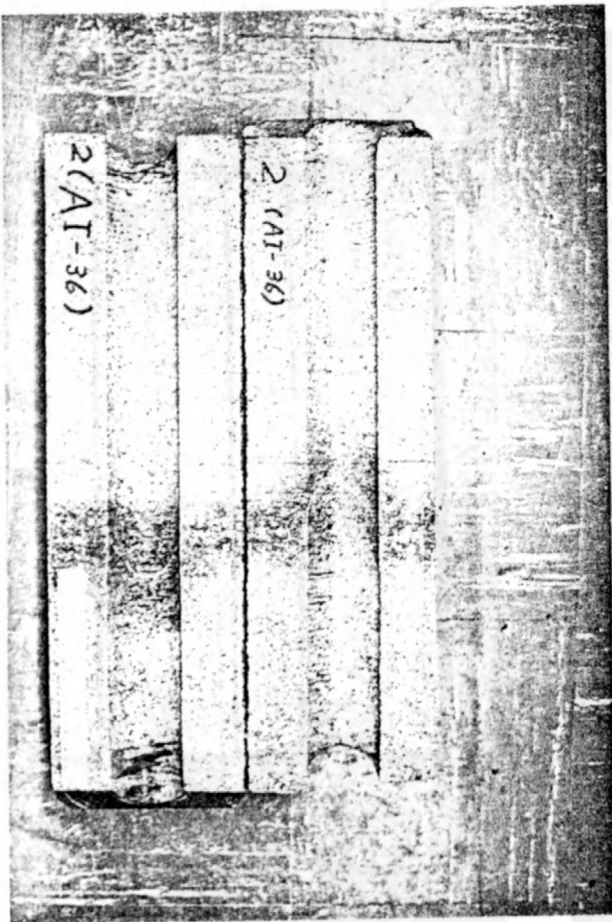
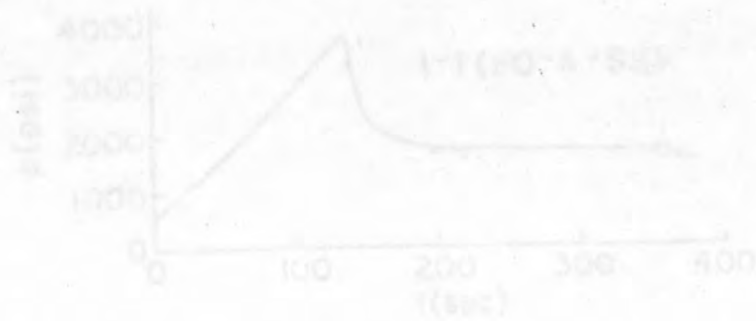


Figure 4.6.5 The 6-inch cores cut in two longitudinally.

( continued )

Figure 4.6.5 shows the core, disclosing the inside.

Some additional 2-inch boring was carried out on several blocks in which fracture was complete. In this way, a record of the fracture path of all elements was built up.

All data were transferred to graph paper representing three dimensional ordinates which were prepared in advance. The resulting traces are shown

Figure 4.6.5. In this figure, the thick lines show the fracture actually

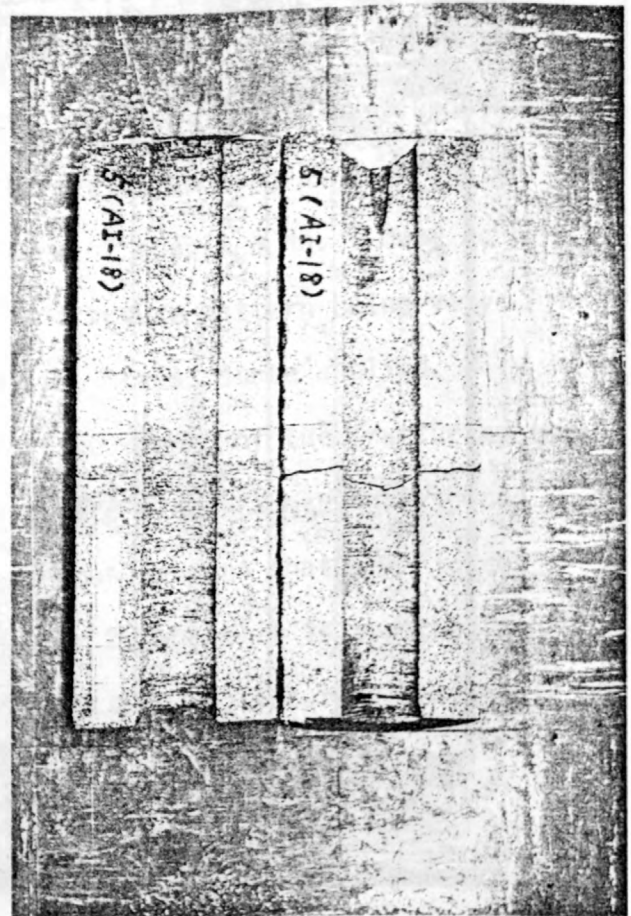
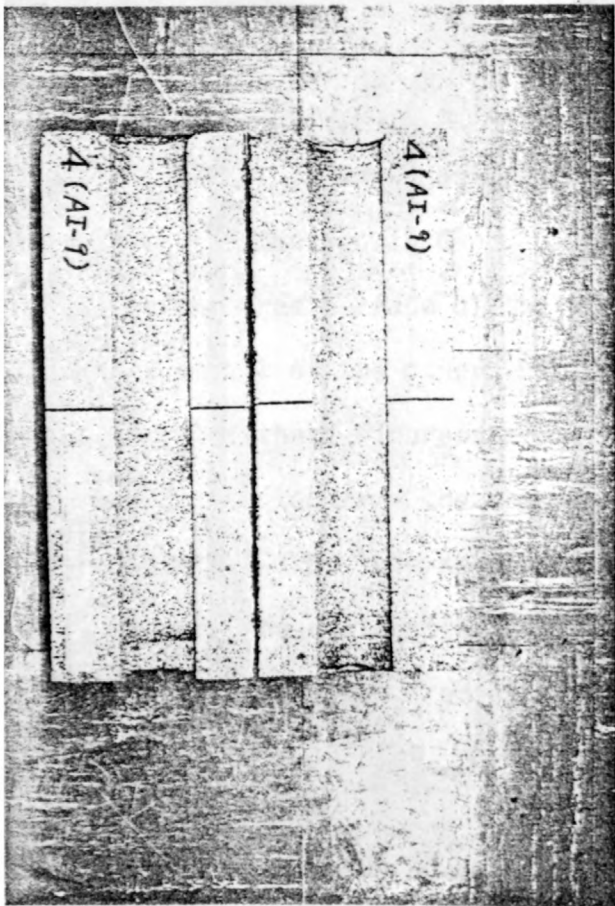


Figure 4.6.5 ( continued )

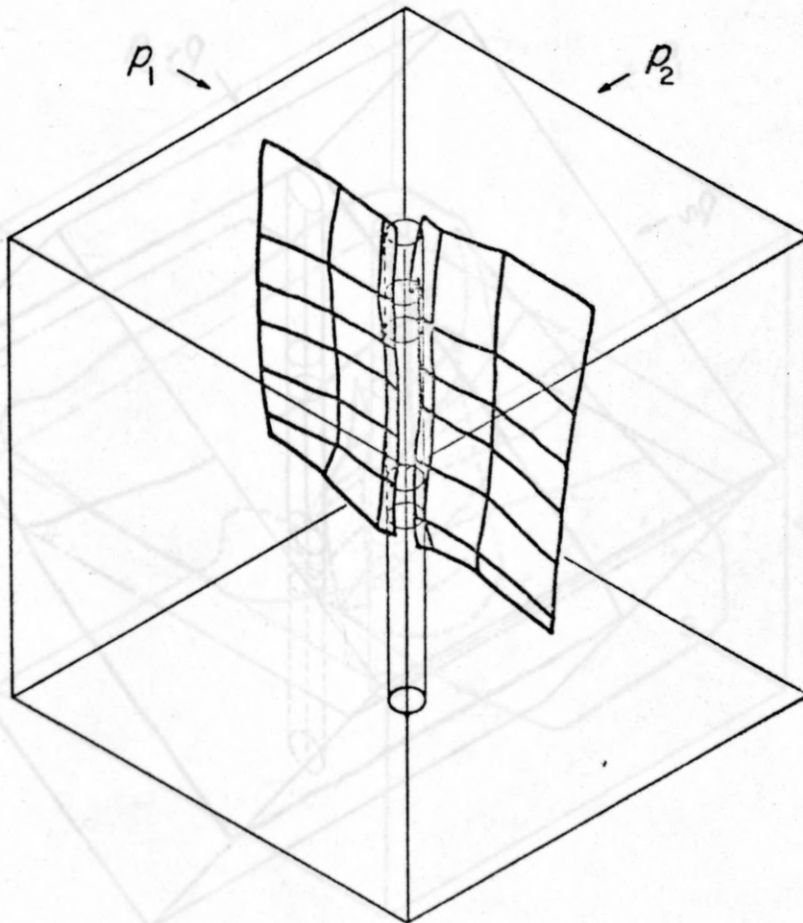
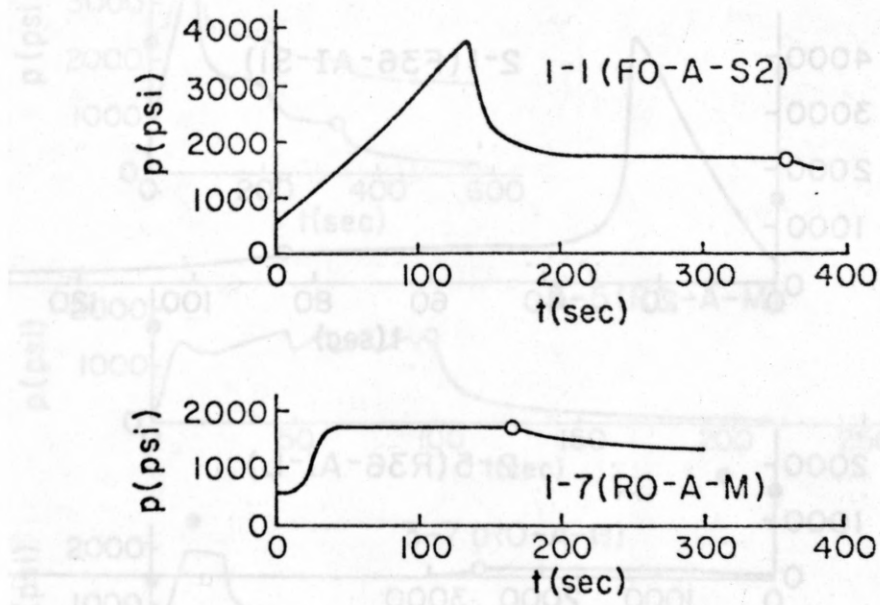


Figure 4.6.6 (1) The fracture trace of specimen No.1

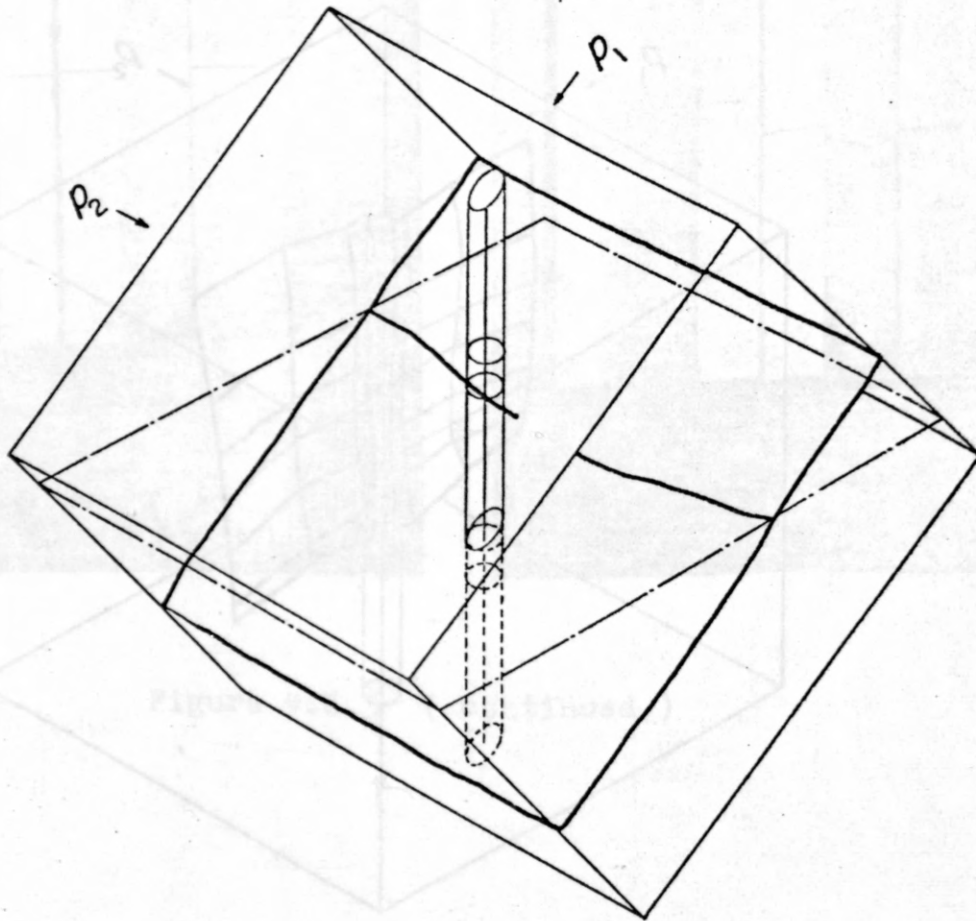
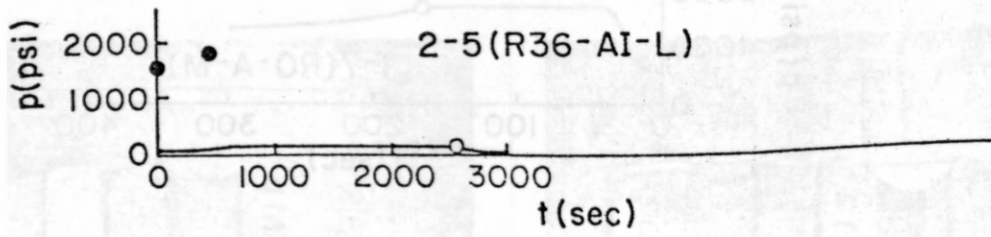
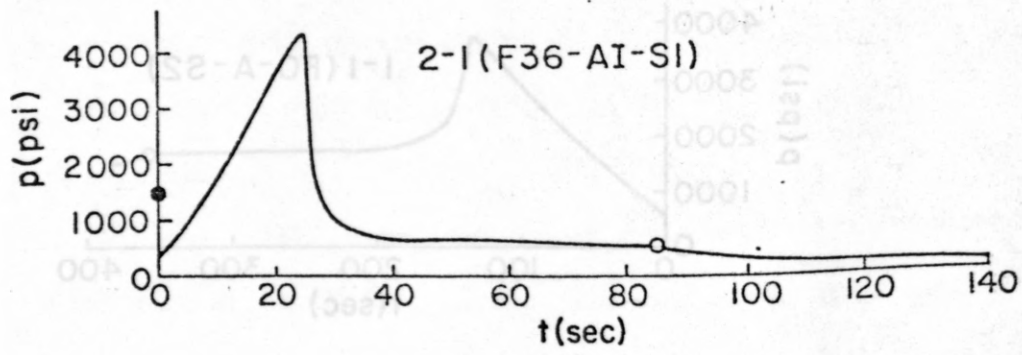


Figure 4.6.6 (2) The fracture trace of specimen No.2



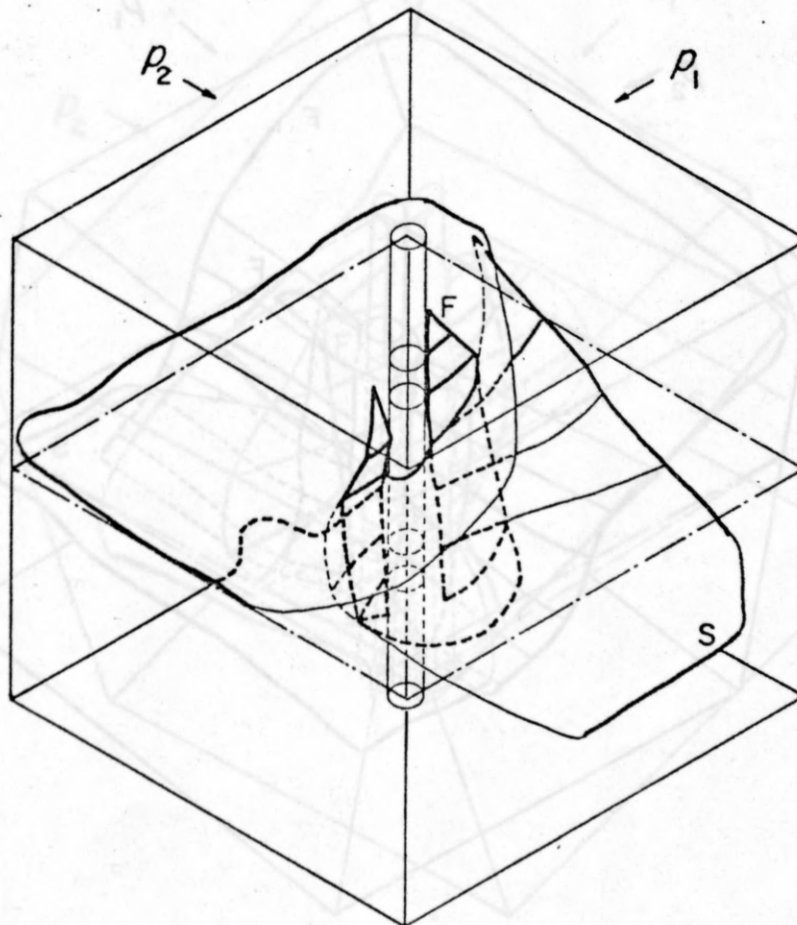
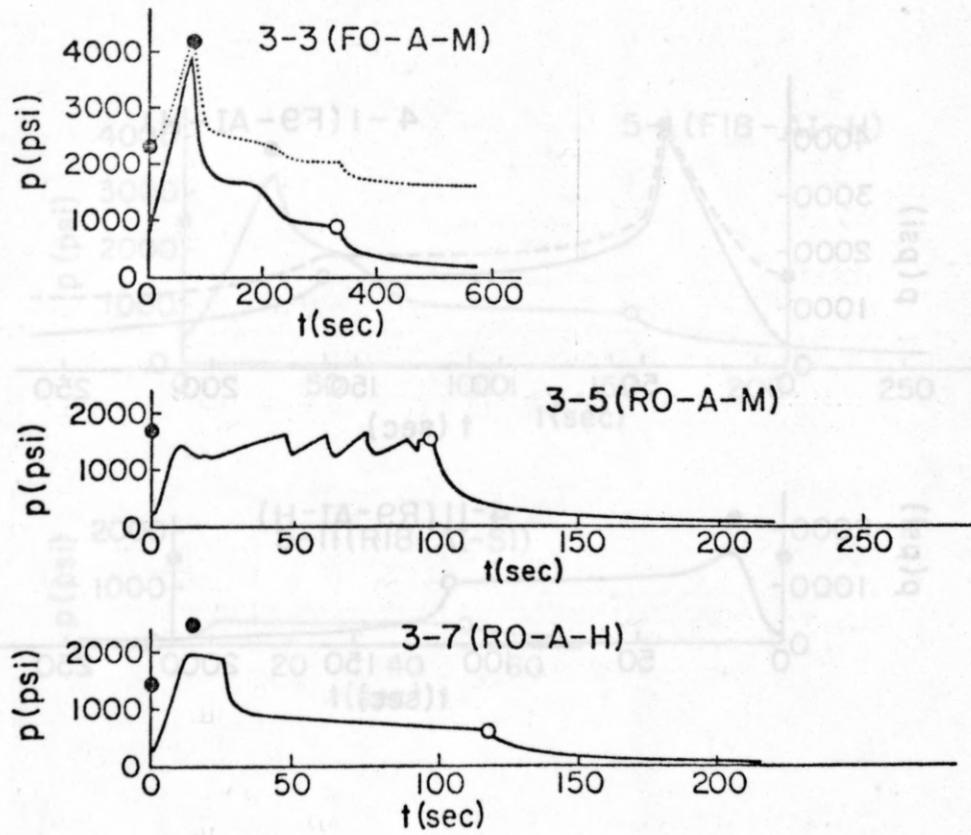


Figure 4.6.6 (3) The fracture trace of specimen No.3

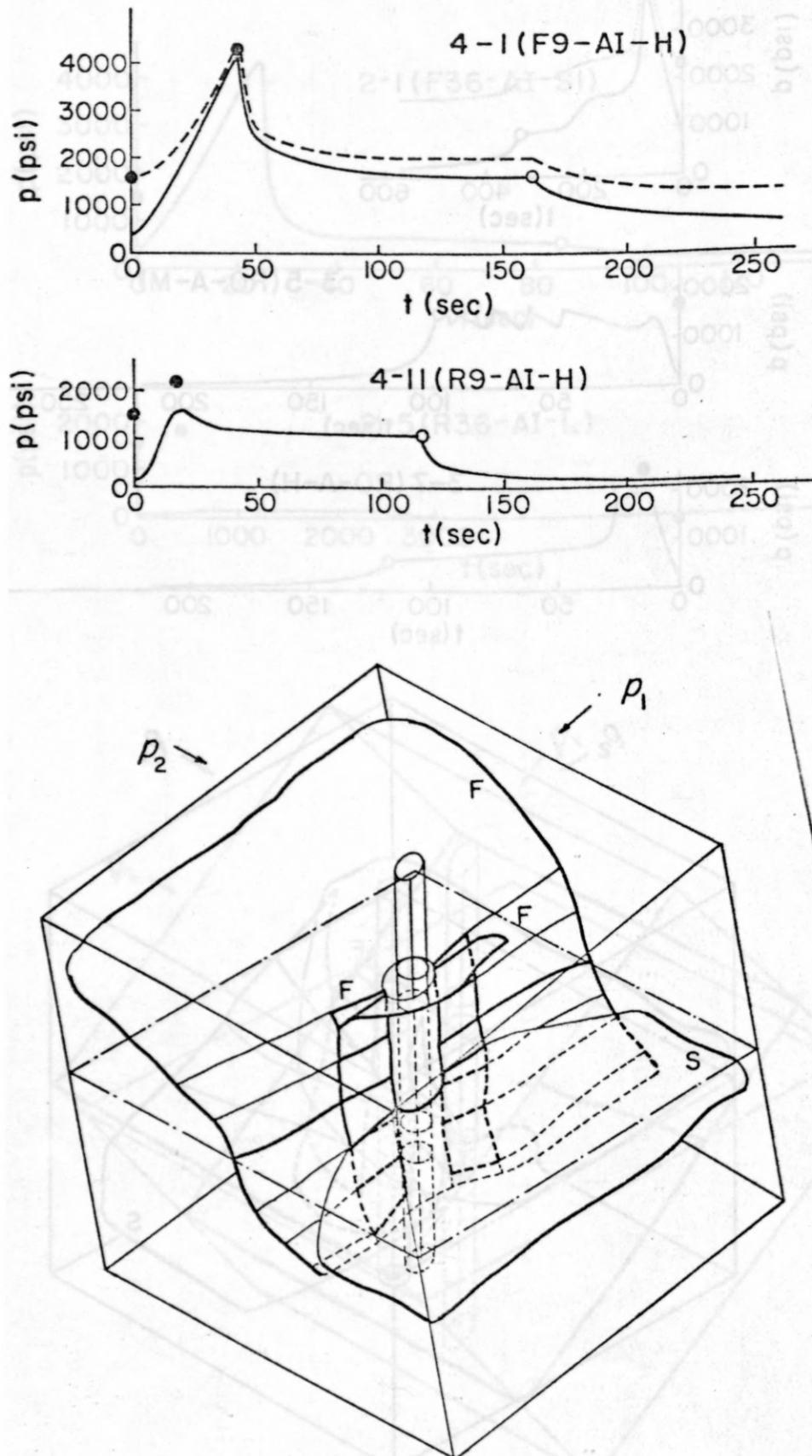


Figure 4.6.6 (4) The fracture trace of specimen No.4

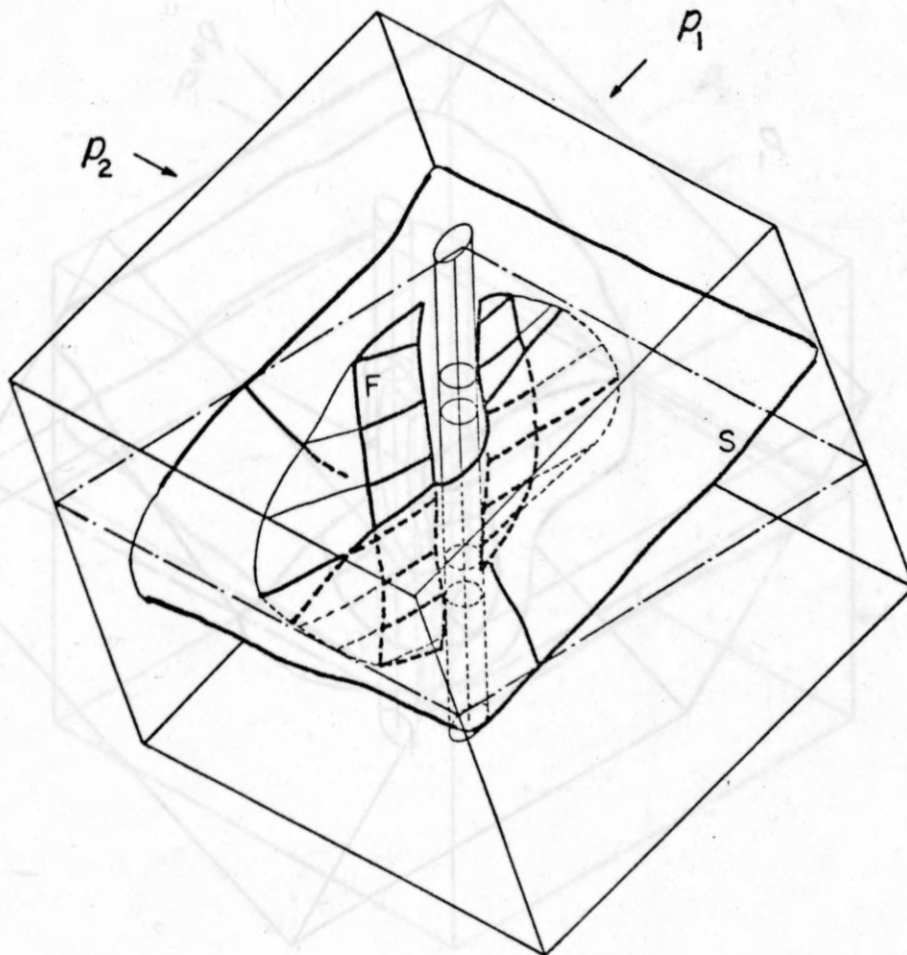
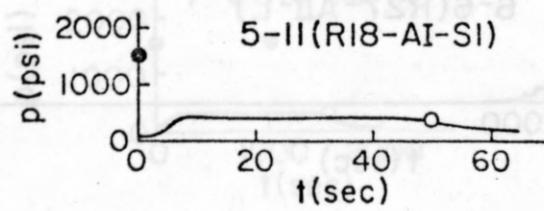
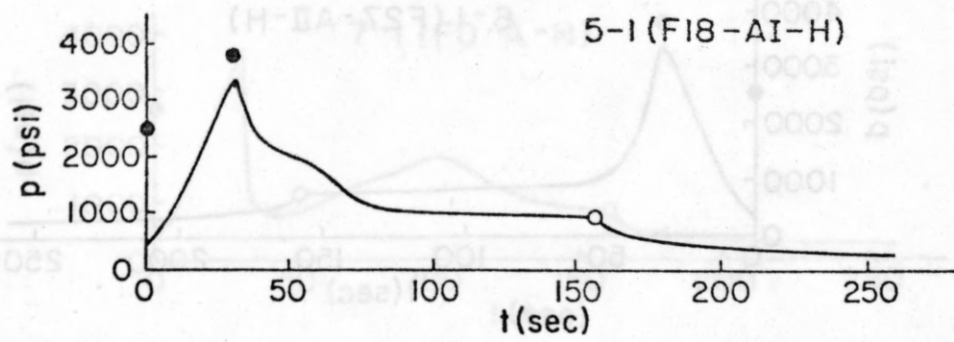


Figure 4.6.6 (5) The fracture trace of specimen No.5

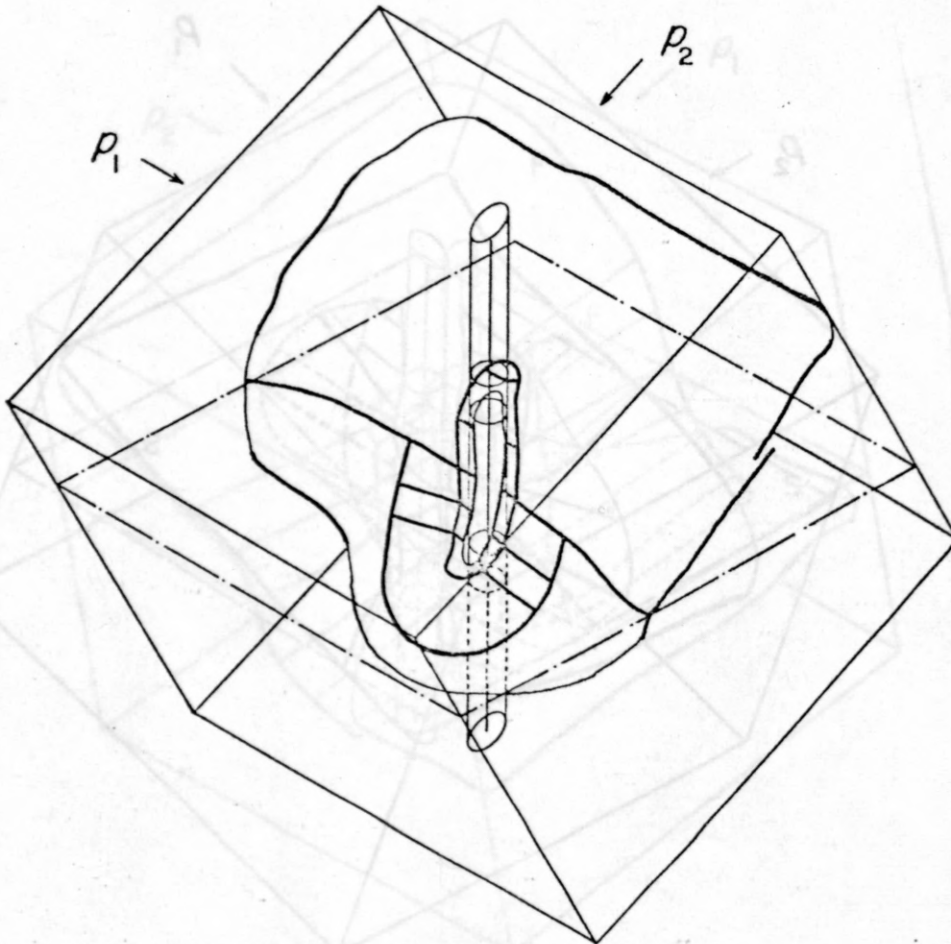
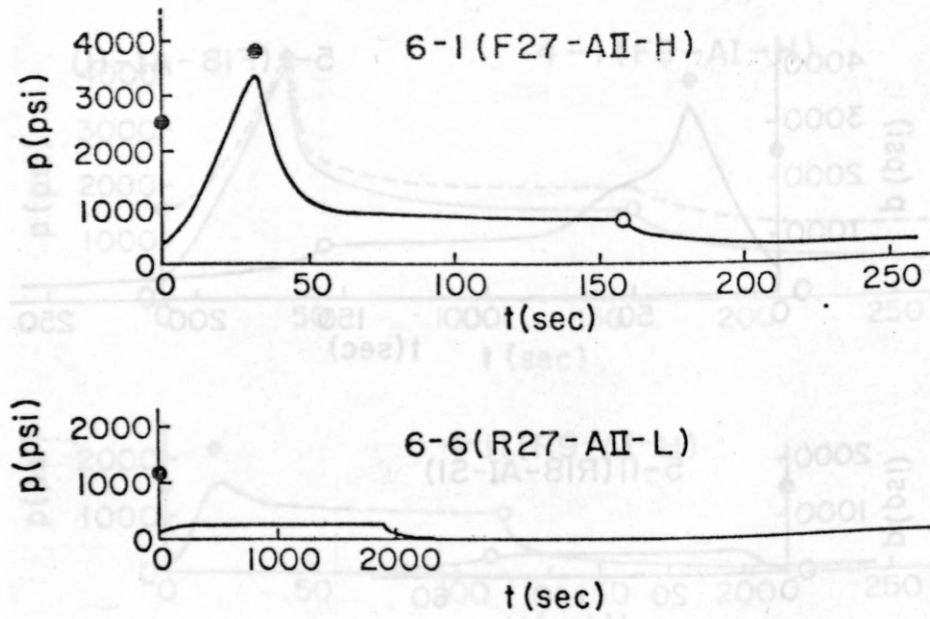


Figure 4.6.6 (6) The fracture trace of specimen No.6

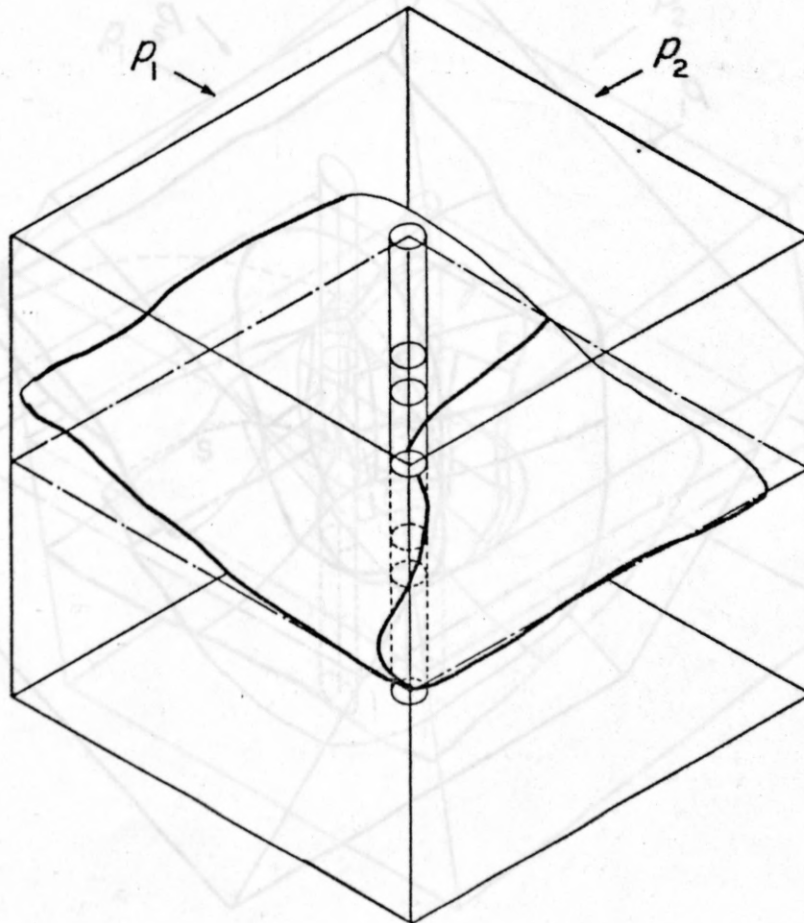
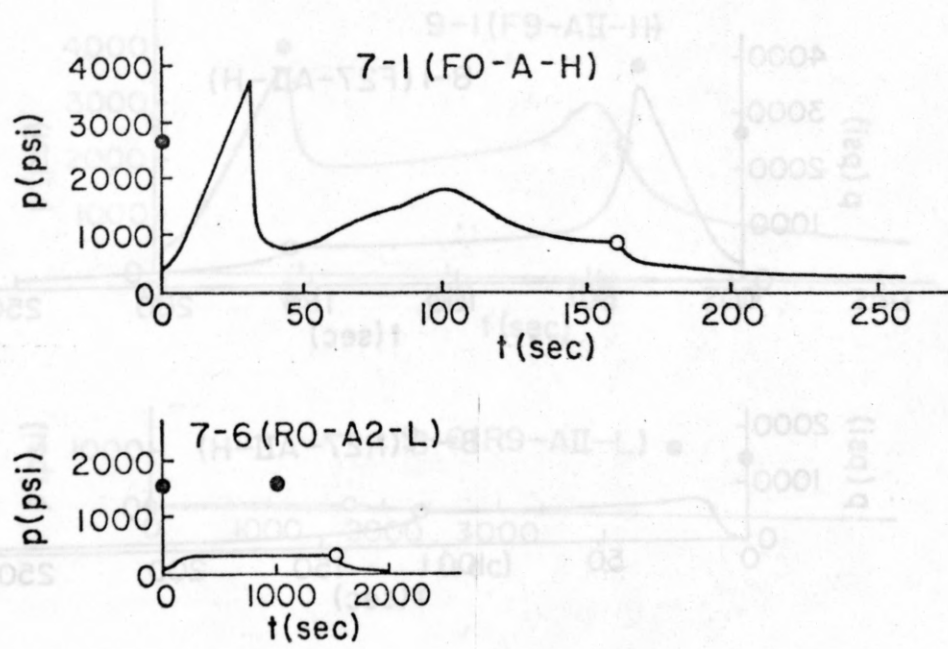


Figure 4.6.6 (7) The fracture trace of specimen No.7



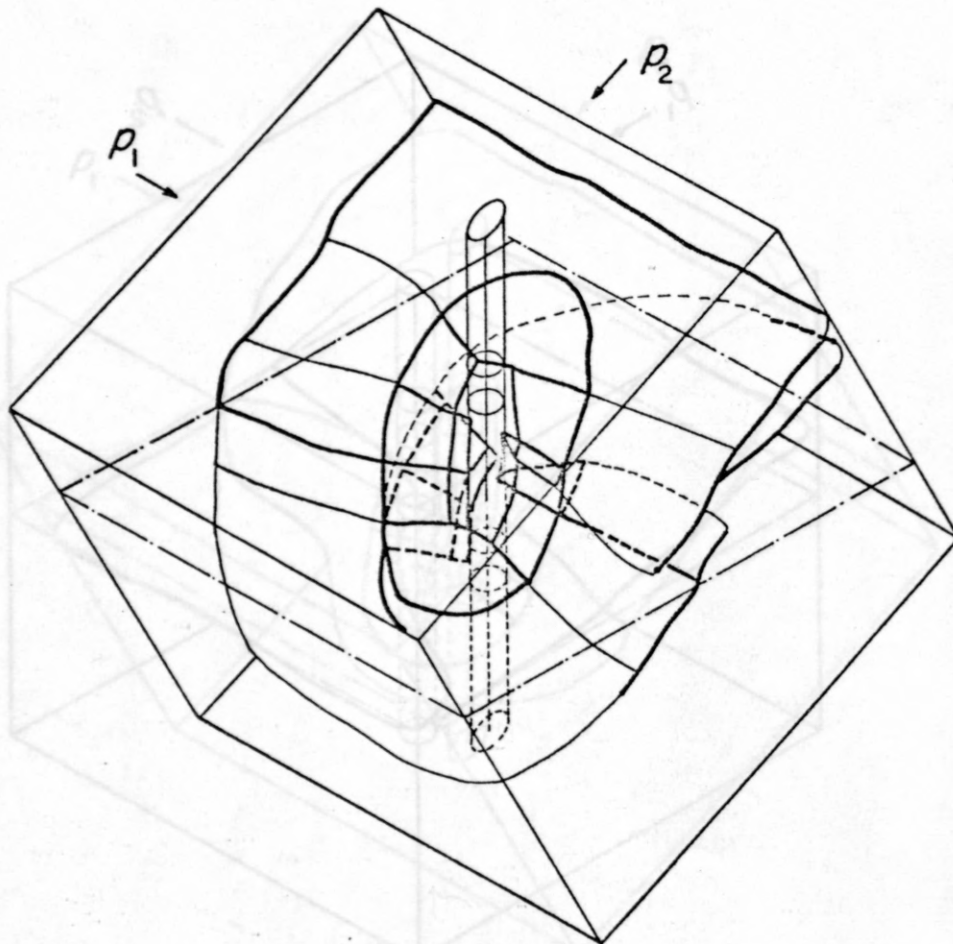
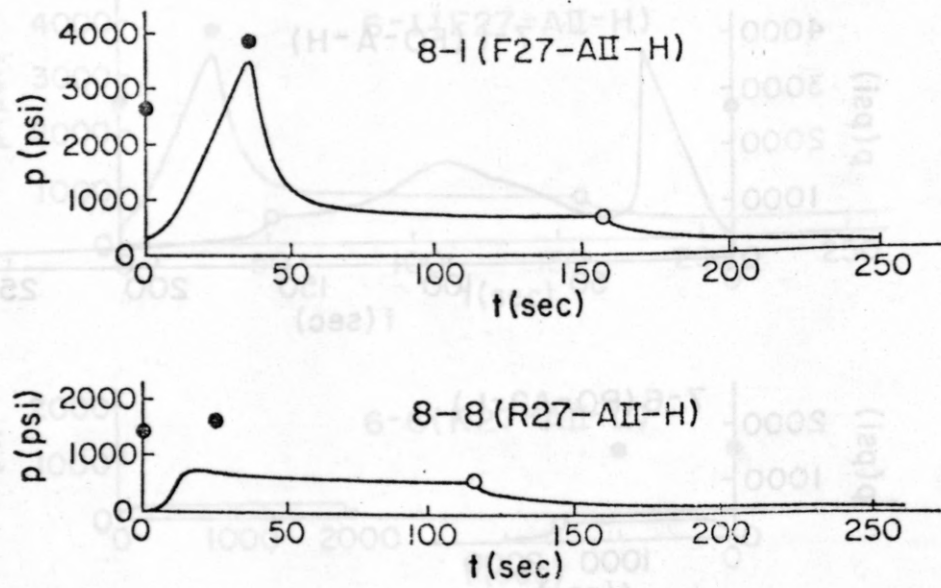


Figure 4.6.6 (8) The fracture trace of specimen No. 8

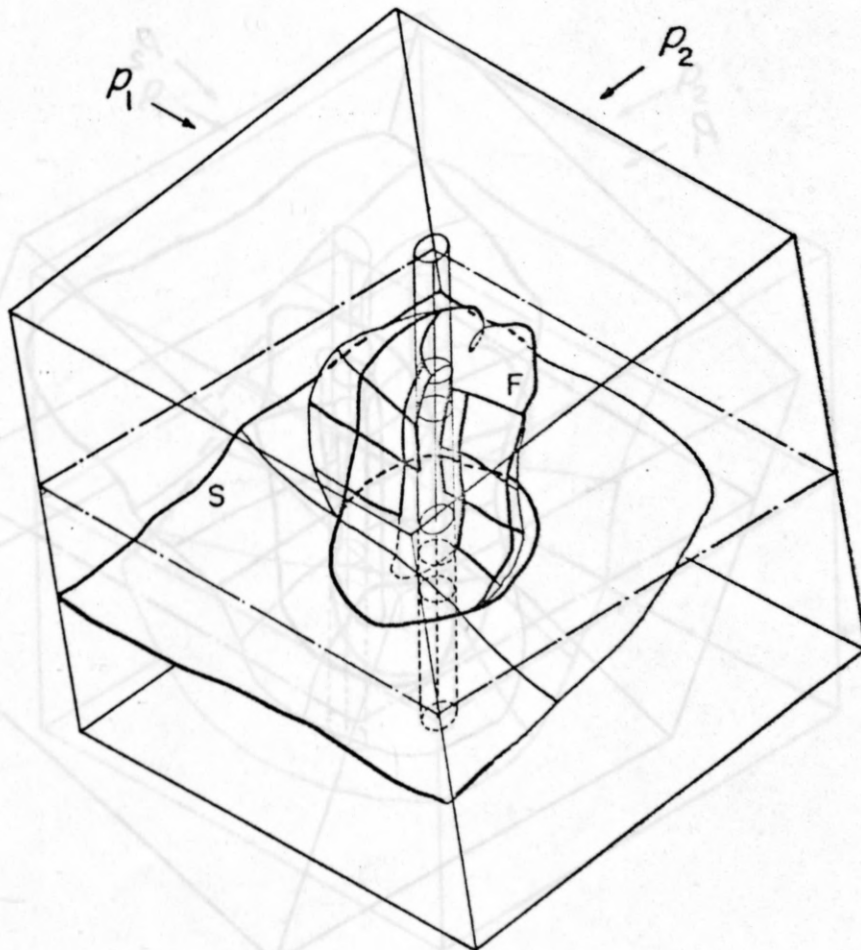
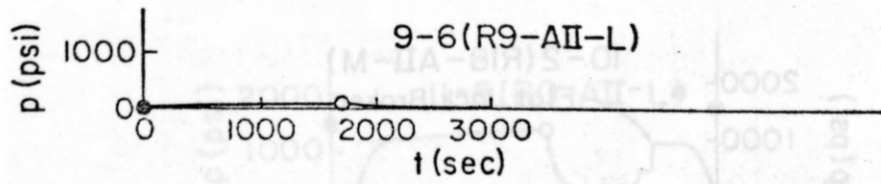
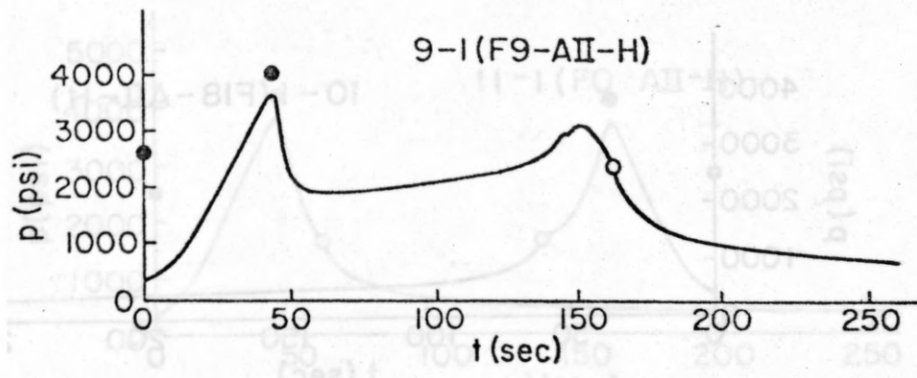


Figure 4.6.6 (9) The fracture trace of specimen No.9

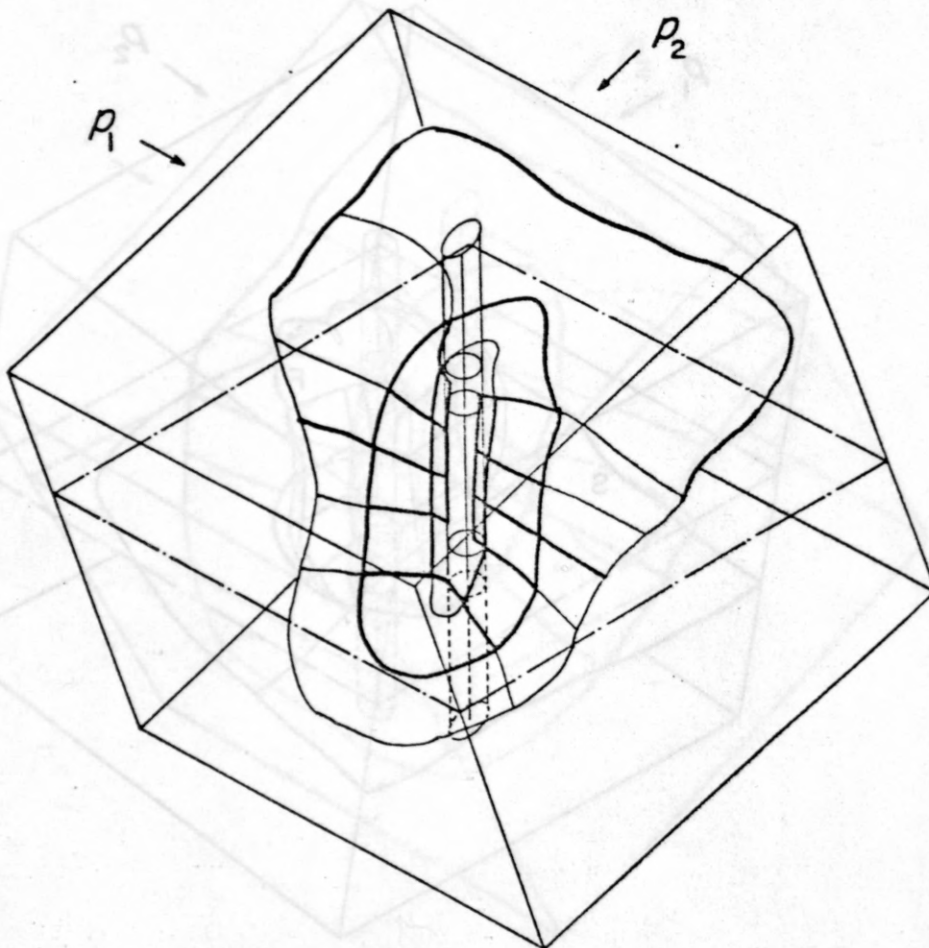
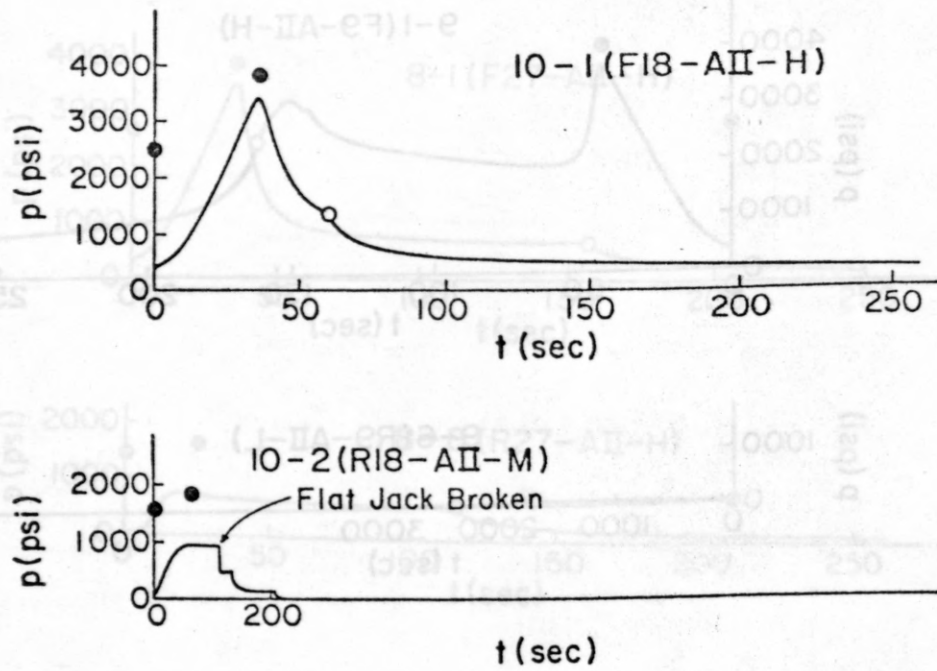


Figure 4.6.6 (10) The fracture trace of specimen No.10

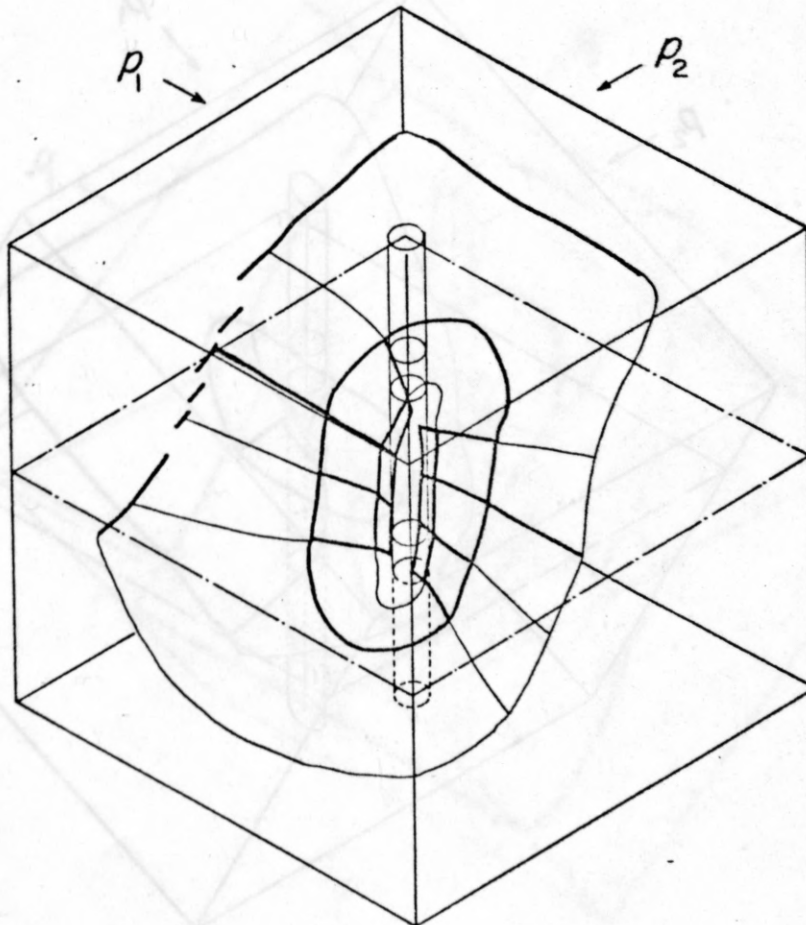
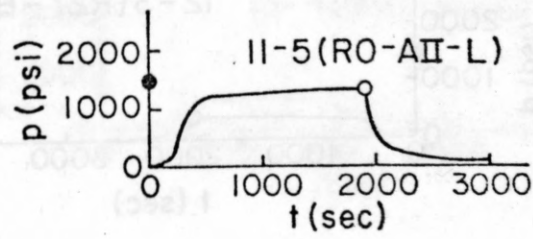
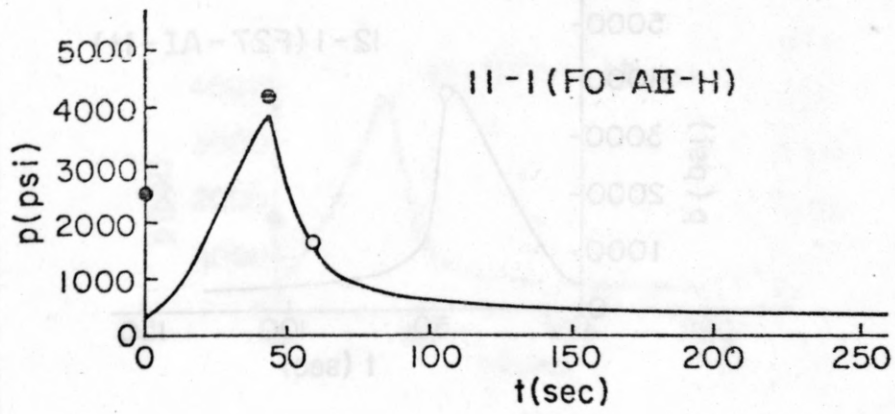


Figure 4.6.6 (11) The fracture trace of specimen No. 11

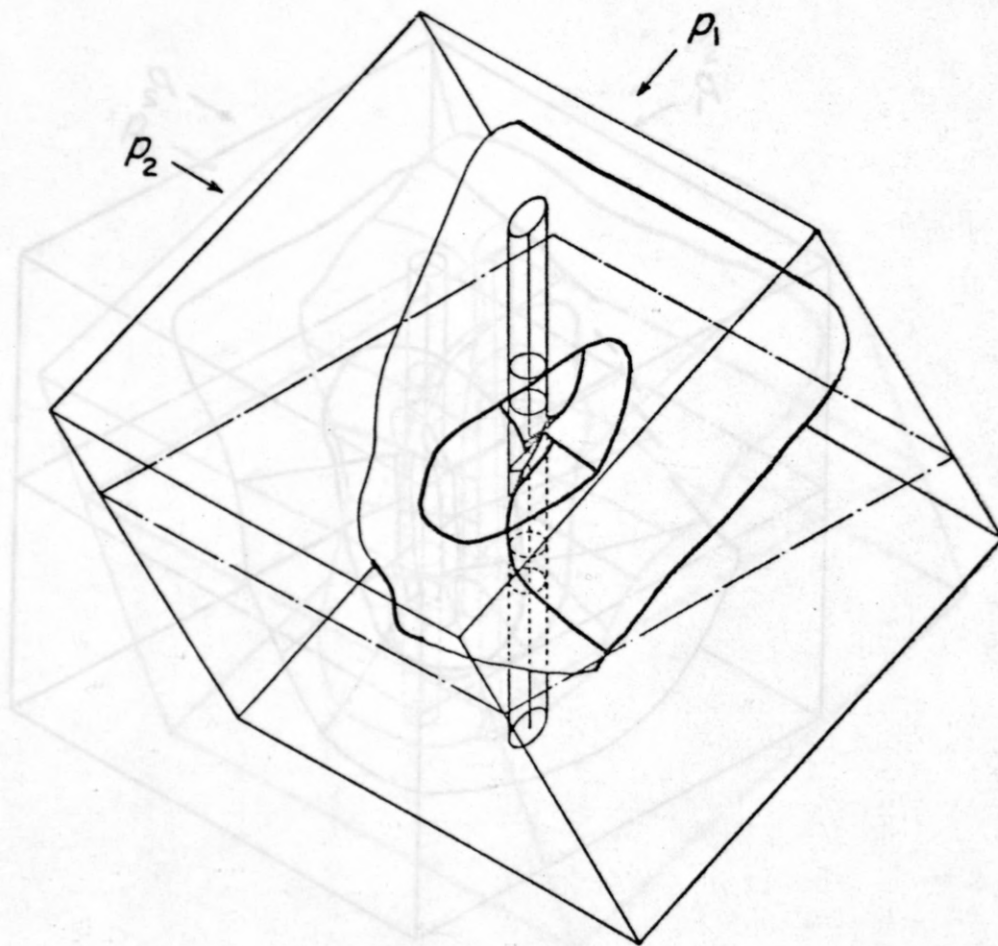
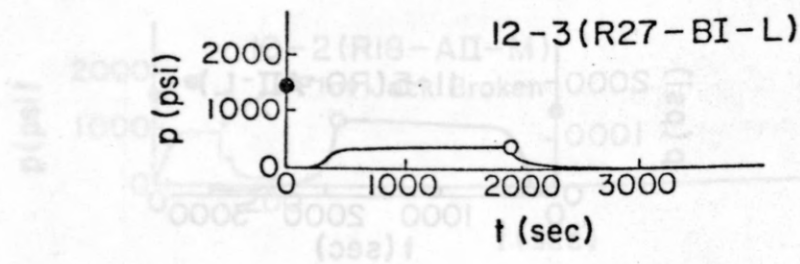
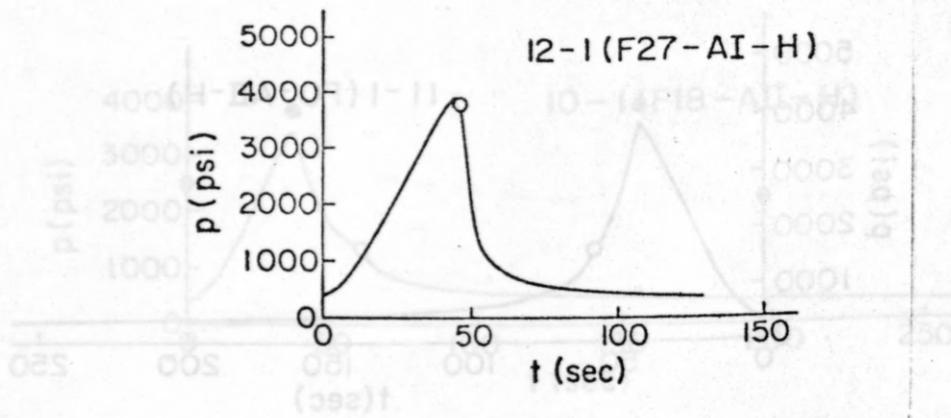


Figure 4.6.6 (12) The fracture trace of specimen No.12



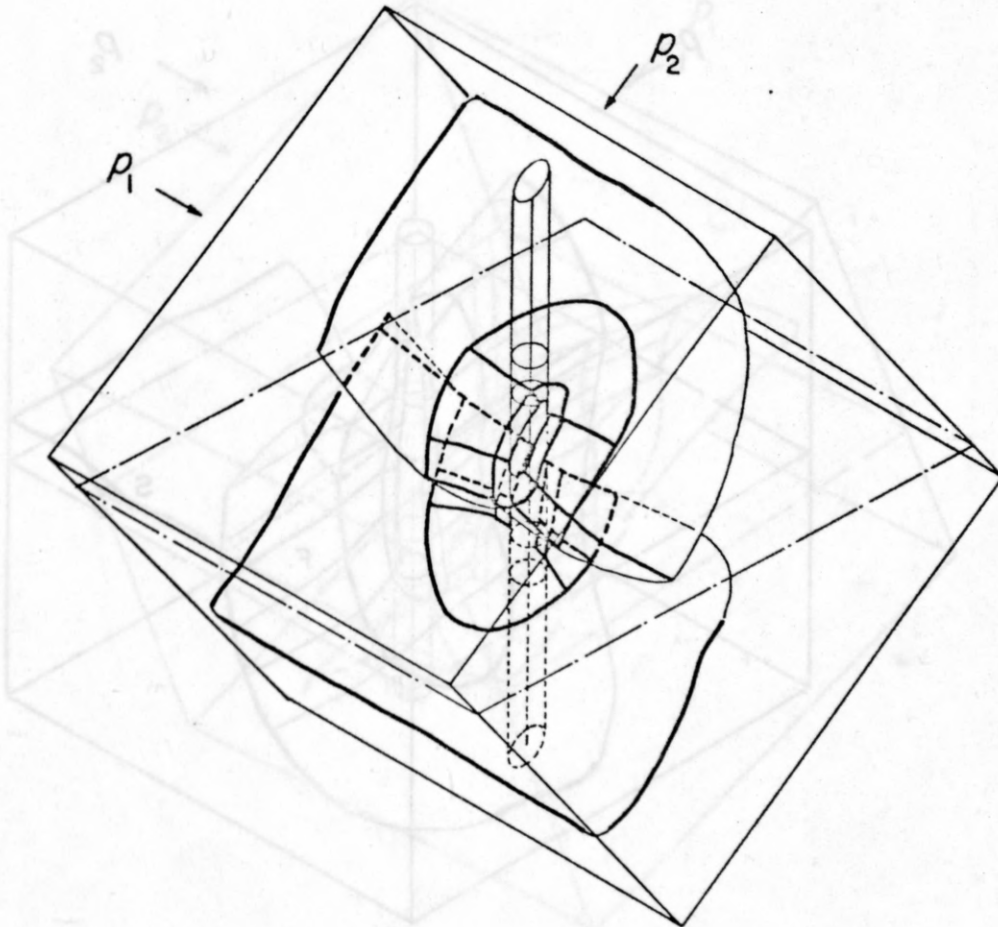
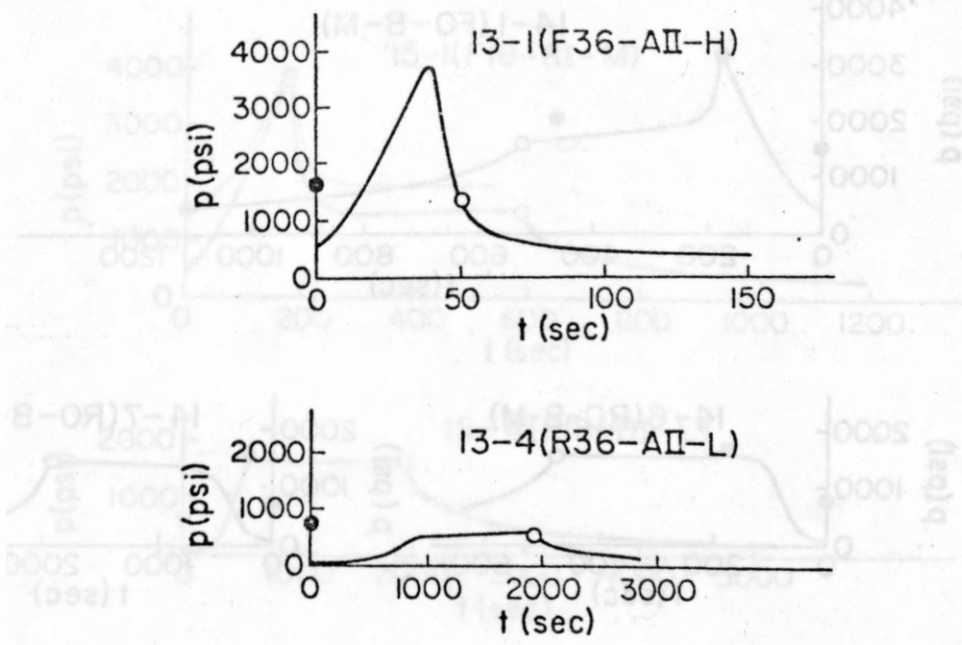


Figure 4.6.6 (13) The fracture trace of specimen No.13

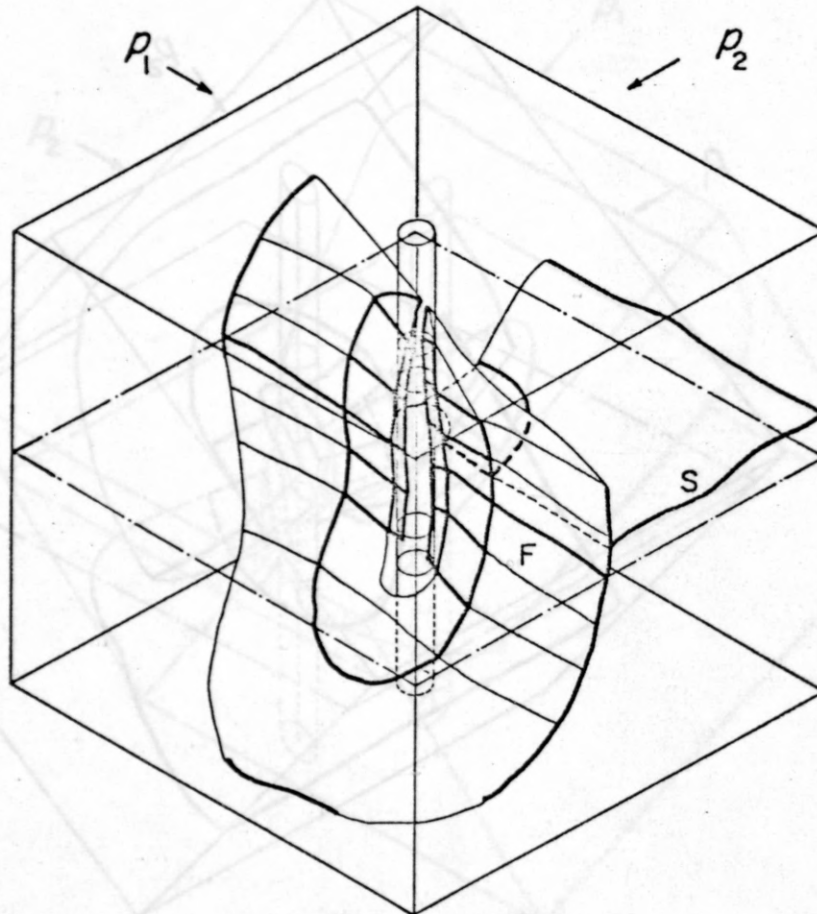
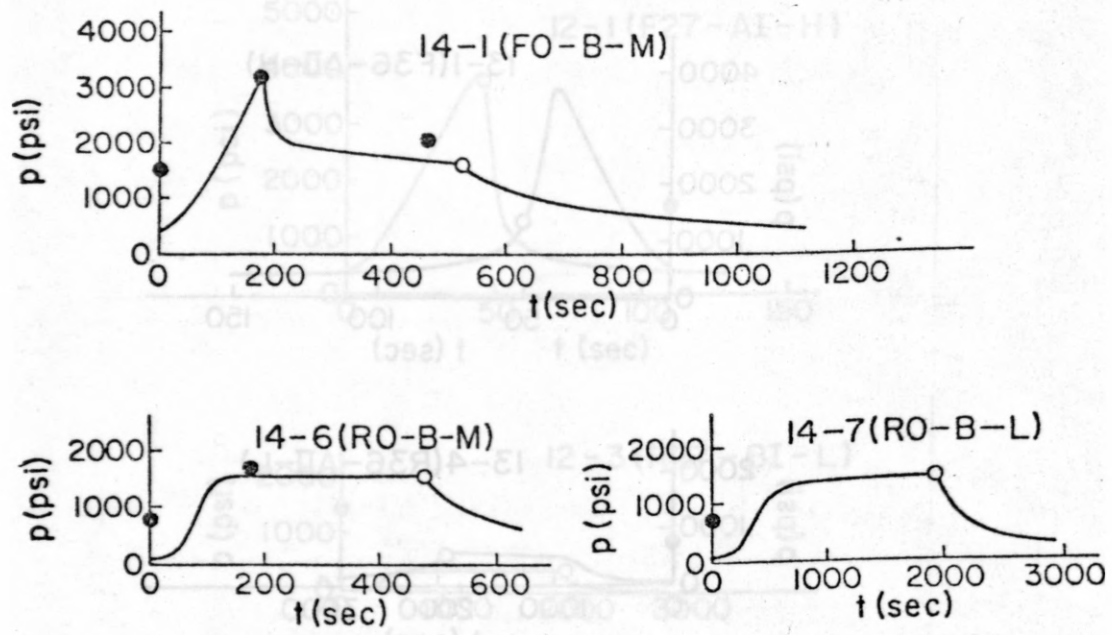


Figure 4.6.6 (14) The fracture trace of specimen No.14

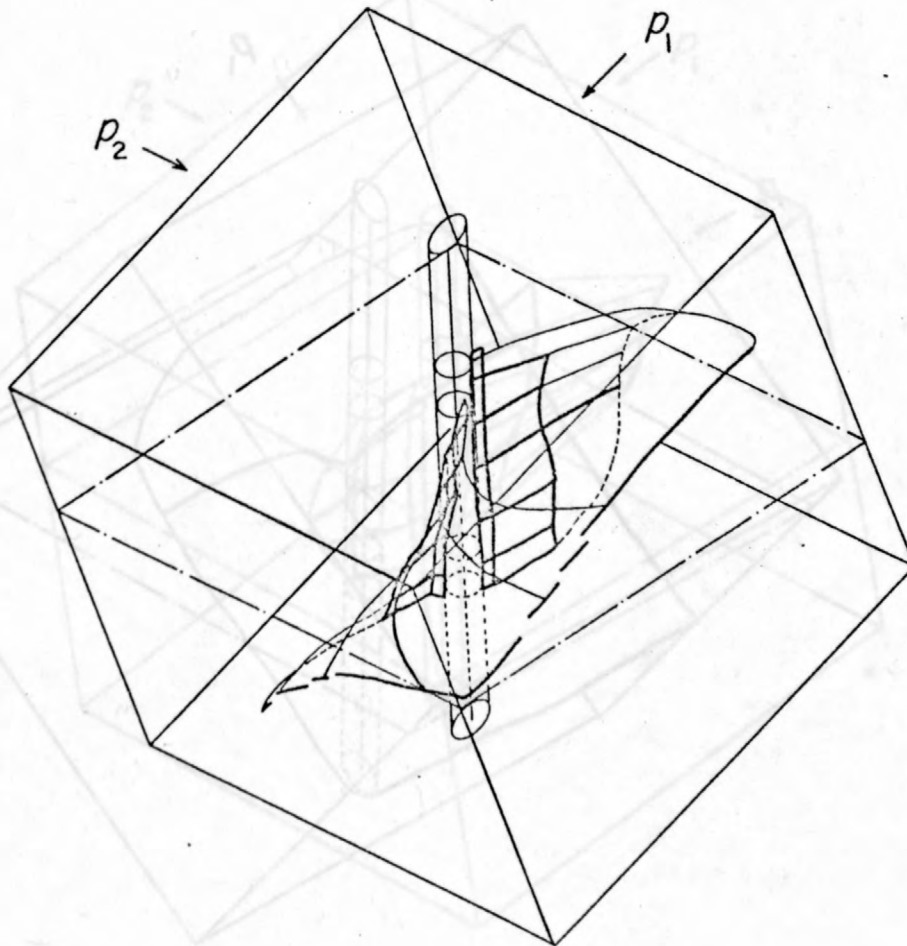
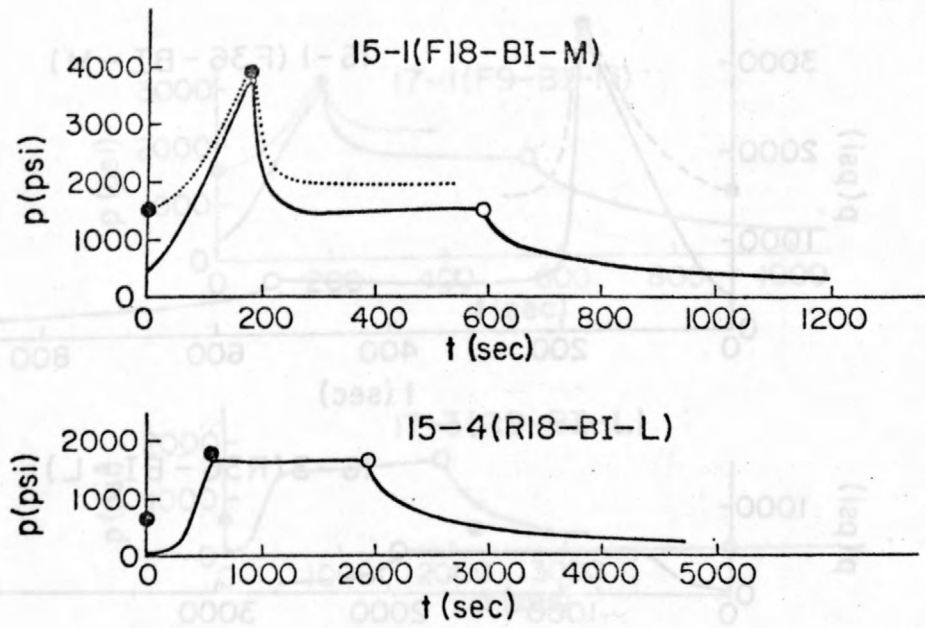


Figure 4.6.6 (15) The fracture trace of specimen No.15

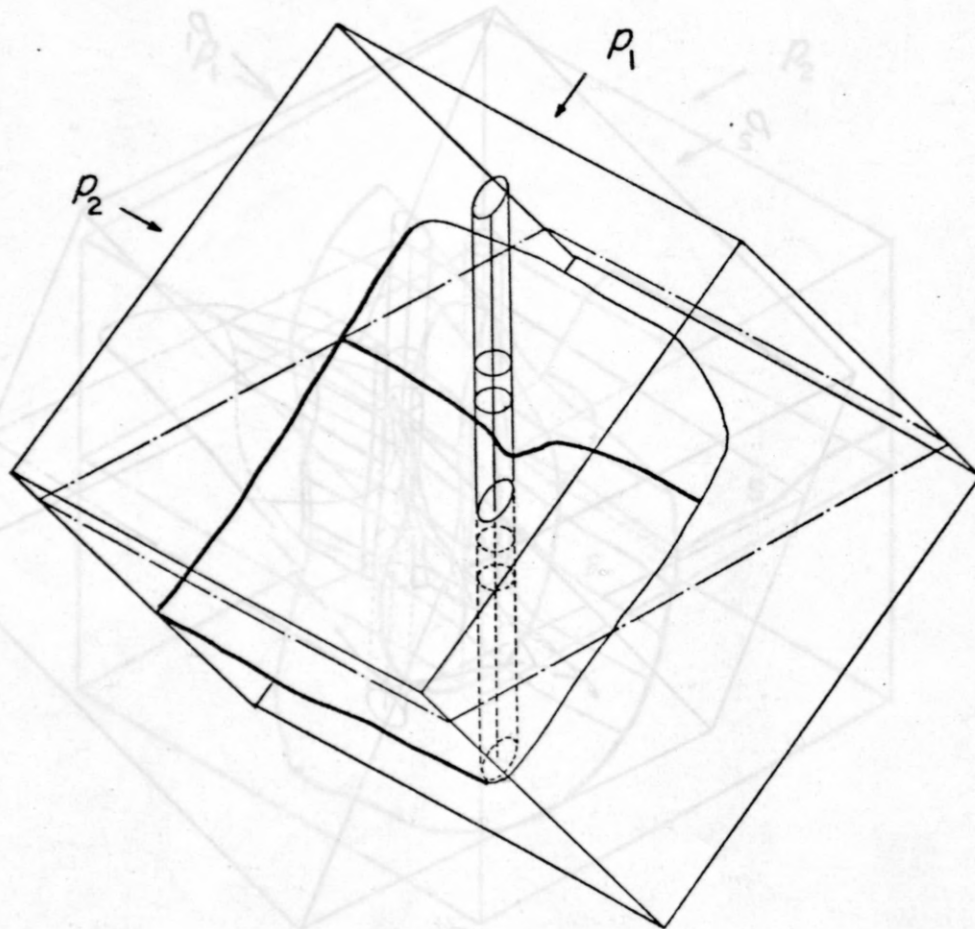
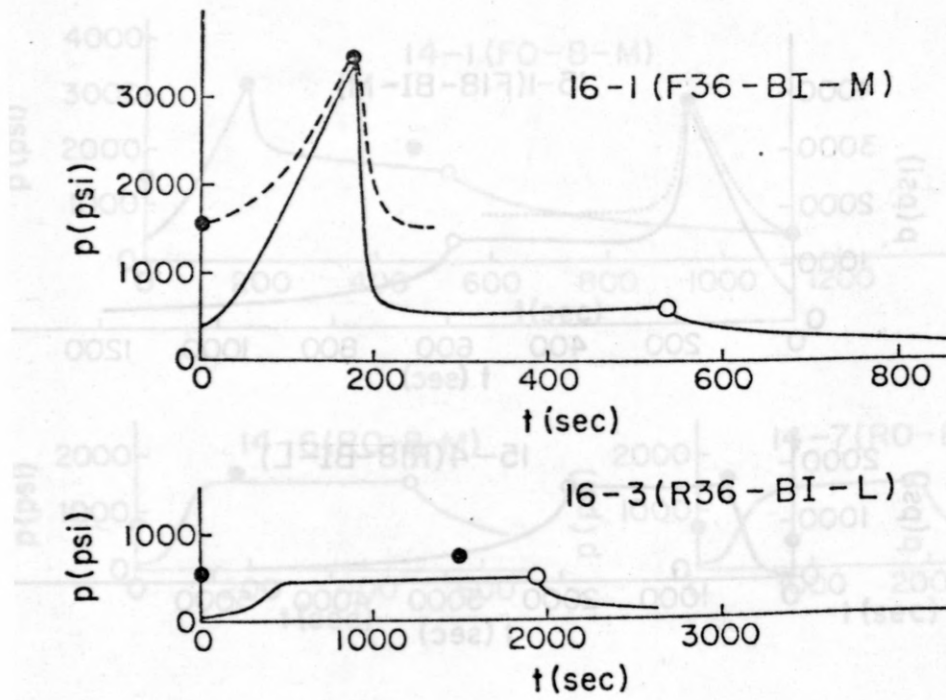


Figure 4.6.6 (16) The fracture trace of specimen No.16

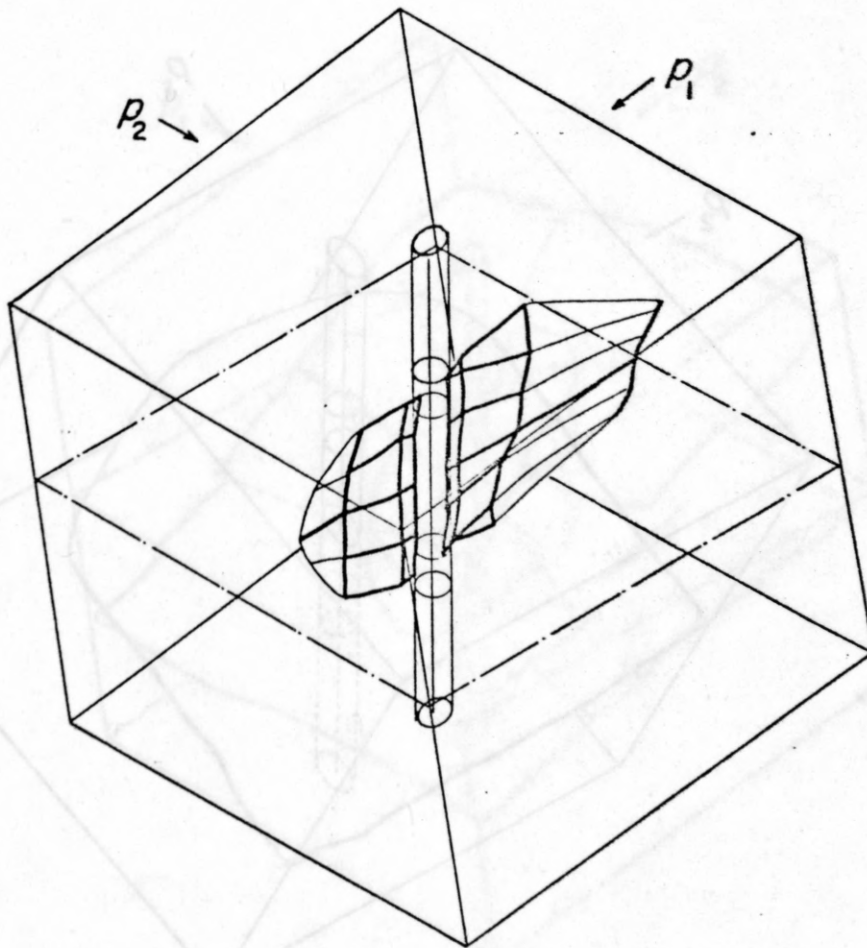
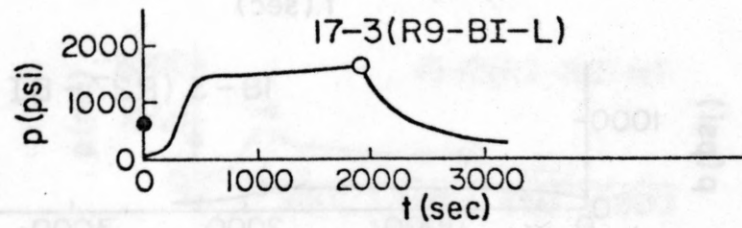
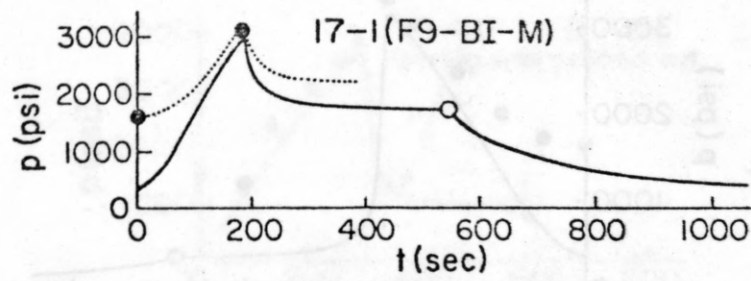


Figure 4.6.6 (17) The fracture trace of specimen No.17



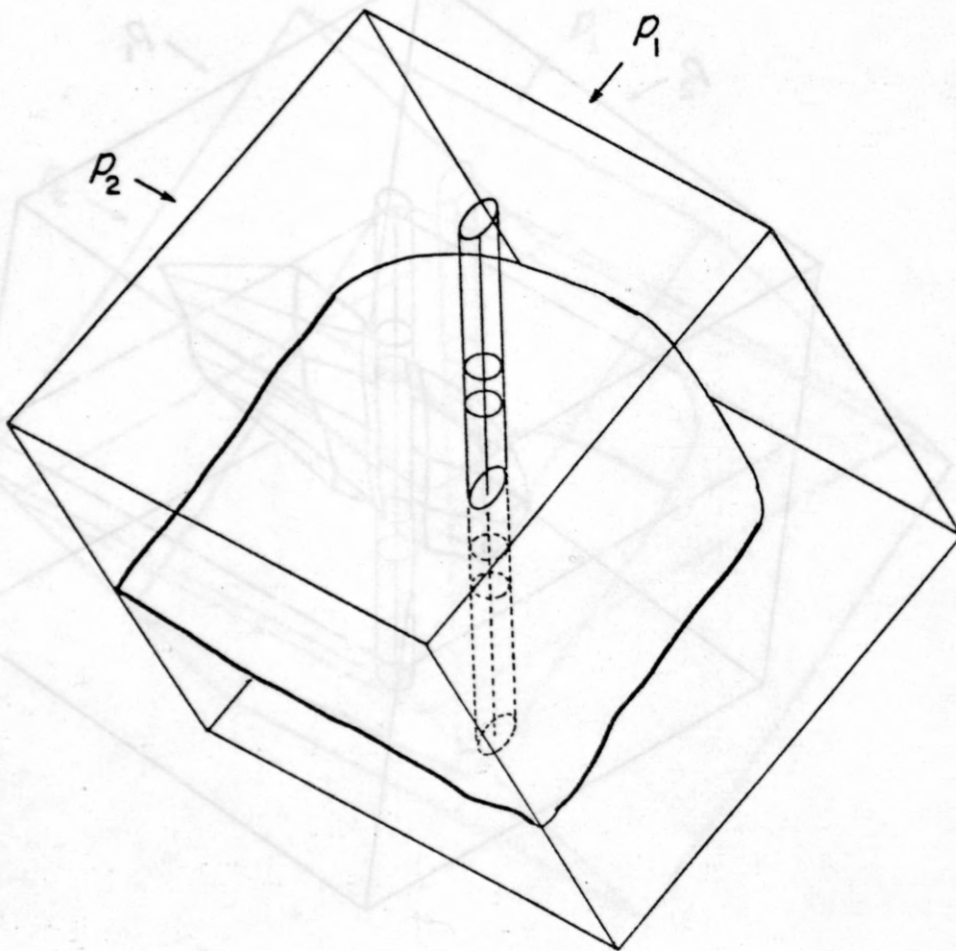
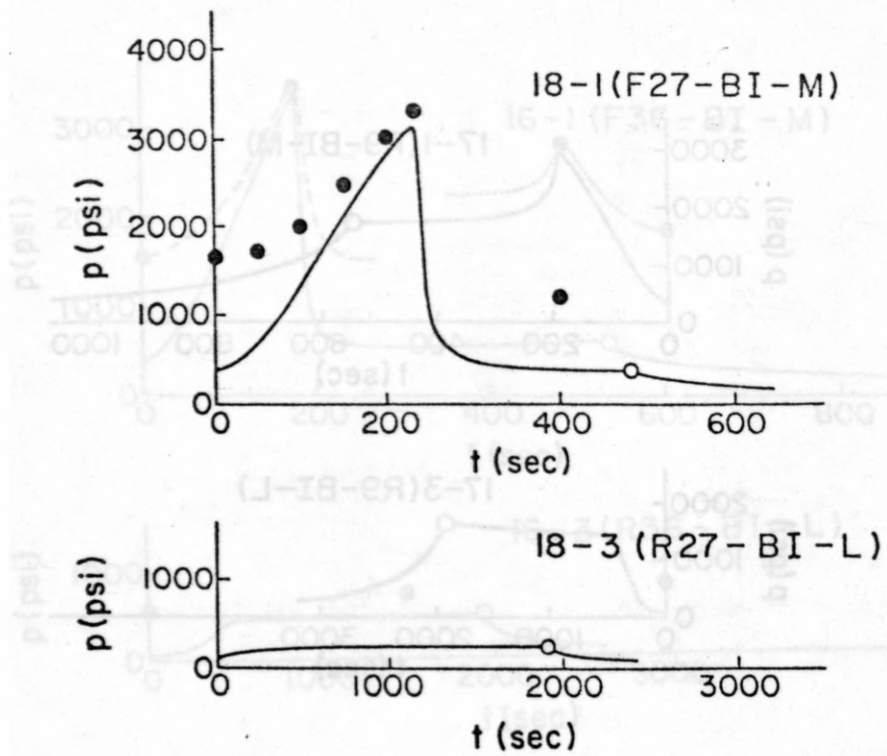


Figure 4.6.6 (18) The fracture trace of specimen No.18

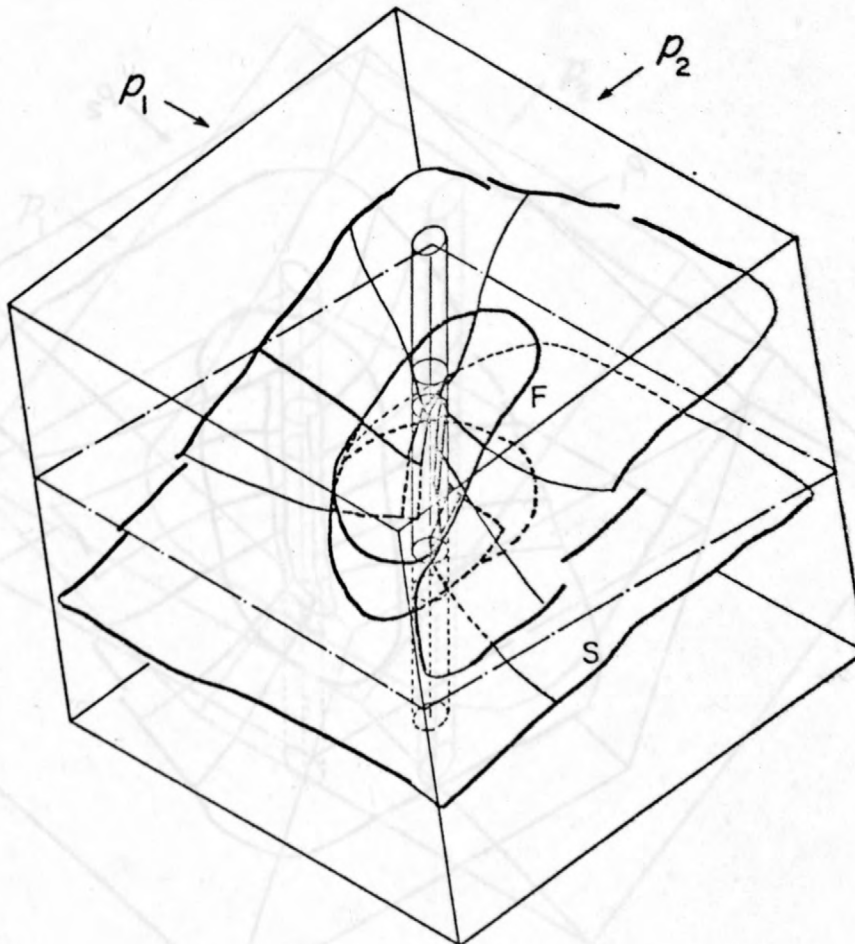
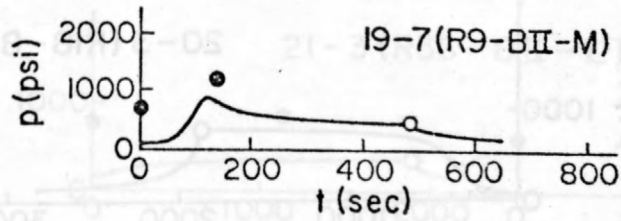
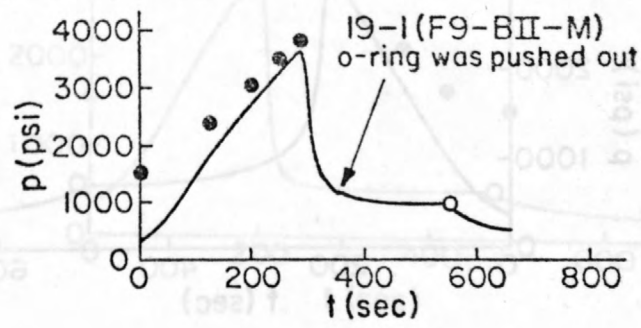


Figure 4.6.6 (19) The fracture trace of specimen No. 19

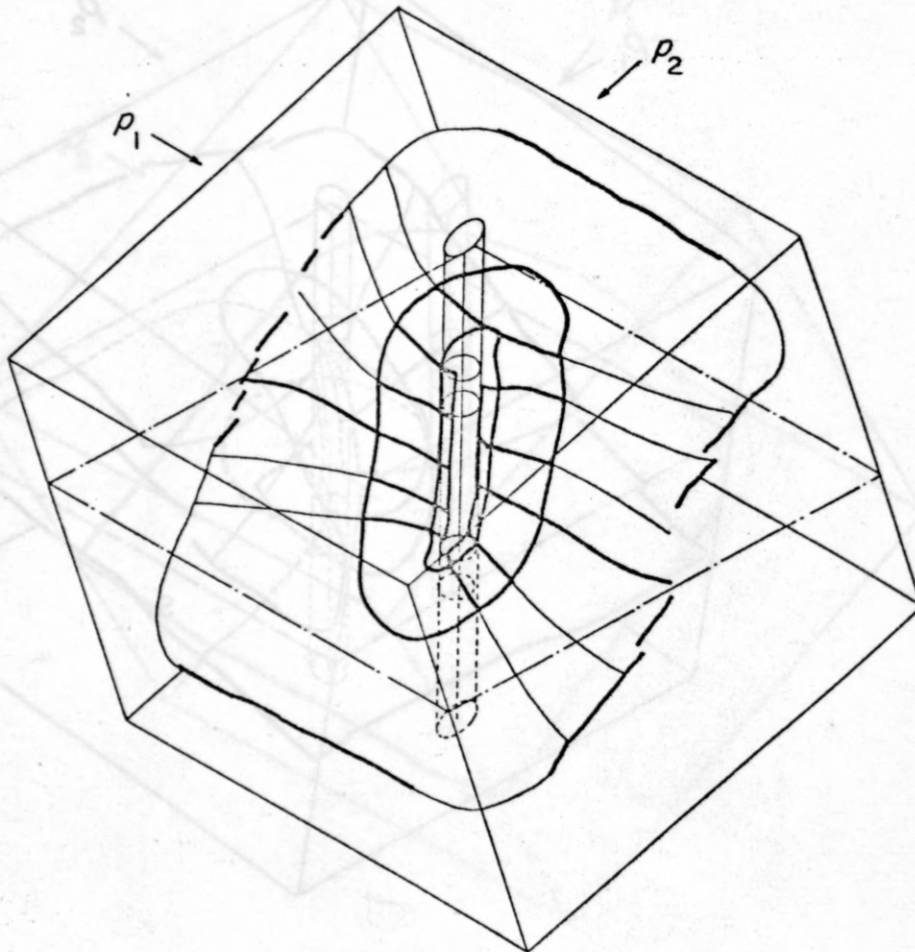
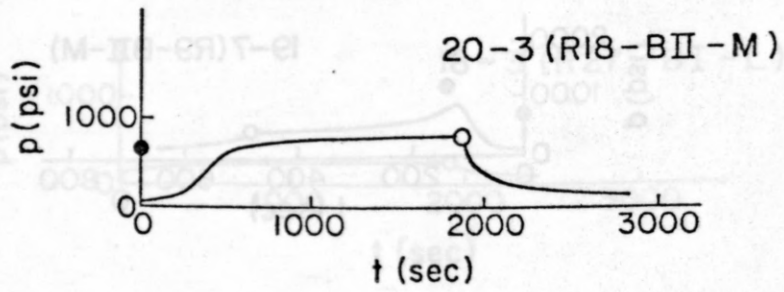
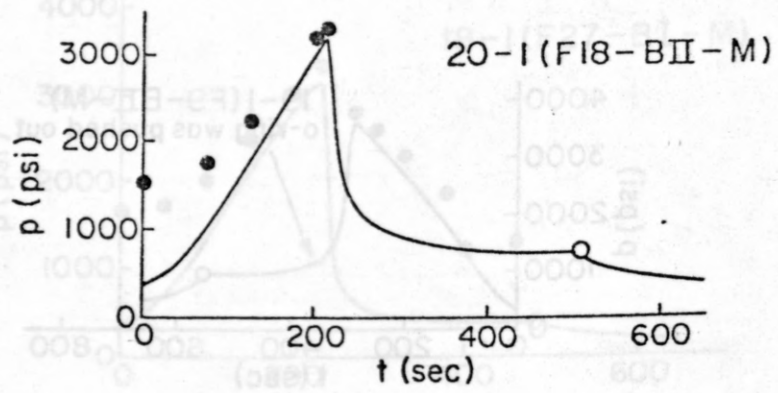


Figure 4.6.6 (20) The fracture trace of specimen No.20

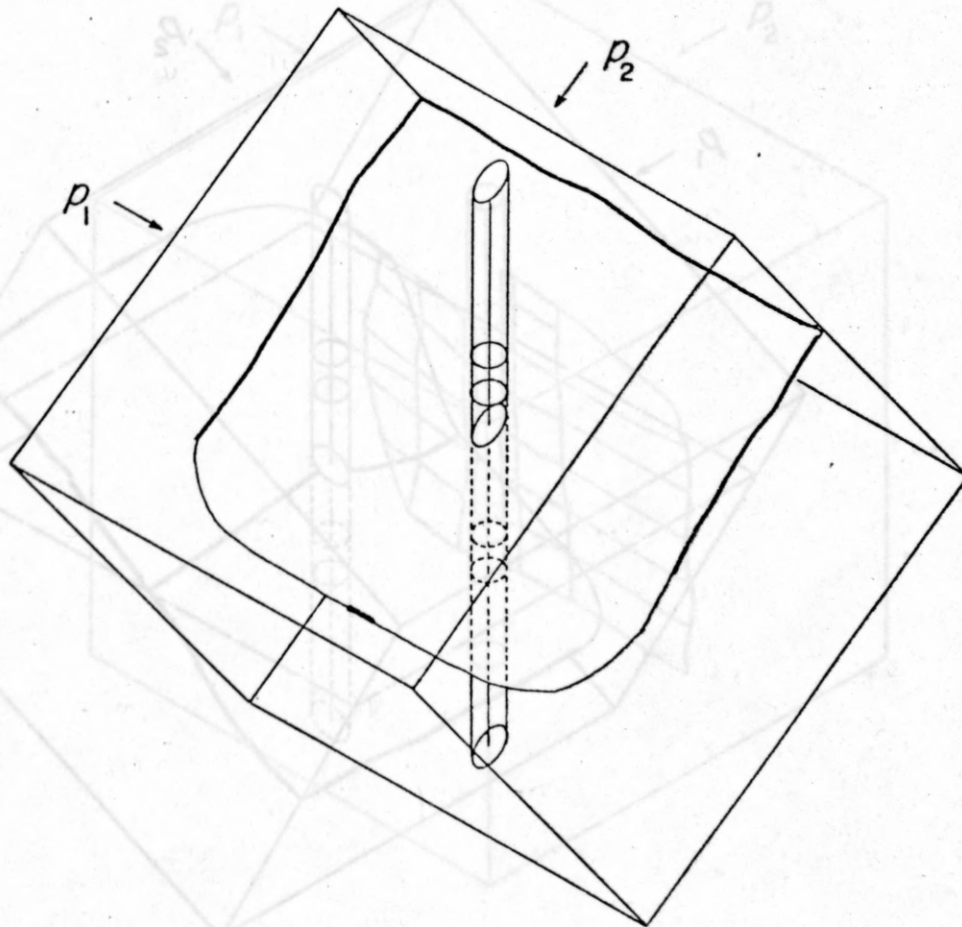
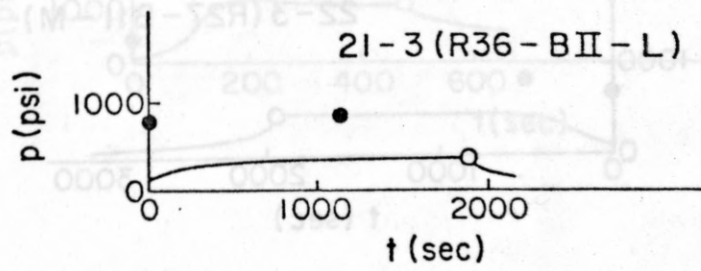
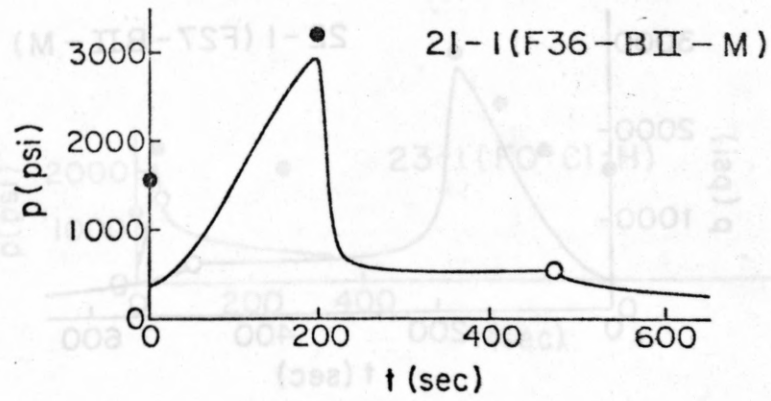


Figure 4.6.6 (21) The fracture trace of specimen No.21

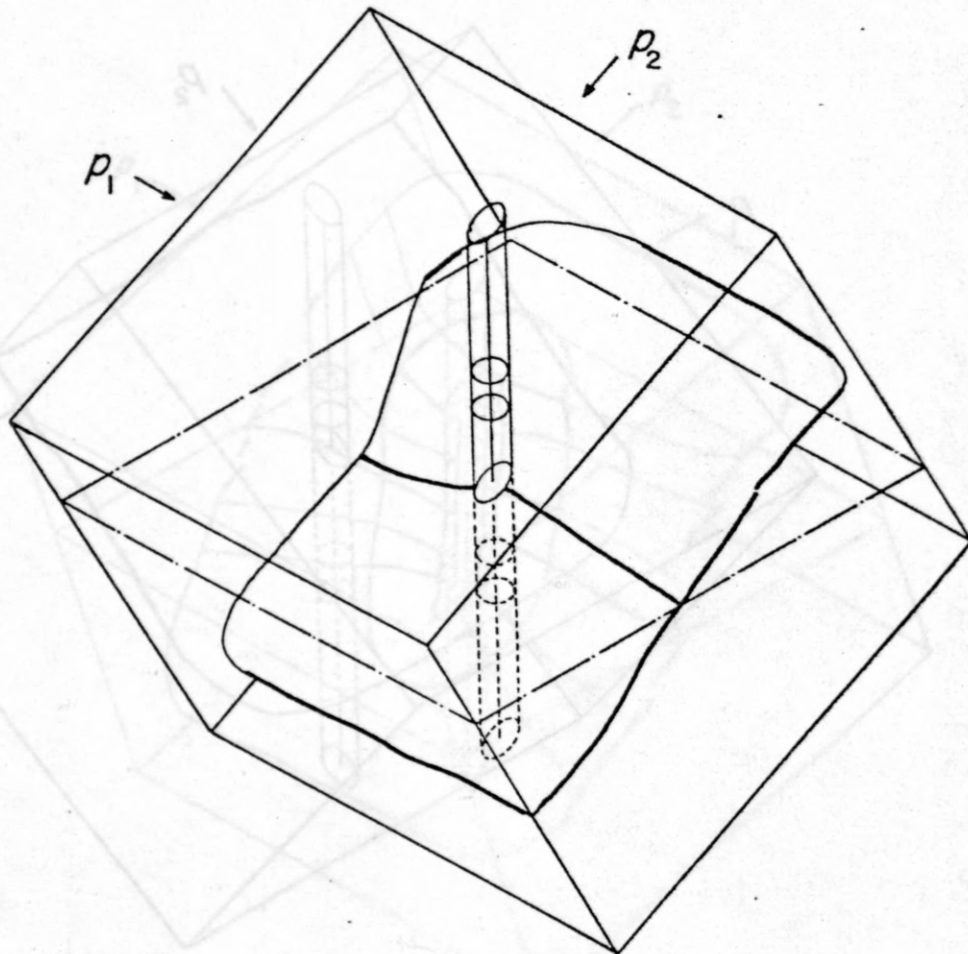
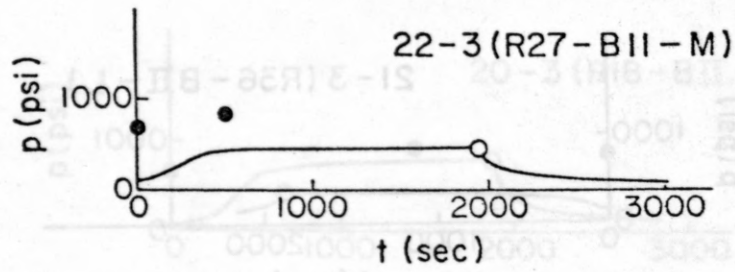
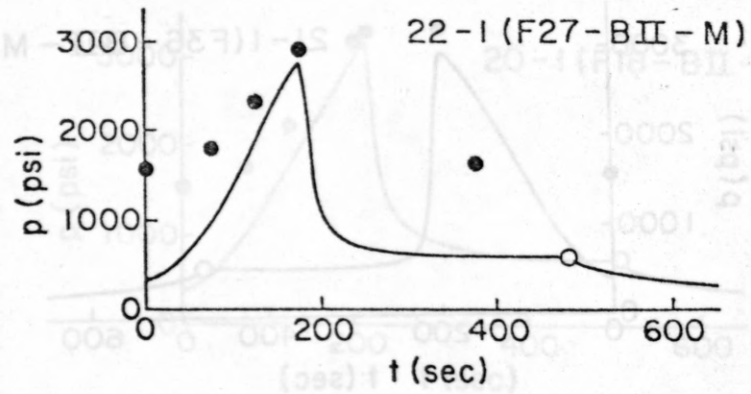


Figure 4.6.6 (22) The fracture trace of specimen No.22



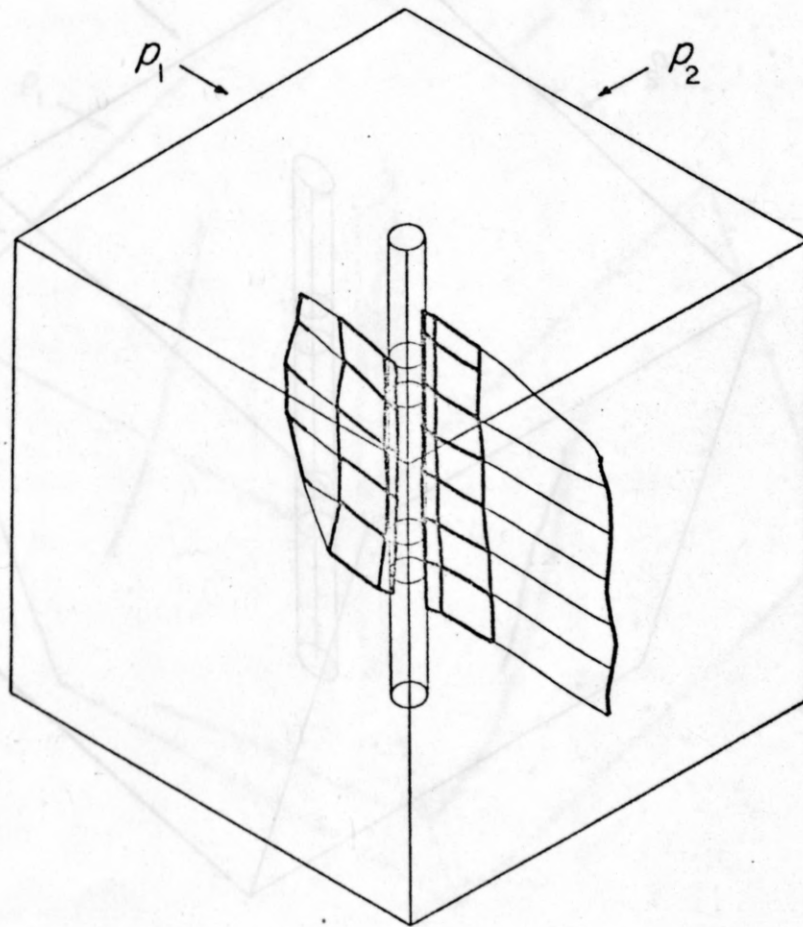
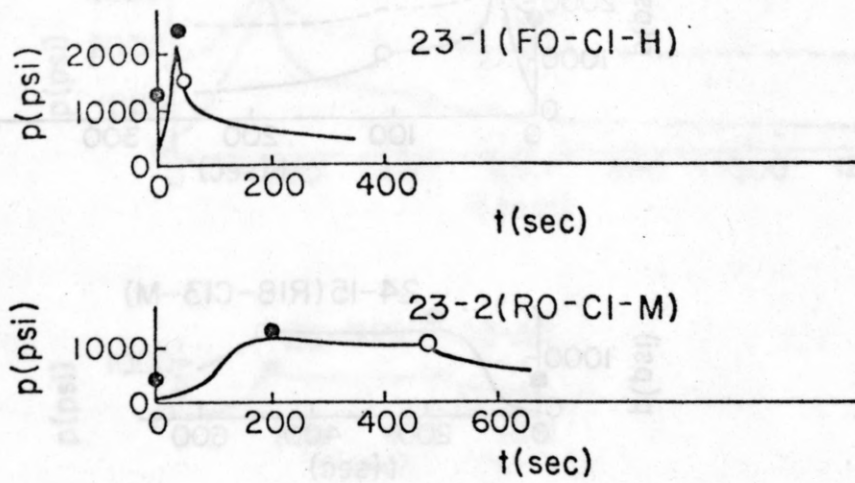


Figure 4.6.6 (23) The fracture trace of specimen No.23

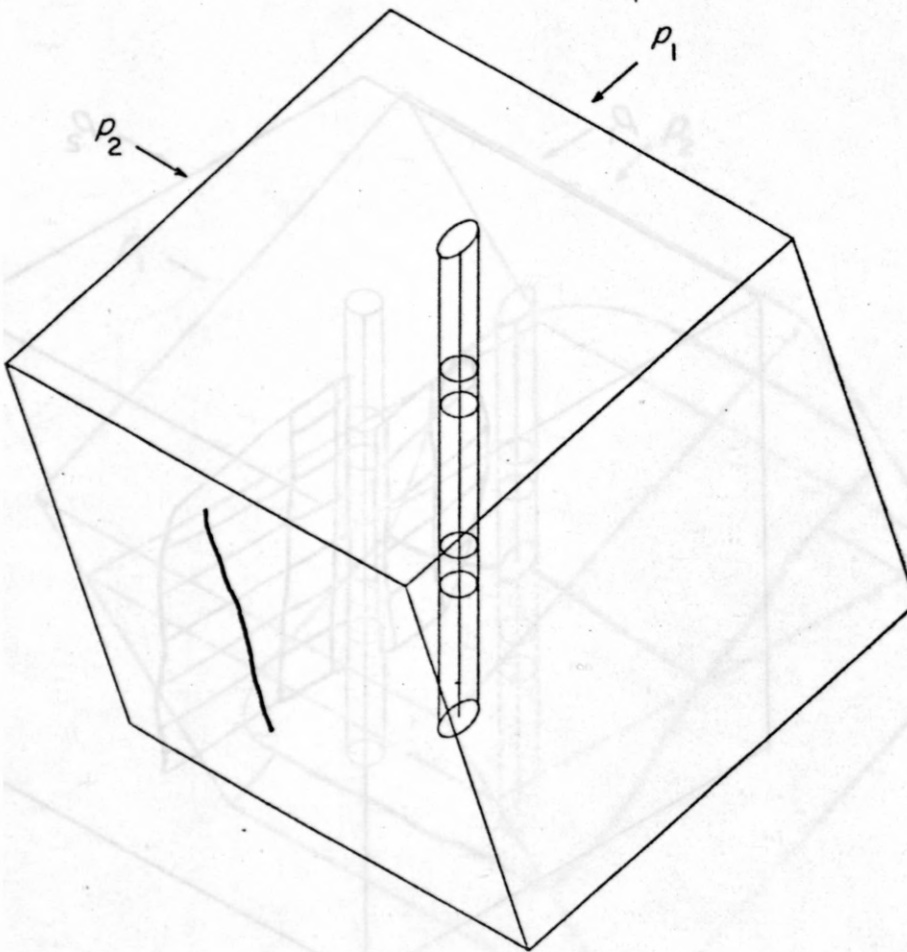
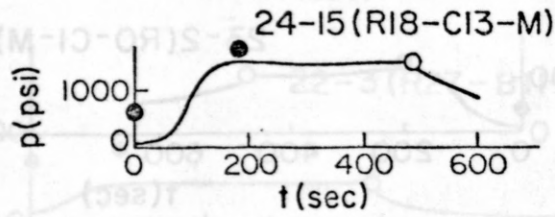
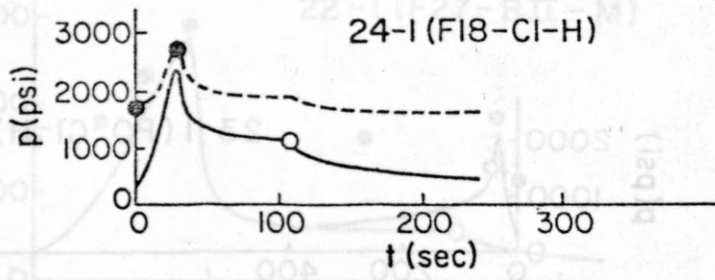


Figure 4.6.6 (24) The fracture trace of specimen No.24

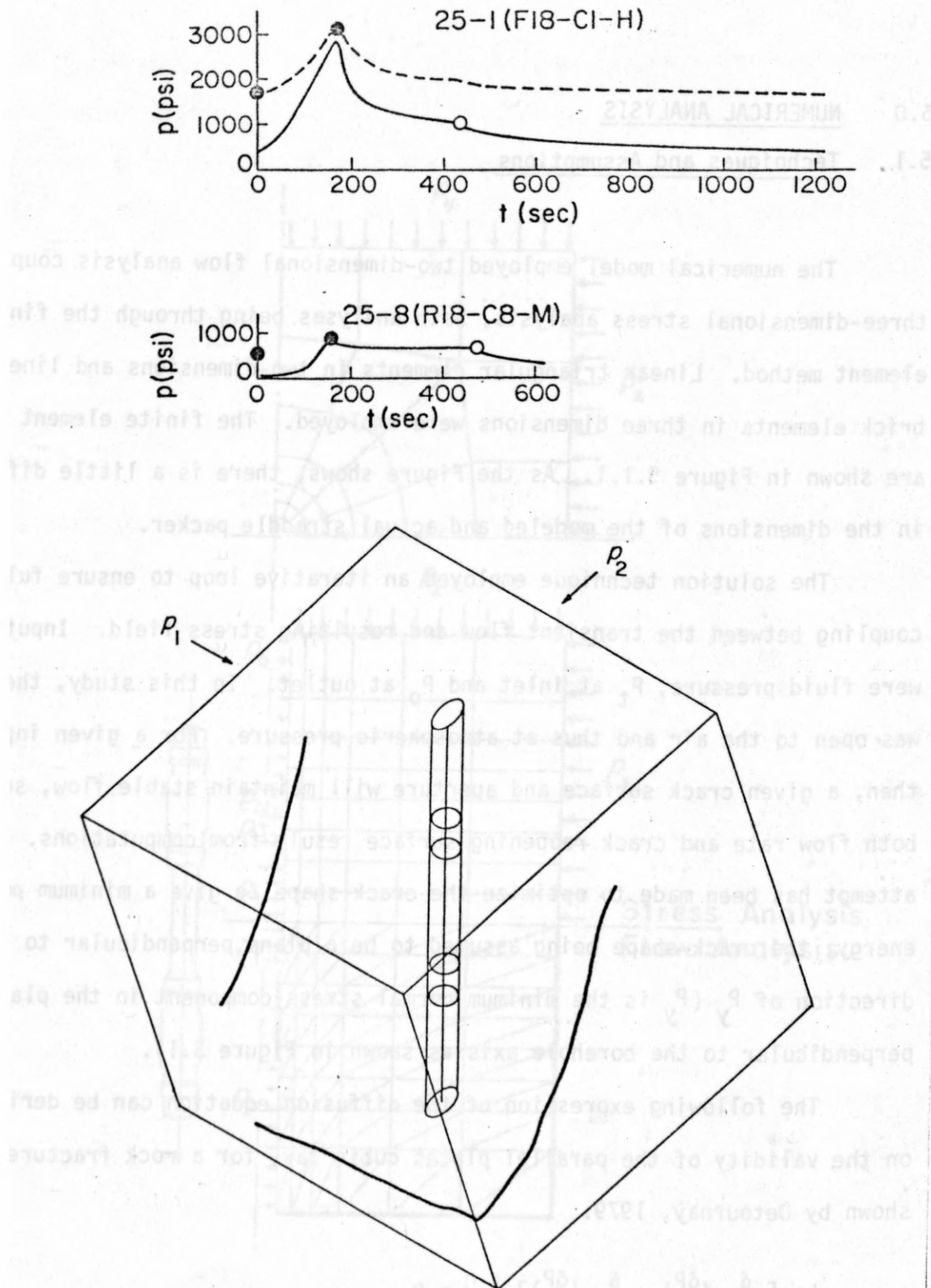


Figure 4.6.6 (25) The fracture trace of specimen No. 25

## 5.0 NUMERICAL ANALYSIS

### 5.1 Techniques and Assumptions

The numerical model employed two-dimensional flow analysis coupled with three-dimensional stress analysis, both analyses being through the finite element method. Linear triangular elements in two-dimensions and linear brick elements in three dimensions were employed. The finite element meshes are shown in Figure 5.1.1. As the Figure shows, there is a little difference in the dimensions of the modeled and actual straddle packer.

The solution technique employed an iterative loop to ensure full coupling between the transient flow and resulting stress field. Input parameters were fluid pressure,  $P_t$  at inlet and  $P_o$  at outlet. In this study, the outlet was open to the air and thus at atmospheric pressure. For a given input pressure then, a given crack surface and aperture will maintain stable flow, so that both flow rate and crack reopening surface result from computations. No attempt has been made to optimize the crack shape to give a minimum potential energy, the crack shape being assumed to be a plane perpendicular to the direction of  $P_y$  ( $P_y$  is the minimum normal stress component in the plane perpendicular to the borehole axis as shown in Figure 3.1).

The following expression of the diffusion equation can be derived, based on the validity of the parallel plates cubic law, for a rock fracture, as shown by Detournay, 1979.

$$ke \left[ \frac{\delta}{\delta x} \left( \frac{\delta P}{\delta x} \right) + \frac{\delta}{\delta z} \left( \frac{\delta P}{\delta z} \right) \right] + \frac{Q}{\Delta} = 0$$

$$k = \frac{1}{\mu} \frac{e^2}{12}$$

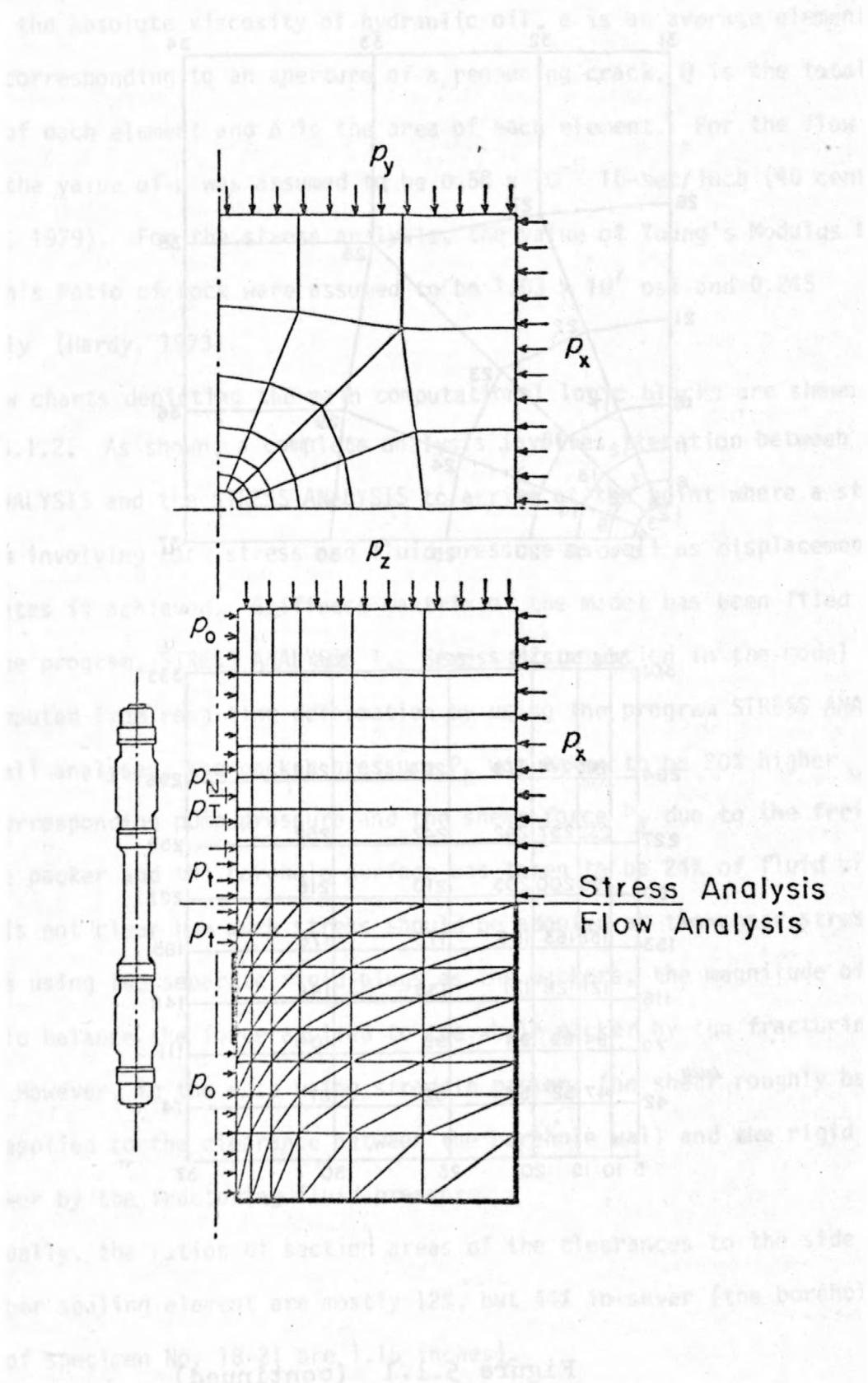


Figure 5.1.1 Finite element meshes used in stress analysis and flow analysis. (continued)



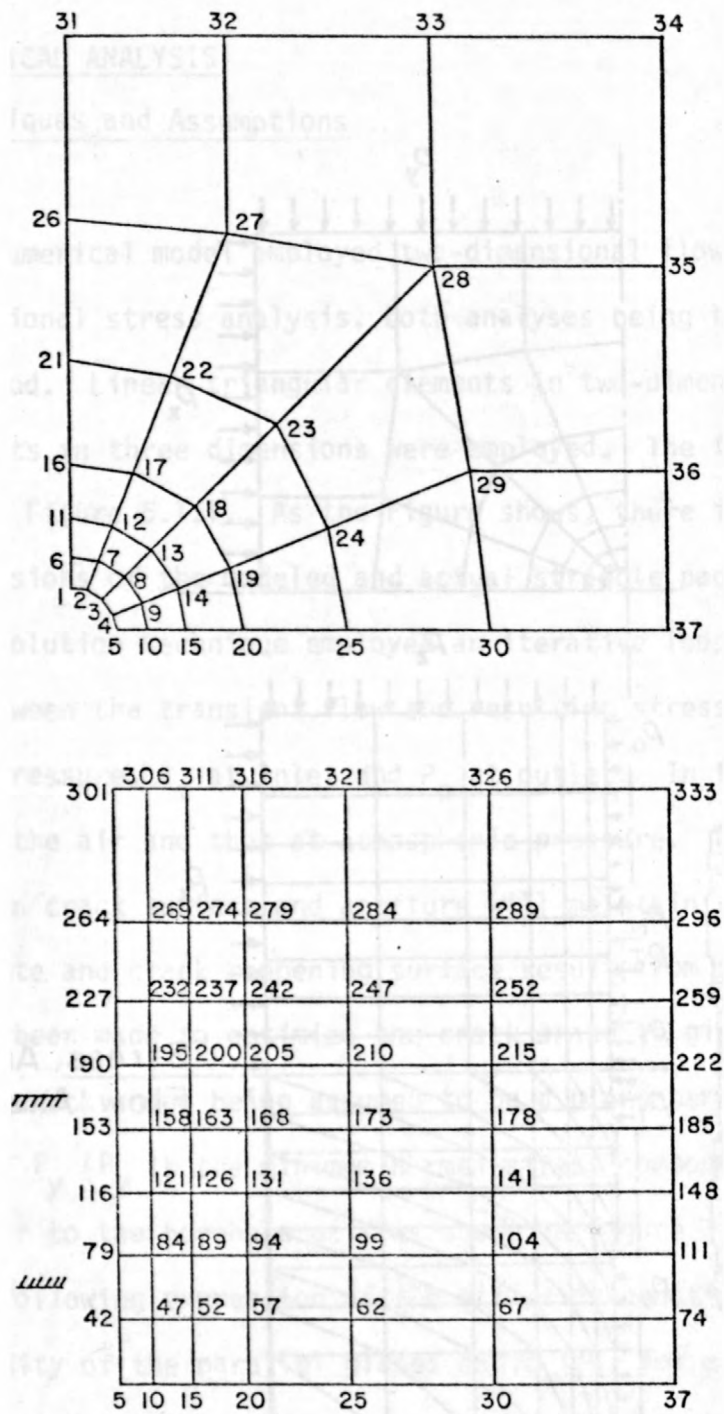


Figure 5.1.1 (continued)

Where  $\mu$  is the absolute viscosity of hydraulic oil,  $e$  is an average element thickness corresponding to an aperture of a reopening crack,  $Q$  is the total discharge of each element and  $\Delta$  is the area of each element. For the flow analysis, the value of  $\mu$  was assumed to be  $0.58 \times 10^{-5}$  lb-sec/inch (40 centpoise, Detournay, 1979). For the stress analysis, the value of Young's Modulus  $E$  and Poisson's Ratio of rock were assumed to be  $1.03 \times 10^7$  psi and 0.245 respectively (Hardy, 1973).

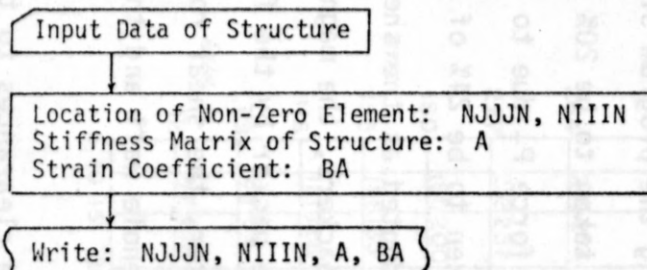
Flow charts depicting the main computational logic blocks are shown in Figure 5.1.2. As shown, a complete analysis involves iteration between the FLOW ANALYSIS and the STRESS ANALYSIS to arrive at the point where a stable equilibrium involving rock stress and fluid pressure as well as displacements and flow rates is achieved. Stiffness matrix of the model has been filed by using the program, STRESS ANALYSIS 1. Stress distribution in the model will be computed from resulting deformation by using the program STRESS ANALYSIS 3.

In all analyses, the packer pressure  $P_N$  was taken to be 20% higher than the corresponding pump pressure and the shear force  $P_T$  due to the friction between the packer and the borehole surface was taken to be 24% of fluid pressure.

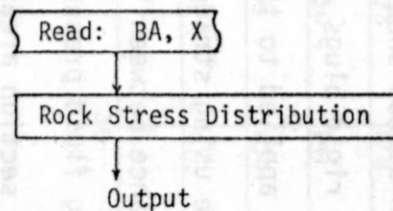
It is not clear how much stress should be adopted as the shear stress  $P_T$ . In the case using two separate rigid plugs as the packers, the magnitude of the shear should balance the force applied to the whole packer by the fracturing fluid pressure. However, in the case using straddle packer, the shear roughly balances the force applied to the clearance between the borehole wall and the rigid part of the packer by the fracturing fluid pressure.

Actually, the ratios of section areas of the clearances to the side area of the rubber sealing element are mostly 12%, but 44% in sever (the borehole diameters of specimen No. 18-21 are 1.15 inches).

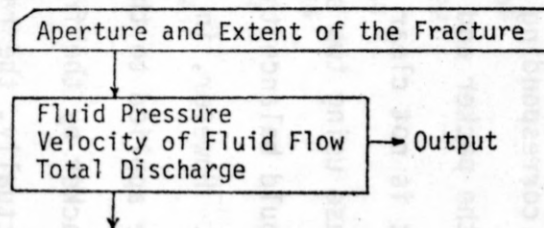
### STRESS ANALYSIS 1



### STRESS ANALYSIS 3



### FLOW ANALYSIS



### STRESS ANALYSIS 2

### STRESS ANALYSIS 2

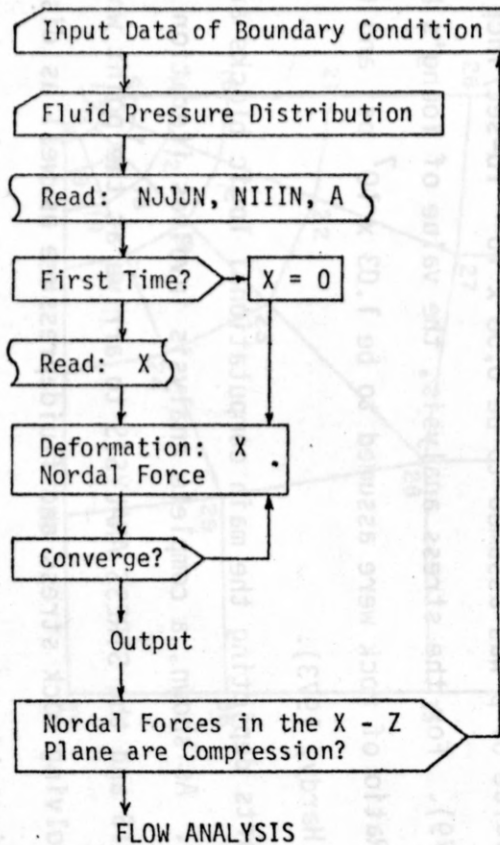


Figure 5.1.2

Flow chart of coupled stress-flow analysis

## 5.2 Results

Numerical results obtained from the analyses on the experimental configurations are shown on Figure 5.2.1 through 5.2.7. Each figure graphically presents the result of fluid injection in terms of:

- (a) crack opening displacements
- (b) fluid pressure distribution in the crack
- (c) normal stress distribution on the continuation of the crack plane in the rock
- (d) fluid velocity field within the crack
- (e) rock specimen deformation in the X-Z plane
- (f) rock specimen deformation in the Y-Z plane

In all cases the Z axis is taken to coincide with the borehole axis, and the Y axis coincides with the direction perpendicular to the fracture (see Figure 3.1).

As shown by the figures, flow rate is almost totally controlled by the outlet aperture. Conversely, for a given flow rate equilibrium considerations will lead to a given aperture, through which fluid will escape past the packers into the borehole. A very large increase in flow rate is required to effect a significant increase in the reopening pressure, implying that the crack opening displacement is a rather sensitive measure of local pressures.

Figure 5.2.8 shows the distribution of  $\sigma_z$  on the X-Z and Y-Z planes under the applied stress state A, with borehole inclination  $\phi = 0^\circ$  and with fluid pressure  $P_t = 1,600$  psi. In the figure, dotted lines represent the theoretical values of  $\sigma_z$  for the case that all forces applying to the wall of the borehole were removed. As expected, the Y-Z stresses do not reflect the presence of the crack to any degree, while the X-Z stresses show the stress reversals that take place due to the presence of the free surfaces of the crack.

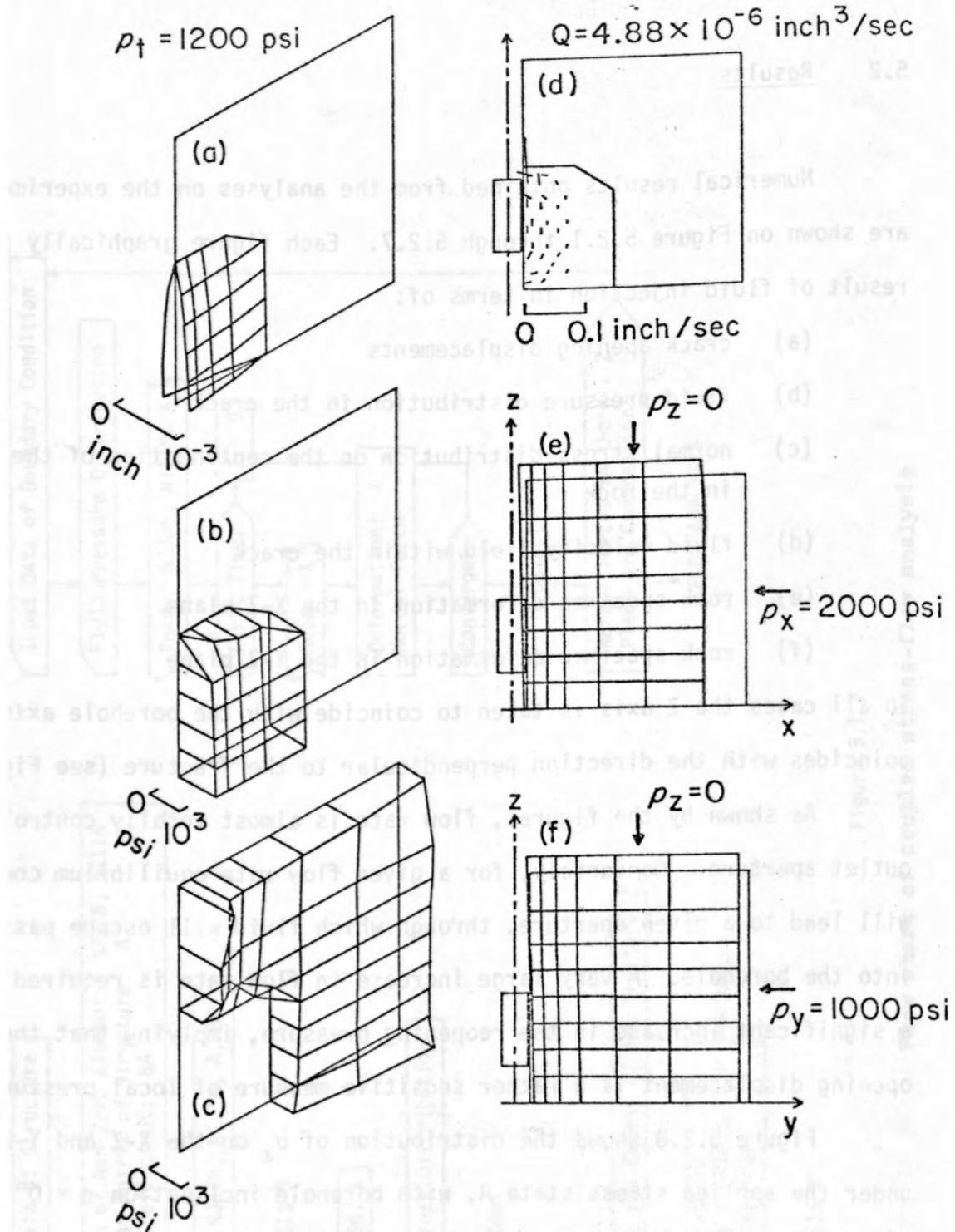


Figure 5.2.1 Computed results for the boundary condition corresponding to the vertical borehole, stress state A and  $P_t = 1200$  psi : crack opening(a), fluid pressure distribution(b), rock stress(c), fluid velocity and total discharge(d) and rock deformations at x-z plane (e) and y-z plane(f).



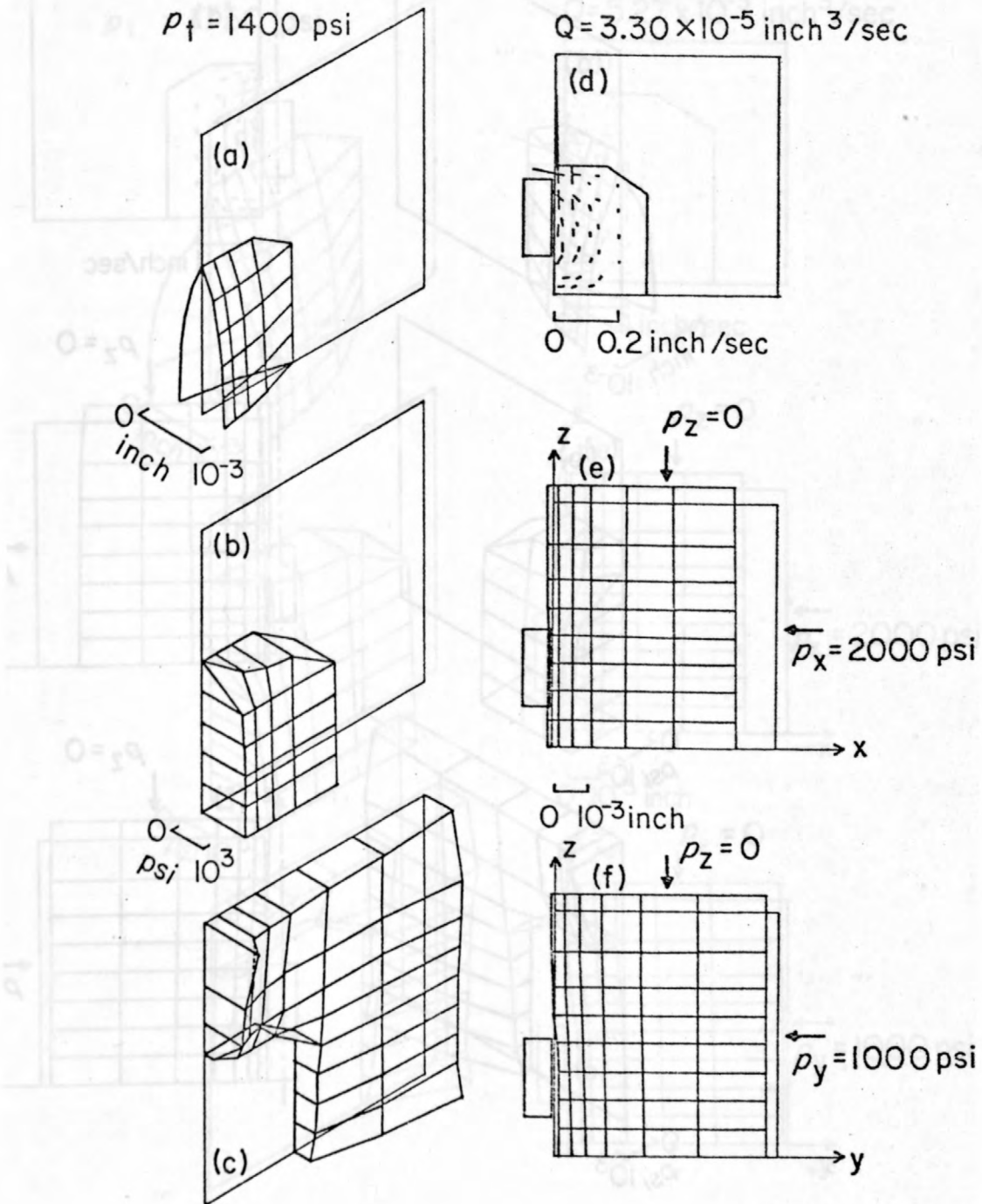


Figure 5.2.2 Computed results for the boundary condition corresponding to the vertical borehole, stress state A, and  $p_t = 1400$  psi.

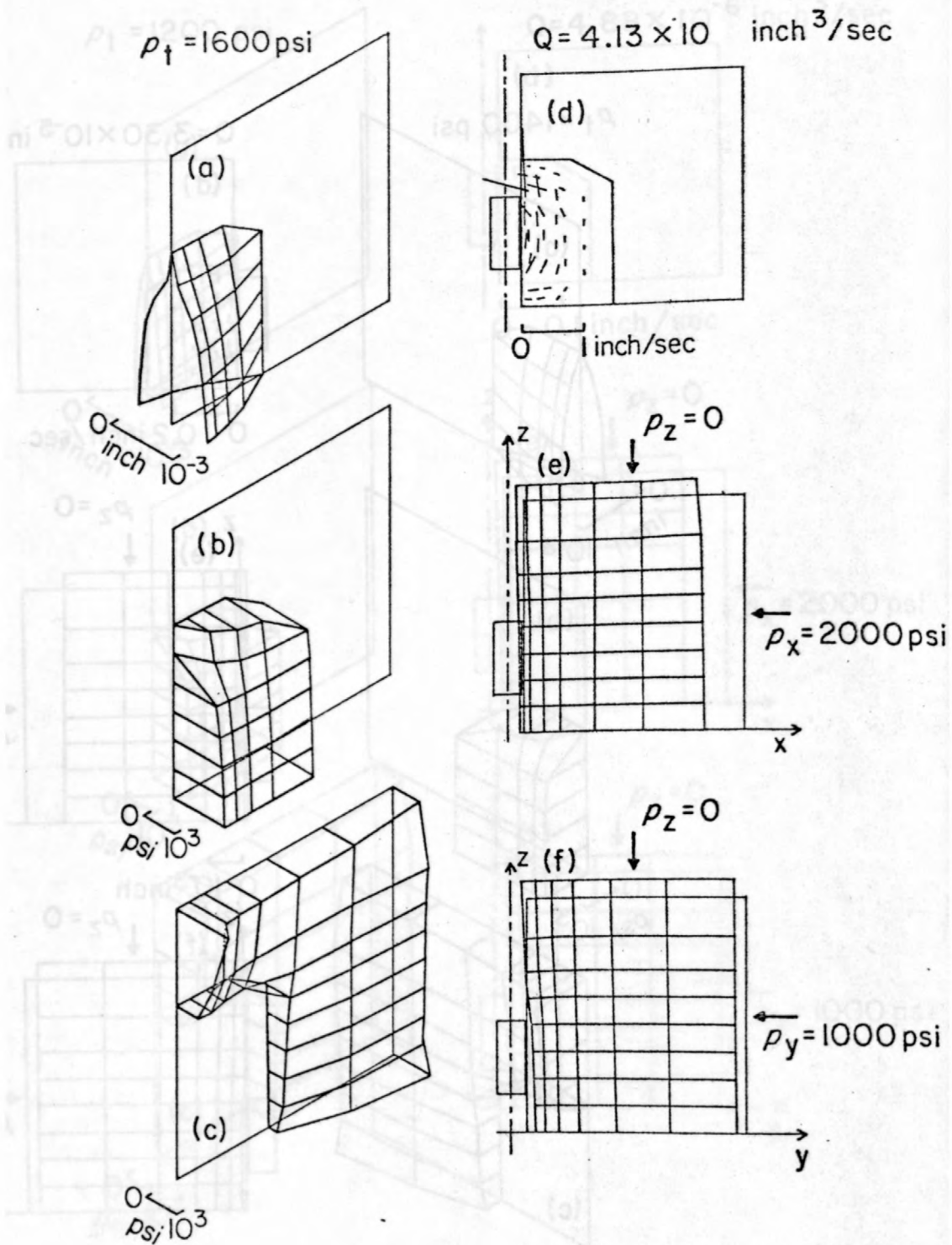


Figure 5.2.3 Computed results for the boundary condition corresponding to the vertical borehole, stress state A and  $p_t = 1600$  psi.

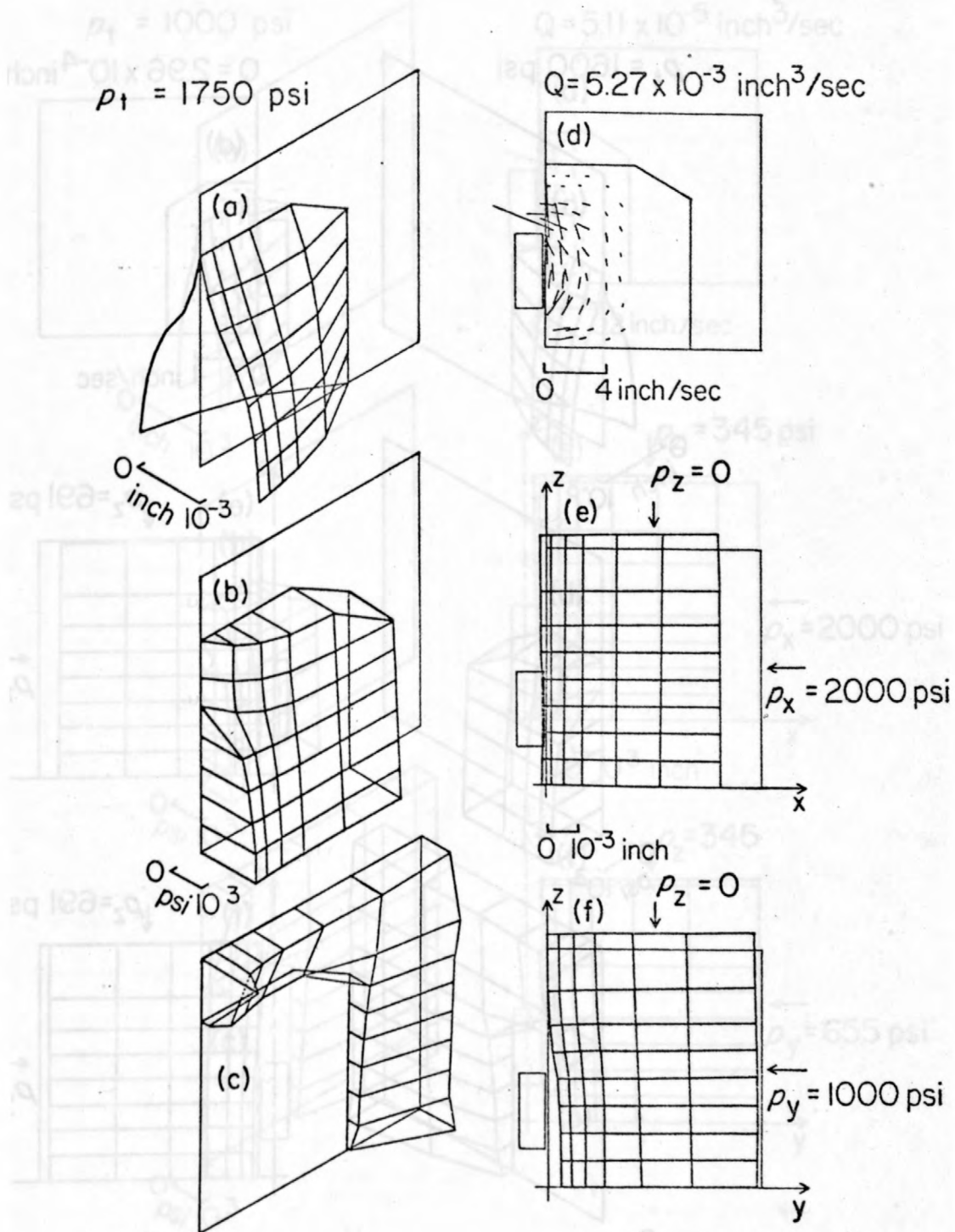


Figure 5.2.4 Computed results for the boundary condition corresponding to the vertical borehole, stress state A and  $p_t = 1750$  psi.

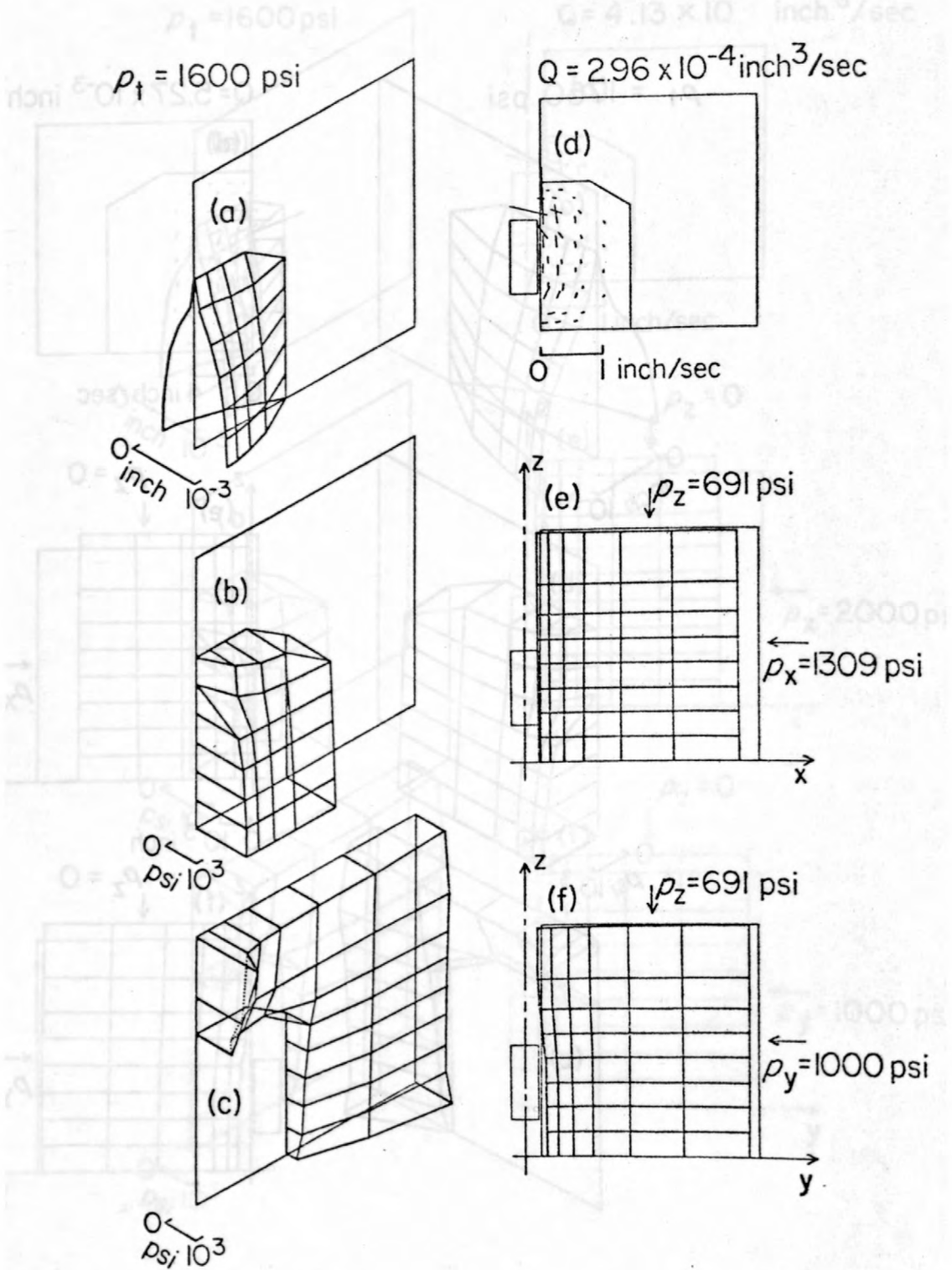


Figure 5.2.5 Computed results for the boundary condition corresponding to the inclined borehole ( $\phi = 36^\circ$ ), stress state A and  $\rho_t = 1600$  psi.

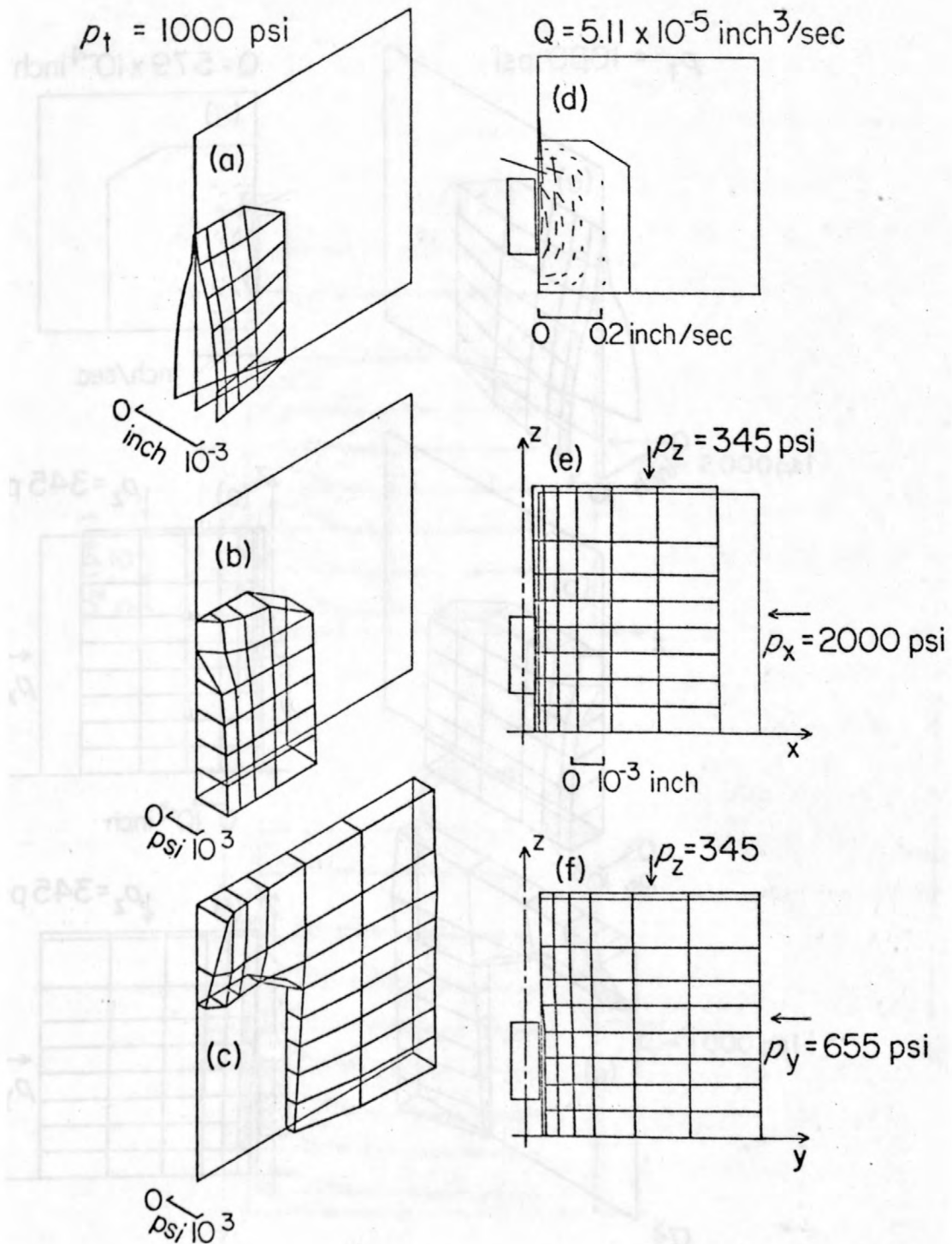


Figure 5.2.6 Computed results for the boundary condition corresponding to the inclined borehole ( $\beta = 36^\circ$ ), stress state A and  $p_t = 1000$  psi.



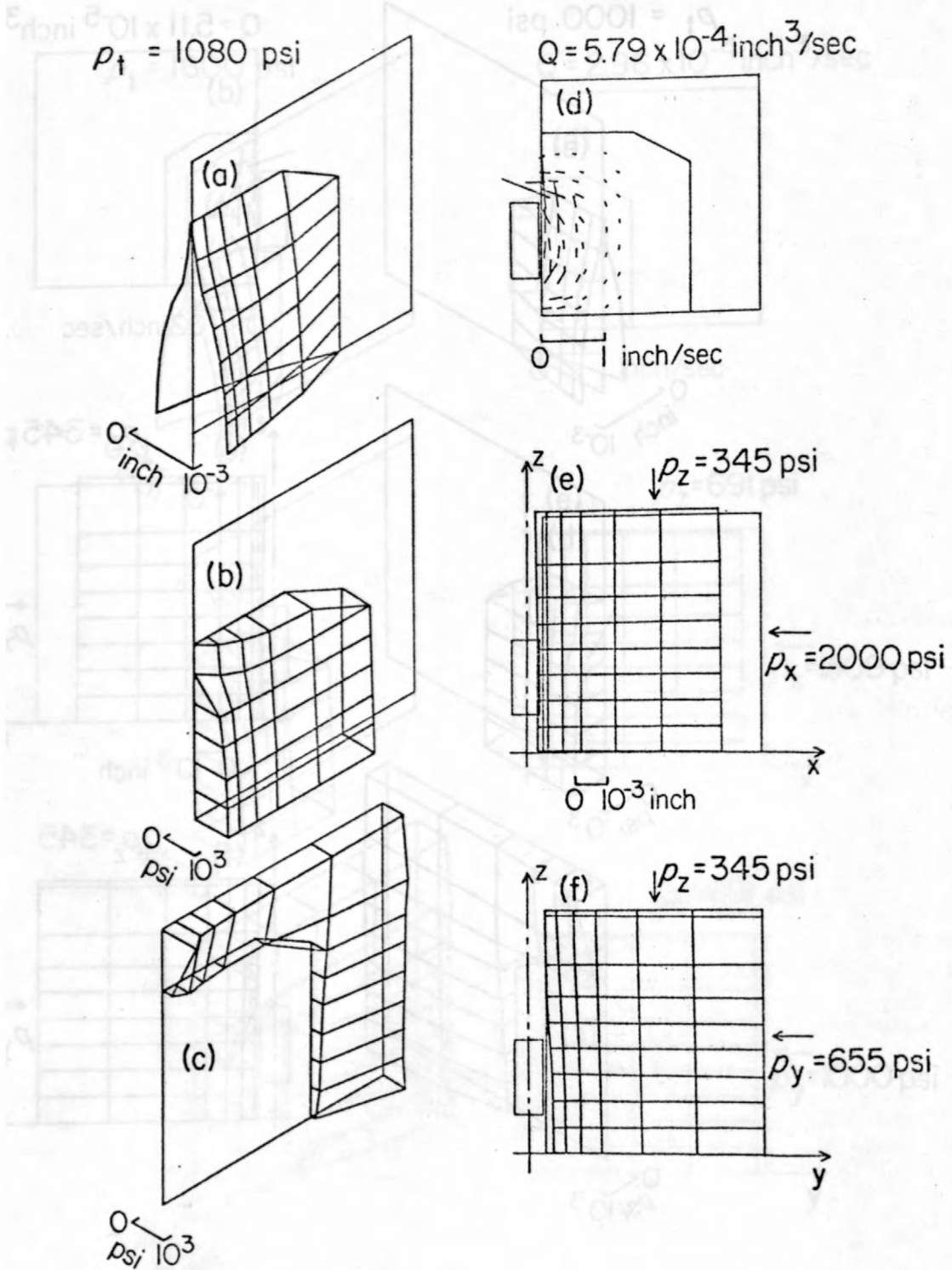


Figure 5.2.7 Computed results for the boundary condition corresponding to the inclined borehole ( $\beta = 36^\circ$ ), stress state A and  $p_t = 1080$  psi.

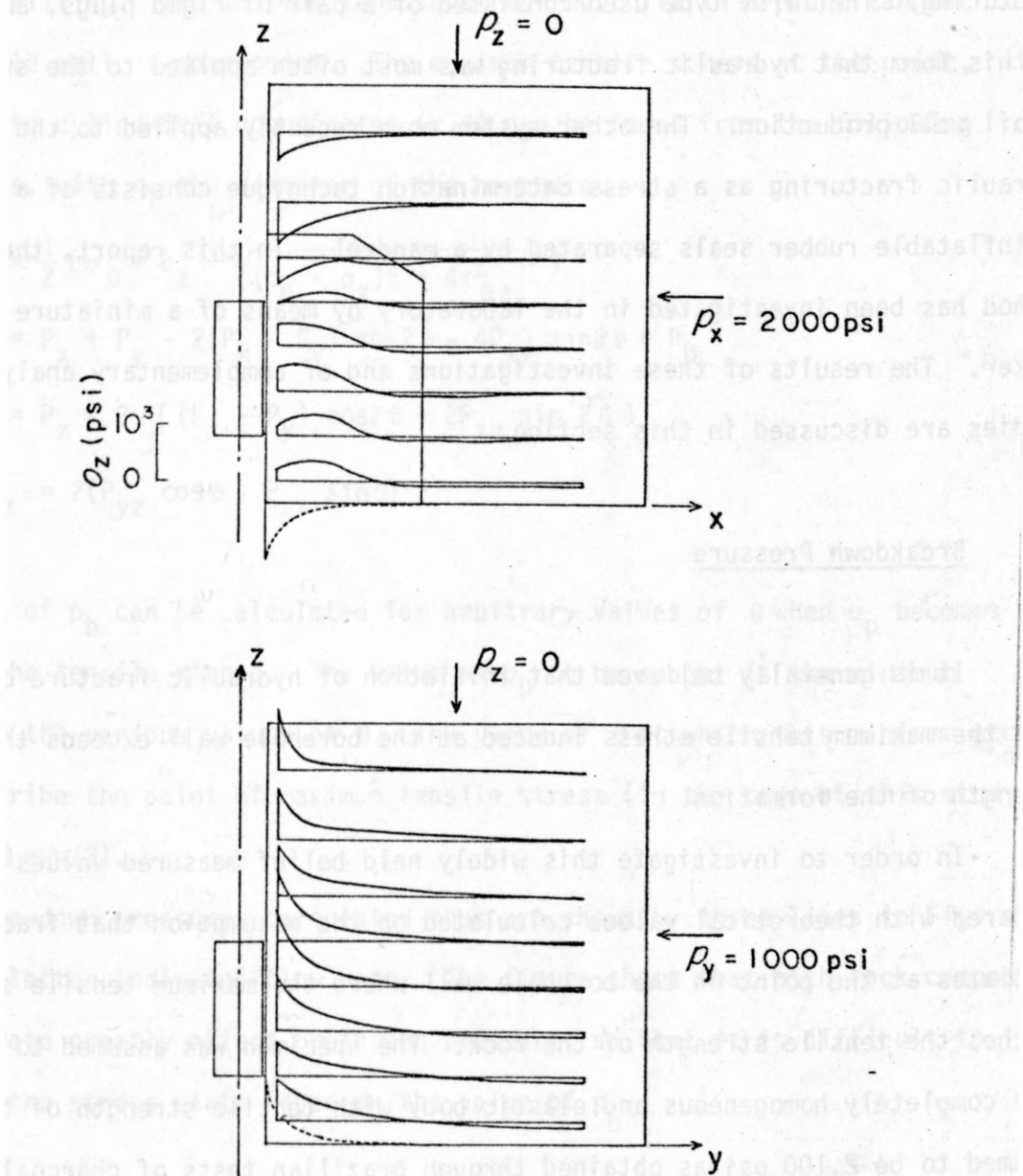


Figure 5.2.8 Stress distribution of  $\sigma_z$  for the boundary condition corresponding to the vertical borehole, stress state A and  $\rho_t = 1600 \text{ psi}$ .

## 6.0 DISCUSSION

### 6.1 Fracturing Tool

Two types of packer systems have been predominantly employed in hydraulic fracturing. The first type used consisted of a pair of rigid plugs, and it was in this form that hydraulic fracturing was most often applied to the stimulation of oil well production. The other system more recently applied to the use of hydraulic fracturing as a stress determination technique consists of a pair of inflatable rubber seals separated by a mandrel. In this report, the latter method has been investigated in the laboratory by means of a miniature straddle packer. The results of these investigations and of complementary analytical studies are discussed in this section.

### 6.2 Breakdown Pressure

It is generally believed that initiation of hydraulic fracture occurs when the maximum tensile stress induced at the borehole wall exceeds the tensile strength of the formation.

In order to investigate this widely held belief measured values were compared with theoretical values calculated on the assumption that fracture initiates at the point on the borehole wall where the maximum tensile stress reaches the tensile strength of the rock. The specimen was assumed to behave as a completely homogeneous and elastic body with tensile strength of the rock assumed to be 2,100 psi as obtained through brazilian tests of charcoal gray granite by Hardy, 1973.

The components of the total stress tensor with respect to the o-xyz coordinate system, namely  $P_{ij}$ , are thus related to the in-situ principal stresses by the expression

$$P_{ij} = \sum C_{ik} C_{jk} P_k$$

where  $C_{ij}$  are the direction cosines of o-xyz with respect to o- $P_1P_2P_3$ .

The presence of a borehole and application of fluid pressure within it will alter the stress field in the vicinity of the borehole from its state prior to drilling. The maximum tensile stress must lie in a plane tangent to the borehole wall at some point. The maximum tensile stress at the point, expressed in cylindrical coordinates  $(r, \theta)$  can be found from the following expressions, with  $r_1$  the diameter of the borehole.

$$\begin{aligned}\sigma_p &= \frac{1}{2} \{ \sigma_\theta + \sigma_z + \sqrt{(\sigma_\theta - \sigma_z)^2 + 4\tau_{\theta z}^2} \} \\ \sigma_\theta &= P_x + P_y - 2(P_x - P_y) \cos 2\theta - 4P_{xy} \sin 2\theta + P_b \\ \sigma_z &= P_z - 2\{ (P_x - P_y) \cos 2\theta + 2P_{xy} \sin 2\theta \} \\ \sigma_{\theta z} &= 2(P_{yz} \cos \theta - P_{zx} \sin \theta)\end{aligned}$$

The values of  $p_b$  can be calculated for arbitrary values of  $\theta$  when  $\sigma_p$  becomes equal to the tensile stress. The value of  $p_b$  to be sought is the minimum respect to the various values of  $\theta$ . The value of  $\theta$  at which this minimum occurs will prescribe the point of maximum tensile stress (in the case of this study,  $\theta = 0$  or  $\theta = \pi/2$ ).

Breakdown pressures calculated thus are shown by three lines in Figure 6.2, where the letter indicates flow rate. The figure shows that both rock composition and flow rate greatly affect breakdown pressure, so that it is difficult to determine the stress state based on the value of  $p_b$ .

### 6.3 Steady Flow Pressure

The pressures  $p_t$  or  $p_f$  obtained from each experimental test performed under various constant flow rates are shown in Figure 6.3.1 (stress state A),

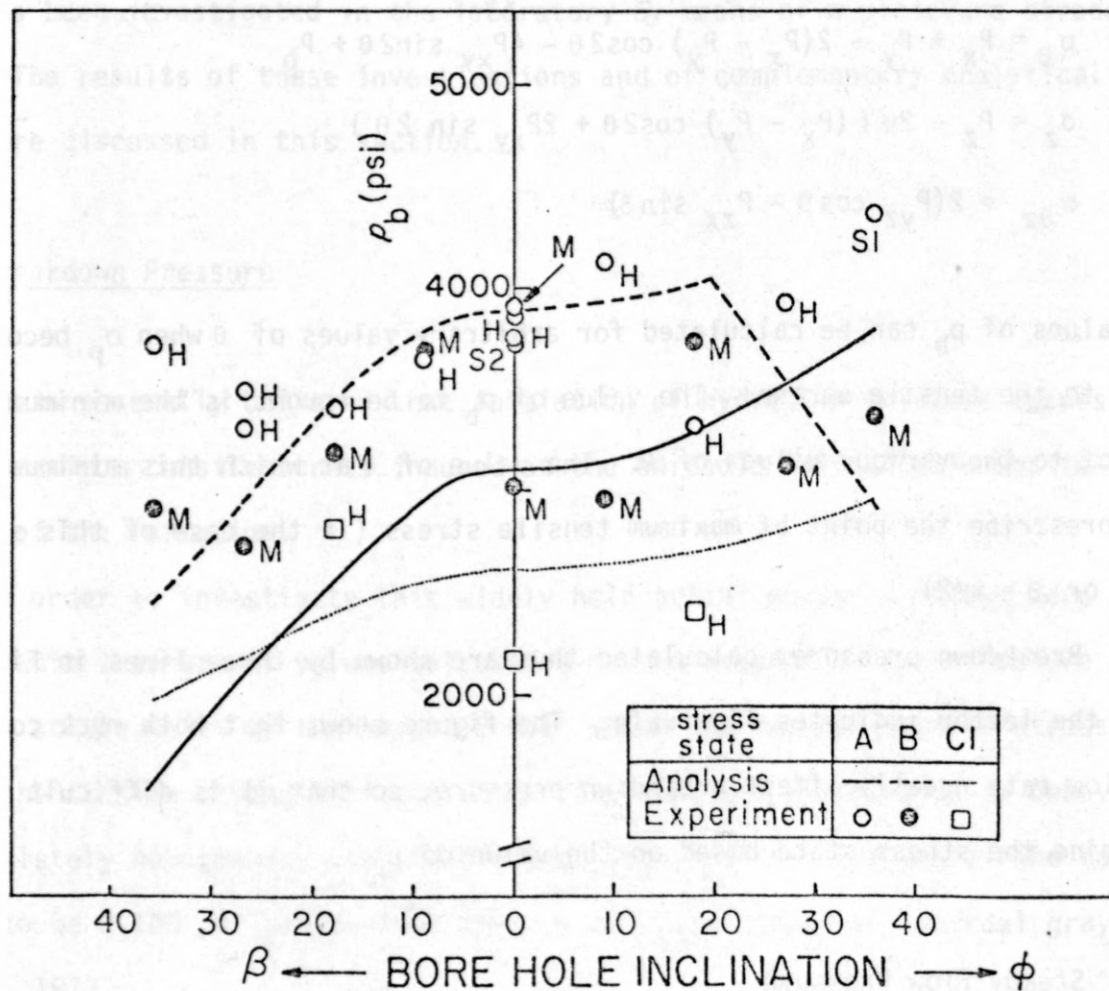


Figure 6.2 Analyzed breakdown pressure-borehole inclination curves and experimental results.



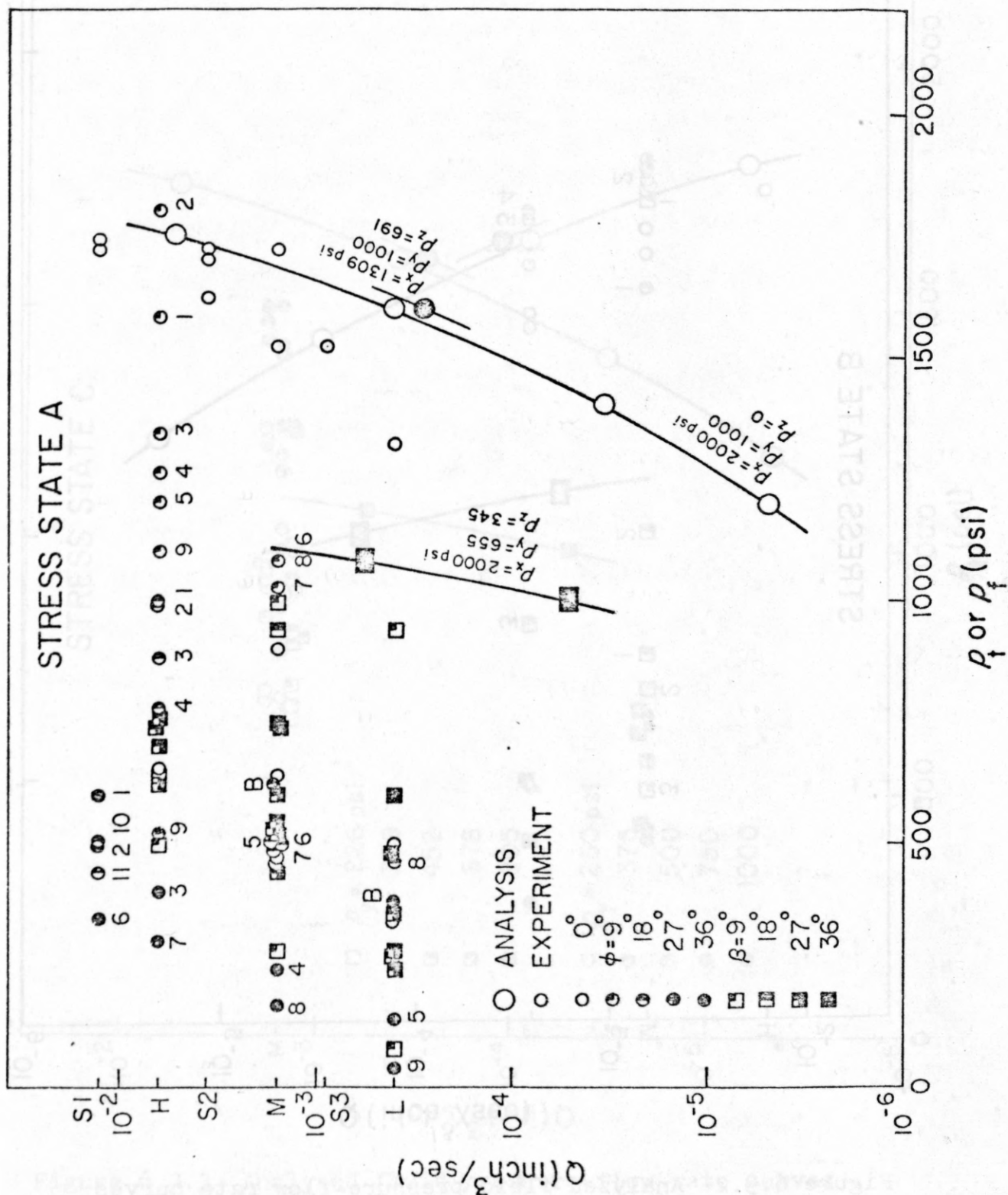


Figure 6.3.1 Analyzed fluid pressure -flow rate curves (stress state A) and experimental results(stress state A).

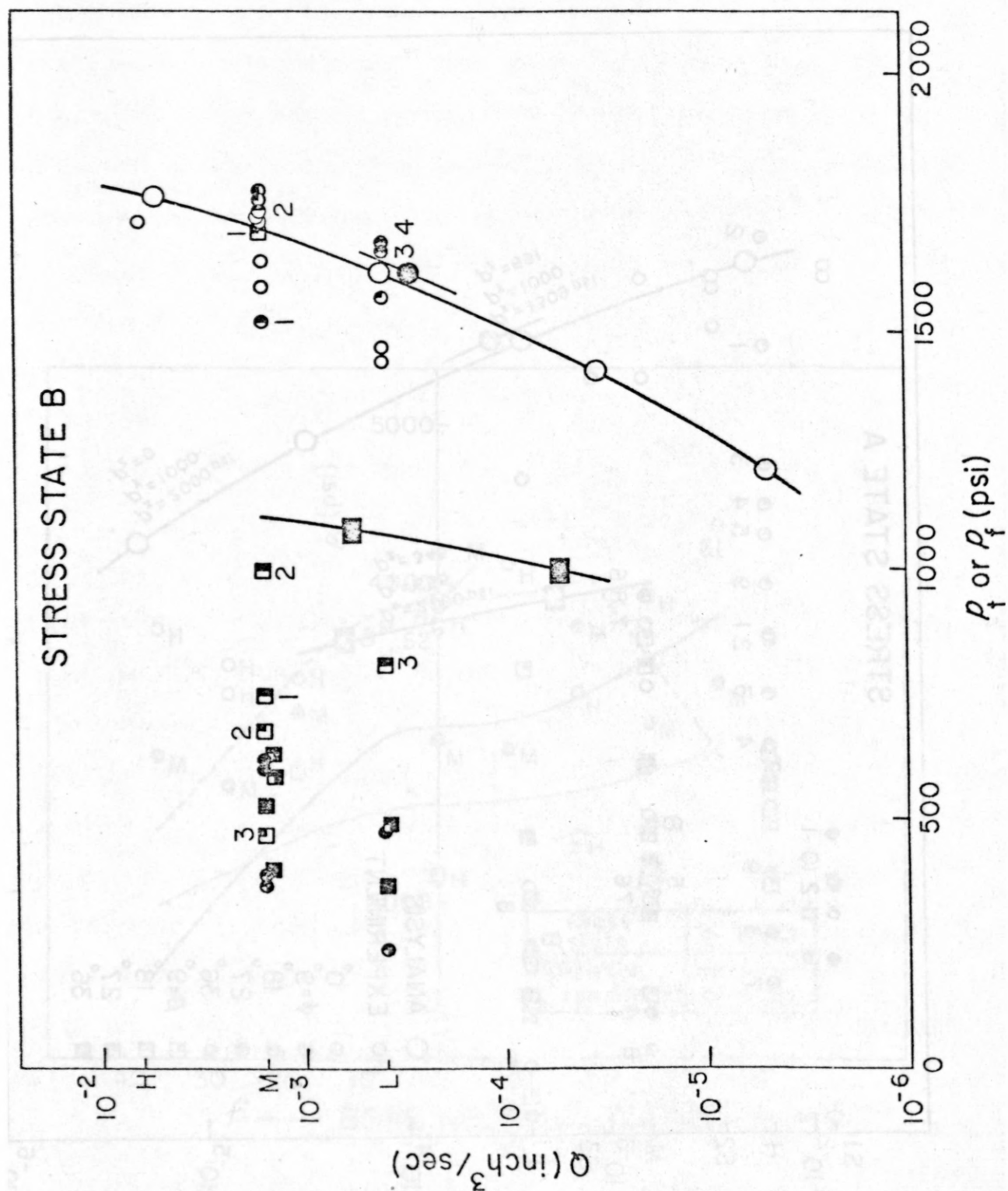


Figure 6.3.2 Analyzed fluid pressure-flow rate curves  
(stress state A) and experimental results(stress state B).

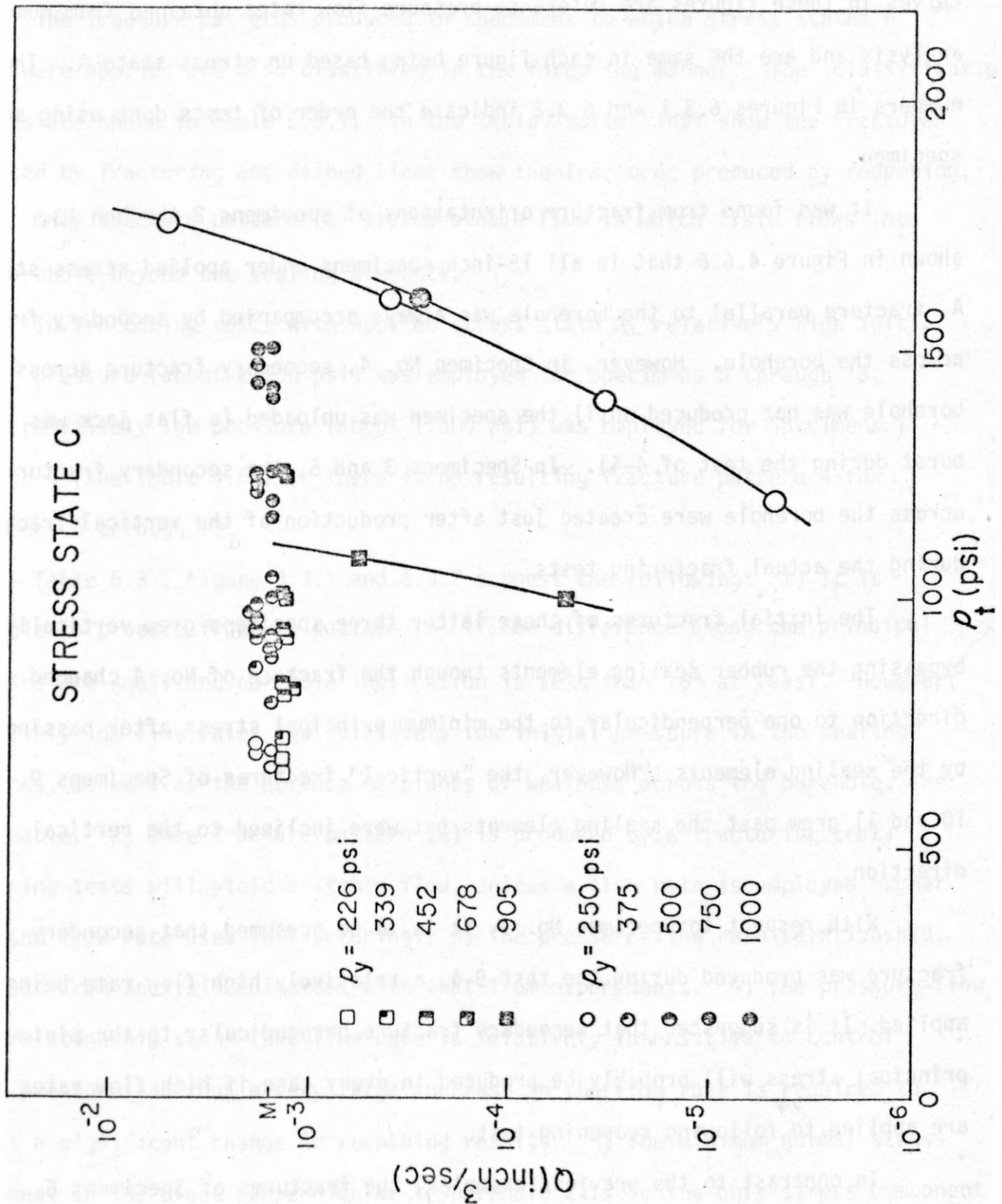


Figure 6.3.3 Analyzed fluid pressure-flow rate curves  
(stress state A) and experimental results(stress state C).

Figure 6.3.2 (stress state B), and Figure 6.3.3 (stress state C). The three curves in these figures are reference pressure-flow rates obtained from numerical analysis and are the same in each figure being based on stress state A. The numbers in Figures 6.3.1 and 6.3.2 indicate the order of tests done using same specimen.

It was found from fracture orientations of specimens 2 through 13, shown in Figure 4.6.6 that in all 15-inch specimens under applied stress state A, fracture parallel to the borehole was always accompanied by secondary fracture across the borehole. However, in Specimen No. 4, secondary fracture across the borehole was not produced until the specimen was unloaded (a flat jack was burst during the test of 4-4). In Specimens 3 and 5, the secondary fractures across the borehole were created just after production of the vertical fractures, during the actual fracturing tests.

The initial fractures of these latter three specimens grew vertically, bypassing the rubber sealing elements though the fracture of No. 4 changed its direction to one perpendicular to the minimum principal stress after passing by the sealing elements. However, the "vertical" fractures of Specimens 9, 10 and 11 grew past the sealing elements but were inclined to the vertical direction.

With respect to Specimen No. 9, it is to be presumed that secondary fracture was produced during the test 9-4, a relatively high flow rate being applied. It is suggested that secondary fracture perpendicular to the minimum principal stress will probably be produced in every case if high flow rates are applied to following reopening test.

In contrast to the previous examples, the fractures of Specimens 6, 8 and 13 initiated vertically, but grew without passing through the rubber sealing element while the fractures of the Specimens 2, 7 and 12 initiated in the direction



perpendicular to the minimum principal stress and propagated in the same plane.

The fracture patterns produced in specimens to which stress states B and C were applied are also classified in the foregoing manner. The classification schemes are shown in Table 6.3.1. In the table, solid lines show the fractures produced by fracturing and dashed lines show the fractures produced by reopening.

Only fracture pattern (a) yields stable flow in which fluid flows into the borehole beyond the sealing elements.

In fracturing tests with applied stress state A, relatively high initial packer pressure (about 2,500 psi) was employed for Specimens 5 through 13, while relatively low pressure (about 1,500 psi) was employed for Specimens 1 through 4 (see Table 4.5.1). There is no resulting fracture pattern A for Specimens 5 through 13.

Table 6.3, Figure 6.3.1 and 6.3.2 suggest the following: 1) It is possible to produce fracture pattern (a) if the difference among the principal stresses are small and borehole inclination is less than  $18^\circ$  at least. However, relatively low flow rates and relatively low initial pressure in the sealing elements, as well as the absence of planes of weakness across the borehole, are desirable. 2) Once fracture pattern (a) is produced by a fracturing test, reopening tests will yield a stable flow, unless a flow rate is employed higher than the flow rate used in fracturing. 3) The pressure-flow rate relationship obtained from analysis coincides with that from experiments. 4) The pressure-flow rate relationship shows that flow rate is relatively insensitive to control fluid pressure and thus a very large increase in the flow rate is required to effect a significant change in reopening results. 5) The minimum normal stress component in the plane perpendicular to borehole axis is the only stress component which affects  $p_t$  (the stable flow pressure) so long as vertical fracture is produced. Both shear stress components  $P_{zx}$  and  $P_{yz}$  have an influence on the possible occurrence of fracture across the borehole. 6) The value of  $p_y$



Table 6.3.1 Classification of fracture pattern

Stress Flow State Rate		FRACTURE PATTERN					
		a	a+b	a'	b'	b	
A	S1 H S2 M						
B	M						
C	M						

(minimum normal stress component in the plane perpendicular to the borehole axis) can be determined by multiplying the value of  $p_t$  by the factor  $f = 0.59$ . This factor "f" is a function of flow rate and the specific value of 0.59 has been obtained from analytical result corresponding to the flow rate M (see Figure 6.3.1). In the condition of this experiment, the peak pressure overshoot on reopening was almost eliminated at the flow rate M.

The factor "f" must be modified for real values of  $p_0$ ,  $\mu$ ,  $E$ ,  $\nu$  and dimensions of double packer. If these parameters are different from the values adopted in this experiment,  $p_t - p_y$  relationship will be also different from the result obtained. However, some flow rate will realize a similar fluid pressure distribution in the crack to the analytical result corresponding to the flow rate M, even though crack opening is different from that. Although this flow rate is different from the flow rate M, the peak pressure overshoot on reopening must be almost eliminated at this flow rate. Hence, the influence of these parameters on the magnitude of  $p_t$  should be much reduced by using the flow rate at which peak pressure overshoot on reopening disappears.

It has been previously suggested that fracture reopening pressure for a given uniform stress state should depend on flow rate and should vary between the limits  $p_y \leq p_b \leq 3p_y$ , the limits applying at very low and very high flow rates respectively. However, these limits were derived from experiments employing two separate rigid plugs (Cornet, 1977). 7) The value of  $P_{yz}$  has a greater influence on the possibility of occurrence of vertical fracture than has the value of  $P_{zx}$ . 8) The direction of  $P_y$  is determined by the fracture trace on the borehole wall. 9) If fracture pattern (a) is produced, the factor "f" must be modified, but modification is rather difficult. In such cases, the modification factor related to the direction of  $P_y$  should be found.

#### 6.4 Fracture Extension Pressure and Shut-In Pressure

Fracture pattern (b) may be produced when the difference among the principal stresses are large or borehole inclination is more than  $27^\circ$  at most. Even if these conditions are reversed, the possibility of occurrence of fracture pattern (b) may increase when high flow rates or high initial packer pressures are employed.

In fracture pattern (b), there is no fluid outlet into the borehole beyond the sealing element. If pumping of fluid is discontinued, therefore, the fluid pressure must balance the stress perpendicular the fracture. That is the minimum principal stress.

The following points are thus suggested:

- 1) If fracture pattern (b) was produced, shear stress components in the plane perpendicular or parallel to the borehole axis may be relatively large, provided low flow rates and relatively low initial packer pressures were employed.
- 2) The fracture of fracture pattern (b) is a plane nearly perpendicular to the minimum principal stress, though a significant plane of weakness across the borehole may interrupt the fracture path.
- 3) The magnitude of the minimum principal stress can be estimated from the shut-in pressure.
- 4) If fracture pattern (b') is produced, it will be difficult to determine the direction of the minimum principal stress. In such cases only the magnitude of the minimum principal stress can be determined.

#### 6.5 Pre-Existing Fracture

In order to examine whether the above mentioned procedure for determination of the normal stress component perpendicular to vertical fracture is a reliable

estimates of the normal stress component perpendicular to a pre-existing vertical fracture, a series C of experiment was performed, employing a vertical or inclined borehole.

A fracture was first produced in a specimen with applied stress state C1 ( $P_1 = 1,000$  psi,  $P_2 = 500$  psi,  $P_3 = 0$ ). In this case, as the differences among the principal stresses are relatively small, a vertical fracture should be produced. In fact, all the fractures appearing on the sides of the specimens were vertical, while no other 15-inch cube, to which stress state A or B was applied, had a similar fracture.

Reopening tests were then performed, under 13 different applied stress states, as shown in Table 3.2. In three of these stress states, normal stress perpendicular to the fracture ( $P_y$ ) is the maximum normal stress component in the plane perpendicular to the borehole axis.

Figure 6.5.1 shows the resulting  $P_y$ - $P_t$  relationship. The analytical result, corresponding to same flow rate (M) in Figure 6.3.1 is also shown in the figure.

It is found from Figure 6.5.1 that the value of  $P_y$  controls the value of  $P_t$ , but that the values of other stress components have little influence, though the effect of  $P_{yz}$  is relatively greater than the others. Figure 6.5.1 also suggests that the trend of experimental results agree with the analytical one but do not fit exactly. The experimental results indicate that the relationship between  $P_y$  and  $P_t$  is not proportional while the inclination of the line representing the  $P_y$ - $P_t$  relationship is less for the experimental results than for the analytical results.

The vertical fracture was produced under the stress state C1 ( $P_y = 500$  psi) and all of the reopening tests for which the other values of  $P_y$  were applied were performed using this fracture. If a vertical fracture was produced under the condition  $P_y < 500$  psi, the fracture would be smaller than the fracture produced under stress state C1. Conversely, if a vertical fracture was produced under the condition  $P_y > 500$  psi, the fracture would be larger.

Once extended and expanded beyond that relevant to a particular stress



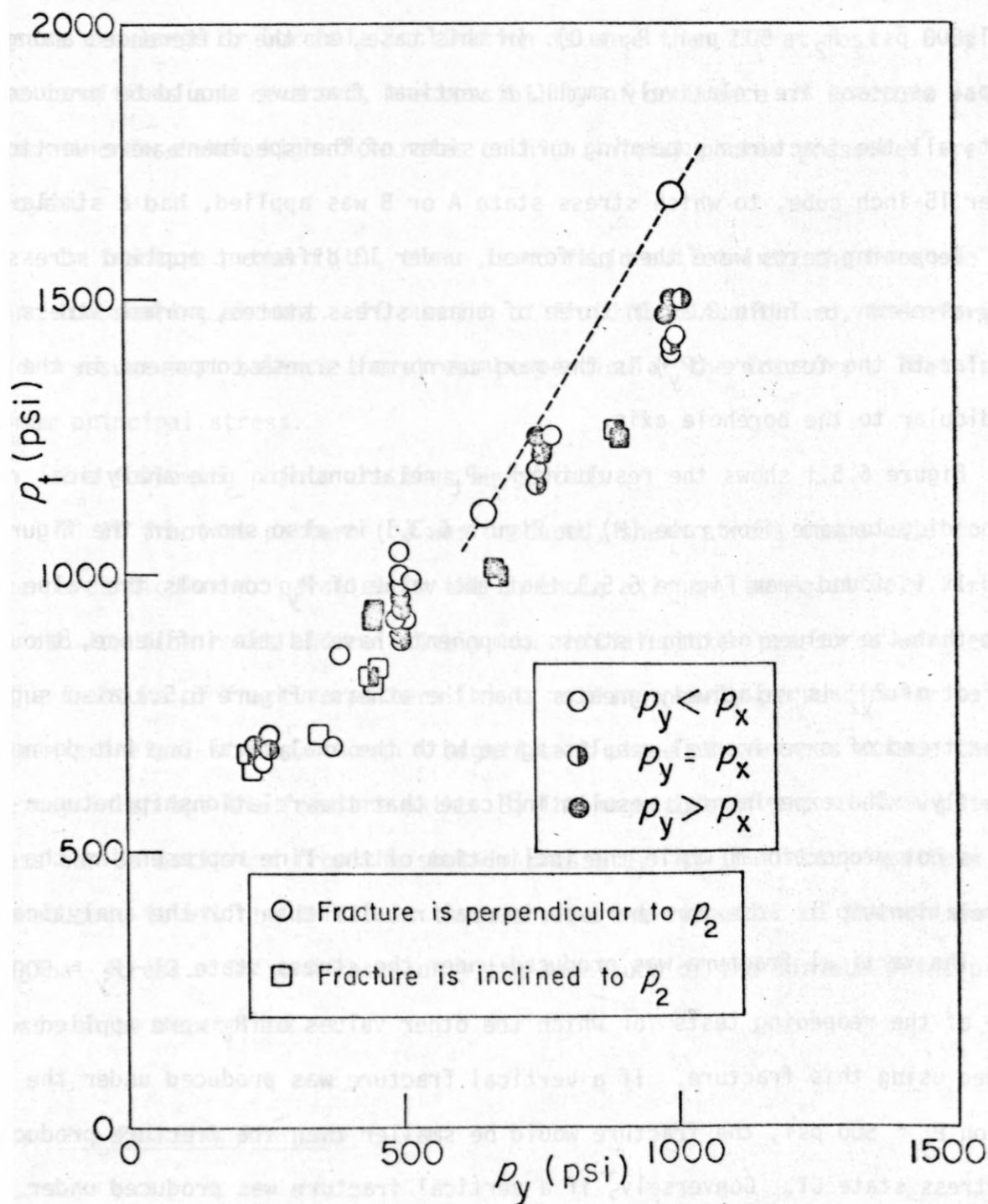


Figure 6.5.1 Comparison of experimental results with analytical results with respect to the relation between stress component perpendicular to the fracture and steady flow pressure.



state, a fracture cannot close completely, or regain any smaller state. If the fracture has not extended as much at fracturing as would be expected for a given stress state, then subsequent reopening under that stress state will not give the expected extension or expansion unless a higher flow rate is employed.

In consequence, the experimental results should be less than the analytical results for  $P_y > 500$  and should be greater for  $P_y < 500$ , though both the values of  $P_t$  coincide for  $P_y = 500$ . If each vertical fracture was produced under same conditions as for the reopening test, the experimental results may well agree with the analytical results.

In the case that the fracture has already been produced in the drilling of the borehole, because of a very high state of stress, the fracture cannot expand before the internal pressurization of the borehole. The creation of a mechanical fracture under the conditions to be employed for reopening tests is therefore desirable.

If the creation of a mechanical fracture perpendicular to the hydraulic fracture (as shown in Figure 6.5.2) is possible, the normal stress component perpendicular to this fracture can be determined. Where the mechanical fracture is created in another section of the same borehole, the normal stress component will be the greatest normal stress component in the plane perpendicular to the borehole axis.

The following points are suggested by the foregoing discussion:

- 1) Even if the fracture has been already produced prior to fracturing is done, (by drilling of the borehole in the case of very high stresses), it may be possible to estimate the normal stress component perpendicular to the fracture.
- 2) If it is possible to create the fracture in a certain direction parallel to the borehole axis by using a mechanical tool before hydraulic fracturing, it may be possible to determine the greatest normal stress component in the plane

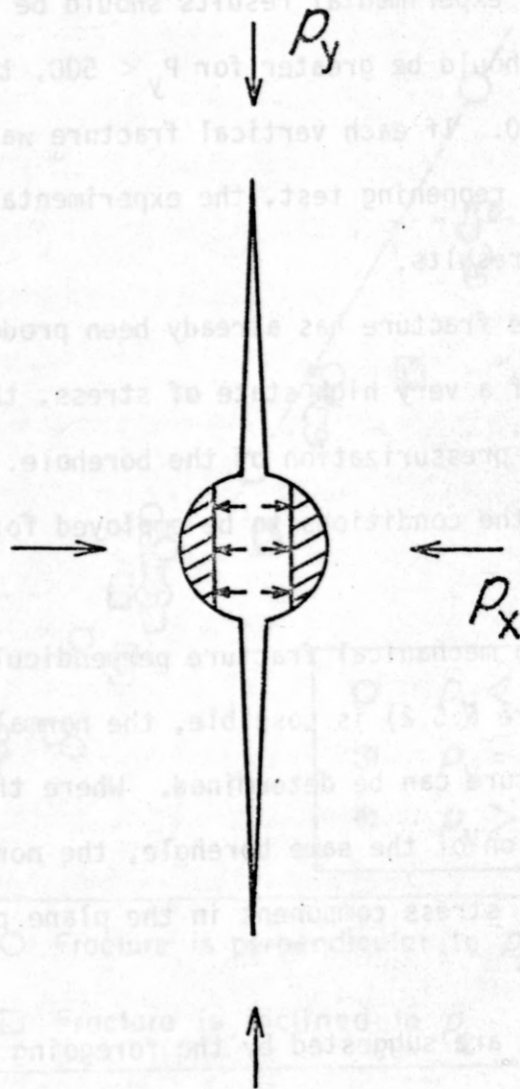


Figure 6.5.2 Mechanical fracture creating perpendicular to the hydraulic fracture.

perpendicular to the borehole axis.

## 7.0 CONCLUSION

Experiments were carried out on relatively large specimens of brittle, competent and impermeable rock containing other vertical or inclined boreholes. These specimens were fractured hydraulically by means of miniature straddle packers under biaxial loading and the fractures reopened by cycling the pressure at different flow rates. Numerical analyses were also carried out on the experimental configurations to assist in the interpretation of experimental data.

Significant results obtained to date are as follows:

- 1) Pressure-time records from hydraulic fracturing are of two types, depending on the fracture orientation at the borehole wall. 2) In the case that a fracture is initiated by fluid pressure for the first time, if the borehole inclination is slight, or if the differences among principal stresses are small, a fracture parallel to the borehole axis is created. The least normal stress component perpendicular to the borehole axis can then be estimated from a first typical pressure-time record obtained from a reopening test, using a relatively low flow rate and its direction will be determined by observation of the fracture on the borehole wall. A hydraulic aperture can be computed for use in hydraulic conductivity equations for prediction of the pressure-flow relation in hydraulic fracturing. 3) If it is possible to create the fracture in a specified direction perpendicular to the borehole axis by using, for instance, a mechanical fracturing tool before hydraulic fracturing, stress components perpendicular to this fracture can be determined. In the case that the direction is chosen to be perpendicular to a fracture which has been induced by fluid pressure applied in a former hydraulic fracturing test, with the mechanical fracture created in

another section of the same borehole, the maximum normal stress component in the plane perpendicular to the borehole axis will be determined.

In the case that the fracture has already been produced by the drilling of the borehole, as in the case of very high in-situ stresses, it is possible to estimate the normal stress component perpendicular to the fracture from the pressure-time record obtained in a reopening test at a low flow rate. In general, pre-existing fracture in the hydraulic fracturing chamber will enable an estimate of the normal stress component perpendicular to the fracture, although the fracture must parallel the borehole axis to some extent. 4) On the other hand, whether the fractures were produced by hydrostatic pressure nor not, the minimum principal stress can be determined from a second type of pressure-time record. This second typical pressure-time trace is obtained through a hydraulic fracturing test using relatively high flow rates.

In the case that a fracture is initiated by hydrostatic pressure for the first time, if the borehole is considerably inclined and the principal stress differences are fairly large, a fracture perpendicular to the minimum principal stress is created. The direction of minimum principal stress can be then determined by observation on the borehole wall. Hence, from tests on the three fractures the minimum principal stress magnitude and direction as well as the magnitudes and directions of the maximum and minimum normal stresses in the plane perpendicular to the borehole axis will be determined. The complete stress state can then be calculated.

In the case where there is a pre-existing fracture, before the hydraulic fracturing tests, the number of known quantities decreases. A couple of tests using other boreholes which have differing inclinations will be required to determine the complete stress state.



## 8.0 REFERENCES

- Haimson, B., "Hydraulic Fracturing in Porous and Non-Porous Rocks and its Potential for Determining In-Situ Stresses at Depth," Technical Report 4-68; Missouri River Division, Corps of Engineers, Omaha, Nebraska, 1968.
- Von Schoenfeldt, M., "An Experimental Study of Open Hole Hydraulic Fracturing as a Stress Measurement with Particular Emphasis on Field Tests," Technical Report MRD-3-70, Missouri River Division, Corps of Engineers, Omaha, Nebraska, 1970.
- Roegiers, J.C., "The Development and Evaluation of a Field Method for In-Situ Stress Determination using Hydraulic Fracturing," Technical Report MRD-1-75, Missouri River Division, Corps of Engineers, Omaha, Nebraska, Ph.D. Thesis, 1975.
- Cornet, F.H., "Crack Propagation in Rocks Normal to the Maximum Compression Stress," Final Report NSF Grant No. GK-41220, 1977.
- Hast, N., "Limits of Stress Measurements in the Earth's Crust," Rock Mechanics, Vol. 11, No. 3, pp. 143-150, 1979.
- Gronseth, J.M. and Detournay, E., "Improved Stress Determination Procedures by Hydraulic Fracturing," Final Report of USGS Grant 14.08.0001.16768, 1979.
- Hardy, M.P., "Fracture Mechanics Applied to Rock," Ph.D. Thesis, University of Minnesota, 1973.
- Daneshy, A.A., "A Study of Inclined Hydraulic Fractures," Society of Petroleum Engineers Journal, Vol. 13, No. 2, pp. 61-68, 1973.
- Detournay, E., "The Interaction of Deformation and Hydraulic Conductivity in Rock Fracture: An Experimental and Analytical Study," Master Thesis, University of Minnesota, 1979.
- Oka, Y., et al., "Introduction of the Matrix Finite Element Method (part 2)," Suiyokaishi, 1975.
- Togawa, H., "Computer Analysis of Matrix Structure," Steel Structure Association, 1970.
- Yokabori, T., "Zairyo Kyodo Gaku," Gihodo, p. 74, 1955.
- Cambeftort, H., Injection des sols, Vol. 1, Eyrolles, Paris, 1965.
- Crouch, S.L., Analytically of Stresses and Displacements around Underground Excavations: An Application of the Displacement Discontinuity Method, Final Report of NSF Grant No. G1-379.268, p. 23, 1977.
- Haimson, B., Design of Underground Power Houses and the Importance of Pre-Excavation Stress Measurements, Design Methods in Rock Mechanics, Sixteenth Symposium on Rock Mechanics, Editors, C. Fairhurst and S.L. Crouch, Am. Soc. of Civil Eng., NY, NY, 1977.



Hubert, M. and Willis, D.G., Mechanics of Hydraulic Fracturing, Vol. 210, p. 153-168, 1957.

Lousi, C., A Study of Groundwater Flow in Jointed Rock and its Influence on the Stability of Rock Masses, Imperial College, Rock Mechanics Report No. 10, London, 1969.

Talobre, J., La mécanique des roches, Dunod, Paris, 1967.





## PROGRAM 1 (Stress analysis)

```

      PROGRAM MAIN(INPUT,OUTPUT,TAPE5=INPUT,TAPE6=OUTPUT,TAPE7,TAPE8
1,TAPE9,TAPE10,TAPE11)
C
C   THREE DIMENSIONAL STRESS ANALYSIS BY FEM
C
C   (SIZE OF AA) = 9*(19LMN-R(LM+MN+NL)+4(L+N+M)-2)+ALFA
C   (SIZE OF NIJ) = 4*(MAX. NO. OF THE ELEMENTS RELATED TO EACH NOD)
C
      DIMENSION XF(4,3),XYZ(333,3)
1,STRESS(6,12),NOD(1200,4),XMK(12,12),E(4),C(4),D(4),PA(6,12)
2,C1(6,6),ZZZ(9),NIJ(112),NOD1(200,8),NOD2(25,4)
3,AA(34641),NIIIN(252,17),NIJJN(333)
      REAL LOAD
C
C   INPUT DATA OF STRUCTURE
C
      READ(5,14) NPOIN1,NLELM2,NDAN
      WRITE(6,14) NPOIN1,NLELM2,NDAN
      READ(5,12) E,V
      WRITE(6,16) E,V
C
C   (XYZ(I,J),J=1,2) ARE : XY COORDINATE ON THE BOTTOM PLANE (Z=0)
C   NODAL POINT NUMBER, ELEMENT NUMBER AND ZZZ ARE : FROM BOTTOM TO TOP
C   ** Z-AXIS IS DIRECTED UPPER **
C   THE SEQUENCE OF NOD2 IS : FROM TOP TO BOTTOM AND LEFT TO RIGHT
C   ** TETA DIRECTION IS UPPER **
C
      READ(5,11)((XYZ(I,J),J=1,2),I=1,NPOIN1)
      WRITE(6,11)((XYZ(I,J),J=1,2),I=1,NPOIN1)
      READ(5,32)(ZZZ(I),I=1,NDAN)
      WRITE(6,33)(ZZZ(I),I=1,NDAN)
      READ(5,17)((NOD2(I,J),J=1,4),I=1,NLELM2)
      WRITE(6,39)((NOD2(I,J),J=1,4),I=1,NLELM2)
12 FORMAT(3F12.3)
11 FORMAT(2F6.2,3Y,2F6.2,3Y,2F6.2,3Y,2F6.2,3Y,2F6.2)
33 FORMAT(10F7.4)
14 FORMAT(10I5)
15 FORMAT(3F7.3,5X,3F7.3,5X,3F7.3,5X,3F7.3,5X,3F7.3)
16 FORMAT(3F15.3)
17 FORMAT(4I4,4Y,4I4)
19 FORMAT(6I4,8Y,6I4)
39 FORMAT(4I4,4X,4I4,4X,4I4,4X,4I4,4X,4I4,4X,4I4)
      NNN=NDAN-1
      NLELM1=NLELM2*NNN
      DO 34 J=1,NPOIN1
34  XYZ(J,3)=ZZZ(J)
      DO 30 T=2,NDAN
      DO 30 J=1,NPOIN1
      NA=NPOIN1*(T-1)+J
      DO 32 K=1,2
32  XYZ(NA,K)=XYZ(J,K)
      XY7(NA,3)=ZZZ(T)
30  CONTINUE
      DO 31 I=1,NNN
      DO 31 J=1,NLELM2
      NA=NLELM2*(T-1)+J
      NE=NPOIN1*(I-1)
      NC=NR+NPOIN1
      DO 31 K=1,4
      NOD1(NA,K)=NOD2(J,K)+NR
      NOD1(NA,K+4)=NOD2(J,K)+NC
31  CONTINUE

```

```

WRITE(6,19)((MCD1(I,J),J=1,8),I=1,NLEEM1)
DO 13 I=1,NLEEM1
  NA=6*(I-1)+1
  NP=NA+1
  NC=NA+2
  ND=NA+3
  NE=NA+4
  NF=NA+5
  MCD(NA,1)=MCD1(I,1)
  MCD(NA,2)=MCD1(I,2)
  MCD(NA,3)=MCD1(I,5)
  MCD(NA,4)=MCD1(I,3)
  MCD(NB,1)=MCD1(I,2)
  MCD(NB,2)=MCD1(I,3)
  MCD(NP,3)=MCD1(I,6)
  MCD(NP,4)=MCD1(I,5)
  MCD(NC,1)=MCD1(I,3)
  MCD(NC,2)=MCD1(I,5)
  MCD(NC,3)=MCD1(I,7)
  MCD(NC,4)=MCD1(I,6)
  MCD(ND,1)=MCD1(I,2)
  MCD(ND,2)=MCD1(I,3)
  MCD(ND,3)=MCD1(I,4)
  MCD(ND,4)=MCD1(I,6)
  MCD(NE,1)=MCD1(I,3)
  MCD(NF,2)=MCD1(I,4)
  MCD(NF,3)=MCD1(I,6)
  MCD(NF,4)=MCD1(I,7)
  MCD(NF,1)=MCD1(I,4)
  MCD(NF,2)=MCD1(I,6)
  MCD(NF,3)=MCD1(I,7)
  MCD(NF,4)=MCD1(I,8)
13 CONTINUE
NLEEM=NLEEM1*6
NPOIN=NPOIN1*NDCAM
WRITE(6,15)((XYZ(I,J),J=1,3),I=1,NPOIN)
WRITE(6,29)((MCD(I,J),J=1,4),I=1,NLEEM)
WRITE(7,39)((MCD(I,J),J=1,4),I=1,NLEEM)
REWIND 7
CC1=F*(1.-V)/(1.+V)/(1.-2.*V)
CC2=E*V/(1.+V)/(1.-2.*V)
CC3=E/2./(1.+V)
C1(1,1)=CC1
C1(1,2)=CC2
C1(1,3)=CC2
C1(1,4)=0.
C1(1,5)=0.
C1(1,6)=0.
C1(2,1)=CC2
C1(2,2)=CC1
C1(2,3)=CC2
C1(2,4)=0.
C1(2,5)=0.
C1(2,6)=0.
C1(3,1)=CC2
C1(3,2)=CC2
C1(3,3)=CC1
C1(3,4)=0.
C1(3,5)=0.
C1(3,6)=0.
C1(4,1)=0.
C1(4,2)=0.
C1(4,3)=0.
C1(4,4)=CC3
C1(4,5)=0.
C1(4,6)=0.

```



```

      C1(5,1)=0.
      C1(5,2)=0.
      C1(5,3)=0.
      C1(5,4)=0.
      C1(5,5)=C02
      C1(5,6)=0.
      C1(6,1)=0.
      C1(6,2)=0.
      C1(6,3)=0.
      C1(6,4)=0.
      C1(6,5)=0.
      C1(6,6)=C02
C
C CALCULATION OF **NIIIN** AND **NUJJN**
C
      KKL=1
      NBR=1
      DO 910 I=1,NPOIN
      DO 920 J=1,17
      920 NIIIN(I,J)=0
      M=0
      DO 930 K=1,NELEM
      DO 940 J=1,4
      IF(1.EQ.NOD(K,J)) GO TO 901
      940 CONTINUE
      GO TO 930
      901 DO 950 J=1,4
      MM=4*M+J
      950 NIJ(MM)=NOD(K,J)
      M=M+1
      930 CONTINUE
      KKL=1
      902 MIN=1000
      DO 960 J=1,MM
      IF(MIN.GT.NIJ(J)) MIN=NIJ(J)
      960 CONTINUE
      IF(MIN.EQ.1000) GO TO 903
      NIIIN(I,KKL)=MIN
      DO 970 JJ=1,MM
      IF(MIN.EQ.NIJ(JJ)) NIJ(JJ)=1000
      970 CONTINUE
      KKL=KKL+1
      GO TO 902
      903 NUJJN(I)=KKL
      KKL=KKL+KKL-1
      IF(NBR.LT."NNBR=MM
      910 CONTINUE
      NAA=KKL-1
      NDAT=(KKL-1)*4
      WRITE(6,991) NAA,NDAT,NBR
      991 FORMAT(1H,4HNAA=I7,10X,5HNDAT=I7,10X,4HNBR=I7)
      WRITE(6,429)(NUJJN(I),(NIIIN(I,J),J=1,17),I=1,NPOIN)
      WRITE(6,429)(NUJJN(I),(NIIIN(I,J),J=1,17),I=1,NPOIN)
      REWIND 6
      429 FORMAT(1PI6)
C
C CALCULATION OF STRUCTURE STIFFNESS MATRIX **AA**
C
      DO 94 I=1,NDAT
      94 AA(I)=0.0
      DO 90 LK=1,NELEM
      DO 95 T=1,4
      JJ=NOD(LK,T)
      XF(I,1)=XYZ(JJ,1)
      YE(I,2)=XYZ(JJ,2)
      95 XF(I,3)=XYZ(JJ,3)

```

```

      DO 400 J=1,12
      DO 400 I=1,12
400   YPK(I,J)=0.
      DO 419 J=1,12
      DO 419 I=1,6
419   STRESS(I,J)=0.
      ORX=(XE(1,1)+XF(2,1)+XE(3,1)+XE(4,1))*0.25
      ORY=(XE(1,2)+XE(2,2)+XF(3,2)+XE(4,2))*0.25
      ORZ=(XE(1,3)+XE(2,3)+XE(3,3)+XE(4,3))*0.25
      DO 500 I=1,4
      XE(I,1)=XE(I,1)-ORX
      XE(I,2)=XE(I,2)-ORY
500   XL(I,3)=XE(I,3)-ORZ
      7K=(XE(3,1)*XL(4,2)-XE(4,1)*XE(3,2))*YE(2,3)+(XE(4,1)*XF(2,2)-XE(2,1)*XE(4,2))*XE(3,3)+(XL(2,1)*YE(3,2)-XE(3,1)*XE(2,2))*XE(4,3)
      7=4.0*7K
      R(1)=(XL(3,2)-XF(4,2))*XE(2,3)+(XL(4,2)-XF(2,2))*XE(3,3)+(XE(2,2)-1*XE(2,2))*YE(4,3)
      R(2)=(XE(1,2)-YE(4,2))*XL(3,3)+(YE(3,2)-XF(1,2))*XE(4,3)+(YE(4,2)-1*XE(3,2))*XF(1,3)
      R(3)=(XE(1,2)-YE(2,2))*XL(4,3)+(XE(2,2)-XL(4,2))*XE(1,3)+(YE(4,2)-1*XL(1,2))*XF(2,3)
      R(4)=(XE(3,2)-XE(2,2))*XE(1,3)+(XE(1,2)-XE(3,2))*XL(2,3)+(XE(2,2)-1*XE(1,2))*XF(3,3)
      C(1)=(XE(3,3)-XE(4,3))*XL(2,1)+(XL(4,3)-XE(2,3))*XL(3,1)+(YE(2,3)-1*XE(3,3))*XF(4,1)
      C(2)=(XE(1,3)-XE(4,3))*XE(3,1)+(XE(3,3)-XE(1,3))*XE(4,1)+(XE(4,3)-1*XE(3,3))*XF(1,1)
      C(3)=(YE(1,3)-XL(2,3))*XF(4,1)+(XE(2,3)-XE(4,3))*XL(1,1)+(XL(4,3)-1*XE(1,3))*YE(2,1)
      C(4)=(XL(3,3)-XF(2,3))*XF(1,1)+(XE(1,3)-XE(3,3))*XL(2,1)+(XL(2,3)-1*XE(1,3))*XF(3,1)
      D(1)=(XL(3,1)-XL(4,1))*XL(2,2)+(YE(4,1)-XL(2,1))*XF(3,2)+(XF(2,1)-1*XF(3,1))*XE(4,2)
      D(2)=(XE(1,1)-XE(4,1))*XE(3,2)+(XE(3,1)-XE(1,1))*XL(4,2)+(XL(4,1)-1*XE(3,1))*XF(1,2)
      D(3)=(XF(1,1)-XL(2,1))*XE(4,2)+(XL(2,1)-XL(4,1))*XE(1,2)+(XL(4,1)-1*XF(1,1))*XL(2,2)
      D(4)=(XE(3,1)-XF(2,1))*XL(1,2)+(XL(1,1)-XE(3,1))*XL(2,2)+(XE(2,1)-1*XE(1,1))*XF(3,2)
      DO 111 I=1,4
      RA(1,3*I-2)=R(I)/7
      RA(2,3*I-2)=0.
      RA(3,3*I-2)=0.
      RA(4,3*I-2)=C(I)/7
      RA(5,3*I-2)=0.
      RA(6,3*I-2)=D(I)/7
      RA(1,3*I-1)=0.
      RA(2,3*I-1)=C(I)/7
      RA(3,3*I-1)=0.
      RA(4,3*I-1)=R(I)/7
      RA(5,3*I-1)=D(I)/7
      RA(6,3*I-1)=0.
      RA(1,3*I)=0.
      RA(2,3*I)=0.
      RA(3,3*I)=D(I)/7
      RA(4,3*I)=0.
      RA(5,3*I)=C(I)/7
      RA(6,3*I)=R(I)/7
111  CONTINUE
      DO 520 J=1,12
      DO 520 I=1,6
      DO 520 K=1,6
520   STRESS(I,J)=STRESS(I,J)+C1(I,K)*RA(K,J)
      VOL=Z/A.
      DO 530 J=1,12

```

```

      DC 530 T=1,12
      DC 530 K=1,6
530  XMK(I,J)=XMK(I,J)+PA(K,I)*STRESS(K,J)*VOL
      DC 56  IT=1,4
      DC 57  JJ=1,4
      I=ND0(LK,IT)
      J=ND0(LK,JJ)
      M=1
      DC 58  N=1,17
      IF(J,50,NILIN(I,N)) GO TO 50
      55  M=M+1
      56  MF=NJJUN(T)+M-1
      DC 90  I1=1,3
      DC 90  I2=1,3
      K=9*MM-3*(4-I1)+I2
      M1=I1+3*(IT-1)
      M2=I2+3*(JJ-1)
      AA(K)=AA(K)+XMK(M1,M2)
      90  CONTINUE
      97  CONTINUE
      96  CONTINUE
      WRITE(9,770)((PA(I,J),J=1,12),I=1,6)
      WRITE(10,220) VOL
      90  CONTINUE
      REWIND 9
      REWIND 10
      WRITE(11,770)(AA(K),K=1,NDAT)
      REWIND 11
770  FORMAT(6F20.10)
220  FORMAT(F20.10)
      STOP
      END

```

## PROGRAM 2 (Stress analysis)

```

PROGRAM MAIN(INPUT,OUTPUT,TAPE5=INPUT,TAPE6=OUTPUT,TAPE8
1,TAPE11,TAPE13 )
C
C   THREE DIMENSIONAL STRESS ANALYSIS BY FEM
C   ** CONJUGATE GRADIENT METHOD **
C
  DIMENSION JP1(100),JF1(109),F(109),LPF1(55),LPF2(55),PF(55)
1,NF1(50),FR(50),NP1(63),XX(999),LOAD(999),Q(999),POAD(999)
2,X(999),Y(999),R(999),P(999),NUM2(63),VF(63),STRES(63)
  COMMON AA(34641),NIIIN(333,17),NJJJN(333)
  REAL LOAD
  READ(5,14)NCASE,MMM,NBEGIN
  WRITE(6,14)NCASE,MMM,NBEGIN
C
C   INPUT DATA OF STRUCTURE
C
  READ(5,20)NPOIN,NELEM,NAA,NDAT
  WRITE(6,20)NPOIN,NELEM,NAA,NDAT
20 FORMAT(4I7)
  READ(8,429)(NJJJN(I),(NIIIN(I,J),J=1,17),I=1,NPOIN)
  REWIND 8
429 FORMAT(18I6)
770 FORMAT(6E20,10)
1331 FORMAT(10E13,5)
C
C   INTRODUCTION OF BOUNDARY CONDITION
C
  READ(5,14)NFORCE,NX,NY,NPRESC,MX
  WRITE(6,14)NFORCE,NX,NY,NPRESC,MX
  READ(5,14)LP,NFRAC,NYPRES
  WRITE(6,14)LP,NFRAC,NYPRES
  READ(5,12)FRIC,PACK
  WRITE(6,12)FRIC,PACK
14 FORMAT(10I5)
12 FORMAT(4F14,3)
33 FORMAT(10F7,4)
  READ(5,14)(JF1(I),I=1,NFORCE)
  WRITE(6,14)(JF1(I),I=1,NFORCE)
  READ(5,33)(F(I),I=1,NFORCE)
  WRITE(6,33)(F(I),I=1,NFORCE)
  READ(5,14)(JP1(I),I=1,NPRESC)
  WRITE(6,14)(JP1(I),I=1,NPRESC)
  READ(5,14)(LPF1(I),I=1,LP)
  WRITE(6,14)(LPF1(I),I=1,LP)
  READ(5,14)(LPF2(I),I=1,LP)
  WRITE(6,14)(LPF2(I),I=1,LP)
  READ(5,33)(PF(I),I=1,LP)
  WRITE(6,33)(PF(I),I=1,LP)
  READ(5,14)(NF1(I),I=1,NFRAC)
  WRITE(6,14)(NF1(I),I=1,NFRAC)
  READ(5,33)(FR(I),I=1,NFRAC)
  WRITE(6,18)(FR(I),I=1,NFRAC)
18 FORMAT(10F10,2)
  READ(5,14)(NP1(I),I=1,NYPRES)
  WRITE(6,14)(NP1(I),I=1,NYPRES)
  IW=3*NPOIN
  DO 775 I=1,IW
775 Q(I)=0.
  DO 165 I=1,NYPRES
165 POAD(I)=0.
  READ(11,770)(AA(K),K=1,NDAT)
  REWIND 11

```

```

READ(5,12)SX,SY,SZ,SP
WRITE(6,12)SX,SY,SZ,SP
READ(5,14)JN1,JN2,JN3,JMP1,JMP2,JMP3
WRITE(6,14)JN1,JN2,JN3,JMP1,JMP2,JMP3
DO 45 I=1,IW
45 LOAD(I)=0.
DO 50 I=1,NFORCE
IF(I.LE.NX)GO TO 1
IF(I.LE.NY)GO TO 2
F(I)=SZ*F(I)
IA=3*(JF1(I)-1)+JN3
GO TO 50
1 F(I)=SX*F(I)
IA=3*(JF1(I)-1)+JN1
GO TO 50
2 F(I)=SY*F(I)
IA=3*(JF1(I)-1)+JN2
50 LCAD(IA)=F(I)
DO 49 I=1,LP
IA=3*(LPF1(I)-1)+LPF2(I)
LOAD(IA)=SP*PF(I)
IF(LP2(I).EQ.3)LOAD(IA)=LOAD(IA)*FRIC
IF(I.GT.16)LCAD(IA)=LOAD(IA)*PACK
49 CONTINUE
DO 47 I=1,NFRAC
IA=3*(NF1(I)-1)+2
47 LOAD(IA)=FR(I)
WRITE(6,1331)(LOAD(I),I=1,IW)
DO 100 II=1,NPRESC
IA=JP1(II)
IB=IA+1
MA=NJJJN(IA)
IF(IA.EQ.NPOIN)GO TO 81
MB=NJJJN(IB)-1
GO TO 91
81 MB=NAA
91 CONTINUE
DO 125 J=MA,MB
DO 125 L=1,3
IF(II.LE.MX)GO TO 160
K=9*(J-1)+3*(JMP3-1)+L
GO TO 125
160 K=9*(J-1)+3*(JMP1-1)+L
125 AA(K)=0.0
M=1
DO 101 N=1,17
IF(IA.EQ.NIIIN(IA,N)) GO TO 102
101 M=M+1
102 MM=NJJJN(IA)+M-1
IF(II.LE.MX)GO TO 60
K=9*MM-4*(3-JMP3)
GO TO 70
60 K=9*MM-4*(3-JMP1)
70 AA(K)=1.0
100 CONTINUE
DO 127 I=1,NYPRES
IA=NP1(I)
IB=IA+1
MA=NJJJN(IA)
IF(IA.EQ.NPOIN)GO TO 80
MB=NJJJN(IB)-1
GO TO 90
80 MB=NAA
90 CONTINUE
DO 135 J=MA,MB
DO 135 L=1,3

```



```

      K=9*(J-1)+3*(JMP2-1)+L
135 AA(K)=C.0
      M=1
      DO 128 N=1,17
      IF(IA.EQ.NIIIN(IA,N))GO TO 129
128 M=M+1
129 MM=NJJJN(IA)+M-1
      K=9*MM-4
      AA(K)=1.0
127 CONTINUE

```

C

C SOLUTION OF EQUATIONS ---CONJUGATE GRADIENT METHOD---

C

```

      WRITE(6,110)
110 FORMAT(1H0,3X,3HNO.,3X,1HI,13X,1HX,16X,2HXX,14X,5HRATIO,13X,
      15HALPHA,13X,4HBETA)
      M=1
      IF(NBEGIN.NE.0)GO TO 56
      DO 55 I=1,IW
155 X(I)=0.0
      GO TO 105
156 CONTINUE
      READ(13,770)(X(I),P(I),R(I),I=1,IW)
      REWIND 13
      IF(NBEGIN.NE.2)GO TO 103
      GO TO 1000
103 CONTINUE
      DO 115 I=1,NYPPRES
      IA=3*(NPI(I)-1)+JMP2
115 X(IA)=0.0
105 CONTINUE
      CALL NZMV(NAA,NPOIN,          IW,X,Y)
      DO 203 I=1,IW
      R(I)=LOAD(I)-Y(I)
203 P(I)=R(I)
1000 CALL VECM(P,R,IW,BUNSI)
      CALL NZMV(NAA,NPOIN,          IW,P,Y)
      CALL VECM(P,Y,IW,BUNBO)
      ALPHA=BUNSI/BUNBO
      DO 303 I=1,IW
      XX(I)=X(I)+ALPHA*P(I)
303 R(I)=R(I)-ALPHA*Y(I)
      CALL VECM(Y,R,IW,BUNSI)
      BETA=BUNSI/BUNBO
      DO 403 I=1,IW
403 P(I)=R(I)-BETA*P(I)
      DO 600 I=1,IW
      IF(XX(I).EQ.0.0) GO TO 701
      RATIO=ABS(X(I)/XX(I)-1.0)
      IF(RATIO-1.0E-2) 600,601,601
701 IF(ABS(XX(I)-X(I))-1.0E-5) 600,601,601
600 CONTINUE
603 DO 503 I=1,IW
503 X(I)=XX(I)
      GO TO 2000
601 WRITE(6,25) M,I,X(I),XX(I),RATIO,ALPHA,BETA
25 FORMAT(1H ,2I5,5E18.6)
      IF(M-PM) 602,603,603
602 M=M+1
      DO 501 I=1,IW
501 X(I)=XX(I)
      GO TO 1000
2000 WRITE(6,26)
26 FORMAT(1H0,2X,5HPOINT,15X,1HU,19X,1HV,19X,1HW)

```

```

      DO 700 I=1,IW
700  Q(I)=Q(I)+X(I)
      DO 172 I=1,NPOIN
      PU=Q(3*I-2)
      PV=Q(3*I-1)
      PW=Q(3*I)
172  WRITE(6,27) I,PU,PV,PW
      27  FORMAT(1H ,I5,3X,3E20.6)
      WRITE(6,28) M
      28  FORMAT(1H ,15HHANPUKU KAISUU=,I5)
      WRITE(16,770)(X(I),P(I),R(I),I=1,IW)
      REWIND 16

```

C

C \*\*\*\*\* CALCULATION OF NODAL FORCE \*\*\*\*\*

C

```

      READ(5,14)(NUM2(I),I=1,MX)
      WRITE(6,14)(NUM2(I),I=1,MX)
      READ(5,33)(VF(I),I=1,MX)
      WRITE(6,33)(VF(I),I=1,MX)
      WRITE(6,773)
773  FORMAT(1H0,3X,10HJUNCT. NO.,8X,11HNODAL FORCE,8X,12HNODAL STRESS)
      READ(11,770)(AA(K),K=1,NDAT)
      REWIND 11
      DO 256 I=1,NYPRES
      IA=NPI(I)
      IB=IA+1
      MA=NJJJN(IA)
      IF(IA.EQ.NPOIN)GO TO 140
      MB=NJJJN(IB)-1
      GO TO 141
140  MB=NAA
141  CONTINUE
      DO 145 J=MA,MB
      JJ=J-MA+1
      DO 145 L=1,3
      K=9*(J-1)+3+L
      II=(NIIIN(IA,JJ)-1)*3+L
145  POAD(I)=POAD(I)+AA(K)*Q(II)
      DO 38 L=1,MX
      IF(IA.EQ.NUM2(L))GO TO 39
38  CONTINUE
      39  STRES(I)=POAD(I)/VF(L)
      WRITE(6,772)IA,POAD(I),STRES(I)
772  FORMAT(I9,9X,E15.6,5X,E15.6)
256  CONTINUE
      STOP
      END

```

```

SUBROUTINE N7MV(NAA,NPOIN , IW,X,Y)
DIMENSION X( 999),Y( 999)
COMMON AA(34641),NIIIN(333,17),NJJJN(333)
DO 1 I=1,IW
1 Y(I)=0.0
DO 2 L=1,NAA
IF(L.LT.NJJJN(NPOIN)) GO TO 3
I=NPOIN+1
GO TO 4
3 DO 5 I=1,NPOIN
IF(NJJJN(I).GT.L) GO TO 4
5 CONTINUE
4 I=I-1
M=L-NJJJN(I)+1
J=NIIIN(I,M)
DO 6 I1=1,3
DO 6 I2=1,3
IAA=3*I+I1-3
JAA=3*J+I2-3
K=9*L-3*(4-I1)+I2
6 Y(IAA)=AA(K)*X(JAA)+Y(IAA)
2 CONTINUE
RETURN
END

```

```

SUBROUTINE VECM(X,Y,N,S)
DIMENSION X( 999),Y( 999)
S=0.0
DO 3 I=1,N
3 S=S+X(I)*Y(I)
RETURN
END

```

## PROGRAM 3 (Stress analysis)

```

PROGRAM MAIN(INPUT,OUTPUT,TAPE5=INPUT,TAPE6=OUTPUT,TAPE7
1,TAPE9,TAPE12)
  DIMENSION STRESS(6,12),NOD(1200,4),STRES(6),CI(6,6),DIS(12)
1,BA(6,12),XX(999),P(999),R(999)
  READ(5,12)E,V
  WRITE(6,12)E,V
  READ(5,14)NELEM,IW
14 FORMAT(10I5)
  READ(7,30)((NOD(I,J),J=1,4),I=1,NELEM)
  REWIND 7
39 FORMAT(4I4,4X,4I4,4X,4I4,4X,4I4,4X,4I4)
12 FORMAT(4F14,3)
  READ(12,770)(XY(I),P(I),R(I),I=1,IW)
  REWIND 12
770 FORMAT(6E20,10)
  DO 530 I=1,6
  DO 530 J=1,6
530 C1(I,J)=0.
  CC1=E*(1.-V)/(1.+V)/(1.-2.*V)
  CC2=E*V/(1.+V)/(1.-2.*V)
  CC3=E/2./(1.+V)
  C1(1,1)=CC1
  C1(1,2)=CC2
  C1(1,3)=CC2
  C1(2,1)=CC2
  C1(2,2)=CC1
  C1(2,3)=CC2
  C1(3,1)=CC2
  C1(3,2)=CC2
  C1(3,3)=CC1
  C1(4,4)=CC3
  C1(5,5)=CC3
  C1(6,6)=CC3
  WRITE(6,190)
190 FORMAT(1H0,3X,11HELEMENT NO.,8X,7HSIGMA X,10X,7HSIGMA Y,10X
1,7HSICMA Z,10X,7H TAU XY,10X,7H TAU YZ,10X,7H TAU ZX/)
190 FORMAT(1H ,19,4X,6F17.5)
  DO 771 LK=1,NELEM
  DO 521 I=1,6
  DO 521 J=1,12
521 STRESS(I,J)=0.0
  READ(9,770)((BA(I,J),J=1,12),I=1,6)
  DO 1P2 J=1,4
  I1=NOD(LK,J)
  IX=3*I1-2
  IY=3*I1-1
  IZ=3*I1
  IJK=3*J-2
  JKL=3*J-1
  KLM=3*J
  DIS(IJK)=XX(IX)
  DIS(JKL)=XX(IY)
  DIS(KLM)=XX(IZ)
182 CONTINUE
  DO 520 J=1,12
  DO 520 I=1,6
  DO 520 K=1,6
520 STRESS(I,J)=STRESS(I,J)+C1(I,K)*BA(K,J)
  DO 1P3 I=1,6
  STRES(I)=0.
  DO 1P3 K=1,12
183 STRES(I)=STRES(I)+STRESS(I,K)*DIS(K)
  WRITE(6,190)LK,(STRES(I),I=1,6)
771 CONTINUE
  REWIND 9
  STOP
  END

```







```

      NR=NPD*(I-1)
      DO 31 K=1,3
31    NPD(NA,K)=NPD(J,K)+NR
      WRITE(6,16)((X(I,J),J=1,2),I=1,NPDIN)
      WRITE(6,18)((NPD(I,J),J=1,3),I=1,NELEM)
      DO 38 J=1,NPRESC
      DO 35 I=1,NPDIN
      IF(JP(J).EQ.NUM2(I))GO TO 37
35    CONTINUE
37    JP(J)=I
38    CONTINUE
      WRITE(6,14)(JP(I),I=1,NPRESC)
      IF(NFORCE.EQ.0)GO TO 22
      DO 40 K=1,NFORCE
      DO 43 I=1,NPDIN
      IF(JF(K).EQ.NUM2(I))GO TO 47
43    CONTINUE
47    JF(K)=I
40    CONTINUE
      WRITE(6,14)(JF(I),I=1,NFORCE)
      DO 50 I=1,NFORCE
      IA=JF(I)
50    LOAD(IA)=F(I)
22    CONTINUE
      DO 25 L=1,NFRAC
      DO 28 I=1,NPDIN
      IF(NUM1(L).EQ.NUM2(I))GO TO 59
28    CONTINUE
59    NUM1(L)=I
25    CONTINUE
      WRITE(6,14)(NUM1(I),I=1,NFRAC)
      DO 60 I=1,NPDIN
      APERT(I)=0.
      DO 60 J=1,JRW
60    ST(I,J)=0.
      DO 88 I=1,NFRAC
      IA=NUM1(I)
88    APERT(IA)=TH(I)
      DO 80 LK=1,NELEM
      THICK(LK)=1.0E-12
      DO 85 K=1,3
      JJ=NPD(LK,K)
      THICK(LK)=THICK(LK)+APERT(JJ)/3.
      XE(K,1)=X(JJ,1)
85    XE(K,2)=X(JJ,2)
      E(LK)=THICK(LK)**2/V/12.
      DO 400 J=1,3
      DO 400 I=1,3
400    XPK(I,J)=0.
      OPX=(XE(1,1)+XE(2,1)+XE(3,1))*0.333333
      OPY=(XE(1,2)+XE(2,2)+XE(3,2))*0.333333
      DO 500 I=1,3
      XE(I,1)=XE(I,1)-OPX
500    XE(I,2)=XE(I,2)-OPY
      ZX(1)=XE(2,2)-XE(3,2)
      ZX(2)=XE(3,2)-XE(1,2)
      ZX(3)=XE(1,2)-XE(2,2)
      ZY(1)=XE(3,1)-XE(2,1)
      ZY(2)=XE(1,1)-XE(3,1)
      ZY(3)=XE(2,1)-XE(1,1)
      ZK=XE(2,1)*XE(3,2)-XE(3,1)*XE(2,2)
      Z=3.*7K
      R(1)=ZX(1)/Z
      C(1)=ZY(1)/Z
      B(2)=ZX(2)/Z
      C(2)=ZY(2)/Z

```

```

      B(3)=ZX(3)/7
      C(3)=ZY(3)/7
      DO 520 J=1,3
      STRESS(1,J,LK)=B(J)
520   STRESS(2,J,LK)=C(J)
      VOL(LK)=.5*7
      DO 540 J=1,3
      DO 540 I=1,3
540   XMK(I,J)=XMK(I,J)+(B(J)*P(I)+C(J)*C(I))*E(LK)*VOL(LK)*THICK(LK)
      DO 5 LL=1,3
      DO 5 KK=1,3
      M=NOD(LK,KK)
      N=NOD(LK,LL)
      NNJ=N-M+1
      IF(NNJ.LE.0)GO TO 5
      ST(M,NNJ)=ST(M,NNJ)+XMK(KK,LL)
5   CONTINUE
80  CONTINUE
      DO 100 II=1,NPRESC
      IA=JP(II)
      ST(IA,1)=ST(IA,1)*0.1E+12
100  LOAD(IA)=ST(IA,1)*FAI(II)
      N=NPOIN
      DO 120 I=1,N
      IP=N-I+1
      IF(IP.GT.JPW)IP=JPW
      DO 120 J=1,IP
      JQ=JBW-J
      IF(JQ.GT.I-1)JQ=I-1
      SUM=ST(I,J)
      IF(JQ.EQ.0)GO TO 122
      DO 124 K=1,JQ
      IK=I-K
      JK=J+K
124  SUM=SUM-ST(IK,K+1)*ST(IK,JK)
122  IF(J.NE.1)GO TO 126
      IF(SUM.LE.0.0)GO TO 1000
      TEMP=1./SORT(SUM)
      ST(I,J)=TEMP
      GO TO 120
126  ST(I,J)=SUM*TEMP
120  CONTINUE
      XX(1)=LOAD(1)*ST(1,1)
      DO 140 I=2,N
      J=I-JBW+1
      IF(I+1.LE.JPW)J=1
      SUM=LOAD(I)
      II=I-1
      DO 142 K=J,II
      IA=I-K+1
142  SUM=SUM-ST(K,IA)*XX(K)
140  XX(I)=SUM*ST(I,1)
      DO 150 I=1,N
      II=N-I+1
      J=II+JBW-1
      IF(J.GT.N)J=N
      SUM=XX(II)
      IF(I.EQ.1)GO TO 150
      IB=II+1
      DO 152 K=IB,J
      IA=K-II+1
152  SUM=SUM-ST(II,IA)*XX(K)
150  XX(II)=SUM*ST(II,1)
      DO 39 T=1,N
39   FORCE(I)=XX(I)*VF(I)
      WRITE(6,27)(I,NUM2(I),XX(I),FORCE(I),I=1,N)

```

```

27  FORMAT(1H ,2I7,3X,2E15.7)
    DO 180 LK=1,NELEM
    DO 182 I=1,3
    I1=NOD(LK,I)
182  DIS(I)=XX(I1)
    DO 183 I=1,2
    STRES(I)=0.
    DO 183 K=1,3
183  STRES(I)=STRES(I)+STRESS(I,K,LK)*DIS(K)*E(LK)
    ZZ=STRES(1)**2+STRES(2)**2
    STRES(3)=SQRT(ZZ)
    ZZZ=STRES(2)/STRES(1)
    IF(STRES(1).GE.0.0)GO TO 3
    GO TO 2
    3  STRES(4)=180.0/3.1415926*ATAN(ZZZ)
    GO TO 573
    2  STRES(4)=180.0*(1.0+1.0/3.1415926*ATAN(ZZZ))
573  CONTINUE
    WRITE(6,190)LK,(STRES(I),I=1,4)
190  FORMAT(1H ,I3,3X,4F15.6)
    DO 55 I=1,3
    PP(I)=0.
    DO 56 J=1,2
    56  PP(I)=PP(I)+STRESS(J,I,LK)*STRES(J)*VOL(LK)*THICK(LK)
    IX=NOD(LK,I)
    55  POAD(IX)=POAD(IX)+PP(I)
180  CONTINUE
    DO 57 I=1,NPRES
    JJ=JP(I)
    57  WRITE(6,58)I,NUM2(JJ),POAD(JJ)
    58  FORMAT(2I6,F16.9)
    GO TO 200
1000 WRITE(6,1002)I,J
1002 FORMAT(1H ,2IHSUM IS NEGATIVE VALUE2I5)
200  STOP
    END

```



APPENDIX B  
COUPLED STRESS FLOW MODEL OF ROCK FRACTURE

By

Emmanuel Detournay





## COUPLED STRESS-FLOW MODEL OF ROCK FRACTURE

### 1 INTRODUCTION

This chapter is aimed to set up a model of steady fluid flow in deformable rock fracture. The model is partly based on the experimental and analytical work reported in Gronseth and Detourney (1979) on the following:

1. Analytical expression for the compression curve of a joint.
2. Justification of the concept of effective stress ( $\sigma_n - p$ ) in fluid saturated fracture.
3. Experimental verification of Darcy's Law for flow of viscous fluid in closed fracture.
4. Variation of the hydraulic conductivity of a fracture with its closure.

To construct the model, one needs, besides, some assumptions about the characteristics and the behavior of the rock surrounding the fracture. Hypothesis of linear elasticity, homogeneity and isotropy is made for the rock. It is also assumed that the rock has no permeability. This last assumption is justified by the existence of a high permeability contrast between rock and fracture. It is also supported by many observations of rock systems where the fluid flow is actually governed by the discontinuities (Cambefort, 1965, Talobre, 1967).

The assumptions and governing equations for a model of steady fluid flow in deformable rock fracture are summarized in Section 2. Section

3 describes the numerical scheme devised to solve the coupled stress flow problem. The numerical analysis involves the displacement discontinuity method for solving the structural problem and a finite difference

technique to carry out the fluid flow analysis. The aim of this analysis is to provide a compatible solution between fluid flow, stress distribution and structural deformation. The fluid flow computer code deals only with horizontal flow in one discontinuity line but it could easily be generalized to more complex situations.

## 2 MATHEMATICAL MODEL

### 2.1 Structural Model

Fractured rock masses can be represented by a model composed of pieces of continuum bounded by major discontinuities.

#### 2.1.1 The continuum

It is assumed to be homogeneous, isotropic, elastic and nonporous. The equations of linear elasticity are applied to describe the displacement, strain and stress fields;

Equilibrium equations:

$$\sigma_{ij,j} = B_i$$

Strain-displacement relationship:

$$\epsilon_{ij} = \frac{1}{2} (u_{i,j} + u_{j,i})$$

Constitutive equations:

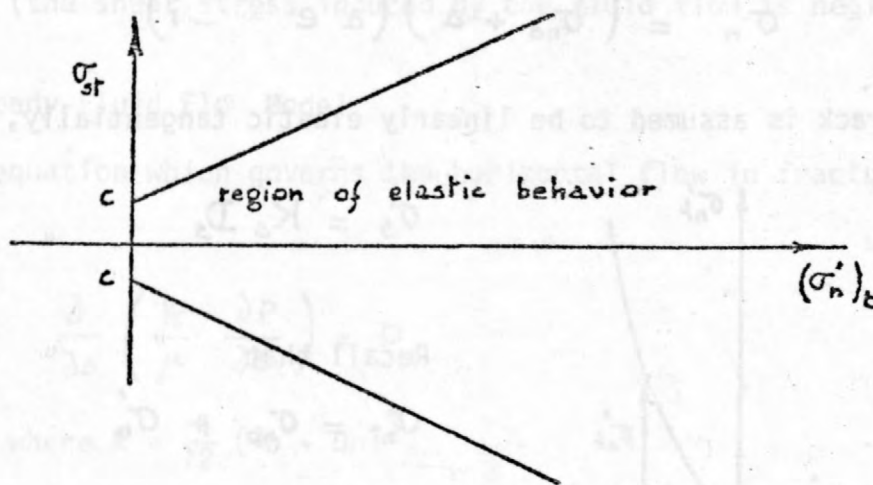
$$\epsilon_{ij} = \frac{1}{2G} \left( \sigma_{ij} - \frac{\nu}{1+\nu} \sigma_{kk} \delta_{ij} \right)$$

#### 2.1.2 Major discontinuities

They are idealized by planar surfaces across which the displacement field can be discontinuous. These discontinuities can be closed or open;

in either case fluid can be present.

If the joint is closed, the effective stress is positive - compression is taken to be positive - i.e. compressional stresses are transmitted across the joint partly through contact spots or rock bridges, partly through fluid if any. There is no strength in tension. The maximum tangential stress to which the joint could be subjected is a function of the effective stress and is assumed to be governed by the Mohr-Coulomb friction model.

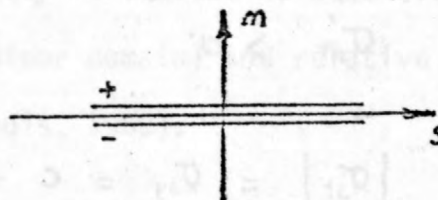


If the joint is open, the effective stress is equal to zero, i.e. no stress is transmitted at all unless fluid is present in the fracture. In that case, only normal stress is conducted - the shear stress induced by the fluid of flow in the discontinuity is neglected in this analysis.

Define  $D_n$ ,  $D_s$  the displacements discontinuities across the joint;

$$D_n = (u_n^- - u_n^+)$$

$$D_s = (u_s^- - u_s^+)$$



To investigate the relations between  $D_n$ ,  $D_s$  and  $\sigma_n$ ,  $\sigma_s$ , several cases have to be distinguished.

## (i) Elastic closed crack

The couple  $(\sigma'_{nt}, \sigma'_{st})$  is inside the Mohr-Coulomb envelope.

This means that,

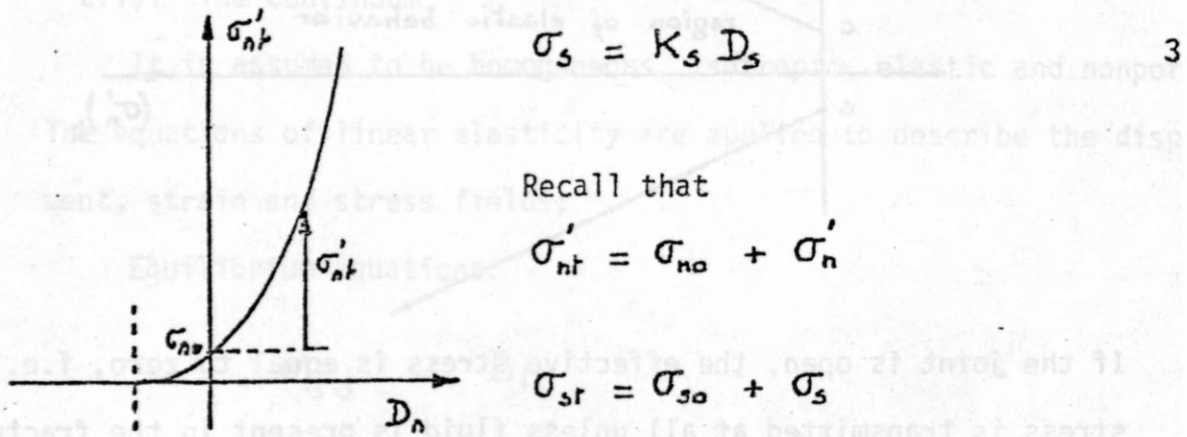
$$\sigma'_{nt} = \sigma_{nt} - p > 0$$

$$\sigma_{st} = c + \sigma'_{nt} \tan \phi$$

From Gronseth and Detourney, Part II, the closure law is given by:

$$\sigma'_n = (\sigma_{no} + a) (a e^{bD_n} - 1) \quad 2$$

The crack is assumed to be linearly elastic tangentially,



## (ii) Slipping closed crack

The couple  $(\sigma'_{nt}, \sigma_{st})$  lies on the Mohr-Coulomb envelope; the normal effective stress is positive.

$$\sigma'_{nt} > 0$$

$$|\sigma_{st}| = \sigma_{sy} = c + \sigma'_{nt} \tan \phi \quad 4$$

The normal constitutive law is given by Eq. 2.



(iii) Open crack

The couple  $(\sigma'_{nt}, \sigma_{st})$  is located at the origin of the axes  $\sigma_s, \sigma_n$ .

$$\sigma'_{nt} = 0$$

$$D_{no} \leq \frac{1}{b} \left[ \ln \frac{1}{2} \sigma_{no} + 1 \right]$$

There are no constitutive equations and

$$\sigma_{nt} = p$$

$$\sigma_{st} = 0$$

(the shear stress induced by the fluid flow is neglected)

4

## 2.2 Steady Fluid Flow Model

The equation which governs the horizontal flow in fracture is given by,

$$\frac{\partial}{\partial s} \left( \frac{k}{\mu} \frac{\partial p}{\partial s} \right) = 0$$

5

$$\text{where } k = \frac{1}{12} (2l_0 - D_n)^3$$

The discharge by unit width of fracture is

$$q = - \frac{k}{\mu} \frac{\partial p}{\partial s}$$

6

Eqs. 5 and 6 apply equally to closed and open fracture. However, in open joints, their validity is limited to conditions where Reynolds number is below 300 (laminar domain) and relative roughness of the fracture less than 0.5 (Louis, 1969).

## 3 NUMERICAL ANALYSIS

## 3.1 Introduction

The stress-deformation and the flow analysis are two independent

parts of the computer code. However, the pressure distribution and the deformed shape of the fracture are quantities common to both programs. The philosophy of the iterative procedure needed to solve the coupled problem, is to loop on the two analyses with the successive approximations of the coupled quantities.

### 3.2 Stress-Deformation Analysis

#### 3.2.1 Displacement discontinuity method

The displacement discontinuity method (Crouch, 1976) belongs to the family of boundary integral equation methods. For an elementary solution, it utilizes the solution of a constant displacement discontinuity, also called dislocation, over a finite length segment in an elastic body. This fundamental solution is used to construct a system of linear equations involving displacements and stresses at boundary elements. Unless modeling natural discontinuities - pressurized crack for example - fictitious dislocations are considered at the boundaries. The system of equations resulting from the displacement discontinuity method is,

$$i = 1, N \quad \left\{ \begin{array}{l} \sigma_s^i = \sum_{j=1}^N A_{ss}^{ij} D_s^j + \sum_{j=1}^N A_{sn}^{ij} D_n^j \\ \sigma_n^i = \sum_{j=1}^N A_{ns}^{ij} D_s^j + \sum_{j=1}^N A_{nn}^{ij} D_n^j \end{array} \right. \quad 7$$

The A's are the influence coefficients. The displacement discontinuity method can also be applied to inhomogeneous problems, but the inhomogeneities have to be restricted to tabular parts of the body or the continuum analyzed. In geomechanical applications, such inhomogeneities are seam or vein deposits, faults, joints etc. The displacement discontinuity method tackles those problems in an approximate way,

because stresses are defined only normally and tangentially to the plane of the inhomogeneity. This approach was shown to be satisfactory (Crouch, 1976).

In that type of problem,  $\sigma_s^i$ ,  $\sigma_n^i$  in Eq. 7 become the induced stresses in element  $i$ . The constitutive equations of the inhomogeneity have to be introduced in the set of Eq. 7.

Let

$$\begin{aligned}\sigma_s^i &= f_s^i(D_s^i, D_n^i) \\ \sigma_n^i &= f_n^i(D_s^i, D_n^i)\end{aligned}\quad 8.$$

be the constitutive equations. If they are introduced in Eq. 7, we obtain

$$i=1, N \quad \left\{ \begin{aligned} f_s^i(D_s^i, D_n^i) &= \sum_{j=1}^N \bar{A}_{ss}^{ij} D_s^j + \sum_{j=1}^N \bar{A}_{sn}^{ij} D_n^j \\ f_n^i(D_s^i, D_n^i) &= \sum_{j=1}^N A_{ns}^{ij} D_s^j + \sum_{j=1}^N \bar{A}_{nn}^{ij} D_n^j \end{aligned} \right. \quad 9.$$

The resultant system of equations is usually no longer linear. In the next section, Eq. 9 will be written down explicitly for a Mohr-Coulomb element which has the crack characteristics enumerated in Section 2.1.2.

### 3.2.2 Equations for a Mohr-Coulomb element

(i)  $i^{\text{th}}$  element closed and elastic

Conditions:  $\sigma_{nr}^i - p^i > 0$

$$|\sigma_{sr}^i| < c + (\sigma_{nr}^i - p^i) \tan \phi$$

$$\sigma_n^i - p^i = (\sigma_{no}^i + a) (e^{b D_n^i} - 1)$$

$$\sigma_s^i = K_s D_s^i$$

Equations 9 become,

$$\dot{p}^i + (\sigma_{no}^i + a) \left( e^{bD_n^i} - 1 \right) = \sum_{j=1}^N \ddot{A}_{ns}^j \dot{D}_s^j + \sum_{j=1}^N \ddot{A}_{nn}^j \dot{D}_n^j \quad 10$$

$$K_s \dot{D}_s^i = \sum_{j=1}^N \ddot{A}_{ss}^j \dot{D}_s^j + \sum_{j=1}^N \ddot{A}_{sn}^j \dot{D}_n^j$$

(ii)  $i^{th}$  element closed and slipping

Conditions:

$$\begin{aligned} \dot{\sigma}_{nr}^i - \dot{p}^i &> 0 \\ |\dot{\sigma}_{sr}^i| = \dot{\sigma}_{sy}^i &= c + (\dot{\sigma}_{nr}^i - \dot{p}^i) \tan \phi \end{aligned}$$

Then,

$$\begin{aligned} \dot{\sigma}_n^i - \dot{p}^i &= (\dot{\sigma}_{no}^i + a) \left( e^{bD_n^i} - 1 \right) \\ \dot{\sigma}_s^i &= \text{sign}(\sigma_s^i) \sigma_{sy}^i - \sigma_{so}^i \end{aligned}$$

Equations 9 become,

$$\text{sign}(\sigma_s^i) \sigma_{sy}^i - \sigma_{so}^i = \sum_{j=1}^N \ddot{A}_{ss}^j \dot{D}_s^j + \sum_{j=1}^N \ddot{A}_{sn}^j \dot{D}_n^j \quad 11$$

$$\dot{p}^i + (\dot{\sigma}_{no}^i + a) \left( e^{bD_n^i} - 1 \right) = \sum_{j=1}^N \ddot{A}_{ns}^j \dot{D}_s^j + \sum_{j=1}^N \ddot{A}_{nn}^j \dot{D}_n^j$$

(iii)  $i^{th}$  element open

Conditions:

$$\begin{aligned} \dot{\sigma}_{nr}^i - \dot{p}^i &= 0 \\ \dot{D}_n^i &\leq -\dot{D}_{no}^i = -\frac{1}{b} \ln \left( \frac{\dot{\sigma}_{no}^i}{a} + 1 \right) \end{aligned}$$

Then,

$$\begin{aligned} \dot{\sigma}_{nr}^i &= \dot{p}^i \\ \dot{\sigma}_{sr}^i &= 0 \end{aligned}$$

Equations 9 become,

$$\begin{aligned} \dot{p}^i - \sigma_{no}^i &= \sum_{j=1}^N \ddot{A}_{ns}^j \dot{D}_s^j + \sum_{j=1}^N \ddot{A}_{nn}^j \dot{D}_n^j \\ -\sigma_{so}^i &= \sum_{j=1}^N \ddot{A}_{ss}^j \dot{D}_s^j + \sum_{j=1}^N \ddot{A}_{sn}^j \dot{D}_n^j \end{aligned} \quad 12$$

### 3.2.3 Resolution technique

With the Mohr-Coulomb element,  $f_n^i$  in equations 9 can be a non-linear function of  $D_n^i$ . An iterative method is therefore needed for solving this system of equations. The technique used is a generalization of Newton-Raphson (see G. Dahlquist and A. Bjorck for example) with the convergence rate accelerated by a relaxation factor.

Equations 9 are written under the following form,

$$i=1,N \begin{cases} F_n^i = f_n^i(D_n^i, D_s^i) - \sum_{j=1}^N \ddot{A}_{ns}^j \ddot{D}_s^j + \sum_{j=1}^N \ddot{A}_{nn}^j \ddot{D}_n^j \\ F_s^i = f_s^i(D_n^i, D_s^i) - \sum_{j=1}^N \ddot{A}_{ss}^j \ddot{D}_s^j + \sum_{j=1}^N \ddot{A}_{sn}^j \ddot{D}_n^j \end{cases} \quad 13$$

The system of equations to solve is

$$i=1,N \begin{cases} \left. \frac{\partial F_n^i}{\partial D_n^i} \right|_{D_n^i = (D_n^i)^k} \left[ (D_n^i)^{k+1} - (D_n^i)^k \right] + F_n^i = 0 \\ \left. \frac{\partial F_s^i}{\partial D_s^i} \right|_{D_s^i = (D_s^i)^k} \left[ (D_s^i)^{k+1} - (D_s^i)^k \right] + F_s^i = 0 \end{cases} \quad 14$$

The superscript k stands for the  $k^{th}$  approximation of the quantity.

Equations 14 are solved iteratively, using a relaxation factor w.

Explicitly, one has

$$\begin{aligned} (D_n^i)^{k+1} &= (D_n^i)^k - \omega F_n^i / \left. \frac{\partial F_n^i}{\partial D_n^i} \right|_{D_n^i = (D_n^i)^k} \\ (D_s^i)^{k+1} &= (D_s^i)^k - \omega F_s^i / \left. \frac{\partial F_s^i}{\partial D_s^i} \right|_{D_s^i = (D_s^i)^k} \end{aligned} \quad 14$$

In the algorithm, the  $D_n$ 's and  $D_s$ 's are updated continuously.

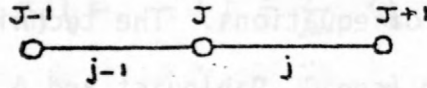
## 3.3 Fluid Flow Analysis

### 3.3.1 Finite differences mesh

The pressure distribution in the fracture is computed by a finite



differences technique (FDT). Due to the flow boundary conditions, the nodes of the finite differences mesh are more conveniently located at the common point of two successive boundary elements.



Let  $P^J$  be the pressure quantity defined at node J.  $p^j$  represents the average pressure acting on element j and is also characteristic of the mid-point of this element.

$$p^j = \frac{1}{2} (P^J + P^{J+1}) \quad 16$$

Let  $K^J$  be the crack conductivity at node J.

$$k^J = \frac{1}{12} (e^J)^3$$

If one assumes that the crack has a constant initial aperture  $e_0$ , then

$$e^J = e_0 - \frac{1}{2} (D_n^{j-1} + D_n^j)$$

At the ends of the crack line:

$$\begin{aligned} e^1 &= e_0 - D_n^1 \\ e^N &= e_0 - D_n^{N-1} \end{aligned}$$

### 3.3.2 Finite differences formulation of the diffusion equation

Assuming the fluid viscosity constant, the diffusion equation is given by

$$\frac{\partial}{\partial s} \left( k \frac{\partial P}{\partial s} \right) = 0$$

An alternative form is

$$k \frac{\partial^2 P}{\partial s^2} + \left( \frac{\partial k}{\partial s} \right) \frac{\partial P}{\partial s} = 0 \quad 17$$

Let  $h$  be the distance between two adjacent nodes. The nodes must be equally spaced in order that  $h$  be constant (convenience for the finite differences technique). The central differences formula ( $O(h^2)$ ) applied at node  $J$  leads to

$$\frac{h^J (P^{J-1} - 2P^J + P^{J+1}))}{h^2} + \frac{(h^{J+1} - h^{J-1}) (P^J - P^{J-1})}{2h} = 0$$

$$(4h^J + h^{J-1} - h^{J+1})P^{J-1} - 8h^J P^J + (4h^J - h^{J-1} + h^{J+1})P^{J+1} = 0 \quad 18$$

Eq. 18 may be written in the following way:

$$a^J P^{J-1} + b^J P^J + c^J P^{J+1} \quad 19$$

$$\text{with} \quad \begin{aligned} a &= 4h^J + h^{J-1} - h^{J+1} \\ b &= -8h^J \\ c &= 4h^J - h^{J-1} + h^{J+1} \end{aligned}$$

### 3.3.3 Introduction of the boundary conditions

(i) Pressure imposed at both ends of the fracture.

$$\text{i.e.} \quad P^1 = P_o \quad ; \quad P^N = P_n$$

$$b^2 P^2 + c^2 P^3 = - (4h^2 + h^1 - h^3) P_o$$

$$a^{N-1} P^{N-2} + b^{N-1} P^{N-1} = - (4h^{N-1} - h^{N-2} + h^N) P_n$$

$$\text{or} \quad \begin{aligned} b^2 P^2 + c^2 P^3 &= d^2 \\ a^{N-1} P^{N-2} + b^{N-1} P^{N-1} &= d^{N-1} \end{aligned}$$

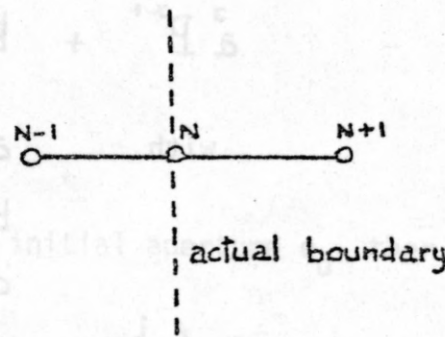
The system of equations to be solved in order to compute the  $\{P^J\}$  is

$$\begin{aligned} b^2 P^2 + c^2 P^3 &= d^2 \\ a^J P^{J-1} + b^J P^J + c^J P^{J+1} &= 0 \\ a^{N-1} P^{N-2} + b^{N-1} P^{N-1} &= d^{N-1} \end{aligned} \quad \text{20}$$

(ii) Pressure imposed at one end, discharge at the other.

i.e.  $P' = P_0$  ;  $-k^N \left( \frac{\partial P}{\partial s} \right)_{J=N} = q_N$

This second condition may be handled by considering a false boundary, i.e. by adding a node numbered  $N+1$

$$\begin{aligned} q_n &= -k^N \left( \frac{\partial P}{\partial s} \right)_{J=N} \\ &= \frac{k^N}{2h} (P^{N-1} - P^{N+1}) \end{aligned}$$


Therefore

$$P^{N+1} = -\frac{2h}{k^N} q_n + P^{N-1}$$

For  $(J=N)$ , Eq. 19 becomes (one imposes  $k^{n+1} = k^{n-1}$ )

$$4 k^N P^{N-1} - 8 k^N P^N + 4 k^N P^{N+1} = 0$$

or  $8 k^N P^{N-1} - 8 k^N P^N = 8 h q_n$

or  $a^N P^{N-1} + b^N P^N = d^N$

The  $\{P^J\}$  are obtained by solving the following system of equations:

$$\begin{aligned} b^2 P^2 + c^2 P^3 &= d^2 \\ a^J P^{J-1} + b^J P^J + c^J P^{J+1} &= 0 \quad J=3, N-1 \\ b^N P^{N-1} + c^N P^N &= d^N \end{aligned} \quad \text{22}$$

The systems of Eqs. 20 and 22 are tridiagonal.

### 3.3.4 Resolution algorithm for a tridiagonal system of linear equations

The elimination algorithm to solve a tridiagonal system of equations is called the Thomas algorithm (Smith, 1971). Consider the following system:

$$\begin{aligned} b^1 x^1 + c^1 x^2 &= d^1 \\ a^j x^{j-1} + b^j x^j + c^j x^{j+1} &= d^j \quad j=2, N-1 \\ a^N x^{N-1} + b^N x^N &= d^N \end{aligned}$$

(i) Transform the matrix of coefficients into one of upper diagonal form.

Let  $a'', b'', c'', d''$  be the coefficients of the new system. Then

$$a^{i''} = 0 \quad ; \quad b^{i''} = 1 \quad i=1, N$$

$$c^{i''} = \frac{c^i}{b^i} \quad ; \quad d^{i''} = \frac{d^i}{b^i}$$

Recurrence

$$c^{i+1''} = \frac{c^{i+1}}{b^{i+1} - a^{i+1''} c^{i''}} \quad ; \quad d^{i+1''} = \frac{d^{i+1} - a^{i+1''} d^{i''}}{b^{i+1} - a^{i+1''} c^{i''}} \quad i=1, N-1$$

(ii) Backwards substitution:

$n^{\text{th}}$  equation is now

$$x^N = d^{N''}$$

and

$$x^i = d^{i''} - c^{i''} x^{i+1} \quad i = N-1, N-2, \dots, 1$$

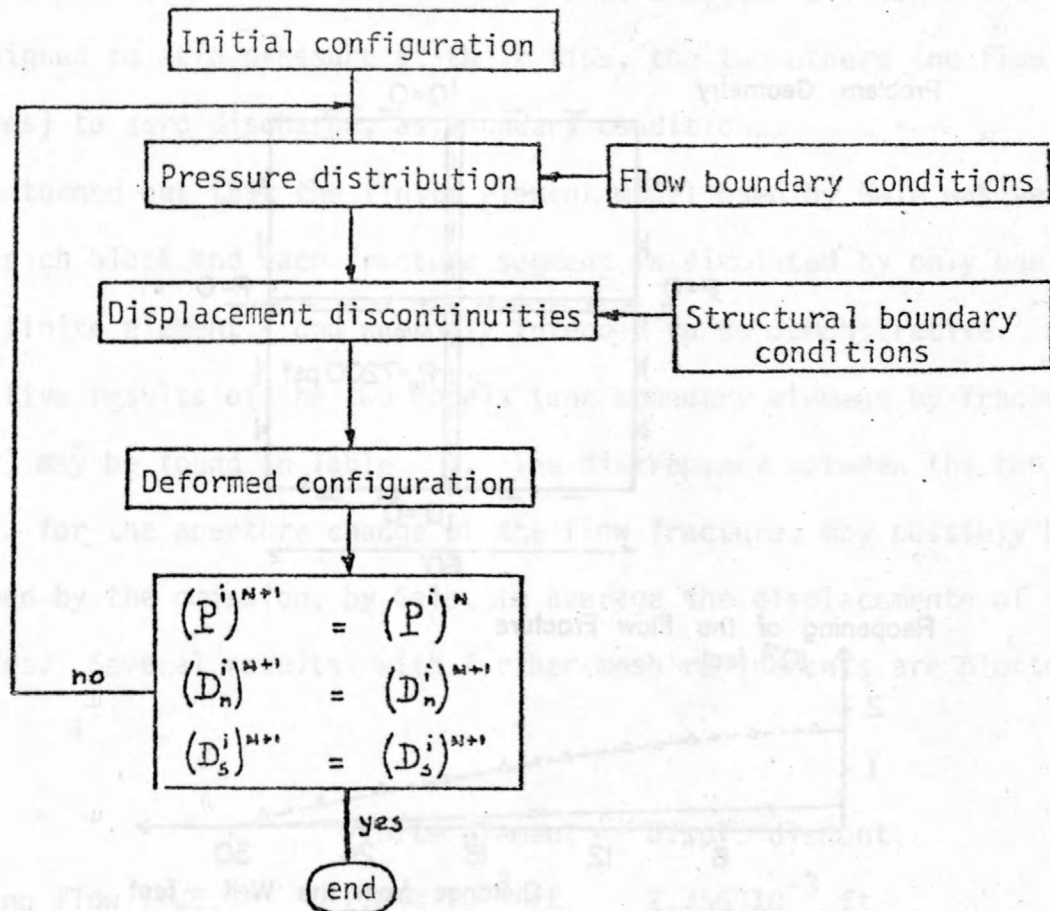
### 4 3.4 Coupled Stress-Flow Algorithm

The choice of the proper mode of coupling the stress-deformation program and the flow program appeared important in order to reduce the computation time. The procedure whose main steps are described below seemed to be the most efficient.

1. A first approximation of the pressure distribution in the fracture is computed according to the flow boundary conditions. This calculation relies upon the initial aperture assigned to the Mohr-Coulomb boundary elements. Actually, this pressure distribution is equivalent to that of a rigid fracture system.
2. Then, the stress-deformation program is entered to compute the displacement discontinuities associated to each boundary element. This computation is based on the structural boundary conditions, the initial state of stress and the first approximation of the pressure distribution in the fracture. The displacement discontinuities are solved iteratively. The number of iterations is chosen so that the results, at this stage of the solving process, are reasonable but not highly accurate. The threshold of "reasonable accuracy is attained when the relative difference between two successive approximations of the same quantity is less than 1%.
3. This step deals with the flow program in which the new apertures of the Mohr-Coulomb elements are introduced. It takes a new approximation of the pressure distribution.
4. The displacement discontinuities are recomputed to fit the new pressure distribution. Remarks given at step 2 are still valid.
5. Steps 3 and 4 are repeated until a 1% level of accuracy is reached for both flow and displacement quantities. The flow chart of the iterative process is sketched below.



B-15  
Flow chart



#### 4 EXAMPLES [values of the parameters are listed in Table 2]

##### 4.1 Four Blocks Model

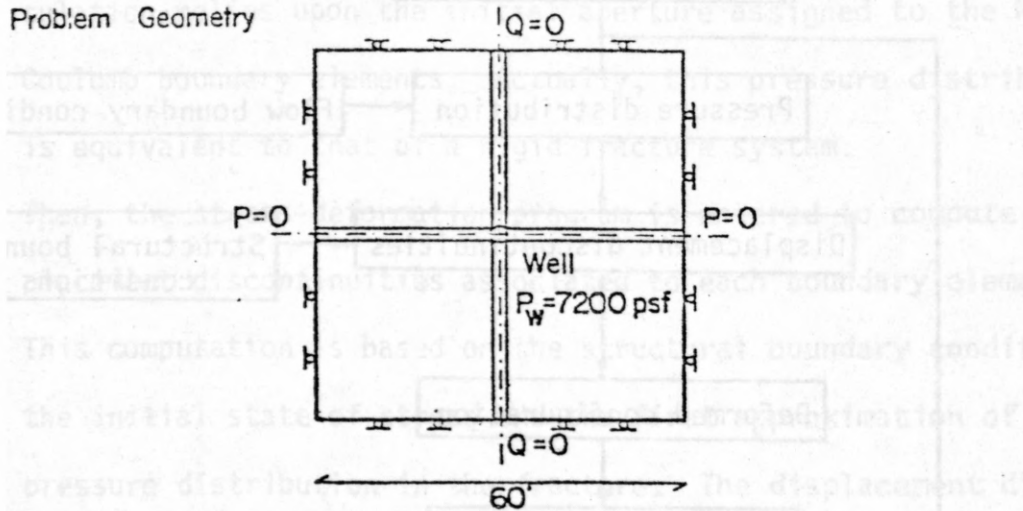
This problem was considered in order to compare the results of this method with those obtained by the coupled finite element method (Gale, 1974) developed at the University of California, Berkeley.

This simple model consists of a horizontal cross section of four rock blocks and four vertical fracture segments (see Fig. 1). The normal joint stiffness is assumed constant.

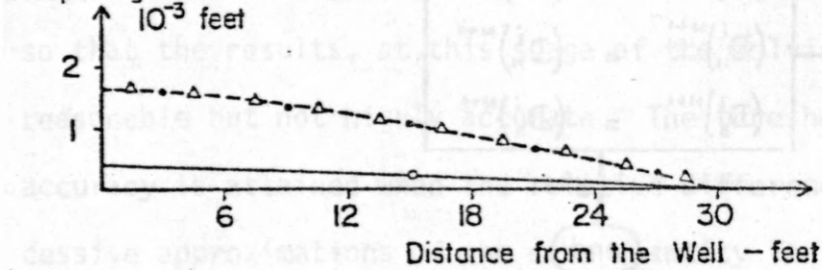
Structural boundary conditions: No movement perpendicular to the boundaries is permitted.

## FOUR BLOCKS MODEL

Problem Geometry



Reopening of the Flow Fracture



Pressure - psf

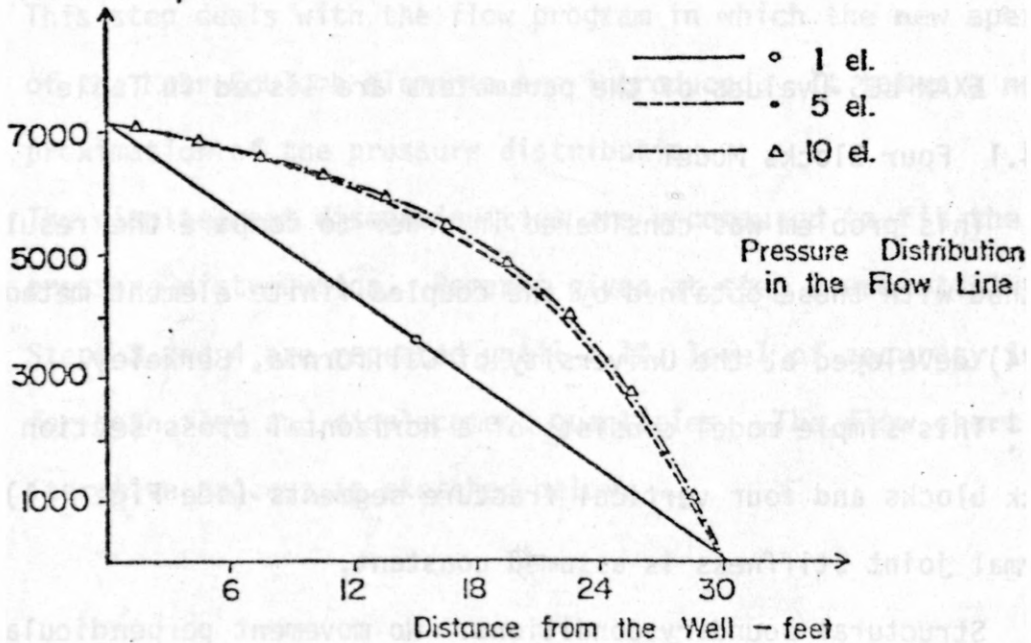


Figure 1

Flow boundary conditions: A fixed pressure is assigned to the well at the center of the model. Two fracture segments (flow fractures) are assigned to zero pressure at their tips, the two others (no flow fractures) to zero discharge, as boundary conditions.

It turned out that the finite element model used by Gale was very rough, each block and each fracture segment is simulated by only one linear finite element - and was only intended to be demonstrative. Comparative results of the two models (one boundary element by fracture segment) may be found in Table 1. The discrepancy between the two methods, for the aperture change of the flow fracture, may possibly be explained by the omission, by Gale, to average the displacements of the two nodes. Several results, with further mesh refinements are plotted on Fig. 1.

	Finite element	Displ. discont.
Dn (no flow frac.)	$2.344 \cdot 10^{-3}$ ft	$2.356 \cdot 10^{-3}$ ft
Dn (flow frac.)	$0.469 \cdot 10^{-3}$ ft	$0.218 \cdot 10^{-3}$ ft
Q (flow frac.)	$6.058 \cdot 10^{-3}$ cfs	$3.461 \cdot 10^{-3}$ cfs

Table 1

#### 4.2 Injection Well

The boundary conditions of this problem are very similar to those of the previous example. Here, all fracture segments are of the flow type. Flow and structural boundary conditions are sketched in Fig. 2. We have investigated the influence of the rock modulus on the pressure distribution in the fracture. Results are plotted on Fig. 2. They show that the pressure distribution becomes more linear when the Young modulus increases.

## INJECTION WELL

Problem Geometry

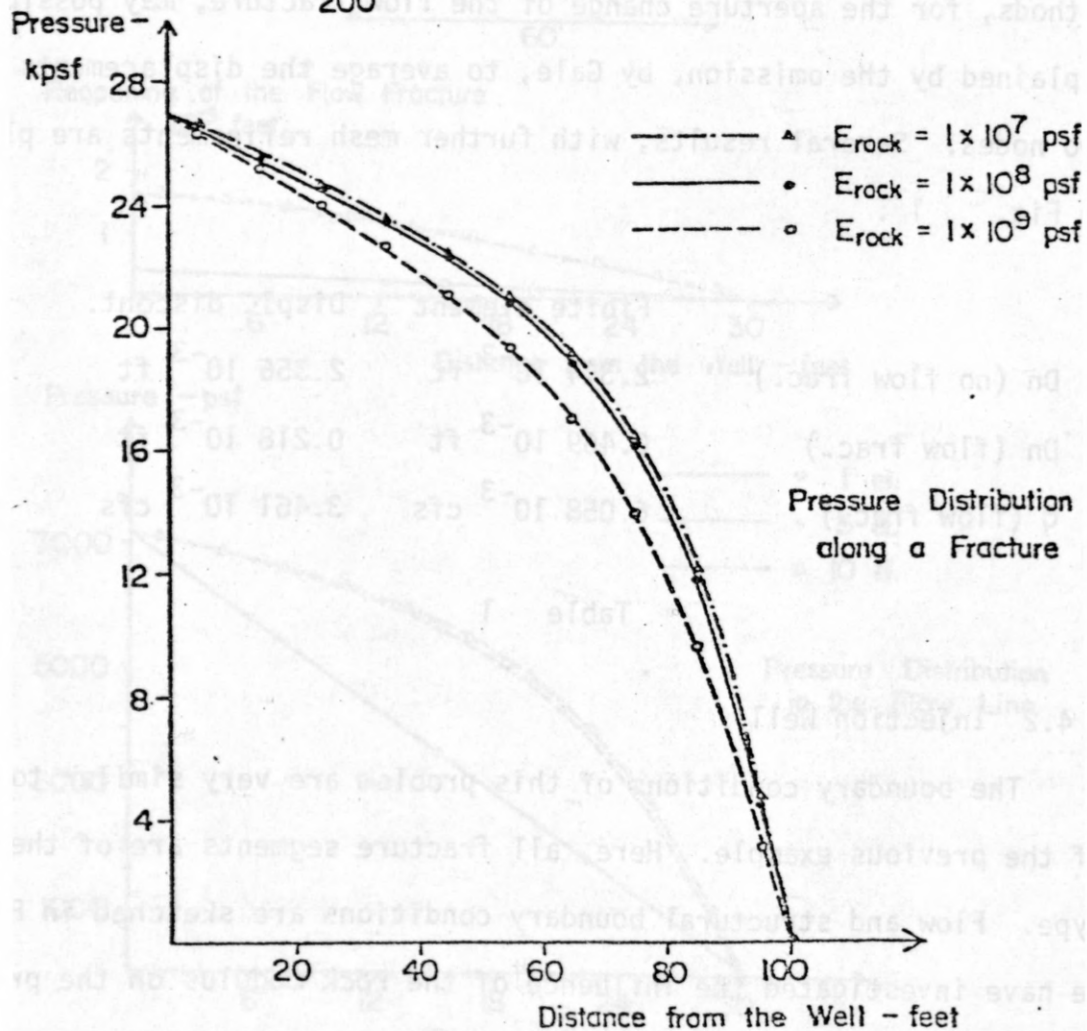
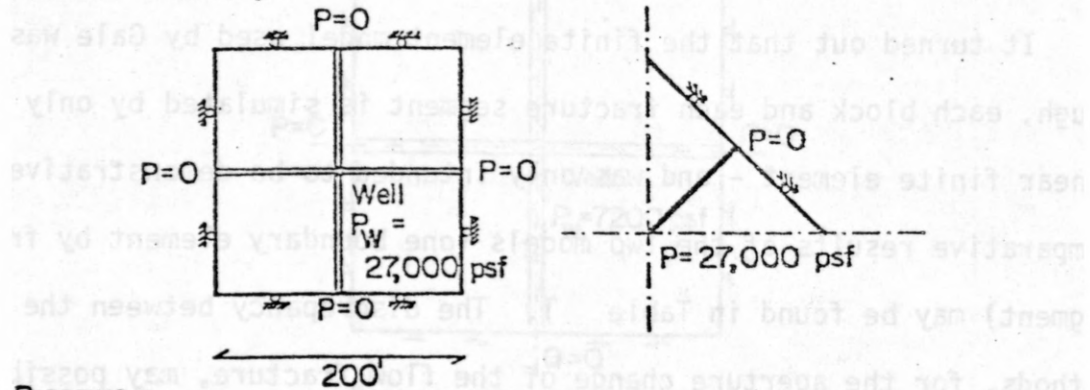


Figure 2

#### 4.3 Simulation of Conductivity Experiment

The intention in carrying out this problem was to try to duplicate the conductivity experiment results and hence validate the model.

The parameters  $a$  and  $b$  of the joint compression curve were computed assuming that the entire load applied to the sample was transmitted through the fluid carrying fracture. The initial aperture was assessed from the conductivity data, see Gronseth and Detourney Part II.

Two conductivity experiments C-201 and C-208 were simulated numerically. The results are sketched in Fig. 3 together with the experimental points. In both cases, the computed relationship between flow rate and gradient of pressure is not linear. As expected from the shape of the compression curve, the departure from linearity is larger in the case where the applied normal stress is smaller. The numerical results show to underestimate the experimental ones in the non-linear range. The most possible explanation is that the actual stress across the fluid fracture is smaller than assessed. Assuming that 80% of the load is transmitted through the fluid fracture, we decreased the differences between the experimental and numerical curves. But, most probably, the normal stress across the fracture is not homogeneous:

- an unknown portion of the load is taken by the sealed edges of the fluid fracture.
- steel tubings cemented in the two holes drilled in the sample have concentrated stresses while releasing them from the inlet of the fluid fracture.
- three dimensional character of the actual test.

These reasons explain the discrepancies between the actual and computed results.



## Numerical simulation of conductivity experiment

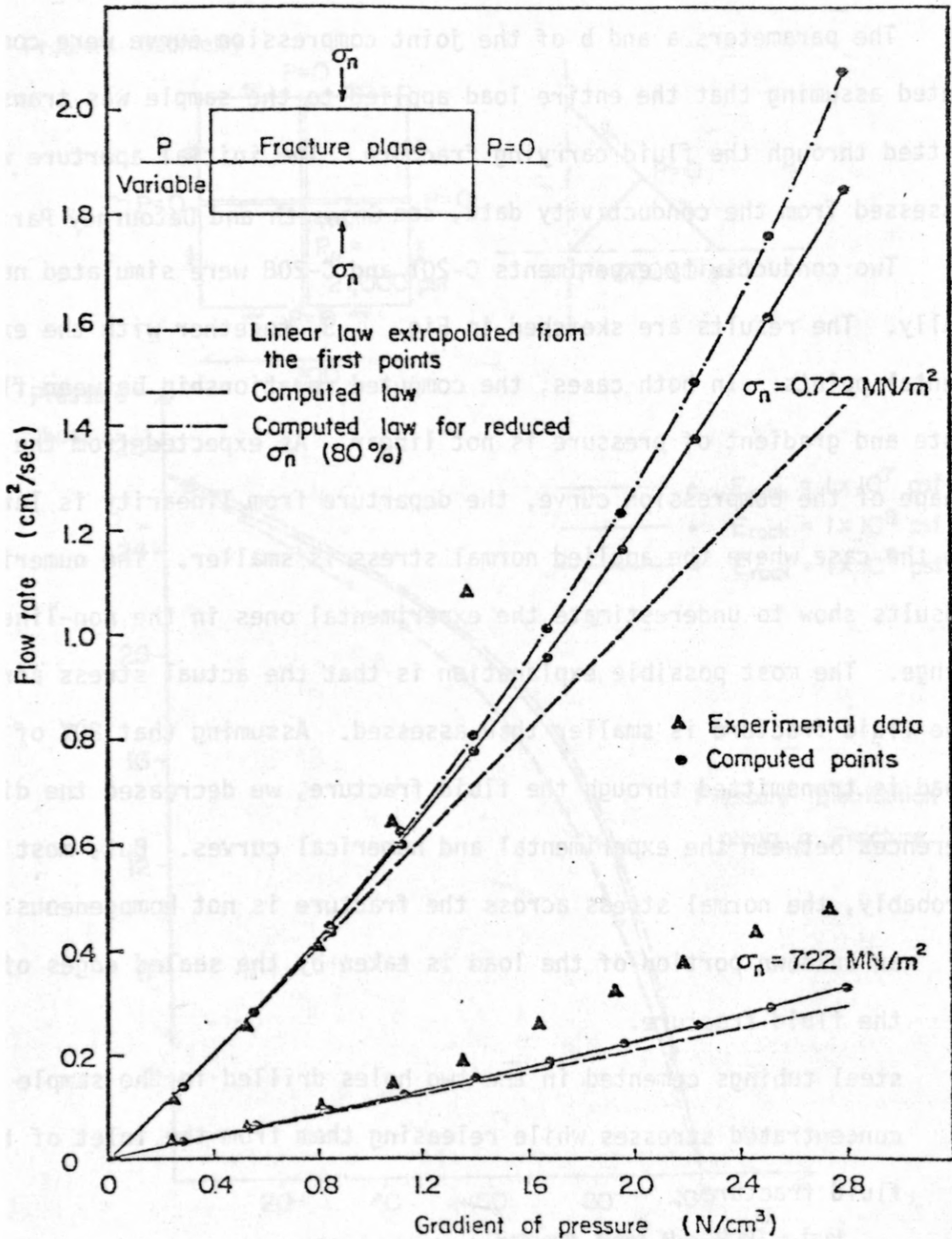


Figure 3

Table 2

Parameters for the four blocks model

ROCK	E	=	$1.44 \cdot 10^8$ PSF
	$\nu$	=	0.25
JOINT	$K_n$	=	$1.44 \cdot 10^{10}$ lb/ft <sup>3</sup>
	$K_s$	=	$1.44 \cdot 10^{10}$ lb/ft <sup>3</sup>
	c	=	0
	$\phi$	=	38°
VISCOSITY	$\mu$	=	$1.045 \cdot 10^{-5}$

Parameters for the injection well model

ROCK	E	variable	See Fig. 2
	$\nu$	=	0.25
JOINT	$K_n$	=	$10^{12}$ lb/ft <sup>3</sup>
	$K_s$	=	$10^{12}$ lb/ft <sup>3</sup>
	c	=	0
	$\phi$	=	20°
VISCOSITY	$\mu$	=	$1.045 \cdot 10^{-5}$

Parameters for the simulation of conductivity experiment

ROCK	E	=	$6.68 \cdot 10^{10}$ N/m <sup>2</sup>
	$\nu$	=	0.32
JOINT	a	=	42420; b = 20142 (Dn in m; $\sigma_n$ in N/m <sup>2</sup> )
	For the case where 80% of the load is transmitted through the fracture: a = 33937; b = 20142		
VISCOSITY	$\mu$	=	40 centipoises







USGS LIBRARY-RESTON



3 1818 00074568 5